Cellular Fatty Acid Toxicity: Extrapolating Yeast Screens into Mammalian Models

Kelly Ruggles

Submitted in partial fulfillment of the
requirements for the degree of
Doctor of Philosophy
under the Executive Committee
of the Graduate School of Arts and Sciences

COLUMBIA UNIVERSITY

2012

©2012
Kelly Ruggles
All rights reserved

ABSTRACT

Cellular Fatty Acid Toxicity: Extrapolating Yeast Screens into Mammalian Models

Kelly Ruggles

Fatty acid deposition in non-adipose tissue leads to a cellular dysfunction known as lipotoxicity. Neutral lipid synthesis is known to protect against lipotoxicity but many additional pathways are likely to be integral in this process. In order to identify pathways protective against lipid induced cell death, we performed a genome-wide unsaturated fatty acid (UFA) sensitivity screen in yeast. Of the ~5,500 gene mutants tested, we identified 156 which resulted in sensitivity to growth on media containing palmitoleate. These genes identified many cellular processes, including vesicular trafficking, lipid metabolism and vacuolar protein sorting. Deletion of three members of the GET complex, a complex essential for tail anchored protein insertion into the ER, caused vulnerability to fatty acids. We went on to assess the role of *GET3* in cellular lipid metabolism and found that ablation of *GET3* results in a defect in vacuolar hydrolysis and a reduction in lipid droplet number; pathways which we hypothesize to be integrally related. Furthermore, a major goal of this study was to find mammalian genes playing an integral role in pathways of lipoprotection. Of the 156 gene deletions found to confer fatty acid sensitivity in yeast, 68 have been conserved in mammals. We demonstrate that two of these mammalian orthologs, *ARV1* and *ASNA1*, are vulnerable to fatty acid treatment upon knockdown in the MIN6 pancreatic β-cell line. These mammalian genes, which were identified through the fatty acid sensitivity screen in yeast, are involved in lipid induced cellular dysfunction in pancreatic β-cells and, in the case of *ARV1*, hepatocytes. Therefore, these genes likely play a role in the progression of the lipotoxic diseases; type 2 diabetes and nonalcoholic fatty liver disease.

TABLE OF CONTENTS

LIST OF FIGURES

LIST OF TABLES

LIST OF ABBREVIATIONS

ACAT	acyl-coenzyme A (coA):cholesterol acyltransferase
Ad	adenovirus
ADP	adenosine diphosphate
AGPAT	acyl-coA:1-acylglycerol-*sn*-3-phosphatase
AHD	arv1 homology domain
APO	apolipoprotein
ARAT	acyl-coA:retinol acyltransferase
ARV1	*ARE2* required for viability
ASNA1	arsA aresenite transporter ATP-binding homolog 1
ASO	antisense oligonucleotide
ATF6	activating transcription factor-6
ATGL	adipose triglyceride lipase
ATP	adenosine triphosphate
BSA	bovine serum albumin
CCT	CTP:phosphocholine ctidylyltransferase
CDP	cytidine diphosphatidylhydrolase
CPT	carnitine palmitoly-transferase
CVD	cardiovascular disease
DAG	diacylglycerol
DIO	diet induced obesity
DMEM	dulbecco's modified eagle's medium
DPM	disintegrations per minute

ER	endoplasmic reticulum
FA	fatty acid
FAS	fatty acid synthase
FBS	fetal bovine serum
FFA	free fatty acid
FXR	farnesoid X receptor
GARP	golgi associated ER trafficking
GET	golgi to ER trafficking
GFP	green fluorescent protein
GPAT	acyl-coA:glycerol-*sn*-3-phosphate acyltransferase
G protein	guanine nucleotide-binding protein
GEF	guanine nucleotide exchange factor
GDP	guanine diphosphate
GPCR	g protein coupled receptors
GRP40	g-protein coupled receptor 40
GSIS	glucose stimulated insulin secretion
GTP	guanine triphosphate
GWAS	genome-wide association study
HAT	histone acyltransferase
HDAC	histone deacetylase
HDL	high density lipoprotein
HSL	hormone sensitive lipase
IRE1	inositol-requiring protein 1

LCAT	lecithin:cholesterol acyltransferase
LC-CoA	long chain-CoA
LCFA	long chain fatty acid
LD	lipid droplet
LDL	low density lipoprotein
LPA	lysophosphatididate
LPL	lipoprotein lipase
MAG	monoacylglycerol
MBOAT	membrane bound O-acyltransferase
MGAT	acyl-coA:monoacylglycerol acyltransferase
NAFLD	nonalcoholic fatty liver disease
NASH	nonalcoholic steatohepatitis
NL	neutral lipid
PA	phosphatidic acid
PAP	phosphatidic acid phosphohydrolase
PAS	pre-autophagosomal structure
PERK	protein kinase RNA (PKR)-like ER kinase
PC	phosphatidylcholine
PE	phosphatidylethanolamine
PI	phosphatidylinositol
PL	phospholipid
PPAR	peroxisome proliferator-activated receptor
PS	phosphatidylserine

PtdIns-3-P	phosphatidylinositol-3-phosphate
RFP	red fluorescent protein
ROS	reactive oxygen species
RT-PCR	real-time polymerase chain reaction
SNARE	soluble NSF attachment protein receptor
SPT	serine palmitoyl-transferase
SRE	sterol regulatory elements
SREBP	sterol regulatory element-binding protein
SRP	signal recognition protein
T2D	type 2 diabetes
TA	tail anchored
TG	triglyceride
TLC	thin layer chromatography
TMD	transmembrane domain
TRC	transmembrane domain recognition complex
s.d.	standard deviation
s.e.	standard error
SE	sterol ester
SFA	saturated fatty acid
UFA	unsaturated fatty acid
UPR	unfolded protein response
VLDL	very low density lipoproteins
VPS	vacuole protein sorting

ACKNOWLEDGMENTS

I am sincerely thankful to my advisor, Dr. Stephen Sturley for his support and guidance throughout my graduate training. His continuous encouragement throughout this process has made the completion of this thesis possible. Furthermore, I would like to thank Dr. Henry Ginsberg for his generous support throughout my graduate tenure, particularly during my last year of thesis work. His mentorship and willingness to allow me to work in his lab have been extremely helpful and I would not have been able to complete this thesis research.

I would also like to thank my thesis defense committee, Dr. Domenico Accili, Dr. Henry Ginsberg, Dr. Liza Pon, and Dr. Anthony Ferrante for their time and effort. My sincere gratitude to the members of my thesis advisory committee, Dr. Henry Ginsbrg, Dr. Domenico Accili, Dr. Wendy Chung and Dr. Anthony Ferrante, for their advice and continuous support throughout this process.

Special thanks goes to the past and present members of the Sturley lab, who have made this process enjoyable and have become some of my most dependable friends. Sturley lab members include Moneek Madra, Dr. Sonia Gulati, Dr. Caryn Trbovic, Dr. Andrew Munkacsi, Matthew Brinkman, Dr. Aaron Turkish, Dr. Jeanne Garbarino, Dina Balderes, James Moon and Kerry Schneider. Particular thanks go to James Moon and Kerry Schneider, who directly contributed to this work. I would also like to thank the Ginsberg lab members, for taking me in as a member of their lab and contributing to my academic development. They are Donna Conlon, Dr. Jing Liu, Dr. Byoung Moon, Dr. Antonio Hernandez-Ono, Dr. Tiffany Thomas and Colleen Ngai.

I would like to thank our collaborator, Dr. Joseph DeGiorgis, from Providence College, for all of his contributions to this work. Thank you to the faculty and staff of the IHN, Dr.

Richard Deckelbaum, Alex Sosa, Leslie DePena, Mary Lou Westberg and Yonnette Beaton, for their continuous assistance. Finally, I would thank to thank Dr. Sharon Akabas and Dr. Debra Wolgemuth for their continuous support and encouragement.

DEDICATION

This thesis is dedicated to my parents, Jeanne and Steven Ruggles, and to my wonderful partner, Sarah Jaramillo. Without their unconditional love, patience and support this thesis work would not have been possible.

CHAPTER 1: LITERATURE REVIEW

The importance of obesity research has been increasing rapidly over the past century. For most of human history, obesity rarely occurred, and when it did was frequently associated with wealth and status. In the late 18th and early 19th century, the number of obese people increased due to increased food access and reduced physical activity, and the medical community began to identify health issues associated with excess weight gain. These issues included shortness of breath, lethargy, depression, poor circulation and skin disorders [1, 2] as well as the primary comorbidities we now associate with obesity, type 2 diabetes (T2D) and cardiovascular disease (CVD) [3, 4].

In 1997 the World Health Organization (WHO) recognized obesity as a global epidemic and obesity and overweight have continued to grow to astounding numbers worldwide. As of 2008, the WHO estimated that 1.5 billion adults were overweight and predict that the number of deaths in 2030 due to cardiovascular disease and diabetes will grow to 23.6 million and 3.4 million, respectively [5]. These metabolic diseases derive primarily from insulin resistance, intracellular lipid accumulation and the resulting cellular dysfunction.

Obesity is associated with impaired insulin signaling in muscle, adipose and liver in addition to decreased glucose stimulated insulin release by pancreatic β-cells leading to broad insulin resistance. Moreover, lipid spill over from adipose tissue during periods of caloric excess leads to lipid accumulation in non-adipose tissues, resulting in cellular dysfunction known as lipotoxicity. Type 2 diabetes (T2D), nonalcoholic fatty liver disease (NAFLD), cardiac dysfunction and muscle insulin resistance are major lipotoxic diseases associated with lipid overload. Studying the cellular processes and genetic components involved in the progression of these disorders is necessary for the development of new treatment strategies.

Part I: Neutral lipid synthesis

Lipid imbalance is a characteristic feature of lipotoxic disease. An accumulation of intracellular lipids in non-adipose tissue induces a lipid challenge, in which the cells are forced to store, or catabolize the excess free fatty acids (FFA). Inability to properly process the incoming lipids by storage or oxidation results in lipid channeling into toxic pathways, such as ceramide biosynthesis and reactive oxygen species (ROS) production. Furthermore, the lipid deposition is often associated with lipid induced cell death known as lipoapoptosis [6]. The first line of defense against excess intracellular lipids is the synthesis and storage of the neutral lipids, triglyceride (TG) and sterol ester (SE) [7].

Neutral lipid synthesis enzymes. Neutral lipids, such as triglycerides (TG) and sterol esters (SE), are a readily accessible storage form of fatty acids and sterols. Both molecules are formed through esterification reactions, in which free sterols are acylated to form sterol ester while triglycerides are synthesized through the acylation of diacylglycerol (Fig 1-1). These lipids have a hydrophobic structure and are insoluble in the cytosol and unable to integrate into membranes at high molar concentrations. Instead, TG and SE are mainly stored within a phospholipid monolayer, forming an organelle known as the lipid droplet (LD). The storage of lipids in the form of TG and SE allows a cell to survive periods of diminished nutrient availability and via their hydrolysis provides membrane building blocks, such as phospholipids and sterols, for cellular maintenance and energy. Neutral lipid synthesis machinery has been well conserved between the budding yeast, *Saccharomyces cerevisiae*, and humans (Table 1-1) and studies in yeast have provided extensive information regarding eukaryotic lipid metabolism.

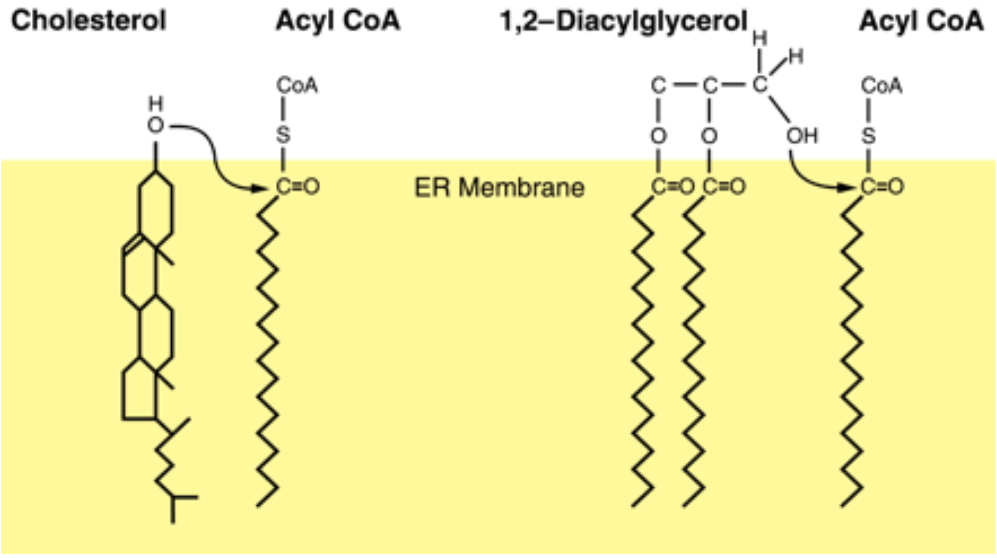

Figure 1-1: Neutral lipids are synthesized through acylation of sterol or diacylglycerol. Figure originally published in Buhman. et al, 2001 [8]. Esterification of diacylgerlycerol (DAG) and sterol occurs through the addition of a fatty acid molecule to a carboxyl group.

There are two primary pathways of TG synthesis, the Kennedy pathway (also known as the glycerol phosphate pathway) and the monoacylglycerol (MG) pathway. The MG pathway is found primarily in the small intestine, where it plays a major role in the synthesis of TG from dietary fat. Diet derived monoacylglycerol and fatty acids enter the enterocytes where they are converted into DAG by an acyl-CoA:monoacylglycerol acyltransferase (MGAT) (Fig 1-2). Humans have three MGAT family members (MGAT1-3) but this pathway of DAG synthesis does not occur in yeast [9].

As an alternate pathway, the Kennedy pathway, named after its founder, functions in all eukaryotic cell types, including yeast (Fig 1-2). The first step in this pathway is the acylation of glycerol-3-phosphate by an acyl-CoA:glycerol-*sn*-3-phosphate acyltransferase (GPAT). In yeast, there are two GPAT enzymes *GPT2* and *SCT1*. The product of this reaction, lysophosphatidate

(LPA), is further acylated by an acyl-CoA:1-acylglycerol-*sn*-3-phosphatase (AGPAT), in yeast known as *SLC1* and *LOA1*, to form phosphatidic acid (PA) [10]. PA is a central regulatory metabolite in the lipid biosynthesis pathway. PA can be converted into cytidine diphosphate (CDP)-diacylglycerol, a key phospholipid precursor, or can be dephosphorylated by a phosphatidic acid phosphohydrolase (PAP) to form DAG. There are three PAP enzymes in mammals, Lipin1-3, and one known yeast ortholog, the phosphoatidic acid hydrolase *PAH1* [11].

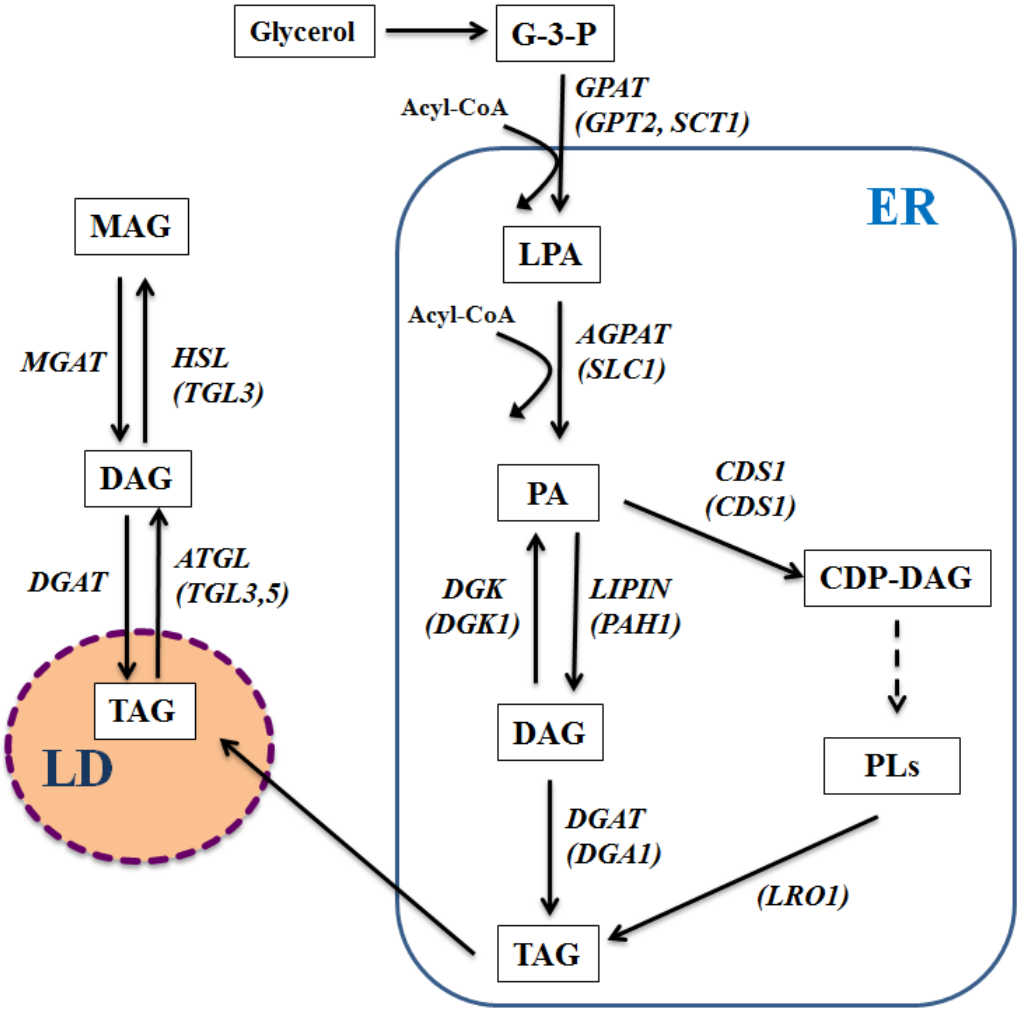

Figure 1-2: Triglyceride synthesis in mammals and yeast. Enzymes indicated for mammals and yeast (in parenthesis) for each synthesis reaction. Adapted from Rajakumari et al., 2008[12]

The final reaction in TG synthesis requires an acyltransferase enzyme, which catalyzes the acylation of diacylglycerol (DAG) (Fig 1-1). In mammals, there are at least two DAG acyltransferase enzymes, DGAT1 and DGAT2 (Fig. 1-2 and Fig 1-3). Both are found at the ER membrane, the site of LD biogenesis, and DGAT2 is also found on the surface of the lipid droplet [9]. Despite their similar function, these enzymes belong to two distinct gene families and do not share sequence homology (Table 1-1).

Human DGAT1 is a member of the membrane bound O-acyltransferase (MBOAT) family, which includes the sterol esterifying acyl-coA:cholesterol acyltransferase (ACAT) enzymes and several enzymes responsible for catalyzing the transfer of fatty acyl moieties onto lipid and protein acceptors [9]. DGAT2 belongs to a gene family known as DAGAT, which includes six other human genes, the three acyl-coA:monoacylglycerol acytransferase genes (MGAT1-3) and the wax monoester synthases (NCBI Conserved Domain Database). Both of these families have been conserved through evolution, with members existing in yeast and plants (Table 1-1) [13]. Though both function in TG synthesis, they differ in substrate specificity and activity. DGAT2 has no known acyltransferase activity outside of TG synthesis, whereas DGAT1 is able to function as a acyl-CoA:retinol acyltransferase (ARAT), catalyzing the synthesis of retinyl esters from retinol, and as both an MGAT and monoester wax synthase in vitro [9]. DGAT1's broad range of substrates is consistent with its known evolution. DGAT1 has two orthologs in yeast, Are1 and Are2, both of which function primarily as sterol esterifying enzymes, but also have a minor role in TG synthesis (< 5%) [14].

Gene Family	MBOAT	DAGAT	LCAT
Humans	ACAT1 ACAT2 DGAT1	DGAT2	LCAT
S. cerevisiae	*ARE1* *ARE2*	*DGA1*	*LRO1*
Lipid Product	SE/TG	TG	SE/TG

Table 1-1: Conservation of neutral lipid synthesis genes between budding yeast (S. cerevisiae) and humans. Neutral lipid synthesis genes from both humans and yeast grouped by gene family. Lipid products (Sterol ester (SE) or triglyceride (TG)) synthesized by the protein transcripts of these genes are also indicated.

In humans, DGAT1 is expressed ubiquitously, with the highest levels in the intestine, colon, testis and adrenal cortex and moderate levels in the heart, skeletal muscle and liver [15]. DGAT2 is also found in all tissue types with specifically high levels of expression in the liver and adipose tissue [16]. The relative role of each DGAT in whole body TG synthesis has been elucidated using gene knockout studies in the mouse model. DGAT2 $^{-/-}$ mice survive for only a few hours after birth, due to skin barrier abnormalities and have a severe (90%) drop in total body TG [17]. In contrast, DGAT1 null mice are viable and have normal plasma TG levels with a decrease in adiposity and resistance to diet induced obesity (DIO) [18]. These studies indicate that DGAT2 is able to partially compensate for a loss in DGAT1 but not vice versa.

In yeast, there are three distinct enzyme families that mediate TG synthesis. The major TG synthesizing enzyme is *LRO1*, an acyl-coA independent acyltransferase (Fig. 1-2 and Fig 1-2) that requires phospholipids (preferentially phosphatidylcholine and phosphatidylethanolamine) as an acyl donor. *LRO1* is both a phospholipase and an acyltransferase [19] and is responsible for the majority of TG synthesis during the log growth phase [13]. *LRO1* has sequence conservation (27%) to the mammalian cholesterol esterification enzyme lecithin-cholesterol acyltransferase (LCAT), an enzyme involved in the lipidation of HDL particles [20]. The sole

yeast ortholog of mammalian DGAT2, *DGA1* (33% identical), functions as an acyl-CoA:diacylgerlycerol acyltransferase, and mediates the majority of TG biosynthesis during stationary growth. The double mutant *dga1Δ lro1Δ* possesses low levels (approximately 5% of control) of triglyceride synthesis, which can be accounted for by residual TG synthesis activity by the sterol esterifying enzyme ARE2 [14].

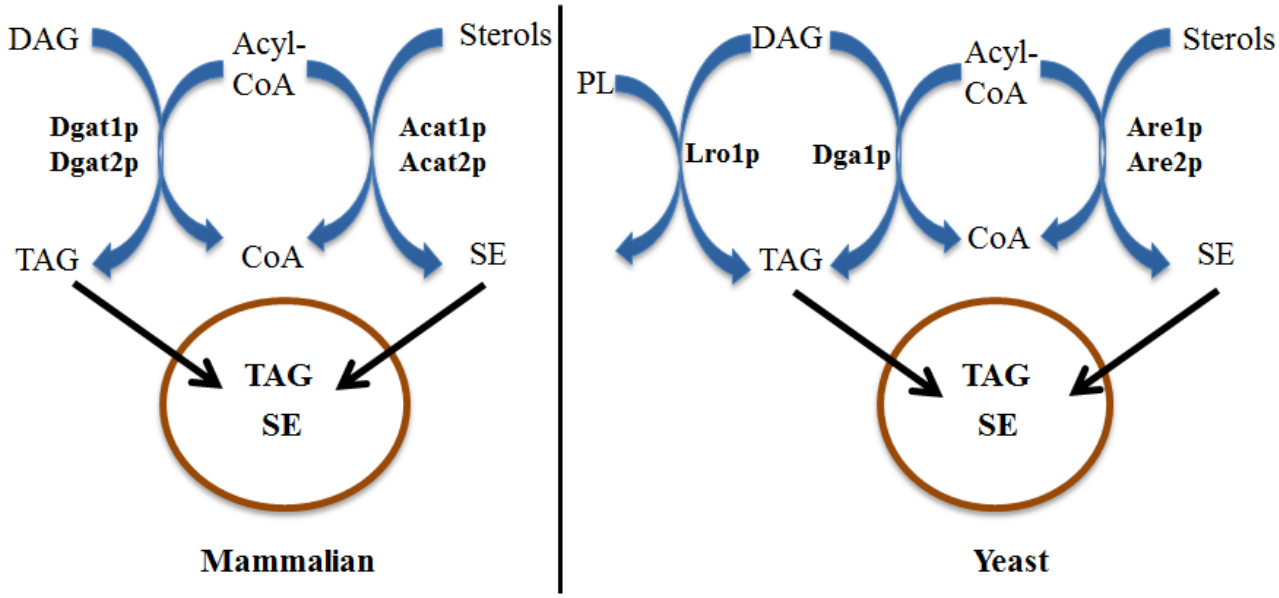

Figure 1-3: Mammalian and yeast neutral lipid synthesis. Neutral lipid synthesis requires action of acyl-coA:cholesterol acyltransferases (ACAT1/2) and acyl-coA:diacylglycerol acyltransferases (DGAT1/2) in mammals and ACAT related enzymes Are1/2 and the triglyceride synthesis enzymes Dga1p and Lro1p in yeast. Lro1p is an acyl-CoA independent acyltransferase.

Synthesis of sterol ester (SE) also requires an acyltransferase enzyme, which act on free sterols (Fig 1-1). This reaction is carried out by two related acyl-CoA:cholesterol acyltransferases, mammalian ACAT1 and ACAT2 (Fig. 1-1 and 1-3) and their yeast orthologs, the ACAT related enzymes 1 and 2 (Are1p and Are2p) (Fig. 1-3). A double deletion of *ARE1* and *ARE2* in yeast eliminates all sterol esterification, proving that these are the lone yeast sterol

esterifying enzymes [21]. Intracellular sterol levels are under tight regulation and increasing free sterol is rapidly esterified for storage in the LD. These esters can then be hydrolyzed, releasing free sterol for use in cellular membranes or steroid hormone synthesis [13].

Triglyceride storage protects against lipotoxicity. Compartmentalization of excess lipids as a storage form in LDs is able to protect the cell from lipotoxic effects. Ablation of TG synthesis in both yeast and mammalian models results in severe lipotoxicity following unsaturated fatty acid (UFA) exposure [7, 22, 23]. High fat diet fed DGAT1 $^{-/-}$ mice have increased toxic metabolites, DAG and fatty acyl-CoA, in nonadipose tissues consistent with the role of neutral lipid synthesis in lipotoxic disease prevention [24]. Interestingly, these mice remain insulin sensitive despite the rise in fatty acid metabolites. Diverting lipids into TG storage is protective, as seen in mice overexpressing DGAT1 or DGAT2 in the liver. These transgenic models develop fatty liver, but do not have hepatic insulin resistance, demonstrating that the synthesis and storage of TG shields against lipid induced cellular dysfunction *in vivo* [25].

Part II: Eukaryotic Lipid Droplets

In addition to a cells ability to synthesize neutral lipids, the biogenesis and homeostasis of the lipid droplet (LD) for neutral lipid storage is fundamental in adapting to intracellular lipid accumulation. Discovered in the 1890s by Richard Altmann and E.B. Wilson [26, 27] , lipid droplets were largely ignored and considered as inert lipid depots for almost a century. With increases in the prevalence of obesity related disease and advances in techniques in molecular biology, the LD is now considered a dynamic organelle integrally involved in the protection of cells against cellular lipid overload.

The lipid droplet is composed of a phospholipid monolayer surrounding a neutral lipid core, made up of TG and sterol esters SE [28-31]. Lipid droplets are found in all eukaryotic cells and range greatly in size from less than 1 μm to 100 μm [32]. In humans, lipid droplets are prominently found in adipocytes where they provide long term energy storage and take up approximately 1/3 of the intracellular space [33]. The ratio of SE to TG stored in the LD differs greatly between cell types. For example, LDs in adipose tissue are composed primarily of TG, whereas the steriodogenic cell types found in the adrenal gland, testis and ovary have LDs enriched in SE. In addition to neutral lipids, LDs in the specialized hepatic steallate cells contain retinyl esters and act as the primary storage form for vitamin A. Nearly equal amounts of TG and SE are found in LDs of the model organism *S. cerevisiae* (budding yeast).

Beyond their role in lipid storage, LDs have been suggested to function as a temporary scaffold for proteins destined for degradation, as seen with the accumulation of α-synuclein on the LD surface in Parkinson's disease [34]. This accumulation may serve to protect the cell from harmful cytosolic protein aggregation. Additionally, recent work has uncovered a role for lipid droplets in the infectivity rate of viruses, such as the hepatitis C virus (HCV). HCV hijacks the LD biogenesis machinery in order to assemble and replicate virus particles [35]. As an integral element for so many metabolic and infectious diseases, investigation into the basic biology of the LD provides valuable knowledge into the cellular mechanisms involved in these disorders.

Lipid droplet associated proteins. The lipid droplet is decorated with an array of proteins, and several proteomic screens in both yeast and mammalian systems have compiled a comprehensive list of lipid droplet associated proteins [36-43] in order to shed light on the function of these surface proteins in lipid droplet biogenesis and metabolism. In mammalian systems, the PAT

protein family, made up of perilipin, adipophilin, TIP47, S3-12 and OXPAT, are important in the maintenance of LD structure. These proteins are able to regulate lipolysis and bind to the droplet via a four-helix bundle resembling that of Apolipoprotein E [44]. Similarly, plant oil droplets are surrounded by oleosin proteins, which cover the droplet and prevent coalescence [45]. Yeast lack orthologs to PAT and oleosin proteins, but do have several known lipid metabolism proteins localized to the LD surface, which regulate TG lipolysis and NL synthesis [46]. These proteins include TG synthesis enzyme DGA1 [47], SE biosynthesis enzymes ERG1, ERG6 and ERG7 [36], TG lipases TGL1,3-5 [46] and the FA synthetase enzymes FAA1, FAA3 and FAA4 [36]. Similarly, mammalian DGAT2 [48] and the TG lipase enzyme, adipose triglyceride lipase (ATGL) [49], are found on the LD surface and regulate droplet lipid levels.

Furthermore, proteins involved in membrane-trafficking (RAB18 [50], ARF1 [51]) and fusion SNARE proteins (SNAP23 [52] and yeast USE1 [46]) have also been identified at the droplet surface and are proposed to be involved intracellular trafficking and fusion of LD. Another well-studied LD protein family known as the CIDE (cell death-inducing DFF45-like effector) family, includes three proteins, CIDEA, CIDEB and FSP27/CIDEC, which all reside on the droplet and all have integral roles in lipid droplet formation and energy homeostasis. Mice deficient in each CIDE protein have a severe deficiency in white adipose LD formation and increased metabolic rate [53].

Lipid droplet biogenesis. LDs form rapidly within discrete regions of the ER in response to increased intracellular FAs, but the exact mechanism for LD biogenesis remains elusive. Several observations support a model for lipid droplet formation at the ER membrane. The phospholipid monolayer of the lipid droplet is similar to that of the ER, with high levels of

phosphatidylcholine (PC) and lower levels of phosphatidylethanolamine (PE) and phosphatidylinositol (PI) [54]. Additionally, many ER-associated proteins are also found at the surface of the lipid droplet, such as DGAT2 [48], and LDs are frequently found associated with the ER membrane [55]. The most supported hypothesis for lipid droplet biogenesis is that neutral lipids are synthesized within the ER bilayer at specialized sites and as the level of lipid increases beyond membrane capacity (2-4 mol %) the membrane leaflets begin to separate. The lipid lens grows toward the cytosol at which point it reaches a critical mass and is able to separate from the ER into an independent organelle (Fig. 1-4 A). Though the intermediate steps of this model have not been demonstrated experimentally, the phospholipid and protein composition of the LD in addition to the localization of NL synthesis genes at the ER are consistent with this explanation.

There are two additional models, which have been proposed in LD biogenesis. The "vesicular budding" model suggests that a membrane vesicle tethers to the ER and is filled with newly synthesized neutral lipids (Fig. 1-4 C) [30]. Corroborating this model, it has been found that knockdown of integral vesicular trafficking proteins alters LD formation [56, 57]. Alternatively, the "bicelle" model posits that once neutral lipids are synthesized between the ER bilayer, the entire lipid lens is excised from the ER. This leaves a transient hole in the ER membrane, which allows proteins typically sequestered in the ER lumen to leak into the cytosol (Fig. 1-4 B). Although this model garners some support from studies that show that reassembled viruses escape from the ER lumen into the cytoplasm, the transient pores produced within the ER may cause significant instability of the organelle and may not be biological feasible [30].

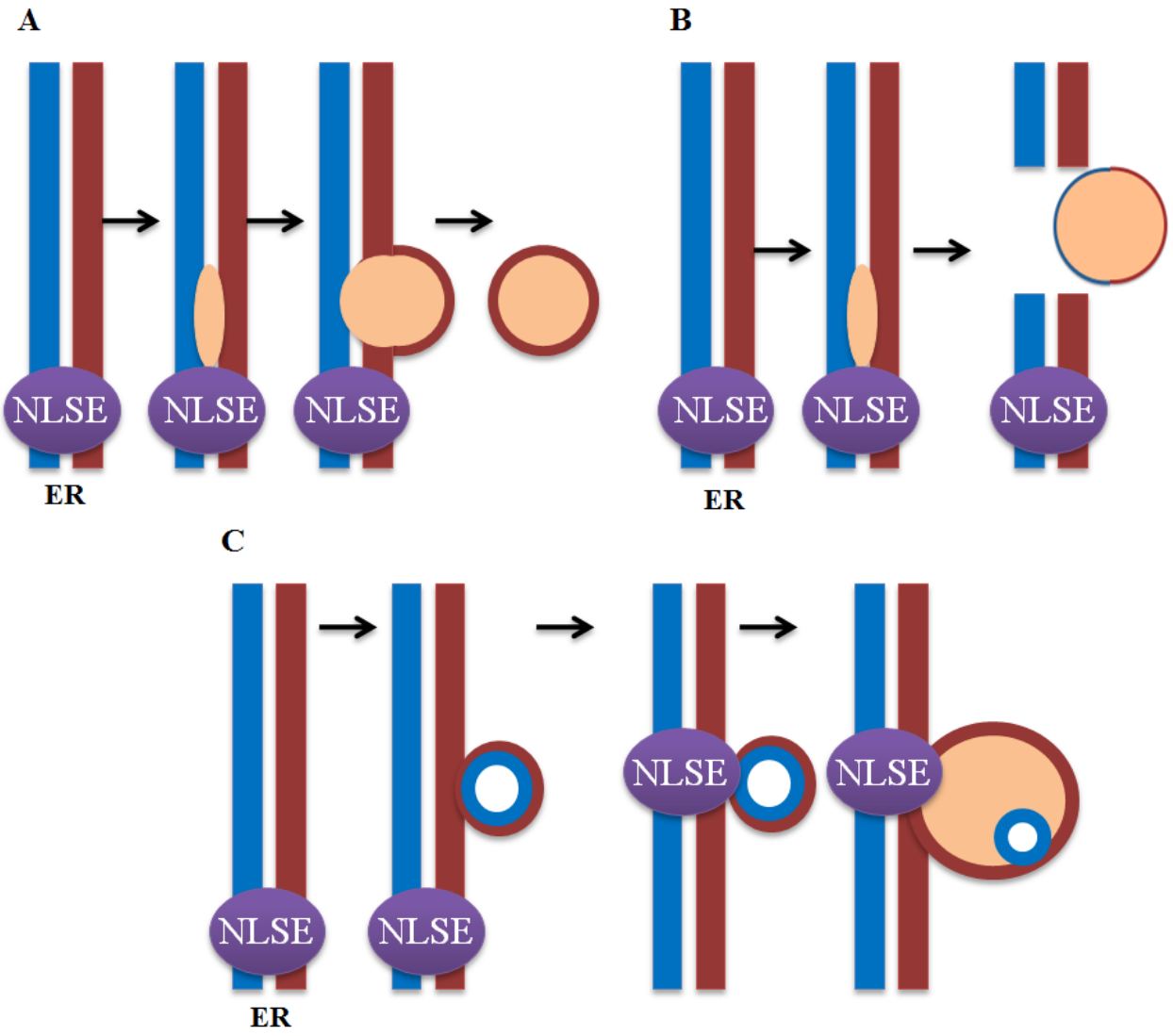

Figure 1-4: Three models of lipid droplet biogeneisis. Adapted from Walther T.C., and R.V. Farese, 2009 [30]. Synthesis of the NL triglyceride and sterol ester occurs at the ER membrane by neutral lipid synthesis enzymes (NLSE). The 3 models of LD formation are as follows: (A) NL build-up within the bilayer forms a lens which buds off as a mature droplet after reaching a critical size. (B) A second model is similar in that the NL forms a lens within the ER leaflets, but is excised from the ER as a "bicelle". The last model (C) involves a bilayer vesicle which binds to the ER and is filled by NLSE. This lipid filling results in a PL monolayer in the majority of the droplet with a small bilayer remaining.

Genome-wide knockout and knockdown screens have been used in the yeast *S. cerevisiae* and *Drosophila* S2 cells respectively, in order to identify genes necessary for lipid droplet biogenesis [56-59]. This work has identified very few genes having a major effect on LD formation, with many more gene knockouts or knockdowns causing a less pronounced, but still significantly altered LD morphology. Two *Drosophila* RNAi screens identified the Arf1-COPI vesicular transport proteins [56, 57] as important regulators in the number and size of droplets. In addition, Guo *et al.*, found that phospholipid biosynthesis proteins *Cct1* and *Cct2* play an important role in providing newly synthesized phospholipids to lipid droplet monolayers during growth [56]. The CCT (CTP:phosphocholine cytidylyltransferase) enzymes are reversibly targeted to the lipid droplet membrane, where they complete the rate limiting step of phosphatidylcholine synthesis and allow for membrane expansion . Knockdown of the genes encoding these proteins results in decreased lipid droplet size due to defects in membrane growth [56].

A yeast genome-wide lipid droplet morphology screen identified a seipin ortholog *FLD1*, which has increased levels of LD fusion after gene knockout [60]. The increased fusion in *fld1Δ* is due to a defect in lipolysis and impaired lipid droplet dynamics and Fld1p is thought to function as a lipid droplet scaffolding protein, moderating ER-lipid droplet interactions [61]. Perhaps more notable than these individual proteins is the broad array of cellular pathways identified in these screens studies. The diverse cellular pathways involved in lipid droplet morphology highlights the complexity of LD formation and homeostasis.

PART III: Neutral lipid catabolism

Intracellular TG levels are dependent on the balance between TG synthesis and catabolism. Under normal conditions, metabolites formed from the breakdown of TG are utilized in signal transduction pathways, membrane biosynthesis and ATP production through β-oxidation. The mobilization of TG is particularly important during nutrient deprivation and is carried out by TG lipases, which cleave a fatty acid from glycerolipids [62]. Because the products of catabolism (DAG, FFA, PA) are also toxic to cells at excess levels, lipase activity may play an important role in the regulation of lipotoxic response. Overexpression of the triglyceride lipase, hormone sensitivity lipase (HSL), in mouse pancreatic β-cells results in increased β-cell lipotoxicity and glucose intolerance [63]. Likewise, genome-wide association studies have identified a link between HSL gene polymorphisms and insulin resistance [64-67].

Furthermore, maintaining tight control of adipocyte lipolysis is critical for whole body metabolism, and small changes in adipose lipolysis levels can have significant effects on circulating FFA [68] . Insulin resistance of adipose tissue results in a deregulation of the lipolysis levels, increasing free fatty acids spill over into non-adipose tissues [6]. Therefore, mobilization of the triglyceride pool is an important factor in cellular lipid homeostasis and the progression of lipotoxic disease.

Triglyceride lipolysis. Mechanisms of mammalian intracellular lipolysis have been studied extensively in the adipose and liver. Degradation of TG is carried out by TG lipases, such as hormone sensitive lipase (HSL) and adipose triglyceride lipase (ATGL). These enzymes have

significant differences in tissue localization and substrate preference but are able to partially compensate for each other in adipose tissue, but not in other tissue types [69].

ATGL is found in most tissues, with the highest expression in brown and white adipose tissue. A deletion in *ATGL* induces a moderate obese phenotype in both mice [70] and *Drosophila* [71], due to defective TG mobilization from adipocyte LD. Likewise, adipose specific overexpression of ATGL results in a lean phenotype through increased TG hydrolysis activity [72]. With high TG specificity, ATGL initiates lipolysis by removal of the first FA from TG, followed by HSL hydrolysis of DAG [73]. The protein CGI-58 (Comparative gene identification -58) is needed for full activation of ATGL, and interaction between these proteins increases TG hydrolysis activity by approximately 20 fold [74].

HSL is critical for complete TG lipolysis, due to its ability to hydrolyze several different substrates, including TG, DAG and MAG [75]. HSL is found primarily in adipose tissue but is also found at low levels in skeletal muscle, pancreas and macrophages [76]. Phosphorylation of HSL by PKA promotes its translocation to the surface of the LD and enhances the lipolysis capacity [77]. HSL knockout mice have a 60% reduction in triglyceride lipase activities, and a 2 fold increase in white adipose tissue size, but are not obese [78]. Additionally, HSL null mice have increased DAG accumulation, in adipose tissue, muscles and testis due to the integral role for HSL in DAG hydrolysis and have impaired insulin sensitivity [75].

In yeast, TG degradation occurs by the three proteins, triglyceride lipase 3, 4 and 5 (TGL3, TGL4 (the ATGL ortholog) and TGL5) all of which are members of the patatin-domain containing family of esterases [79, 80]. These proteins are found at the phospholipid surface of the LD and all have similar structure, with a conserved sequence motif GXSXG and catalytic domains consisting of parallel β-sheet structures connected by helical loops. Knockout of *TGL3*

or *TGL4* results in a significant TAG accumulation and altered cell cycle progression due to defects in membrane precursor availability [81]. A *TGL5* deletion does not cause changes in TG hydrolysis but exhibits increased levels of very long chain fatty acids in TG [82]. All *TGL* mutants have decreased levels of sphingolipid biosynthesis and increased turnover of sphingolipids, suggesting that aberrations in lipolysis affect sphingolipid metabolism [83].

Sterol ester hydrolysis. Lipid droplet homeostasis also depends on the rate of sterol ester mobilization, a reaction which is carried out by sterol ester hydrolases to yield a fatty acid and a free sterol. Three SE hydrolases, TGL1, YEH1 and YEH2 have been identified in yeast, two of which localize to the LD (TGL1 and YEH1) and one to the plasma membrane (YEH2) [12]. In mammals, sterol esters are hydrolyzed by the neutral cholesterol ester hydrolase (nCEH) and enzymatic activity of this enzyme is protective against foam cell formation and atherosclerosis [84].

Lipophagy. Recent work has shown that autophagy plays an important role in lipid droplet metabolism and in a myriad of metabolic diseases including obesity, insulin resistance and T2D [85-87]. Autophagy, or "self-eating" is a lysosomal pathway used by a cell during periods of nutrient deprivation to recycle intracellular organelles and proteins. There are three classes of autophagic response, macroautophagy (for "bulk flow"), microautophagy (for cytosolic recycling) and chaperone mediated autophagy. In classical macroautophagy, autophagosomes sequester cytosolic organelles and proteins, and fuse with lysosomes to form an autophagolysosome. The low pH and enzymes within the autophagolysosome degrade the internalized content and release recovered nutrients into the cytosol. Originally thought to be a

nonspecific process, macroautophagy has been shown to have specific targeting capabilities for the mitochondria (mitophagy)[88], ER (reticulophagy) [89] and peroxisomes (pexophagy) [90].

Macroautophagy can also specifically target lipid droplets for degradation, a process known as lipophagy. During lipophagy, LDs are sequestered in autophagosomes which then fuse with lysosomes. The components of the LD are broken down by lysosomal lipases, freeing up FFAs for β-oxidation. This process was first described in hepatocytes, where inhibition of autophagy caused decreased rates of lipolysis resulting in increased NL levels and increased LDs [91]. Additionally, autophagy functions in the differentiation of cultured preadipocytes into mature adipocytes, with a block in autophagy resulting in decreased differentiation gene induction and reduced TG levels. Blockage of autophagy in adipose tissues through ablation of the autophagy gene, ATG7, results in decreased white adipose tissue mass, decreased TG content and resistance to high fat diet induced insulin resistance [87]. The conflicting results in autophagy inhibition and TG levels in hepatocytes and adipocytes indicates that additional research regarding the connection between TG metabolism and autophagic flux is necessary.

Fatty acid oxidation. Once TG breakdown has occurred, the major degradative pathway for FA is through β-oxidation [92]. Acyl-CoA molecules can enter into the mitochondria or peroxisomes where they are used for energy production through β-oxidation. In mammalian cells, fatty acids are activated by acyl-coA synthetase to form an acetyl-CoA and transported across the mitochondrial membrane by carnitine-acyltransferase. The acyl-CoA is degraded by four fatty acid oxidation reactions, generating large quantities of ATP. Fatty acid oxidation also occurs in peroxisomes, which generate H_2O_2 through the FA breakdown. The peroxide produced can then be further broken down into water, and is particularly important in the kidney and liver

for detoxification. In yeast all β-oxidation occurs in the peroxisome, which uses β-oxidation to produce NADH and NADPH for the generation of energy [92].

Part IV: Free fatty acid synthesis and uptake.

In addition to triglyceride synthesis and catabolism, fatty acid uptake from the environment and *de novo* fatty acid synthesis play significant roles in the maintenance of intracellular lipid levels. The balance of lipids can be described as an equation, with de novo lipogenesis and FA uptake increasing intracellular lipids and FA catabolism and utilization as degrading these lipids in the form of energy or membrane building blocks. Under conditions of increased circulating free fatty acids (FFA), intracellular FA uptake and accumulation occurs, requiring an increase in FA oxidation to maintain the lipid balance [93]. A similar increase in oxidation is needed to compensate for elevations in *de novo* FA synthesis. Without oxidative compensation, lipid accumulation occurs, initially as increased neutral lipid storage and eventually resulting in lipid induced cellular defects including ER stress, altered mitochondrial membrane integrity and apoptotic initiation.

De novo lipogenesis. Fatty acid biogenesis through *de novo* lipogenesis requires acetyl-CoA which can be derived from multiple metabolic pathways, including glycolysis and pyruvate oxidation. In mammals and yeast, two acetyl-CoA carboxylase (ACC) genes, cytosolic ACC1 (yeast *ACC1*) and mitochondrial ACC2 (yeast *HFA1*) catalyze the initial step of FA synthesis through acetyl-CoA carboxylation forming the metabolic intermediate malonyl-CoA. This process, which occurs through several catalytic steps, requires the action of one gene in mammals, FASN, and two genes in yeast, FAS1 and FAS2. Following malonyl-CoA formation,

fatty acid synthesis (FAS) enzymes catalyze the final steps of FA biosynthesis. These fatty acids can then be elongated, by long chain elongases (mammalian ELOVL proteins and yeast ELO1, FEN1 and ELO3) and desaturated (mammalian stearoyl-CoA desaturase 1 (SCD1) and yeast OLE1) to meet cellular lipid requirements [94].

Free fatty acid uptake. The alternate mode of intracellular fatty acid increase is through long chain fatty acids (LCFA) uptake. LCFAs are essentially insoluble in aqueous solutions, but when bound to proteins, such as albumin, can exist in an aqueous environment at much higher concentrations. The two main mechanisms for fatty acid transport into cells are passive diffusion and protein-mediated transport. Transfer of the lipid from the outer to the inner leaflet of the membrane has been shown to occur through a fatty acid 'flip-flop' [95]. Though this passive diffusion model of FA uptake is likely to occur to some degree, recent literature supports that the majority of FA uptake occurs through a protein mediated mechanism.

Protein mediated lipid uptake takes place in one of two ways, through membrane bound fatty acid transporters or receptor mediated uptake of lipoprotein particles. Fatty acid transporters function to sequester FA at the membrane for subsequent transport. The major membrane bound fatty acid transporters in mammals are CD36, plasma membrane associated fatty acid-binding protein (FABPpm), the fatty acid transport protein family (FATP1-6) and caveolin [96].

The mechanisms of fatty acid uptake in yeast are still unclear. Like that described in mammals, one model is through a "flip-flop" entry, independent to protein transporters. In addition, membrane bound proteins Faa1p, Faa4p and Fat1p have been implicated in fatty acid uptake. Protein mediated uptake in yeast likely occurs through "vectorial acylation", in which

proteins activate FAs through addition of an acyl-CoA, which traps the FA within the cell [97-99]

Receptor mediated lipid uptake occurs through protein endocytosis of lipoprotein particles into cells, a process used by many mammalian cell types but not by yeast. Lipoproteins are lipid-enriched particles made up of a neutral lipid core surrounded by a phospholipid monolayer, with a structure analogous to that of the LD. Lipoproteins are classified into four main groups based on their characteristic density, chylomicrons having the lowest density, very low-density lipoproteins (VLDL), low-density lipoproteins (LDL), and high-density lipoproteins (HDL). A distinguishing surface protein known as an apolipoprotein (apo) marks each lipoprotein class and acts in particle recognition [100].

After a meal, the enterocytes of the small intestine absorb cholesterol and TG and incorporates these lipids into a chylomicron with a single apo B48 protein. Chylomicrons are then secreted into the lymphatic and circulatory system where TG in the particle core is hydrolyzed by lipoprotein lipase (LPL) on the surface of the capillary endothelium. The product of this hydrolysis, FFA, enters the adipose or muscle cells through the flip-flop or protein mediated transport mechanisms. Chylomicron remnants are then taken up by the liver through receptor-mediated uptake through interaction with a cell surface protein known as the LDL receptor [100].

The liver is able to package and secrete TG and SE into a VLDL particle through lipidation of apo B100 in the ER of the hepatocytes. Like chylomicrons, lipolysis of VLDL triglyceride occurs through LPL-dependent hydrolysis, and this lipolysis results in increasingly dense particles and an eventual conversion to LDL. Interaction between LDL and the LDL receptor forms clathrin-coated vesicles and internalization of the particle into the cell. Once

internalized, the vesicle fuses with the late endosome and lysosome, releasing sterols and FAs for cellular use [100]. The rise in circulating free fatty acids associated with obesity results in increased FFA flux through these protein mediated lipid uptake mechanisms and lipid accumulation due to increased uptake is a major determinant of lipotoxic disease progression.

Part V: Mammalian Lipotoxicity

As previously discussed, lipotoxicity is defined as a cellular dysfunction triggered by the accumulation of fat in nonadipose tissue. This term was first coined by Dr. Roger Unger in 1994 when he described the role of FFA in the pathogenesis of type 2 diabetes in obese Zucker rats [101]. The most extreme example of lipotoxic disease occurs in complete lipodystrophy, where patients lack adipose tissue and lipids accumulate in ectopic tissues such as liver, muscle and pancreas [102]. Lipodystrophies can be either genetic or acquired, and are characterized by a loss or mislocalization of body fat and severe insulin resistance. A similar increase in ectopic lipids has been shown to occur in obesity and has been observed in obese rodent models such as the high fat fed mouse [103] and Zucker rat [101].

The lipotoxicity seen in lipodystrophy highlights the importance of adipocytes in protecting nonadipose tissue against insults of excess lipid exposure. Adipocytes have evolved as a storage depot for fuel during extended periods of famine, in which excess calories are stored in the adipocyte LD and mobilized for use by other organs when nutrients are scarce. Conversely, during periods of caloric excess, adipocytes buffer against increases in nutrient load through nutrient sequestration in the form of neutral lipids [104]. In addition to fat storage, adipocytes are important endocrine organs, secreting the energy regulatory hormones adiponectin and leptin.

Normally, adipose is very insulin sensitive and small increases in insulin results in robust inhibition of lipolysis [105].

In many cases of obesity the adipocyte becomes dysfunctional and undergoes hypertrophy, experiences macrophage infiltration, and becomes insulin resistant. This dysfunction likely result from an increase in ER stress and a failure in adequate cell proliferation, leading to both increased inflammatory adipokine and free fatty acid (FFA) release into circulation [106, 107]. High circulating FFAs promote fat deposition into peripheral tissues such as pancreatic β cells, hepatocytes and muscle. In an effort to attenuate lipotoxicity, these tissues increase lipid stores in the form of lipid droplets.. Although the LDs themselves are protective, an increase in lipid droplet number is indicative of an associated FA load. With chronic exposure, nonesterified fatty acids (NEFA) are able to enter into toxic pathways, eventually causing cellular injury [108].

Mammalian Mechanisms of Lipotoxicity: The primary form of circulating FAs are long chain FAs (LCFA) containing 16 carbons or more, which can be classified as saturated, monounsaturated and polyunsaturated based on the number of double bonds. The most abundant circulating fatty acids are the unsaturated fatty acids (UFAs) oleate (C18:1) and palmitoleate (C16:1) and the saturated fatty acids (SFAs) palmitate (C16:0) and stearate (C18:0). In most mammalian tissue types UFA exposure increases TG synthesis and storage while SFAs enter into more toxic pathways, eventually resulting in lipotoxicity and lipid induced apoptosis (lipoapoptosis) [109-113]. Though typically less potent compared to SFA, UFAs have been shown to cause lipoapoptosis through alternate cellular pathways in certain cell types [114-124].

Evidence indicates that SFA induced lipotoxicity occurs through increased *de novo* synthesis of ceramides [111] and reactive oxygen species (ROS) production [125]. Ceramide is

a lipid molecule consisting of a sphingosine and a FA moity (typically palmitoly-CoA). With increases in cellular palmitate, ceramide levels rise through the activity of the rate limiting enzyme serine palmitoyltransferase (SPT1). Ceramides, like many sphingolipids, are signaling molecules involved in an array of cellular processes including cell proliferation and apoptosis [126]. Ceramide induces apoptosis through the formation of channels within the mitochondrial membrane, allowing for the release of mitochondrial apoptotic mediators, such as cytochrome c, and increased mitochondrial permeabilization [127]

Ceramide independent pathways of SFA mediated lipotoxicity also occur, as seen with increased ROS [110, 111]. A rise in FAs increases ROS production via FA flux through β-oxidation. Newly formed ROS can react with mitochondrial DNA, proteins and lipids inducing oxidative damage and mitochondrial dysfunction. These effects result in a compromised mitochondrial membrane and release of pro-apoptotic factors resulting in a caspase dependent cell death cascade [125].

UFA has been shown to induce lipoapoptosis in various cell types, including HUVEC cells [116], the liver cell lines HepG2 [119] and McA-RH7777 [124] and primary rat β-cells [123]. Unlike SFA, this process involves the phosphorylation/dephosphorylation cycle of protein phosphatase type 2C and endoplasmic reticulum (ER) stress response. Interestingly, genetic ablation of DGAT1 activity in CHO cells causes SFA and UFA to become equally toxic [7].

ER stress response has proven to be important in both SFA and UFA induced lipotoxic dysfunction. Classical ER stress occurs through an accumulation of misfolded proteins in the ER lumen and activation of PKR-like kinase (PERK), inositol-requirement enzyme 1 (IRE1) and activating transcription factor 6 (ATF6) (Fig 1-5). The activation of these proteins occurs

through the dissociation of the ER chaperone immunoglobin heavy chain binding protein (BiP also known as GRP78) and leads to downstream signaling known as the unfolded protein response (UPR). The UPR is an adaptive mechanism for restoration of ER function through decreasing cellular protein load and increasing the ER folding capacity. If activation of these pathways is unable to restore ER homeostasis, pro-apoptotic pathways are initiated. Activation of the pro-apoptotic factors, CHOP, JNK and caspase 12 as well as inhibition of the anti-apoptotic Bcl-2 following prolonged ER stress lead to cell death [128].

In addition to misfolded proteins, both saturated and unsaturated FFAs are able to trigger ER stress [129-131] in part through decreased ER Ca^{2+} stores causing a secondary protein-folding defect. Additionally, palmitate is incorporated into lipid components in the ER where it disrupts the ER structure leading to a protein independent ER stress response [132].

Studies in rodent models have concluded that increased lipid exposure typical of obesity causes increased ER stress response marker expression in β-cells, adipocytes and hepatocytes [133]. Pancreatic beta cells are particularly susceptible to ER stress due to their primary function in protein secretion and increased ER protein load [112]. Therapies that increase cellular resistance to ER stress could attenuate the lipotoxic cellular dysfunction in these tissues. Chaperone administration and attenuation of downstream UPR targets have been shown to increase ER protein folding capacity and correct for systemic insulin resistance, hepatic lipid accumulation and pancreatic β-cell lipotoxicity [128].

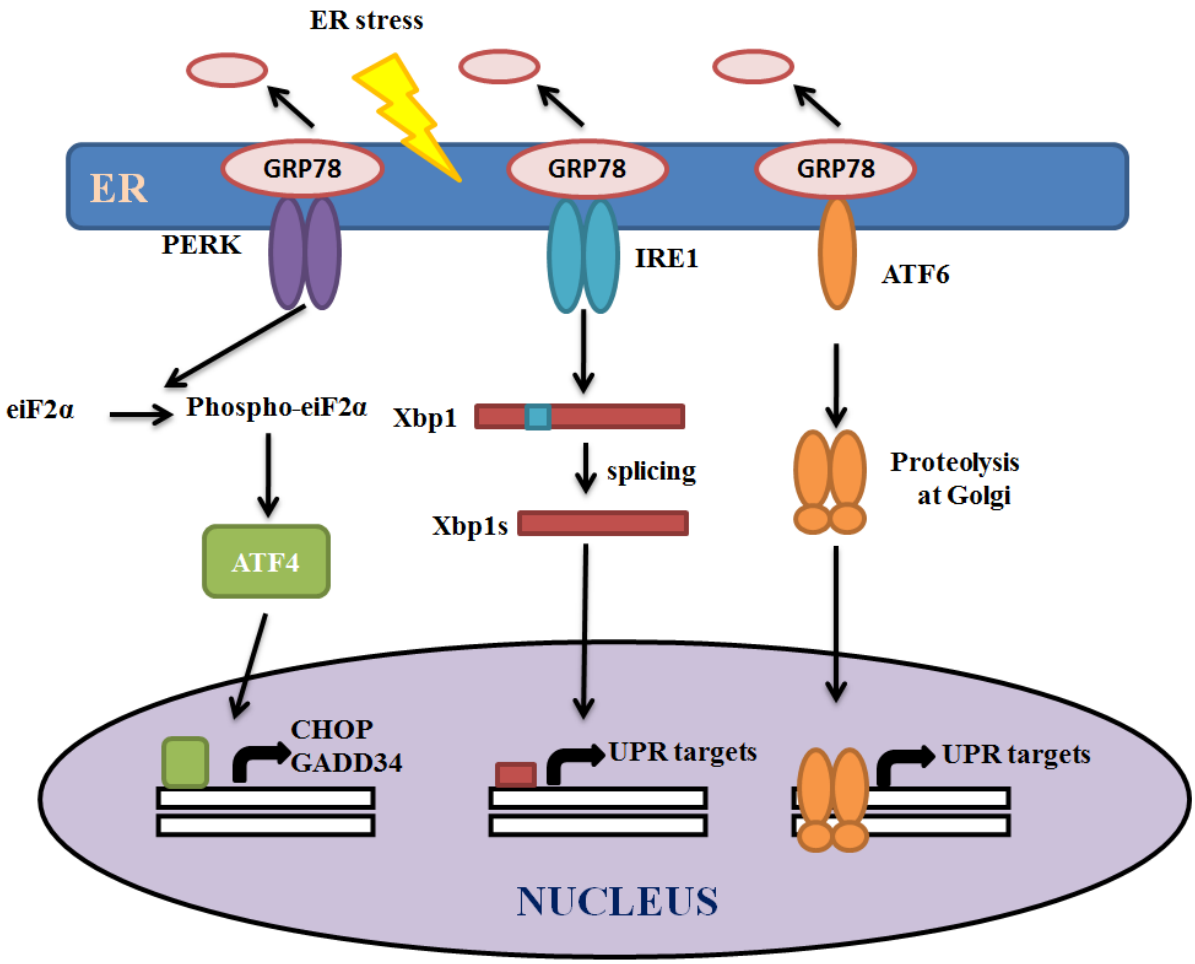

Figure 1-5: Mammalian ER stress response pathways. There are 3 branches of mammalian ER stress response. Activation of these pathways occurs through the release of GRP78 from its binding partners (PERK, IRE1 and ATF6) in the ER. This initiates PERK dimerization and trans-auto-phosphorylation. PERK then phosphorylates the α-subunit of elongation initiation factor 2 (eIF2) which results in decreased protein translation and the activation of proapoptotic CHOP. Similarly, upon activation, IRE1 oligomerizes and trans-auto-phosphorylates initiating splicing of the XBP1 transcript which can then translocate in the nucleus and bind to UPR response elements. Lastly, movement of ATF6 from the ER to the Golgi occurs following GRP78 release. At the Golgi, ATF6 undergos proteolysis, allowing it to translocate to the nucleus and activation UPR target genes.

Type 2 Diabetes and pancreatic β cell failure. Type 2 Diabetes (T2D) is a disease characterized by defects in insulin action and insulin secretion. Though obesity and overnutrition have been continually associated with T2D progression, research has highlighted the importance of genetic

makeup in determining pancreatic β-cell adaptation to glucose and FA excess. Those with both increased circulating FFA and a pancreatic β-cell susceptibility are the most prone to T2D. Genome-wide association studies (GWAS) have identified several gene variants responsible for this apparent susceptibility, including polymorphisms in the insulin receptor substrate IRS1 [134], the β-cell potassium subunit KCNJ11[135] and the gene encoding transcription factor-7 like 2 (TCF7L2) [136].

Under normal physiological conditions, the β-cell responds to increases in circulating glucose with insulin release. The circulating insulin then acts on liver, muscle and adipose to regulate carbohydrate and fat metabolism. There are two phases to insulin release; the first is triggered in response to increased blood glucose levels stimulating the release of previously synthesized, docked, insulin containing secretory vesicles (Fig 1-6). Glucose enters the β-cell through the GLUT2 transporter, initiating the first phase of insulin secretion. The rise in intracellular glucose causes increased glycolysis and mitochondrial respiration resulting in an increased ATP/ADP ratio in the cytosol. K_{ATP} channels close in response to the rise in ATP, triggering membrane depolarization and Ca^{2+} influx through voltage gated calcium channels. The Ca^{2+} signal then stimulates the release of insulin containing granules through exocytosis [137]. The second response step requires mobilization and priming of newly synthesized population of insulin granules to the plasma membrane for docking and fusion. Approximately 1% of the total number of granules present release insulin in the first phase whereas the second phase occurs at a rate of 5-40 granules per second over a period of hours [138].

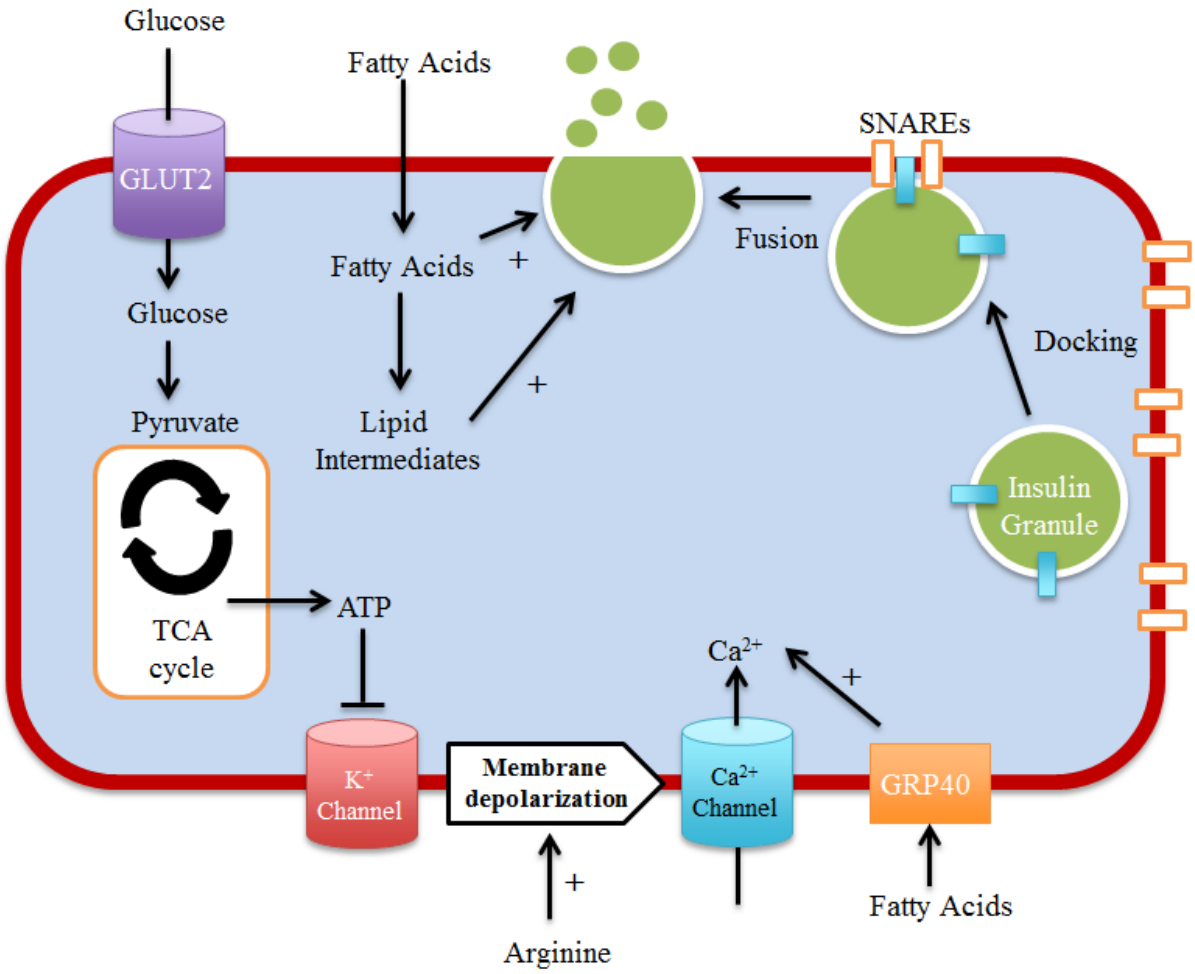

Figure 1-6: Mechanisms of glucose and fatty acid stimulated insulin secretion in pancreatic β-cells. Role of glucose in insulin secretion stimulation and potentiation of the response with fatty acid or amino acid treatment.

In addition to glucose, several other molecules are able to stimulate insulin release. These include hormones and neurotransmitters, which bind to β-cell membrane receptors and activate a neurohormonal activation pathway. Fatty acids also serve as insulin secretagoges (Fig 1-6) through glucose stimulated insulin stimulation (GSIS) potentiation by activation and binding to the fatty acid binding receptor GRP40. Binding of FA to this receptor activates the $G_{\alpha q}$-phospholipase C (PLC) pathway, triggering the release of luminal ER Ca^{2+} stores and subsequent increases in cytosolic Ca^{2+} levels [139]. Accumulation of LCFAs and lipid

intermediates, such as DAG, have also been shown to alter acylation of insulin regulatory proteins and enhance insulin vesicle fusion. Due to these effects, acute FA treatment improves insulin release with glucose stimulation, however chronic FFA exposure causes a reduction in GSIS, due to lipotoxic dysfunction.

Defects in insulin secretion and β-cell function may occur prior to the development of impaired glucose tolerance. In the pancreas of T2D patients, β-cell volume is decreased by approximately 30% and frequently shows markers of apoptosis based on autopsy results [140, 141]. Though significant, this loss in mass does explain the insulin response defect seen in T2D, rather β-cell dysfunction in the remaining cells likely accounts for the full disease condition. Triglyceride accumulation in pancreatic islets is associated with β-cell loss, impaired insulin secretion and type 2 diabetes [142, 143]. Detailed studies on glucose stimulated insulin release in T2D patients and rodent models have shown that islets from diabetic donors have decreased glucose responsiveness, decreased insulin content and a defect in GSIS [144, 145]. In addition to impaired GSIS, T2D islets have decreased insulin content, decreased mature insulin granules, a reduction in insulin mRNA expression and increased levels of proapoptotic caspase3 and 8 [142]. β-cells are particularly sensitive to increased FFA levels due to their limited lipid storage capacity, driving excess lipids into toxic metabolic pathways (eg, ceramide and DAG synthesis). Chronic exposure to glucose (glucotoxicity) also causes some level of β-cell dysfunction in model systems but the extent to which this occurs in humans is still undetermined [143].

Nonalcoholic Fatty Liver Disease. In addition to pancreatic β-cell lipotoxicity, an accumulation of intracellular lipids in hepatocytes, known as nonalcoholic fatty liver disease (NAFLD), results in a similar lipid induced cellular dysfunction. NAFLD encompasses all phases of fatty liver, the

early stages of hepatic steatosis as well as the progressive inflammatory stages of steatohepatitis (NASH) and cirrhosis [68]. The most common cause of NAFLD in the developed world is overnutrition and obesity and seventy-five percent of obese patients exibit some level of hepatic steatosis [146].

Excess levels of FFA or glucose have been shown to cause hepatic steatosis, with increased glucose channeling into the *de novo* FA synthesis pathway [147]. Both FFA and glucose uptake into the liver occurs by an insulin-independent mechanism. For this reason, an increased level of either metabolite in the circulation results in uptake by the liver regardless of circulating insulin. Once within the cell, hepatic FFAs can be stored in the lipid droplet as TG, used as energy through β-oxidation, or assembled with apolipoprotein B 100 (ApoB) to form a very-low density lipoprotein (VLDL). VLDL particles are then secreted into circulation, and are able to deliver lipids to peripheral tissues such as the adipocyte [68].

Though one main function of the liver is to repackage lipids for distribution, it has a limited lipid storage capacity. As the lipid level saturates lipid droplet storage, inflammatory and lipotoxic responses rise, furthering NAFLD disease progression. On a molecular level, this hepatic lipid accumulation likely occurs through a combination of cellular changes. Increased lipid uptake from circulation or elevated *de novo* lipogenesis increases lipid levels and defects in fatty acid oxidation or impaired lipoprotein secretion or synthesis decrease clearance of lipid from the liver.

Insulin resistance is considered to be the primary source for these cellular alterations. In order to understand the connection between insulin sensitivity and hepatic steatosis, the role of insulin in normal physiology will be briefly described. In peripheral tissues such as the adipose and skeletal muscle, insulin has two main functions. The first is to stimulate the translocation of

glucose transporter 4 (GLUT4) transporters to the plasma membrane, resulting in increased glucose uptake. Insulin is also able to decrease peripheral lipolysis through inactivation of hormone sensitive lipase (HSL). In the liver, glucose uptake occurs through the insulin-independent GLUT2 transporter, and therefore is unaffected by changing insulin levels. Instead, hepatic insulin action results in the inhibition of gluconeogenesis through FOXO1 phosphorylation, increased hepatic *de novo* lipogenesis and decreased levels of fatty acid oxidation [68].

Insulin resistance in adipocytes results in a loss of insulin induced suppression of lipolysis, thus increasing levels of circulating albumin bound FFA. Hepatic uptake of free fatty acids from circulation is insulin independent, and therefore this rise in circulating FFA results in increased lipid uptake. In the liver, there is a mixed insulin resistance characterized by impaired insulin mediated gluconeogenesis suppression, but no change in insulin stimulated *de novo* lipogenesis. The combination of increased FFA flux into the liver and increased lipogenesis results in hepatic lipid overload. In order to lessen lipid load, the hepatocyte increases VLDL secretion but in many cases in unable to compensate for the chronically high levels of intracellular TG typically seen with type 2 diabetes [68].

Lipid overload in the hepatocyte activates several signaling pathways altering cellular metabolism and increasing the susceptibility of the cell to damage. This increased vulnerability is the result of impaired mitochondrial function and subsequent increases in oxidative stress. FFAs are able to increase the permeability of the mitochondrial membrane, increase ROS generation, induce ER stress response and increase JNK-dependent lipoapoptosis. The oxidative stress resulting from the mitochondrial dysfunction is able to induce proinflammatory signaling pathways, which lead to the progression of NAFLD to NASH [148].

Part VI: Yeast as model system for lipid disorders

Many aspects of lipid metabolism and LD structure have been conserved across eukaryotic evolution. This conservation provides us with a useful and easily manipulated biological model to study complex pathways involved in human lipid disorders. Genes that have been highly conserved across evolution are likely to be involved in essential cellular processes. Being that lipid homeostasis is critical for cellular function, it is not surprising that there has been a high level of conservation in both sequence and function between integral lipid metabolism proteins of yeast and mammalian systems.

Yeast is a commonly used model organisms that is useful for the study of basic biological pathways due to its fast growth rate, availability of a deletion library containing a single deletion of all non-essential open reading frames (ORF), ease of genetic manipulation through use of homologous recombination or episomal plasmid transformation, and a high number of human orthologs [149]. The metabolic processes of NL synthesis (Table 1-1), β-oxidation, and lipolysis have an exceptional level of conservation and research using yeast has had a major impact on our current knowledge of eukaryotic lipid biology.

Lipotoxicity in Yeast: The process of lipotoxicity also occurs in yeast, and shares several parallels to mammalian lipid disorders. Yeast undergoes cell death in response to exogenous fatty acids under certain genetic manipulations. In yeast, a strain with deletions in all four of the genes encoding the NL-synthesis enzymes Are1p, Are2p, Dga1p and Lro1p contains no lipid droplets (Fig. 1-7) but is viable under normal growth conditions. This mutant is highly sensitive to treatment with unsaturated fatty acids (UFA) such as oleate (C18:1) and palmitoleate (C16:1) (Fig. 1-7) while surprisingly unaffected by the saturated fatty acid (SFA) palmitate (16:0) [23,

150]. Following UFA supplementation, the NL-deficient strain shows increased oxidative stress and activation of the UPR, eventually leading to cell death. Eliminating neutral lipid biosynthesis results in channeling of incoming FA into phospholipids, causing massive ER membrane proliferation and alterations in the phospholipid acyl chain composition [22]. Co-supplementation of palmitate and oleate partially protects the NL-synthesis mutant from these defects, highlighting the importance of a balanced unsaturated/saturated fatty acid ratio in cellular function [23].

Phosphatidic acid (PA) is an important central intermediate in TG and PL synthesis. A mutation in the PA hydrolase, Pah1p, has markedly reduced levels in DAG and TG, and a channeling of lipids into phospholipid synthesis results in nuclear envelope expansion. The defect in TG synthesis seen in *pah1Δ* renders the cell highly sensitive to UFA treatment, similar to that seen in the neutral lipid deficient strain [151]. Mutations in the mouse ortholog of *PAH1*, LPIN1, results in a lipodystrophy characterized by white adipose tissue loss, fatty liver, insulin resistance and hypertriglyceridemia [152]. Consistent with the mouse and yeast phenotype, the human LPIN1 gene has been linked to fat mass and glucose homeostasis through linkage studies [153].

Though monounsaturated fatty acids (MUFAs) are the more toxic lipid in yeast, whereas SFAs are widely accepted as being more toxic in mammals, the lipotoxic mechanisms between the two organisms share many commonalities. The resistance to palmitate toxicity in yeast is not due to a lack of uptake or incorporation. FA profiling of yeast exposed to palmitoleate show that it is rapidly elongated and desaturated to match the cellular phospholipid requirements [154]. Yeast with a desaturase activity defect have increased palmitate induced toxicity due to their inability to alter chain saturation to meet cellular needs [131]. Likewise, human arterial

endothelial cells overexpressing the mammalian desaturase SCD-1 rescues SFA induced lipotoxicity [155]. Collectively, these results indicate that desaturation of palmitate in both yeast and human systems is protective against SFA induced lipotoxicity and the composition of fatty acyl chains (both length and degree of desaturation) is important in maintaining membrane structure and cellular function.

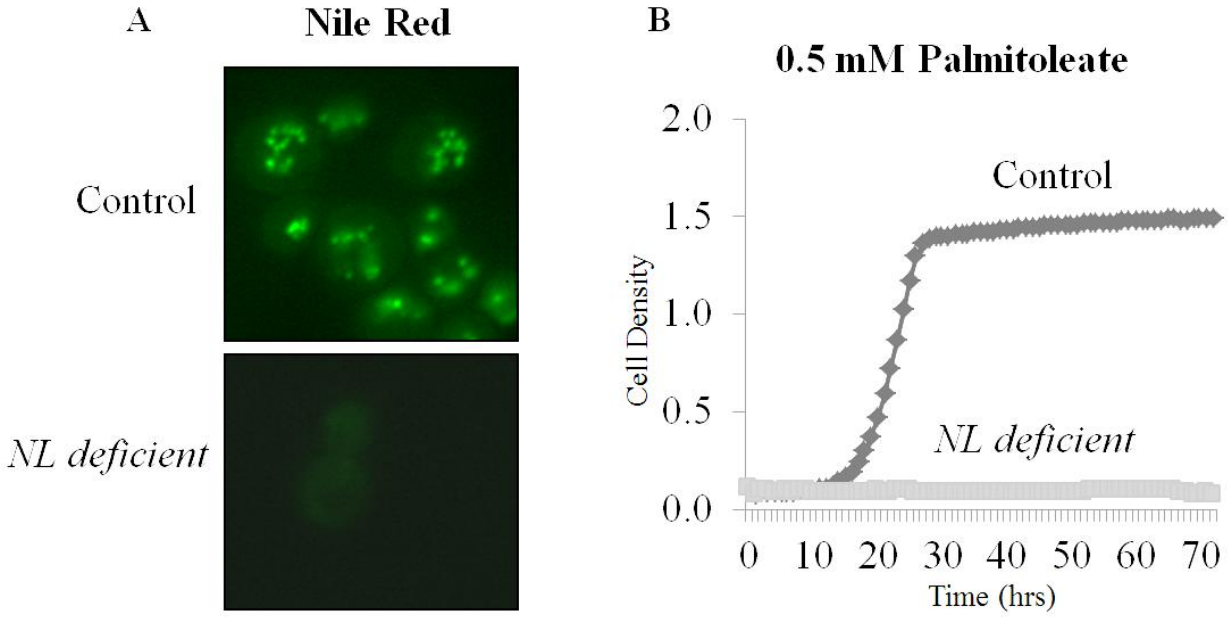

Figure 1-7: Neutral lipid deficient strain lacks all cytoplasmic lipid droplets and is sensitivity to unsaturated fatty acid treatment. (A) Lipid droplets from normal and the neutral lipid deficient strain (*are1Δ are2Δ dga1Δ lro1Δ*) were stained by the lipophilic dye, Nile Red. (B) Cell growth in the presence of 0.5 mM palmitoleate in liquid rich media over time.

Part VII: The Aims and Findings of this Thesis

The purpose of this thesis was to identify novel mammalian genes involved in the progression of lipotoxic disease. In Chapter 2, we analyze the results of a yeast genome-wide

palmitoleate (C16:1) sensitivity screen, which identified genes deletions resulting in increased lipotoxicity. From this screen, we determined that ablation of 156 genes result in a significant growth defect in response to unsaturated fatty acid treatment. Of these genes, many encode proteins involved in lipid metabolism, mitochondrial respiration, mitochondrial fatty acid synthesis, vesicular trafficking, and histone modification.

From these genes we concentrated on those which have high evolutionary conservation between yeast and mammals in order to identify novel pathways involved in mammalian lipotoxicity. We chose to focus on two conserved proteins, the tail-anchored protein insertion complex members, mammalian *ASNA1* and yeast *GET3*, and the putative sterol transporters, mammalian and yeast *ARV1*. In Chapter 3 we used the yeast model system to complete basic mechanistic studies on the role of *GET3* in eukaryotic lipid metabolism and lipid droplet dynamics. We demonstrate that a loss in *GET3* results in increased apoptosis in response to unsaturated fatty acid treatment, decreased neutral lipid synthesis and altered lipid droplet homeostasis due to defects in vacuolar nutrient recycling. We also identify a relationship between *GET3* and the yeast diacylglycerol acyltransferase, DGA1, in lipid droplet homeostasis.

In order to clarify a potential role for mammalian *ASNA1* and *ARV1* in lipotoxic disease, we took advantage of RNAi and adenoviral technology to knockdown and overexpress these genes in pancreatic β-cell line, MIN6, and the rat McA-RH7777 hepatoma cell line. In Chapter 4, we focus on the role of *ASNA1* in lipid induced apoptosis and alterations in fatty acid effects on glucose stimulated insulin secretion (GSIS) in MIN6 cells. We demonstrate that *ASNA1* is involved in saturated fatty acid induced lipoapoptosis and the potentiation of GSIS in pancreatic β-cells.

In Chapter 5 we build upon research previously reported by Dr. Ying Liu, demonstrating that overexpression of human *ARV1* in mouse liver induces hepatic lipid accumulation through increased TG synthesis [156]. We found that this lipid accumulation could not be explained by decreased VLDL secretion following *ARV1* overexpression in McA-RH7777 hepatoma cells. We also report that knockdown of *ARV1* in pancreatic β-cells results in decreased TG synthesis and increased apoptosis in response to both palmitate and palmitoleate and propose a model for the role of *ARV1* in triglyceride homeostasis. Finally in Chapter 6 we discuss the potential mechanisms of *GET3, ASNA1* and *ARV1* in pathways of eukaryotic lipotoxicity and propose future experiments to clarify their role in maintaining cellular lipid balance.

Chapter 2: Identification of novel genes involved in palmitoleate sensitivity in yeast

ABSTRACT

Under conditions of excess lipid exposure, a cells primary line of defense is the esterification of fatty acids into neutral lipids and their subsequent storage in the lipid droplet. Lipid accumulation beyond the cells storage capacity results in a spillover of fatty acids into toxic metabolic pathways leading to lipotoxicity and apoptosis. An accumulation of lipids in skeletal muscle, hepatocytes and pancreatic β cells is associated with the development of lipotoxic diseases such as type 2 diabetes and steatohepatitis. Identification of gene mutants associated with a predisposition to fatty acid induced toxicity is essential in understanding the progression of these diseases. In order to identify novel genes involved in eukaryotic lipotoxicity, we performed a genome-wide unsaturated fatty acid sensitivity screen using the model organism *Saccharomyces cerevisiae*. Of the ~5,500 gene knockouts and knockdowns tested, we identified 156 gene mutant strains with significant sensitivity to the unsaturated fatty acid palmitoleate. Of these genes, many are involved in lipid metabolism, vesicular trafficking, mitochondrial respiration and transcriptional regulation. Additionally, 68 of the 156 yeast genes identified by the screen have been highly conserved throughout evolution, 11 of which have been previously associated with lipotoxic disease phenotypes in rodent models and/or human subjects. Therefore, this screen has identified novel genes and pathways involved in lipid homeostasis in both yeast and human systems, many of which are potential treatment targets for lipotoxic disease.

INTRODUCTION

Ectopic fatty acid deposition in non-adipose tissues, such as pancreatic β-cells, muscle and liver, is strongly associated with obesity related diseases such as type 2 diabetes (T2D) and nonalcoholic fatty liver disease (NAFLD). The limited lipid storage capacity of these tissues results in cellular dysfunction and apoptotic initiation, known as lipotoxicity and lipoapoptosis, respectively. Lipotoxicity occurs in many mammalian cells types, including pancreatic β-cells [157-159] and hepatocytes [160, 161], as well as the eukaryotic model organisms *Drosophila* [162] and *Saccharomyces cerevisiae* [22, 163].

Saturated fatty acids (SFA), such as palmitate are considered to be the primary toxic fatty acids (FAs) in mammalian cells [110, 111, 164, 165], but under certain circumstances, unsaturated fatty acids (UFA) can be equally as toxic [116, 117, 119-122]. For example, DGAT1 $^{-/-}$ fibroblasts are as sensitive to UFA as they are to SFA due to their inability to channel UFA into triglyceride synthesis and lipid droplet (LD) storage [7]. Interestingly, wild type yeast are resistant to lipid induced cell death under normal growth conditions [22, 163, 166]. Ablation of all four neutral lipid synthesis enzymes (*ARE1*, *ARE2*, *DGA1*, and *LRO1*) however, results in severe sensitivity to the monounsaturated fatty acids oleate (C18:1) and palmitoleate (C16:1) [22, 163]. This yeast strain is analogous to the DGAT $^{-/-}$ fibroblast cells, in that the UFA induced lipotoxicity can be attributed to the neutral lipid synthesis defect.

Mechanisms of lipotoxicity in eukaryotic cells are still somewhat elusive, particularly the pathways of UFA-induced lipotoxicity. The model organism, *S. cerevisiae* (‘yeast’), is a useful tool to examine these mechanisms due to its ease of use and the availability of a nearly complete (~96%) library of single deletion knockouts or knockdowns [167, 168]. The knockout library allows for relatively simple full genome screening and identification of genes involved in many

aspects of eukaryotic biology. In the past, these screens have revealed genes integral for nutrient metabolism [169, 170], drug sensitivities [171, 172], cell cycle regulation [173] protein degradation pathways [174, 175], lipid droplet homeostasis [58-60] and fatty acid utilization [166, 176].

In this study, we use a genome-wide screen in yeast to determine genes necessary for growth on the unsaturated fatty acid palmitoleate (C16:1). Of the ~5,500 haploid gene mutants tested, 156 conferred sensitivity to fatty acid treatment compared to control. We demonstrate that many protein transcripts of the palmitoleate sensitive genes are members of the same protein complex or function within the same biological pathway. Additionally, forty four percent of the yeast gene hits have been conserved throughout evolution with orthologs in mice and humans.

MATERIALS AND METHODS

Yeast General. Molecular biology and yeast procedures were performed according to conventional methods [177]. Complete (YPD; yeast extract, peptone, dextrose), synthetic complete (SC) and selective media were prepared as described previously [177]. All yeast strains used in this study were derived from s288C (Open Biosystems), with the exception of SCY2021 (*are1::HIS3 are2::LEU2 dga1::URA3 lro1::URA3*) which is derived from W303[178]. All single mutants were obtained from Open Biosystems Yeast Knock Out (YKO) Strain collection (Cat # YSC1053). When indicated, fatty acids were added to media in 0.6% ethanol:tyloxapol (5:1, v/v) at the designated molar concentration (Sigma; palmitoleate and oleate as a 10% w/v stock in ethanol). For liquid growth assays, overnight cultures were used to inoculate liquid media such that the starting optical density was 0.1 (A600 nm) and growth curves were obtained using a Microbiology Workstation Bioscreen C (Thermo Electron Corp.) and Research Express Bioscreen C software (Transgalactic Ltd). Three isolates per genotype were normalized to an absorbance (OD600) of 0.1 and 10 µl of each strain was added to 290 µl of media per well and grown at 30° for 4 days and averaged in order to produce the final growth curve.

Genome-Wide UFA Sensitivity Screen and Validation. The palmitoleate screen was carried out using the set of MATa haploid deletion strains (Open Biosystems) and a portion of essential gene knockdown DAmP (Decreased expression through mRNA perturbation) strains (Open Biosystems) maintained in the 96 well format setup by the supplier. Frozen stocks were thawed and inoculated into YPD + 200 mg/liter geneticin G418 media in 96 well dishes using a singer RoToR HDA replicator robot. Cultures were grown for 2 days at 30°C and diluted 1:100 in

water. 1 µl of the culture was pinned onto rectangular SC + 2% dextrose agar plates with and without 0.5 mM palmitoleate and grown for 2 days at 30°C . Growth on plates was quantified using Image J software. Growth normalization was done by dividing each colony size by the average growth of each on YPD. The normalized growth of each quadruplicate was then averaged to quantify the growth of each strain. Differential growth was determined by using the $\log_2$ ratio between control plate values (SCD) and experimental plate values (SCD+ palmitoleate). P-values comparing these normalized growth variables ('calculated ratio') were completed and a $p<0.05$ was considered as significant.

Screen Validation using MATLAB Curve Analysis. Strains showing decreased growth on palmitoleate compared to fatty acid free media were then validated using the liquid growth assay. Growth curve variables obtained from this assay were then used to determine statistically significant changes in growth compared to a normal strain. Three variables: maximum OD (A600), maximum growth rate (ΔA600/hr) and time at which maximum growth rate (in hours) were obtained using MATLAB numerical computing program for three isolates per genotype were normalized to wild type values and analyzed using ANOVA and t-tests against wild type values to determine significance.

The MATLAB program was created to find the slope of the growth curve at each time point, and identify the maximum slope (or growth rate) for each triplicate in each strain. The time (in hours) at which this slope was reached was also stored in a new matrix table. Maximum OD was calculated as the highest OD600 value of the curve. Values of these variables were calculated for each individual growth curve and normalized to wild type control. The values were calculated as follows:

$$WT_{norm} = \frac{WT_{SCD}}{WT_{SCD+PO}} \qquad RateRatio = \frac{avg(WT_{norm})}{avg(xxx\Delta_{norm})}$$

$$t_{norm} = t_{SCD+PO} - t_{SCD} \qquad TimeRatio = t_{norm(xxx\Delta)} - t_{norm(WT)}$$

$$OD_{norm} = \frac{OD_{SCD}}{OD_{SCD+PO}}$$

Variable Glossary:

WT_{SCD}: Maximum growth rate for wild type strain in SCD media

$WT_{SCD + PO}$: Maximum growth rate for wild type strain in SCD media supplemented with palmitoleate

WT_{norm}: Maximum growth rate of wild type in SCD normalized to SCD with palmitoleate

***$xxx\Delta_{SCD}$*:** Maximum growth rate of growth for deletion strain in SCD media

$xxx\Delta_{SCD + PO}$: Maximum growth rate of growth for deletion strain in SCD media supplemented with palmitoleate

***$xxx\Delta_{norm}$*:** Maximum growth rate of deletion strain in SCD normalized to SCD with palmitoleate

RateRatio: Ratio of normalized growth rates in deletion strain compared to wild type. The higher this value, the more sensitive the deletion strain is to palmitoleate

t_{SCD}: Time at which maximum growth rate occurs in SCD media

$t_{SCD + PO}$: Time at which maximum growth rate occurs in SCD media with PO

t_{norm}: Maximum growth rate time in SCD normalized to time in SCD with palmitoleate.

TimeRatio: Ratio of normalized time values in deletion strain compared to wild type. The larger this value the longer it takes for the deletion strain to reach log phase growth (lag).

OD_{SCD}: Maximum OD600 Absorbance value in SCD media

$OD_{SCD + PO}$: Maximum OD600 Absorbance value in SCD media with palmitoleate

OD_{norm}: Maximum OD in SCD normalized to maximum OD in SCD + palmitoleate

OD_{Ratio}: Ratio of normalized OD in deletion strain compared to wild type. The lower this value the less saturated the culture with time.

In subscreens testing for the sensitivity of each mutant in nystatin, myriocin, and temperature stress, only 74 gene deletions were tested. These gene deletions are those, which had a significant difference in 'Max OD' and/or 'Rate' variables compared to control.

Plating Assays. Sensitivity to media containing fatty acids (0.5 mM palmitoleate, oleate, linoleate), Nystatin (2.5, 5, 10 and 15 μg/ml), myriocin (500 ng/ml) and temperature (16°C or 37°C) were determined by serial dilutions of yeast strains after OD normalization. Plates were incubated at 30°C, unless otherwise indicated, for 2 days. Growth was compared to wild type grown under the same conditions.

Fluorescence Microscopy. Yeast cells were grown in specified media to saturation. Lipid droplets were stained with Nile Red (1 μg/ml) (Sigma-Aldrich N3013) and visualized with a long pass GFP filter (excitation 440 nm). All microscopy was performed using a Zeiss Axiovert 200 M using a 63x oil immersion objective and images taken using a Hamamatsu Orca-ER camera.

RESULTS

A genome-wide screen identifies palmitoleate sensitive single mutants in yeast. In yeast, a neutral lipid (NL) deficient *are1Δ are2Δ dga1Δ lro1Δ* strain was found to have a severe sensitivity to unsaturated fatty acids (UFA) but is unaffected by saturated fatty acid (SFA) treatment [22]. We therefore hypothesized that sensitivity of other mutant yeast strains to UFA would identify previously unreported lipotoxic pathways. In order to determine additional genes important in yeast lipid tolerance, we performed a genome-wide screen for sensitivity to the monounsaturated fatty acid palmitoleate.

We chose to carry out a fatty acid sensitivity screen in the yeast system for several reasons. Multiple genome-wide screens have been completed in model organisms focusing on gene mutants resulting in altered lipid droplet morphology [56-60]. Surprisingly, there has been very little overlap in the genes identified by these screens and they have not been productive in terms of lipotoxic pathway identification. The investigators focused on the role of two particular genes, the yeast seipin ortholog, *FLD1*, and the COPII vesicular trafficking complex, in the regulation of lipid droplet formation and size. Furthermore, to our knowledge, no screen for mutants with increased susceptibility to fatty acid induced death has been completed in any organism and therefore this screen will provide a novel outlook on eukaryotic lipid metabolism. There have been two screens identifying mutants which are resistant to palmitate induced cell death in Chinese hamster ovary (CHO) cells, which demonstrate a role for the elongation factor 1A-1 (eF1a1) and 3 small nucleolar RNAs (snoRNAs) in the resistance to lipotoxicity [179, 180]. We hoped to complement these studies by examining lipotoxicity from a different angle, with an outcome of sensitivity versus resistance. Lastly, the yeast model system is useful in the study of lipid metabolism, due to its ease of use and high evolutionary conservation in lipid

homeostatic pathways. Moreover, the large number of human orthologs in yeast makes it a good model for the identification of genes involved human disease.

The use of palmitoleate for the screen stemmed from the observation that NL-deficient yeast is more sensitive to palmitoleate (C16:1) than any other fatty acids tested (palmitate (C16:0), stearate (C18:0), myristate (C14:0), oleate (C18:1) and linoleate (C18:2) [22]. The haploid (MATa) deletion collection with deletions in ~4,800 nonessential genes and a knockdown DAmP (Decreased expression through mRNA perturbation) collection of ~700 essential genes were plated on synthetic complete media with 2% dextrose +/- 0.5 mM palmitoleate.

Growth sensitivity to palmitoleate was determined by comparing the normalized colony size on fatty acid containing media to no treatment media for each single deletion. Analysis of each strain in quadruplicate found that 256 single deletion strains caused sensitivity ($p<0.05$) to palmitoleate compared to the wild type control, as measured by comparative growth rate (SCD versus SCD + palmitoleate) (Fig 2-2). For screen validation, we grew each of these 256 deletion strains in rich liquid media (YPD) with and without 0.5 mM palmitoleate and monitored growth over a 4 day period (Fig 2-2). Growth curves were analyzed using MATLAB software for 3 variables; maximum optical density reading ("Max OD" in OD600), maximum rate of growth ("Max Rate" in OD600/hour) and time at which the maximum rate of growth was reached ("Time" in hours) (Figure 2-1). These three variables were normalized to a wild type control and used to validate gene deletions with significant growth defects in palmitoleate containing media (see Methods for further explanation).

We considered a significant increase in any of the three variables (Max Rate, Max OD or Time) to indicate that the mutant was sensitive to palmitoleate compared to control. From this

validation we narrowed down our list from 256 to 156 gene mutants with sensitivity to palmitoleate in both liquid and solid media (Table 2-1, Fig 2-2, Table S2-1). Forty-seven of the 156 genes identified have defects in at least two of the three growth variables. The majority (136 gene mutants) of the 156 had a significant growth lag, in which the time to reach maximum growth rate ('Time') was increased compared to control. Thirty-eight gene mutants had decreased maximum cell density ('Max OD') and forty-three had a significant defect in maximum growth rate ('Rate') (Table S2-1).

Growth resembling that of wild type would have a "Time" of 0, a "Max Rate" of 1 and a "Max OD" of 1 (see Methods for details). Gene mutants were ranked based on the sum of these variables ("Time" + "Max OD" + "Max Rate") with the highest value indicating the most sensitive strain (Table S2-1). A control curve without UFA sensitivity would have a variable sum equal to 2. The highest variable summation value occurred with a deletion in *ARV1*, which had a variable sum of 47, making it the most sensitive strain identified in the collection (Table S2-1). There were several strains that had a sum indicating wild type growth (~2) but because these mutants had significant values indicating a growth defect in at least one of the three variables they were included in the data set.

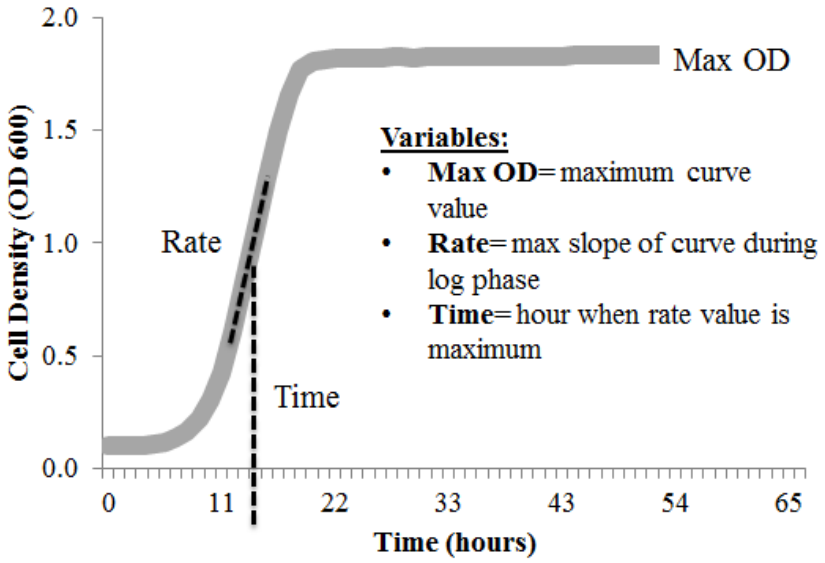

Figure 2-1: Yeast growth curve variables for screen validation. Schematic for growth curve analysis. Values for each curve were calculated and normalized compared to wild type control (See Materials and Methods for details).

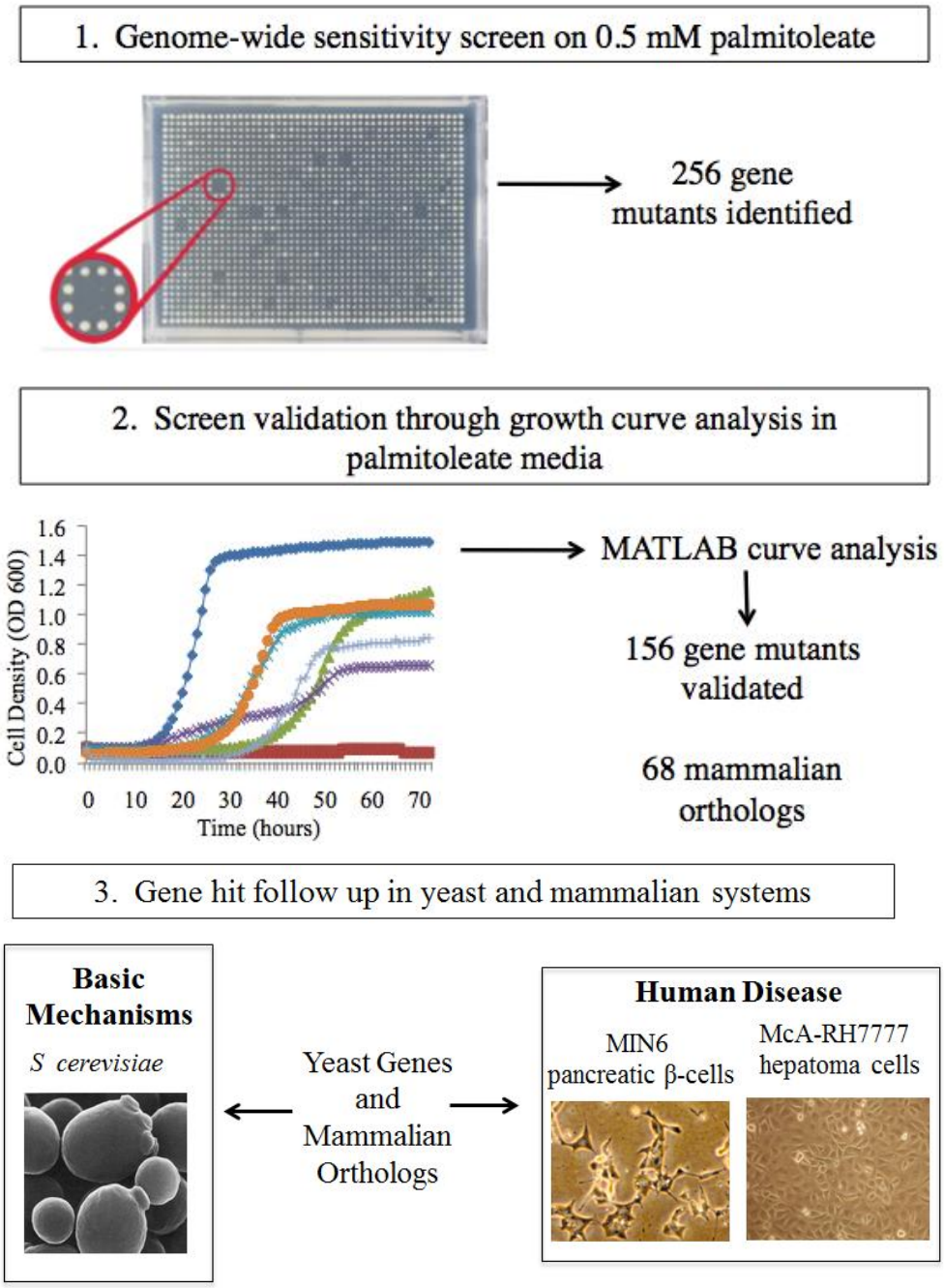

Figure 2-2: Screen validation and follow-up methodology. (1) Genome-wide screen of yeast knockout and knockdown collection on 0.5 mM palmitoleate. 256 gene mutants were identified as being sensitive relative to wild type. (2) Growth curve analysis in liquid media. MATLAB program was used to determine statistical significance between mutant growth in 0.5 mM palmitoleate (see Methods for details). 156 gene mutants were validated as having significant sensitivity. Of the 156 yeast genes, 68 have human orthologs. (3) Yeast and mammalian models will be used to determine the role of these genes in the basic mechanisms of lipid metabolism and lipotoxic disease.

Table 2-1: Deletion of 156 genes confers significant growth defects on palmitoleate A yeast deletion library containing haploid single deletion strains was plated on SCD ± 0.5 mM palmitoleate in quadruplicate. Strain sensitivity was validated by growth curve analysis in liquid media with 0.5 mM palmitoleate. Cellular process determined using Saccharomyces Genome Database (SGD) Gene Ontology (GO) Slim Mapper

Cellular Process	Genes
Amino Acid Metabolism	*ARO1 ARO2 TRP2 TRP5*
Carbohydrate Metabolism	*GCR2 HOC1 MNN4 TCO89 TPS1*
Cell Cycle	*GRR1 HSL7 MRC1 NIP100 NPR3 SIC1*
Cellular Homeostasis	*SAG1 VMA1 VMA7 VMA21*
Cellular Respiration	*BCS1 CBP1 COX11 CYT1 MRPL51 PET309 QCR7 QCR8*
Chromosome Organization	*BUB1 CTF4 CTF8 HTB2 LGE1 NGG1 RTG2 VPS71*
Cofactor Metabolism	*CAT5 COQ3 COQ6*
Lipid Metabolism	*ARV1 CEM1 CSH1 DEP1 ETR1 FEN1 LOA1 MCT1 SAC1 SCS7*
Mitochondrial Organization	*AEP1 ATP11 ATP25 CCE1 COX23 CRD1 GGC1 IFM1 IMP2 MDM32 MRP10 MRPL7 PCP1 PET54 PET117 PET123*
Protein Modification and Protein Folding	*AIM22 KEX2 MDJ1 PFD1 SLI15 WSS1*
RNA/DNA Metabolism	*CBP2 COX18 ELP3 FRA2 GCN5 IES6 LDB7 LHP1 LSM7 MEC3 MTF2 MSW1 NPL6 PHO23 PHO80 QCR8 RAD6 RPB9 RPS14A RPS16A RRP8 RSC1 RTF1 SHE3 SKY1 SLX8 SPT21 SRB8 SSN3 STP2 YAF9 YNL296W*
Translation and Transcription	*AIM10 FES1 HAP3 MRPL9 RPL8A RPS28B RSM22 RSM27 SNT1*
Transport	*FPS1 CTR1 ITR1 MTM1 SPF1 VPS61 VPS63 VPS64 VPS69*
Vesicle Mediated Transport	*EMP24 ERV14 GET1 GET2 GET3 GLO3 GOS1 RIC1 PEP3 VPS51 VPS52 VRP1*
Unknown	*GFD2 MGR2 MTC1 SOV1 YBL094C YBL100C YBR144C YBR196C-A YDL009C YDL041W YDR149C YDR230W YDR417C YER084W YGR219W YHR009C YLR184W YLR202C YLR374C YML095C-A YMR031W-A YMR135W-A YNL198C YOR331C YPR153W*

The liposensitivity screen confirms previously identified unsaturated fatty acid sensitive mutants. Prior to this screen, several genes had been identified as causing sensitivity to unsaturated fatty acids [22, 151, 166, 181]. In order to ensure that our screen was consistent with these known phenotypes, we investigated if these mutants were also found by our screening methods. Garbarino *et al*., determined that mutations in GET complex members *GET2* and *GET3* were vulnerable to growth on 0.5 mM palmitoleate in minimal media (SCD) [22]. As we expected, these knockout strains were also identified in our screen as having palmitoleate sensitivity (Table 2-1). In addition, Fakas *et al*., showed that mutations in the phosphatidic acid hydrolase, *PAH1*, cause increased sensitivity to palmitoleate, oleate, and palmitate [151]. *pah1Δ* was not found by our screening methods only because it was not included in our yeast knockout library. We tested this strain using our validation techniques and found that it too had a significantly increased sensitivity to UFA (Fig 2-5A).

Furthermore, two yeast screens assessing unsaturated fatty acid (UFA) utilization have been previously completed, both of which used oleate as a sole carbon source and identified several peroxisomal synthesis genes as integral in fatty acid utilization [166, 181]. The study completed by Lockshon *et al*. assessed viability defects in single mutant strains grown on UFA containing media lacking glucose [181] whereas Smith *et al*., investigated fatty acid utilization defects in strains by their ability to form "clear zone" of used FA in the media [166]. The purpose of both studies was to identify genes necessary for fatty acid utilization and not for lipotoxic pathway identification. Despite this difference, we did see moderate overlap (19 of 156) between the genes found in our screen and these studies (Table 2-2). The majority of commonality between the these screens and ours occurred in genes involved in lipid metabolism

(*FEN1, LOA1* and *SAC1)*, cellular transport (*SPF1, VPS64, VPS69*) and RNA/DNA metabolism (*LBD7, LSM7, NPL6, RSC1* and *SPT21)* (Table 2-2).

The overlap found between our screen and the two FA utilization screens is not particularly surprising. Though their prime focus was in the determination of genes integral in fatty acid utilization as a sole carbon source, some genes which are highly sensitive to UFA may not be able survive on FA in the absence of glucose due to their liptoxic response. Our screen is unique from these in that we focused on lipotoxicity, in which glucose was supplemented to the media and cells did not require FA utilization for viability. Furthermore, our screen highlights the effect of glucose and lipid in combination (glucolipotoxicity) in eukartyoic systems as a mediator of lipid induced cell death.

Table 2-2: Overlap of palmitoleate sensitive gene mutants with previous fatty acid and lipid droplet genome-wide yeast screens. A. Gene mutants identified in three lipid droplet morphology screens (Fei [58] Fei [60] and Szymanski [59]) and two oleate utilization studies (Lockshon [181] and Smith [166]) as having a lipid metabolism phenotype. 'More' or 'Less' indicates the reported lipid droplet morphology change in the literature.

Genes identified in palmitoleate sensitivity screen	**Previously Published Screen(s)**				
	Fei [58]	Fei [60]	Szymanski [59]	Lockshon [181]	Smith [166]
ARV1	More	More			
BUB1	More				
CTF8					X
FEN1				X	X
GET1	More				
GET2	Less				
GGC1				X	
LOA1			Smaller	X	
LBD7					X
LSM7					X
NGG1					X
NIP100				X	
NPL6					X
RPL8A		Less		X	
RSC1					X
SAC1		More		X	
SPF1				X	X
SPT21				X	
SSN3		More			
VMA1	Less		Larger		
VMA21	More	More			
VPS51			More		
VPS64		More			X
VPS69	More	More		X	X
VPS71				X	
YAF9				X	
YDR149C					X

Effect of chain length and saturation on toxicity. It has been well established that the level of toxicity of fatty acids is largely due to their degree of saturation and chain length [182-184]. In yeast lacking the neutral lipid (NL) synthesis enzymes (*are1Δ are2Δ dga1Δ lro1Δ*), both mono- and poly- unsaturated fatty acids are toxic (Fig 2-3A), but they are unaffected by treatment with saturated fatty acids (Fig 2-3B). In order to determine if the gene mutants identified in this screen are vulnerable to only palmitoleate or if their sensitivity is a more general FA-mediated effect, we tested 74 gene mutants which had significant defect in either growth rate or maximum OD (defined in Materials and Methods) on media containing the saturated fatty acids myristate (C14:0) and palmitate (C16:0), the monounsaturated fatty acid oleate (C18:1) and the polyunsaturated fatty acid linoleate (C18:2). We found that in general, the palmitoleate (C16:1) sensitive gene mutants had a less severe sensitivity phenotype to FAs with increased chain length (oleate, C18:1) and increased desaturation (linoleate, C18:2) (Figure 2-3A).

Despite the robust sensitivity of the NL-deficient mutant to all unsaturated fatty acids tested, this strain is not vulnerable to saturated fatty acid treatment (Fig 2-3B). This is likely due to the ability of yeast to rapidly elongate and desaturate SFA to meet the cellular requirements for membrane phospholipids [22, 163]. UFAs are also integrated into the acyl-chains of membrane phospholipids, but do not undergo the alterations in chain length or saturation prior to integration [163]. Only one of the palmitoleate sensitive mutants, *fen1Δ*, exhibited sensitivity to the saturated fatty acid palmitate (16:0) in both solid and liquid growth media (Fig 2-3B,C). *FEN1* is a fatty acid elongase which mediates the elongation of fatty acids up to 24 carbons long. Of all of the yeast fatty acid elongases, *FEN1* has the highest affinity for substrates with less than 22 carbons, like palmitate (C16:0), palmitoleate (C16:1) and oleate (C18:1) [185]. A balance in both saturation (UFA:SFA) and fatty acyl chain length (C16:C18) are integral in membrane

fluidity and cellular health and it has been proposed that the ability of palmitate to rescue oleate induced toxicity in the NL-deficient mutant is due to a restoration in the saturation balance of phospholipid acyl chains [23]. Similarly, yeast mutants with a defect in desaturase activity are sensitive to palmitate, likely due to their altered PL acyl chain balance [23]. The sensitivity of *fen1Δ* to both palmitoleate and palmitate can be explained by its inability to properly elongate exogenous FA to meet the cellular requirements of the cell and leading to an accumulation of acyl chains with the same chain length and a subsequent membrane phospholipid imbalance.

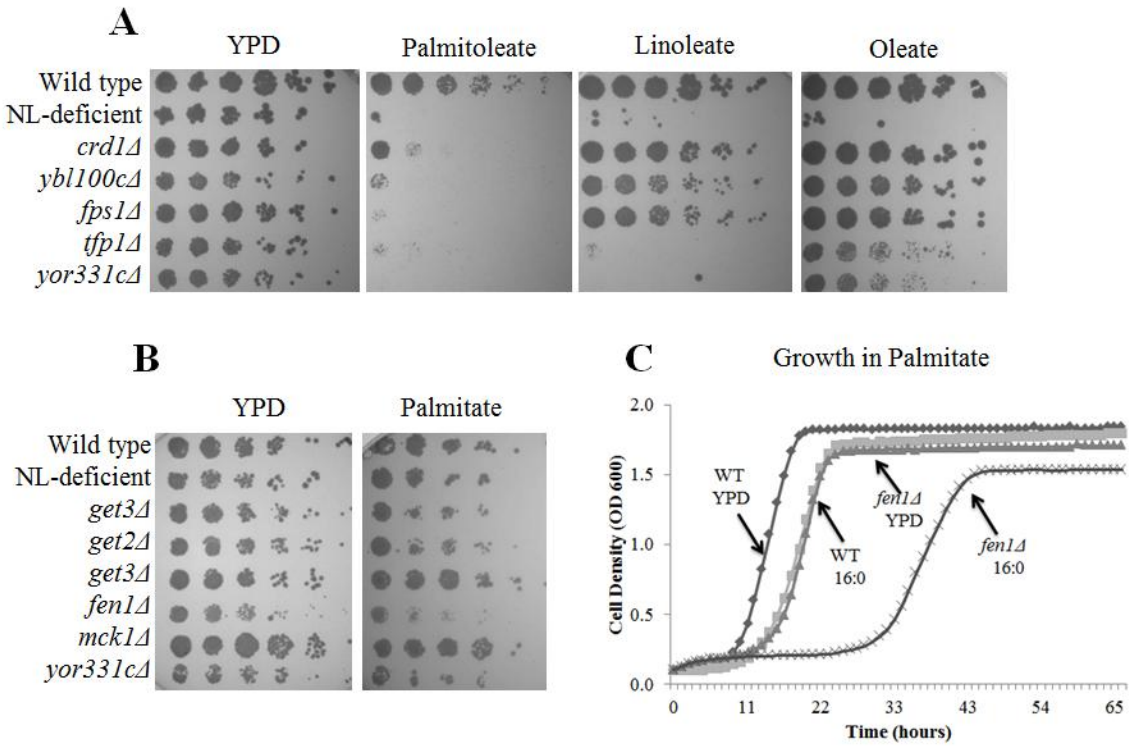

Figure 2- 3: Toxicity of fatty acid depends on degree of unsaturation and chain length
(A) Subset of palmitoleate sensitive gene mutants grown on media containing 0.5 mM of the monounsaturated oleate (18:1) and the polyunsaturated linoleate (18:2). (B) Single deletion mutants grown on 0.5 mM palmitate (16:0) (C) Growth curve of *fen1Δ* tested in liquid media with 0.5 mM palmitate.

Lipid droplet sub-screen. Given that triglyceride storage in the form of lipid droplets is a cells primary defense against increased fatty acid exposure [22, 81, 186], we performed a lipid droplet screen of the 156 palmitoleate sensitive gene mutants. We used this screening method to determine if palmitoleate sensitivity was due to defects in lipid droplet status. Each single mutant was grown overnight in rich media (YPD) and stained with the lipophilic dye Nile Red, and images were classified as having less (Class I), control (Class II) or more (Class III) lipid droplets compared to a wild type (Fig 2-4). 89 of the 156 gene mutants screened (57%) had a normal number of droplets, 47 (30%) showing decreased droplet number and only 20 (13%) with increased lipid droplets (Table 2-3).

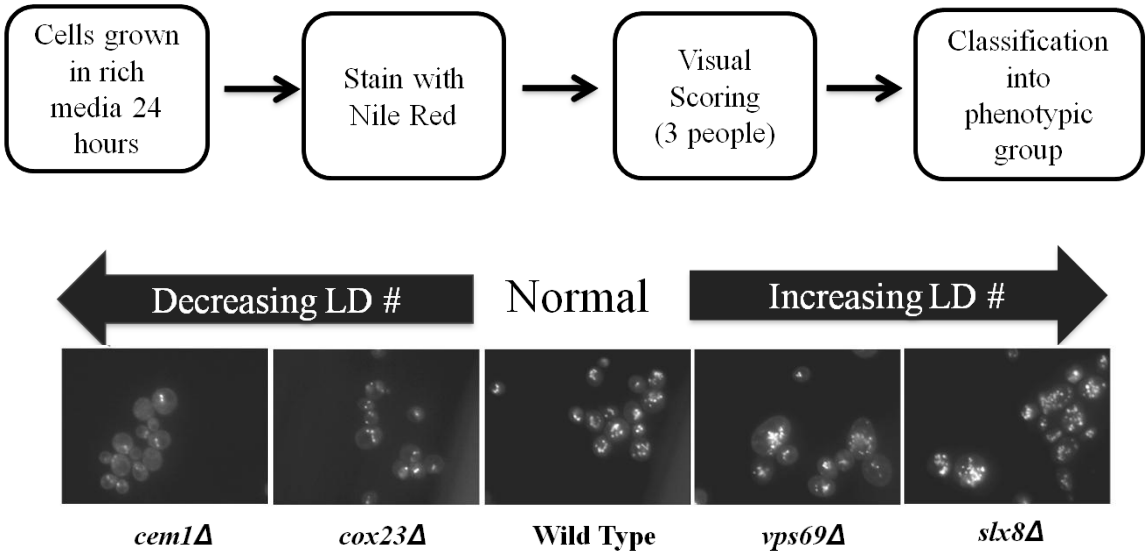

Figure 2-4: Lipid droplet morphology sub-screen methodology. Single deletion mutants were grown overnight in YPD and stained with Nile Red to visualize lipid droplets. Five or more images were captured and visual scoring was completed by three people in order to determine if the strains had abnormal lipid droplet number or size.

***Table 2-3: Lipid droplet phenotypes of palmitoleate sensitive single mutants*.**
Classification of single deletion strains from palmitoleate sensitivity screen based on lipid droplet phenotype (more, less or control number of droplets). Complexes or biological pathways highly represented in each phenotypic class were also identified.

LD Phenotype	Genes identified by palmitoleate sensitivity screen	Complexes
Class I (Less)	*AEP1 AIM10 AIM22 ATP25 BCS1 CEM1 COQ3 COX11 COX18 CTF4 CTR1 CYT1 ETR1 GCN5 GET1 GET3 GGC1 GRR1 HTB2 IFM1 IMP2 LBD7 LSM1 MDJ1 MRPL51 MRPL9 MSW1 MTF2 MTM1 NPR3 PET117 PET309 QCR8 RPS28B RSM22 SAG1 SOV1 SSN3 VMA1 WSS1 YBL100C YLR202C YMR135W-A YNL198C YOR331C YPR153W*	Fatty Acid Synthesis GET complex Cytochrome C oxidase Cytochrome bc1 complex
Class II (Control)	*ARO1 ARO2 ATP11 ARV1 BUB1 CAT5 CBP1 CCE1 COQ6 CRD1 CSH1 CTF8 DEP1 ELP3 EMP24 ERV14 FPS1 FRA2 GCR2 GET2 GFD2 GLO3 GOS1 HOC1 HSL7 IES6 ITR1 KEX2 LGE1 LHP1 LSM7 MCT1 MDM32 MEC3 MGR2 MNN4 MRC1 MRP10 MRPL7 MTC1 NGG1 NIP100 NPL6 PCP1 PEP3 PET54 PHO23 PHO80 RAD6 RIC1 RPB9 RPS14A RPS16A RRP8 RSM27 RTF1 RTG2 SAC1 SCS7 SHE3 SIC1 SKY1 SLI15 SNT1 SPF1 SPT2 SPT21 TCO89 TPS1 TRP2 TRP5 VMA21 VMA7 VPS52 VPS63 VRP1 YAF9 YBL094C YBR144C YDL009C YDL041W YDR149C YDR417C YER084W YGR219W YHR009C YLR184W YML095C-A YMR031W-A*	Amino Acid Metabolism Carbohydrate Metabolism Sphingolipid Metabolism Histone deacetylation
Class III (More)	*CBP1 FEN1 FES1 HAP3 LOA1 PFD1 PGI1 RPL8A RSC1 SLX8 SRB8 VPS51 VPS61 VPS64 VPS69 VPS71 VPS72 YL096C-B YLR374C YNL296W*	Class B Vacuolar Mutants SWR-1 complex

The proteins encoded by these genes tended to group within the droplet phenotype categories based on their biological process or protein complex (Table 2-3). Gene mutants with protein transcripts involved in fatty acid synthesis and members of the cytochrome bc or vesicular GET complex have decreased droplet number while those with altered amino acid, carbohydrate or sphingolipid metabolism had no change in lipid droplet status. Mutations in

genes needed for histone deacetylation also had normal lipid droplet number. Only those genes belonging to the class B vacuolar mutant family or SWR1 complex had increased lipid droplet number upon mutation. (Table 2-3)

There have been three previously published yeast genome-wide screens using neutral lipid dyes Nile Red [58, 60] or BODIPY 493/503 [59] to determine single gene deletion alleles resulting in altered lipid droplet morphology. Through comparison of our palmitoleate screen with these previous studies, we find 12 of 156 gene mutants have been previously reported to have altered lipid droplet morphology (Table 2-2). Of these 12, we independently identified 7 to have a LD phenotype in our Nile Red sub-screen. There is surprisingly little overlap within these morphology screens, indicating that even slight changes in growth conditions can cause significant alterations in lipid droplet morphology and the subjectivity of morphology screens may lead to high variability.

This screen also demonstrates that there are many pathways that do not affect LD biogenesis that can alter lipid vulnerability. To determine if mutants known to affect LD morphology cause changes in lipid vulnerability, we tested four single gene deletions known to cause severe defects in LD morphology in yeast (*pah1Δ* [187], *fld1Δ* [60], *tgl3Δ* [81], *snf1Δ*[188]) for palmitoleate sensitivity. We found that all except for one (*pah1Δ*) had normal growth with FA treatment (Fig 2-5). Mutations in the phosphatidic acid hydrolase, *PAH1*, causes a smaller number of larger droplets due to its role in diacylglyceride (DAG) synthesis and targeting of neutral lipids into the lipid droplet [187]. Triglycerides accumulate within the ER bilayer of *pah1Δ,* possibly contributing to its sensitivity to unsaturated fatty acids [151] (Fig 2-5A).

The three other genes inducing changes in LD morphology are *FLD1*[60], *TGL1* [81] and *SNF1* [188]. *FLD1* is an ortholog of human seipin, a gene associated with congential lipodystrophy. Deletion of *FLD1* results in giant lipid droplets, likely due to increased fusion [60] or defects in the ER lipid droplet contact sites [59] (Figure 2-5C). Deletion in the triglyceride lipase, *TGL3*, causes increased lipid droplets due to decreased triglyceride turnover [80] (Figure 2-5B). Lastly, *SNF1* is a central kinase regulating the transcription of glucose-repressed genes [188]. Deletion of *SNF1* causes a massive increase in lipid droplet number when grown in minimal media (SCD) (Figure 2-5E). Despite the significant changes in lipid droplet morphology, deletion in any of these genes did not alter the sensitivity of cells to treatment with palmitoleate (Fig 2-5B-D). Together, this data demonstrates that although an essential protective mechanism against intracellular lipid accumulation, sensitivity to palmitoleate also occurs through pathways that do not alter NL-storage or synthesis. Additionally, changing LD morphology or size does not predict an associated effect on the lipotoxic vulnerability of the cell. Studying these pathways that effect lipotoxicity independent from neutral lipid synthesis is integral in understanding the full array of mechanisms a cell uses to survive periods of lipid accumulation.

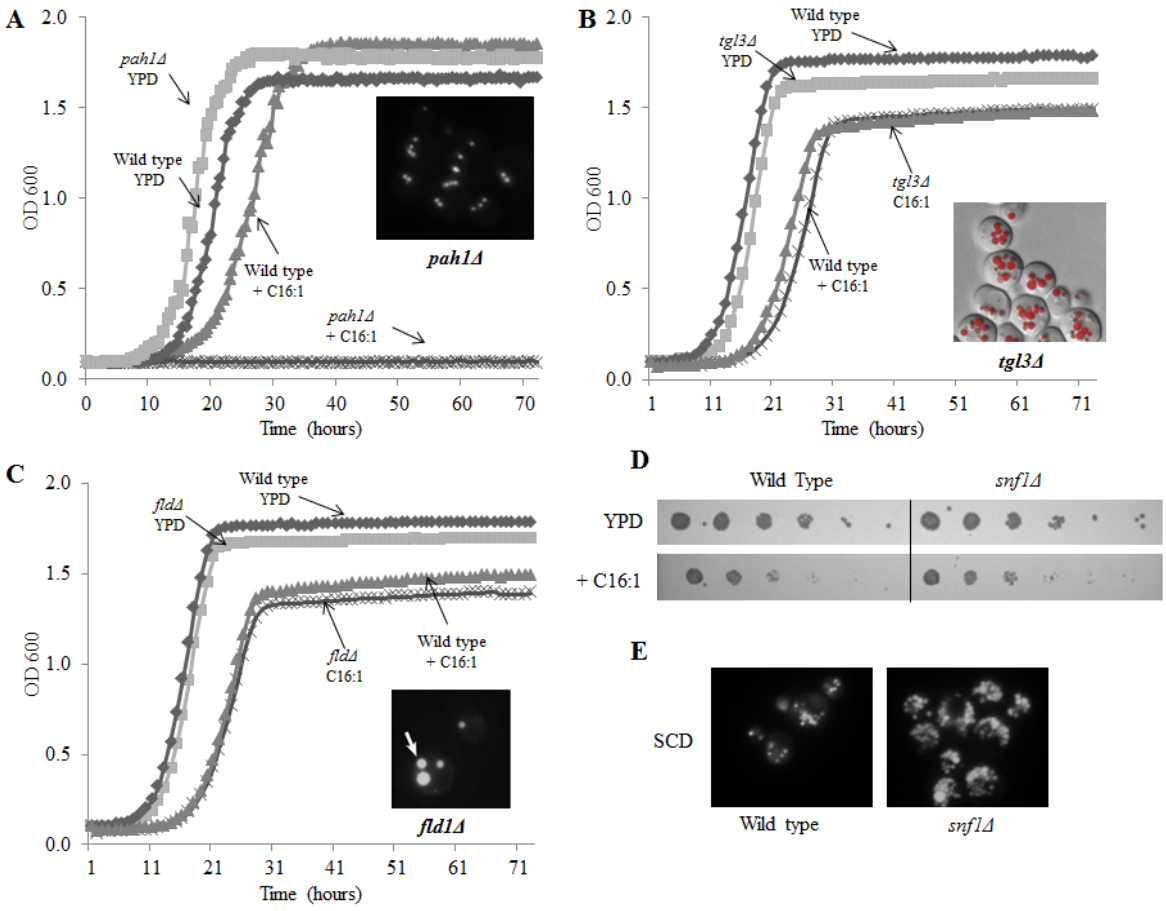

Figure 2-5: Defects in lipid droplet morphology does not always predict sensitivity to exogenous fatty acid. Growth curves of four single deletion strains (*pah1Δ*, *fld1Δ, tgl3Δ, snf1Δ*) known to cause defects in lipid droplet morphology in liquid (A-C) YPD with and without 0.5 mM palmitoleate (C16:1). (A) *pah1Δ* grown overnight in YPD and stained with Nile Red to confirm lipid droplet defects. (B) Oil Red O image of lipid droplet defects in *tgl3Δ* obtained from (Kohlwein *et.al*). (C) Nile Red images of *fld1Δ* [60]. (D) Serial dilutions of wild type and *snf1Δ* on YPD with and without 0.5 mM palmitoleate (C16:1). (E) Lipid droplet defects in *snf1Δ* grown overnight in SCD and stained with Nile Red.

Unsaturated fatty acid sensitive strains share several other sensitivity phenotypes. The 74 genes that had significant defects in "Max OD" and "Rate" growth curve variables, were tested under several additional growth conditions known to target sterol, sphingolipid and cellular stress pathways. We chose these conditions based on the known connections between fatty acid metabolism and other lipid pathways in order to gain insight into how these genes may be functioning in lipotoxicity.

Targeting sterol homeostasis with nystatin treatment. In yeast, oleate causes major changes in membrane phospholipid composition and increases membrane fluidity, which is thought to be a major cause of oleate induced toxicity [23]. Under conditions of oleate treatment, triglyceride synthesis and lipid droplet formation is increased but sterol ester (SE) synthesis is decreased through inhibition of the sterol acyltransferase, Are2p. It has been proposed that the inhibition of sterol esterification compensates for the changes in membrane fluidity, through an accumulation of membrane free sterols inducing increased membrane rigidity [189]. Therefore, defects in sterol homeostasis or an inability to properly regulate membrane SE levels could alter a cells ability to properly respond to UFA treatment.

In order to determine if palmitoleate sensitive mutants were defective in sterol metabolism, we used the polyene antibiotic, nystatin, which induces defects in the plasma membrane through binding of the drug with membrane free sterols. This binding results in the formation of transmembrane channels composed of polyene and sterol molecules followed by intracellular ion and metabolite leakage through these channels, leading to cellular dysfunction and death [190]. Consistent with the interaction between nystatin and sterol homeostasis, a mutation in sterol transporter gene, *ARV1*, sensitizes the cells to nystatin-induced cell death [58].

We tested the palmitoleate sensitive strains on several concentrations of nystatin (2.5, 5, 10 and 15 μg/ml) and found that the 66% of the 74 mutants tested were sensitive to nystatin compared to wild type (Fig 2-6 and Table S2-3). Screens for polyene antibiotic sensitivity in yeast have identified genes important in not only sterol homeostasis, but have also revealed a potential role for fatty acid pathways [191] and antioxidative defense mechanisms [192] in nystatin vulnerability. The commonality in gene deletions conferring sensitivity to both palmitoleate and nystatin are consistent with these previous studies, and demonstrate an interesting connection between FA-induced lipotoxicity and sterol metabolism.

Focusing on defects in sphingolipid metabolism using myriocin treatment. Sphingolipids are integrally involved in lipotoxicity, particularly in response to saturated fatty acid treatment [111]. Increased saturated fatty acids (SFAs) can enter the ceramide biosynthesis pathway, through action of serine palmitolytransferase (SPT). Ceramide is a potent inducer of apoptosis, and acts through the formation of channels in the mitochondrial membrane leading to protein release and mitochondrial permeabilization. Due to the role of sphingolipid metabolism in lipotoxicity and apoptosis, we tested the palmitoleate sensitive mutant strains for defects in sphingolipid homeostasis using the serine palmitolytransferase (SPT) inhibitor, myriocin.

Inhibition of the yeast SPT enzymes with myriocin blocks the rate-limiting step of sphingolipid biosynthesis, and depletes the cell of ceramide and complex sphingolipids IPC, MIPC and $M(IP)_2C$ [193]. Gene deletions vulnerable to myriocin are likely involved in an integral sphingolipid related pathway. Growth of the palmitoleate sensitive deletions on myriocin supplemented media caused growth inhibition in only three mutant strains, *aep1Δ, get3Δ* and *vma1Δ* (Table S2-3). Since palmitoleate does not channel into ceramide biosynthesis, it is not

surprising that there is little overlap between palmitoleate sensitive deletions and those inducing myriocin sensitivity and demonstrates that palmitoleate induced cell death in yeast is likely a ceramide independent process.

Targeting a mutant's ability to adapt to temperature stress. Adaptation to increased or decreased temperature depends on the "heat-shock" or "cold-shock" response respectively. These response mechanisms serve to alter gene expression for conservation of cellular function. Adaptive response to a shift in growth temperature includes alteration in sterol concentrations in the plasma membrane and modification of membrane phospholipid fatty acyl chains, both of which affect membrane fluidity. For instance, in response to cold stress in yeast, PL synthesis genes *INO1* and *OPI3* are upregulated and there is an immediate increase in the expression of the FA-desaturase *OLE1* [194, 195]. Action by these enzymes causes a small decrease in saturated phospholipid acyl chains and an increase in total unsaturated acyl chains, with increased C16:1 but decreased C18:1 [196], which together increase membrane fluidity and survival.

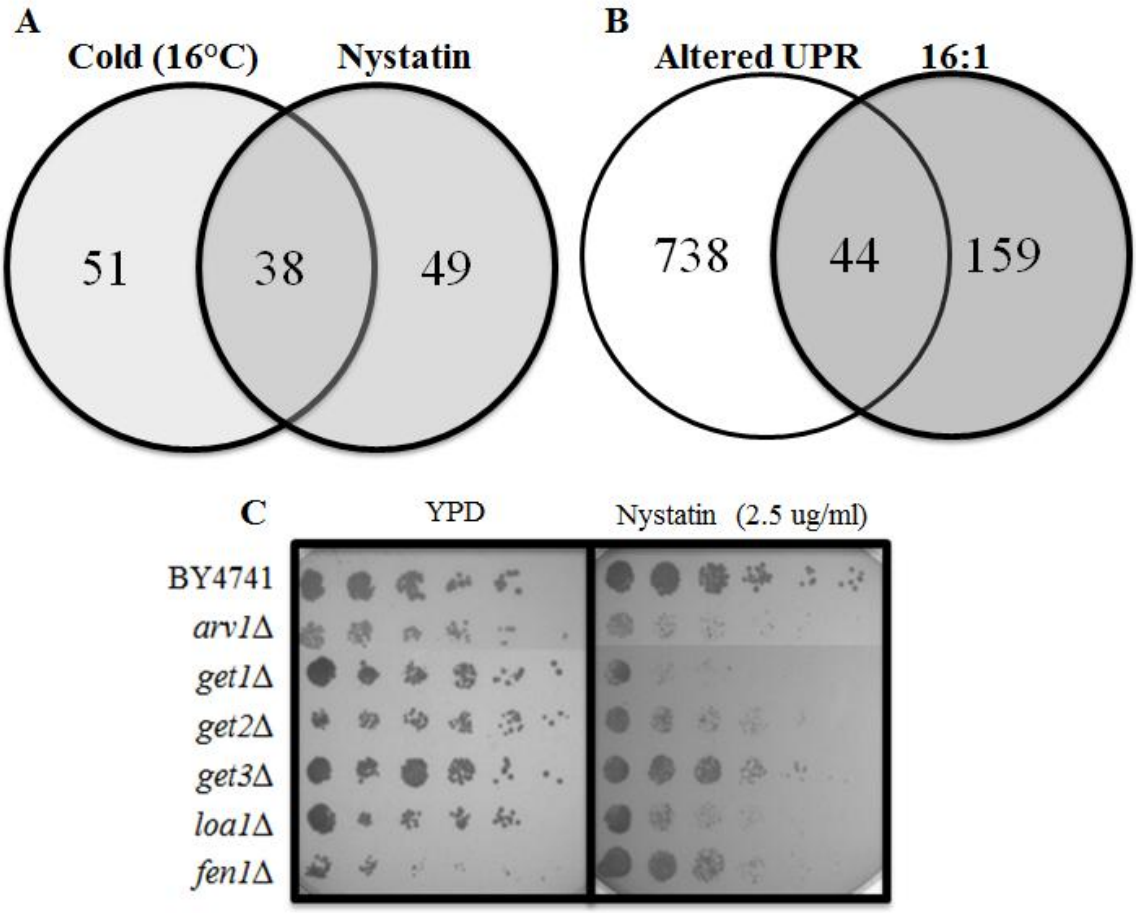

Figure 2-6: Gene mutations conferring sensitivity to palmitoleate sensitivity also have altered basal unfolded protein response (UPR) induction nystatin and cold sensitivity. **(**A)Top 80 16:0 sensitive mutants plated on rich media containing 2.5-15 μg/ml nystatin X myriocin and also under growth conditions of cold (16°) and heat (37°) stress for 3 days. Deletions were found to be sensitive to nystatin cold stress or in many cases both. (B) Gene hits from screen were compared to a HAC1 reporter screen in yeast tested for altered levels of basal UPR in single deletions [197] ~30% of palmtioleate sensitive hits were also identified in this screen. (C) Example of nystatin sensitivity in a subset of gene single deletions.

Since the response to a shift in temperature is so reliant on UFA levels and the integration of unsaturated fatty acyl-chains into membrane phospholipids, mutant strains sensitive to palmitoleate due to altered membrane FA composition may also be vulnerable to changes in growth temperature. In order to determine growth levels of the palmitoleate sensitive mutants in

conditions of temperature stress, we grew serial dilutions of each strain in high (37°C) and low (16°C) growth temperatures. Of the mutant strains tested, sixty-seven percent were sensitive to low temperature growth (16°C) (Fig 2-6 A and Table S2-3). The overlap between the palmitoleate sensitivity and cold sensitivity indicate that these strains have a defect in the ability to properly modulate the acyl chain distribution, membrane fluidity, and/or stress response associated with both lipid influx and cold shock.

Alternatively, there was a small number (10%) of palmitoleate sensitive mutants also sensitive to high temperature growth (Fig 2-6 A and Table S2-3). Mirroring cold shock response, growth of yeast at high temperatures is correlated with decreased unsaturation of lipids in order to counter the more "fluid" state of membranes at higher temperatures [198]. Heat shock induces a general down regulation of transcription for energy conservation, and an accumulation of trehalose and glycogen [199]. It is unclear why we see an obvious difference in susceptibility of palmitoleate sensitive single deletions to heat vs. cold stress but perhaps genes necessary for cold resistance are more reliant on unsaturated fatty acid detoxification and stress response mechanisms than heat stress.

Lipotoxicity and the UPR. ER stress is involved in both saturated and unsaturated fatty induced toxicity in both mammalian [142, 164] and yeast systems [22, 154]. Induction of ER stress typically occurs due to an accumulation of unfolded proteins, but can also be triggered by FFAs [129]. In yeast, ER stress induction occurs through stimulation of the transmembrane sensor Ire1p resulting in an activation of the Hac1p transcription factor [200]. Hac1p transcriptionally upregulates unfolded protein response (UPR) genes in order to adapt to altered ER homeostasis [201] . Using a Hac1p-GFP reporter construct Jonikas *et al.*, monitored basal levels of UPR in

the yeast knockout library and identified several hundred gene knockouts causing significantly altered levels of UPR [197]. There was a significant overlap (28%) between gene mutants found to be palmitoleate sensitive in this screen with those found to affect the UPR (Fig 2-6B and Table S2-3).

Together, these sub-screens demonstrate that many gene deletions inducing palmitoleate sensitivity are also sensitive to drugs targeting membrane sterols (nystatin) and conditions inducing alterations in membrane fluidity (16°C growth) but are not sensitive to an inhibition in ceramide biosynthesis (myriocin treatment). In addition, almost thirty percent of palmitoleate sensitive mutants had altered levels of UPR, a factor which likely contributes to their lipotoxic vulnerability.

Biological categories of palmitoleate sensitive gene deletions. The cellular processes represented most by the genes found causing palmitoleate sensitivity upon mutation include mitochondrial organization, RNA and DNA metabolism, cellular and vesicular transport, lipid metabolism, cellular respiration and a large number of genes with unknown function (Table 2-1 and Fig 2-7). Of the twenty-six genes with unknown function, three dubious open reading frames (ORF) overlap or are chromosomally adjacent to recognized yeast genes also identified in our screen. For example, the start codons between *YER084W* and *GET3 (YER083C)* are separated by only 34 base pairs (bp). The other two dubious open reading frames overlap with known genes, with a 16 bp overlap between *YNL198C* and *GCR2* (*YNL199C)* and a 302 bp overlap between *MRPL9* (*YGR220C*) and *YGR219C*. Therefore, these dubious ORF may alter the expression of their overlapping genes, and the palmitoleate sensitivities may instead be due to decreased expression of *GET3*, *GCR2* or *MRPL9*.

More detailed analysis of the 156 gene deletions revealed that 48 encode proteins from 12 protein complexes (Fig 2-7), implicating a role of these complexes in yeast lipid metabolism. Of the complexes identified, six are involved in RNA and DNA metabolism including the chromatin remodeling complexes SWR-1/INO80, and RSC; the histone acetyl/deacetylation complexes Rpd3L and SAGA-like (SILK); and the spliceosomal protein complex U6 snRNP. Additionally, genes encoding proteins involved in the cellular respiration complexes III and IV, both mitochondrial and cytoplasmic ribosomes and two vesicular trafficking complexes (GARP and GET) were identified as playing a role in protection against palmitoleate induced cell death (Fig 2-7). If a complex is involved in lipotoxic processes, we expect that a mutation in any part of the complex would impact palmitoleate sensitivity. Therefore, independent identification of several complex members increases screen confidence and highlights the importance of each complex in pathways involved in lipid sensitivity.

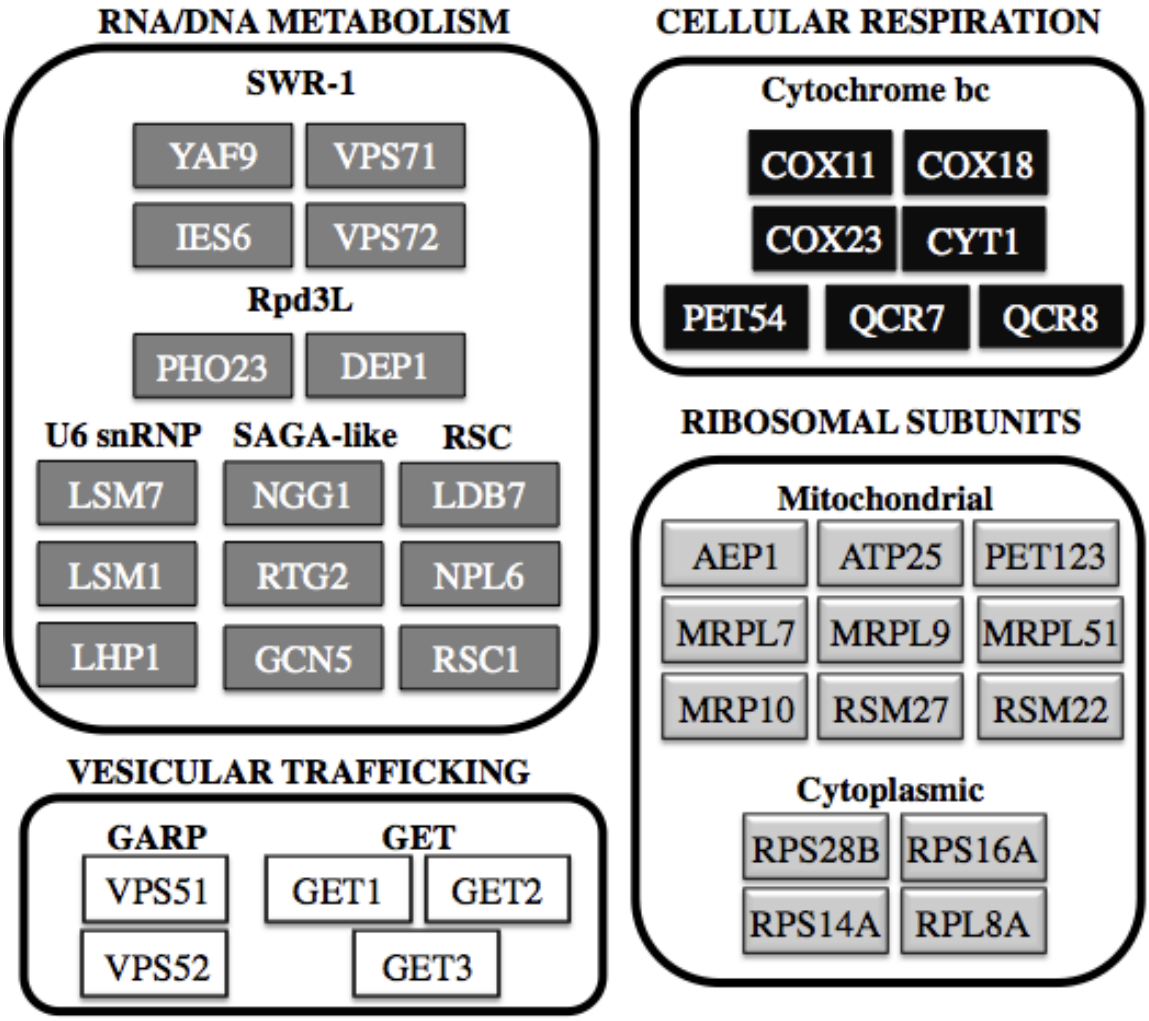

Figure 2-7 Yeast protein complexes represented by palmitoleate screen and grouped by cellular function. Complex information obtained from *Saccharomyces* genome database (SGD).

Lipid metabolism and transport. Past studies have highlighted the importance of triglyceride synthesis [7, 22, 23], fatty acid desaturation [155, 202-204] and elongation [202] in the maintenance of cellular function during periods of excess fatty acid exposure. Consequently, it is not surprising that mutations in multiple genes encoding lipid metabolism proteins cause increased palmitoleate sensitivity. The ten lipid metabolism genes identified are involved in

multiple metabolic pathways, including sphingolipid biosynthesis, lipid transport, mitochondrial fatty acid synthesis and phospholipid regulation.

Sterol and sphingolipid metabolism. The putative sterol transporter, *ARV1*, was the most sensitive deletion mutant identified by this screen (Table S2-1). As seen with the NL-deficient strain, *arv1Δ* was completely inviable in media containing 0.5 mM palmitoleate. Knockout of *ARV1* induces a defect in sterol transport from the ER to the plasma membrane, resulting in sterol accumulation in the ER membrane and a constitutively active unfolded protein response (UPR) [205, 206]. In addition to this gene effecting sterol transport, two sphingolipid metabolism genes, *CSH1* and *SCS7*, are sensitive to palmitoleate upon deletion (Table 2-1and Table S2-1). Protein transcripts of these genes are involved in the synthesis and hydroxylation of the long chain sphingolipids IPC, MIPC and $M(IP)_2C$ [207]. Sphingolipids and sterols been implicated in mammalian toxicity, with increased ceramide [111] and free sterols inducing cell death [206]. It is likely that mutations in these genes sensitize cells to lipid induced apoptosis through similar pathways to FA induced toxicity, including mitochondrial permeabilization [127], increased reactive oxygen species production [125] and the induction of ER stress[129].

Fatty acid modification. Modification of fatty acids through desaturation and elongation are common mechanisms of cellular adaptation to lipid load through their ability to moderate the levels of membrane lipid species [22, 23] and regulate channeling of FA into TG stores [7]. Knockout of the fatty acid elongase *FEN1* and the acyl-CoA dependent lysophosphatidic acid acyltransferase (LPAAT), *LOA1*, results in decreased viability with palmitoleate exposure (Table 2-1 and Table S2-2). Loa1p is involved in the maintenance of TG stores through synthesis of the

central lipid metabolite phosphatidic acid (PA) [10]. Though no other phospholipid synthesis gene mutants exhibited palmitoleate sensitivity, our screen identified a phospholipid gene regulator, transcription factor *DEP1* as important in the response to FA accumulation (Table 2-1 and Table S2-2). Mutations in these FA modification genes results in altered FA composition and storage within the cell both of which are necessary processes for protection against excess lipid load.

Alterations in acyl chain ratios (in either chain length or degree of unsaturation) or defects in pathways of lipid storage can result in oxidative damage [208] and ER stress [23, 80, 129] .

Mitochondrial fatty acid synthesis. In addition to cytosolic lipid metabolism genes, mutations in the mitochondrial localized fatty acid synthase (FAS) II confer sensitivity to palmitoleate, as identified by our screen. The mitochondrial FAS II complex differs from the eukaryotic FAS I system in that independent polypeptides enzymes carry out each reaction step and a deletion in any complex member results in a cell deficient in respiratory function [209]. Three of the five major FAS II enzymes were identified by our screen as being important regulators of palmitoleate tolerance. These enzymes are the predicted malonyl-CoA:ACP transferase (MCT1), the 3-ketoacyl-ACP synthase condensing enzyme (CEM1) and enoyl thioester reductase (ETR1) [209] (Table 2-1and Table S2-2). The end product of this pathway is the 8 carbon saturated fatty acid, octanoic acid (C18:0). Mitochondrial membrane phospholipid composition is altered in yeast with disrupted FAS II, supporting the idea that fatty acids synthesized by this complex are able to integrate into phospholipid acyl chains [210]. We therefore propose that dysfunction in FAS II results in altered mitochondrial phospholipid

membrane content and mitochondrial integrity, which is further compromised by a rise in intracellular UFA, leading to apoptotic initiation.

Mitochondrial Respiration. Reactive oxygen species (ROS) exist as either oxidants (such as hydrogen peroxide $H_2O_2^-$) or as reductants (such as superoxide O_2^-) and high levels of ROS can induce significant oxidative damage. These molecules are the major toxic metabolites responsible for lipid induced cellular dysfunction. Mitochondria are integral to eukaryotic lipotoxicity, and mitochondrial dysfunction results in the release of pro-apoptotic factors which initiate the cell death cascade [183]. ROS are produced during aerobic respiration, mainly through the leakage of electrons from the mitochondrial respiratory chain [211]. Mutations in key respiratory chain proteins are associated with increased mitochondrial reactive oxygen species production (ROS) and this rise in ROS is particularly high in mutants affecting the functions of respiratory chain complex III and IV [212]. We found that deletions in genes from both complex III and IV conferred sensitive to growth on palmitoleate. Three of the cytochrome bc1 (complex III) associated genes, cytochrome C1 (CYT1), and two ubiquinol cytochrome c reductase complex members (QCR7 and QCR8) were found by our screen to induce palmitoleate sensitivity upon deletion. Moreover, four gene deletions whose corresponding proteins are involved in respiratory complex IV function, *COX11, COX18, COX23* and *PET117,* were identified by our screen (Table 2-1and Table S2-2). Increased ROS resulting from deletions in these genes likely increase the cells susceptibility to lipid induced ROS production.

Vesicular trafficking. Vesicles are responsible for the transport of protein cargos between different organelles. This trafficking requires coat protein machinery (COPI/COPII), Rab-

GTPases for vesicle fusion and SNAREs for membrane tethering [213] . Screens for lipid droplet defects in yeast and *Drosophila* have demonstrated a relationship between vesicular trafficking and lipid droplet homeostasis [56, 57, 59, 60]. Knockdowns in components of the COPI machinery in *Drosophila* S2 cells results in larger, more dispersed droplets [56, 57] and blockage of retrograde trafficking (COPII) in yeast causes a lipid droplet accumulation, likely as a protective mechanism against secretory stress.

In this screen, deletions in genes encoding proteins of two vesicular trafficking complexes, GARP and GET, were found to be vulnerable to growth on palmitoleate containing media (Fig 2-7). The Golgi-Associated Retrograde Protein (GARP) complex is involved in endosomal tethering from the endosome to the Golgi, a key step in retrograde trafficking [214]. The GET, or Golgi to ER Trafficking, complex was initially described through a yeast secretory pathway screen as an important mediator of retrograde trafficking [215], but has now been identified as a required complex for tail anchored protein insertion [216]. Tail anchored (TA) proteins contain a C-terminal hydrophobic domain and an N-terminal cytosolic domain, and lack a signal peptide for organelle targeting. Instead, ER localized TA proteins require the GET machinery (Get1-3p) for targeting and insertion into the ER, by a signal recognition particle (SRP) independent mechanism [216].

Both the GET and GARP complexes have a role in retrograde vesicular transport, particularly in endosomal trafficking pathways. In addition to its role in TA protein insertion, Get3 functions as an endosomal gunanine nucleotide exchange factor. Get3p facilitated binding of GTP to the guanine nucleotide binding protein (G-protein) Gpa1 at the endosome initiates the production of phosphatidylinositol-3-phosphate [217], which has been implicated in endosomal maturation [218]. As a SNARE responsible for endosomal tethering, the GARP complex also

plays an important role in cellular processes requiring endosomal trafficking. The identification of these complexes in our screen introduces a potential role for endosomes in lipid homeostasis.

Vesicular transport is necessary for the exchange of lipids and proteins between organelles. Defects in trafficking causes protein mislocalization, induces the unfolded protein response (UPR) and increases cellular stress [22]. To date, it is unclear if the lipid droplet morphology phenotypes observed in vesicular transport mutants are due to a broad membrane trafficking defect or specific to particular complexes. These results indicate that palmitoleate sensitivity is specific to these complexes (GARP and GET) and not a general defect of altered cellular trafficking.

Vacuolar protein secretion mutants. *VPS* mutants are characterized as single deletions causing a sorting defect of the vacuolar glycoprotein carboxypeptidase Y (CPY) resulting in CPY secretion. Vacuolar proteins, such as CPY, are first inserted into the ER, travel to the Golgi through the secretory pathway and are sorted through the Golgi to the vacuole [219, 220]. The 61 *VPS* mutants have been grouped into 5 classes based on their vacuolar morphology, which can be visualized by fluorescent vacuolar membrane stains such as FM4-64 [221]. Class A has normal vacuolar morphology with three to ten sub-compartments within the cytosol. Class B has fragmented vacuolar structure, with twenty or more vacuole-like compartments. Class C mutants have no vacuolar structure whereas class D mutants have defects in vacuolar segregation resulting in a single large vacuole. Class E mutants have large prevacuolar compartments due to defects in the formation of intralumenal vesicles at the multivesicular body (MVB). Lastly, class F mutants have a central vacuole surrounded by many fragmented vacuolar structures [222] . Due to the high representation of vacuolar protein secretion (*VPS)* mutants identified in our

screen, we re-plated 61 *VPS* mutants [223] on palmitoleate to check for additional gene deletions that result in fatty acid sensitivity within this protein family.

This screen validated our original hits and identified several additional palmitoleate sensitive *VPS* deletions including the GARP complex members, *VPS53* and *VPS54*, Class D mutants *VPS15* and *VPS45* and Class C mutants *VPS16* and *VPS18* (Fig S2-2 and Table 2-4). The class B *VPS* mutants had the highest number of gene knockouts causing increased palmitoleate sensitivity (Table 2-4). These include the GARP complex members *VPS51, 52, 53* and *54* as well as *LOA1, VPS69, VPS71, VPS72* and *VPS73.* NL-deficient yeast have highly fragmented vacuoles, characteristic of that seen in Class B *VPS* mutants [23] and a similar vacuolar phenotype has been reported in mutants defective in fatty acid elongation [224], phosphatidic acid hydrolysis [225] and phospholipase C metabolism [226]. Defects in vacuolar fusion are evidently associated with altered lipid homeostasis though the mechanism explaining this connection this has yet to be identified

Table 2-4: Sensitivity of vacuolar protein sorting (VPS) mutants to palmitoleate. Sensitivity phenotype indicated as either completely inviable (++) or sensitive (+) compared to wild type, '--' indicates normal growth. See Figure S-1 for growth images.

***VPS* Class**	**Gene**	**Sensitivity phenotype**	***VPS* Class**	**Gene**	**Sensitivity phenotype**	***VPS* Class**	**Gene**	**Sensitivity phenotype**
Class A	*VPS8*	--	Class C	*VPS11*	--	Class F	*VPS1*	--
	VPS10	--		*VPS16*	++		*VPS26*	--
	VPS13	--		*VPS18*	++		*VPS62*	--
	VPS29	--		*VPS33*	--		*VPS65*	+
	VPS30	--	Class D	*VPS2*	--		*VPS68*	--
	VPS35	--		*VPS3*	--			
	VPS38	--		*VPS6*	--			
	VPS55	--		*VPS8*	--			
	VPS63	+		*VPS9*	--			
	VPS70	--		*VPS15*	++			
	VPS74	--		*VPS19*	--			
Class B	*VPS5*	--		*VPS21*	--			
	VPS17	--		*VPS45*	+			
	VPS17	--	Class E	*VPS4*	--			
	VPS39	--		*VPS20*	--			
	VPS41	--		*VPS22*	--			
	VPS43	--		*VPS23*	--			
	VPS51	+		*VPS24*	--			
	VPS52	+		*VPS25*	--			
	VPS53	+		*VPS27*	--			
	VPS54	+		*VPS28*	--			
	VPS64	--		*VPS31*	--			
	VPS66	++		*VPS32*	--			
	VPS69	++		*VPS36*	--			
	VPS71	+		*VPS37*	--			
	VPS72	+		*VPS44*	--			
	VPS73	+		*VPS46*	--			
	VPS75	--						

Histone modification, acetylation and deacetylation. In response to oleate exposure, cells alter their gene expression profile through the induction of genes required for fatty acid metabolism [227]. These gene expression changes result in increased peroxisomal β-oxidation, decreased protein translation and repressed glycolysis in order to adapt to the new source of energy [227-229]. Transcriptional regulation controls these changing expression patterns through chromatin remodeling processes controlled by chromatin binding of the histone variant Htz1p. Movement of Htz1p (H2A.Z) onto the nucleosome in exchange for the chromatin bound histone H2A requires the SWR1 complex [230]. This screen identified knockouts of three SWR1 complex members, *YAF9*, *VPS71* and *VPS72* as being sensitive to palmitoleate (Table 2-1 and Table S2-2). In addition, transcriptional activation of a portion of oleate responsive promoters requires the acetylation of Htz1p by Gcn5p/Esa1p [230]. A deletion in *GCN5* also had a significant growth defect on palmitoleate containing media (Table 2-1) further supporting a role for Htz1p transcriptional regulation in the activation of pathways protective against lipotoxicity.

Histone acetylation status contributes to gene activation and expression pathways, and is controlled through histone acetylases (HATs) and deacetylases (HDACs). We have found that 9 of the yeast genes associated with sensitivity to palmitoleate have histone acyltransferase or deaclyltransferase activity (Table 2-1 and Fig 2-2). Genes encoding the histone deacyltases HDAC complex, Rpd3L (*PHO1* and *DEP1*), are sensitive to palmitoleate upon deletion (Fig 2-2). The Rpd3-L complex is required for repression and induction of Environmental Stress Response (ESR) genes under several different conditions, lack of which causes major defects in the initiation of stress response. Additionally, three of the palmitoleate sensitive deletion strains belong to the SAGA-like (SLIK) histone acyltransferase complex (*NGG1*, *RTG2* and *GCN5*)

(Fig 2-2). This complex is required for gene regulation under conditions of mitochondrial dysfunction [231].

Together the identification of the Htz1 associated proteins (SWR-complex and GCN5) as well as the HAT and HDAC genes from this screen demonstrates that a proper transcriptional response to palmitoleate treatment may be necessary for the induction of protective pathways able to compensate for intracellular lipid accumulation.

DISCUSSION

In this study, we identified novel genes and pathways integral in the protection against lipid induced cell death in the yeast model organism *S. cerevisiae*. Our screen is unique in that we focused on sensitivity to lipids in rich media containing both glucose and fatty acids, a condition which caused severe toxicity in the NL deficient mutant (*are1Δ are2Δ dga1Δ lro1Δ*). Ablation of the triglyceride synthesis enzyme DGAT1 in mouse fibroblasts results in severe sensitivity to unsaturated fatty acids, similar to that seen in the NL-deficient yeast strain [7, 22, 23]. Unsaturated fatty acids have also been shown to induce toxicity in some mammalian cell types including liver cell lines [119, 124] and primary rat pancreatic β- cells [123] without genetic manipulation. The concentration needed to induce toxicity with UFA tends to be greater (~1.0 mM) than that needed to induce toxicity with SFA (~0.25 mM) but gene mutations resulting in sensitivity to either UFA or SFA will increases susceptibility for lipotoxic disease progression. Thus identification of mammalian genes involved in these processes is crucial in understanding the genetics of obesity related disease.

A primary goal of this study was in the identification of mammalian genes that play a role in lipotoxic diseases such as type 2 diabetes. Using methods of sequence alignment (NCBI: Basic Local Alignment Search Tool) we determined that a large proportion of the 156 yeast genes identified by this screen have been conserved throughout evolution with 68 (44%) genes having human and murine orthologs (Table S2-2). Since the concentration of fatty acid used in this study (0.5 mM) is at a level of similar to that normally occurring in human serum [232] many of these orthologs may have a similar fatty acid sensitivity upon knockdown in mammalian cell types.

Eleven of these orthologs have been previously associated with metabolic diseases, diabetic phenotypes or stress induced apoptosis (Table 2-5). This provides an interesting connection between known metabolic genes and lipotoxic pathways and provides a potential mechanism for these associations. The diabetic phenotypes linked to these orthologs include defects in glucose homeostasis, altered insulin secretion, and genetic association with T2D in human populations. ASNA1, the *GET3* ortholog, was shown to positively regulate insulin secretion in both *C. elegans* and mammalian pancreatic β-cells [233] though the mechanism of this regulation is still unclear. Moreover, altered expression of the mouse ortholog of yeast palmitoleate sensitive gene, *ITR1* (mouse GLUT2) results in pancreatic β-cells dysfunction. Specifically, mammalian GLUT2 is an insulin-independent glucose transporter integral in glucose sensing in pancreatic β-cells. Inactivation of GLUT2 in mice by homologous recombination resulted in hyperglycemia, hypoinsulinemia and high plasma free FA [234].

Genome-wide association studies reported polymorphisms in mammalian orthologs of *PCP1* (presenilin associated, rhomboid-like (PARL), *IFM1* (mitochondrial initiation factor 2 (MTIF2)) and *FEN1* (elongation of very long chain fatty acids protein 6 (ELOVL6)) to be associated with increased risk for type 2 diabetes [235, 236]. The identification of the yeast orthologs of these genes in our screen indicates a potential connection between the diabetic phenotypes associated with these mammalian genes and cellular dysfunction due to increased lipid sensitivity.

The mammalian ortholog of yeast *GCN5* (also known as GCN5) is a histone acyltransferase (HAT) that directly acetylates peroxisomal proliferators gamma coactivators PGC1α and PGC1β [237, 238]. The PGC1 family of transcriptional coactivators is involved in broad glucose and lipid metabolism regulation and a potential target in the treatment of

metabolic disorders. GCN5 repression of PGC1β in primary skeletal muscle cells results in decreased GLUT4 expression and reduced insulin mediated glucose transport [237].

Table 2-5: Mammalian orthologs of screen identified yeast genes previously associated with glucose homeostasis insulin secretion dyslipidemia or oxidative stress. Associations determined through the National Center for Biotechnology (NCBI) database National Human Genome Research Institute catalog of published genome-wide association studies (genome.gov) and HuGE Navigator human genome database.

Palmitoleate sensitive yeast gene	Human Ortholog	Previous associations with the metabolic syndrome
GET3	ASNA1 (46.5%)	ASNA-1 positively regulates insulin secretion in C. elegans and mammalian cells. [233]
PCP1	PARL (32.3%)	Leu262Val polymorphism of PARL is ssociated with earlier onset of T2D [235]
ARV1	ARV1	Decreased expression of ARV1 results in cholesterol retention in the endoplasmic reticulum and abnormal bile acid metabolism. [239]
GCN5	GCN5 (46%)	GCN5-mediated transcriptional control of the metabolic coactivator PGC1β through lysine acetylation [237]
FPS1	AQP9 (28%)	Gene expression of paired abdominal adipose AQP7 and liver AQP9 in patients with morbid obesity: relationship with glucose abnormalities. [240]
IFM1	MTIF2 (36%)	Genetic association analysis of 13 nuclear-encoded mitochondrial candidate genes with type II diabetes mellitus: the DAMAGE study. [241]
ITR1	GLUT2 (27%)	GLUT2 was thus demonstrated to be required to maintain normal glucose homeostasis and normal function and development of the endocrine pancreas [234]
MDJ1	DNAJB9 (46%)	MDG1/ERdj4 an ER-resident DnaJ family member suppresses cell death induced by ER stress. [242]
FEN1	ELOVL6 (30.6%)	ELOVL6 genetic variation is related to insulin sensitivity[236]
MGR2	ROMO1 (43%)	Serum deprivation-induced reactive oxygen species production is mediated by Romo1 [243]
ETR1	MECR (36.4%)	Structural enzymological studies of 2-enoyl thioester reductase of the human mitochondrial FAS II pathway: new insights into its substrate recognition properties. [244]

As seen with the yeast system (Fig 2-7), many of the human orthologs can be grouped into the cellular processes of DNA and RNA metabolism, mitochondrial respiration and vesicular trafficking (Fig 2-8). Several deletions of yeast mitochondrial respiration complex III and IV members and genes essential for mitochondrial DNA maintenance were identified as palmitoleate sensitive by our screen (Table 2-1 and Table S2-2). Mammalian mitochondrial respiratory genes BCS1L, COX11 and COX18 genes have all been conserved in sequence and function to their yeast orthologs *BCS1* (50% identity), *COX11* (54% identity) and *COX18* (24.7% identity) (Table S2-2). Furthermore, the retrograde trafficking SNARE, GOSR1 and the vesicular trafficking GTPase, Arfgap2 were also found to have high sequence identity to two genes identified by our screen, *GOS1* and *GLO3*. Deletions in these genes results in vesicular trafficking defects, specifically in retrograde (Golgi to ER) transport, and likely function in lipid metabolism similarly to the yeast system.

Yeast is a powerful model system for studying mammalian lipid disorders due to the high evolutionary conservation of lipid metabolism machinery [149]. Regardless, there is an obvious difference in the vulnerability of yeast and mammals to saturated fatty acids (SFA) such as palmitate. SFA are considered more toxic than UFA in mammalian cells [182], whereas yeast are resistant to SFA induced cell death [22, 23]. This resistance may be explained by yeasts ability to rapidly elongate and desaturate SFAs to meet the requirements of the cell [23].

Despite this obvious difference, there are many parallels in the mechanisms of lipotoxicity between yeast and mammals. For instance, deletion of the yeast fatty acid elongase, *FEN1*, results in sensitivity to the SFA, palmitate, likely due to its inability to properly elongate fatty acids and maintain “normal” proportions of phospholipid acyl-chain species (ie C16:C18 ratio) (Fig 2-3C). In mammals, overexpression of the ortholog of *FEN1*, the FA elongase

ELOVL6, increases SFA sensitivity in pancreatic β-cells through increased elongation of palmitate to stearate [202]. Altered acyl-chain ratios have been shown to cause major changes in membrane fluidity and increase vulnerability to ER stress [176] and regulation of FA elongation in both yeast and mammalian systems increases levels of lipotoxicity. Moreover, disruption of the yeast phospholipid synthesis through deletions in the phosphatidylethanolamine methyltransferase (PEMT) genes, *OPI3* or *CHO2,* in a TG-deficient (*dga1Δ lro1Δ*) background results in a marked sensitivity to 0.5 mM palmitate. This further highlights the essential connection between neutral lipid and phospholipid synthesis, where loss of both results in fatty acid vulnerability [22].

In conclusion, this screen has identified a comprehensive list of eukaryotic gene deletions resulting in UFA sensitivity and provided new information regarding pathways essential in cellular response to lipid accumulation. In addition, we have implicated 68 mammalian genes in lipotoxic disease through sequence homology, 55 of which are unprecedented. Future research into the role of these genes in human metabolic disease is necessary, and may provide significant insight into lipid induced cellular dysfunction in mammalian systems.

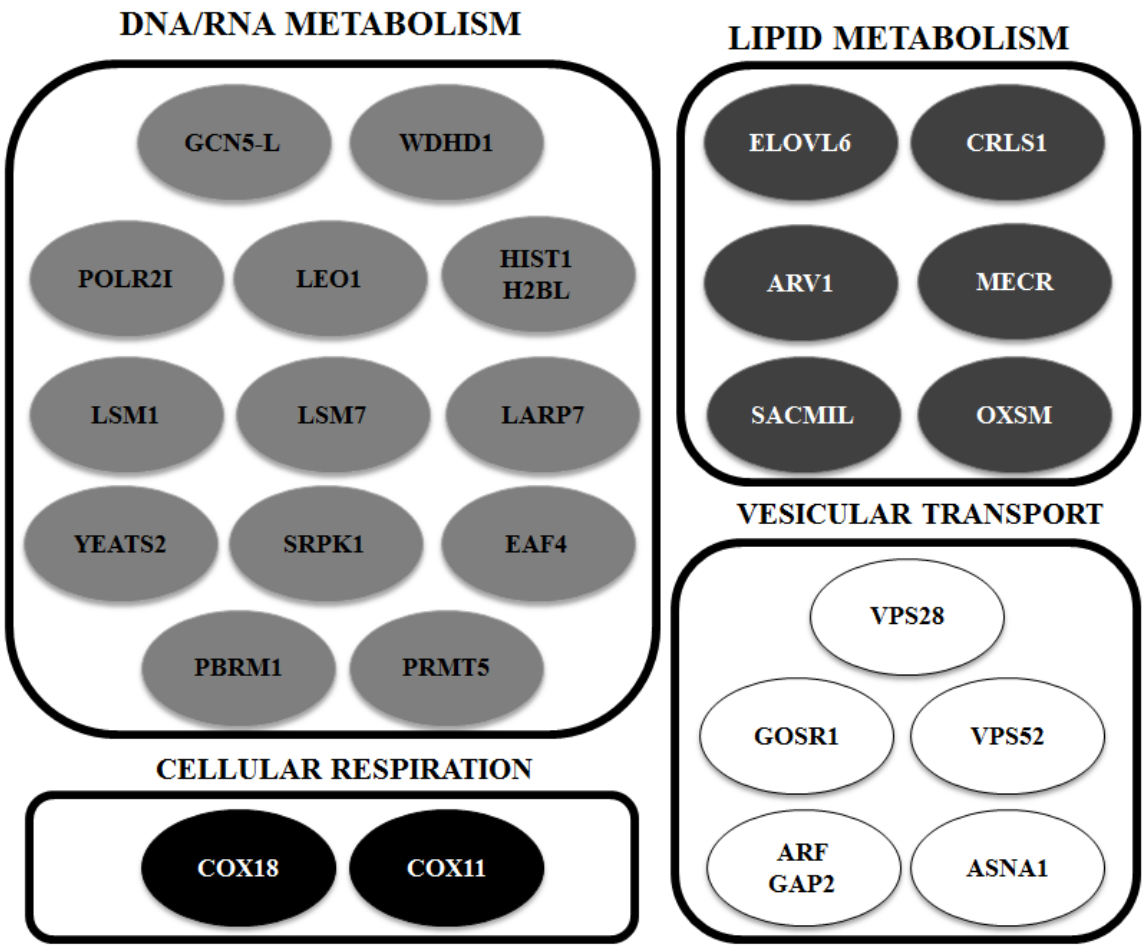

Figure 2-8: Mammalian orthologs represented by palmitoleate screen grouped by cellular function. Biological function information from National Center for Biotechnology (NCBI) and Biobase PROTEOME database.

CHAPTER 3

Golgi to endoplasmic reticulum trafficking protein, GET3, plays an integral role in lipid droplet homeostasis through regulation of vacuolar lipolysis.

ABSTRACT

A genome-wide palmitoleate sensitivity screen in yeast identified the Golgi to ER Trafficking (GET) complex as having an important role in yeast lipid metabolism and lipotoxicity. The GET complex is integral to tail-anchored protein insertion into the ER membrane and ablation of this complex results in inefficient protein insertion and localization. Due to its high evolutionary conservation we focused on the cytosolic member of the complex, Get3p. Deletion of *GET3* causes a reduction in lipid droplet number, decreased neutral lipid synthesis and a vulnerability to palmitoleate-induced apoptosis. Additionally, a double mutant lacking both *GET3* and the triglyceride synthesis gene *DGA1* had a significant reduction in lipid droplet number compared to both single deletion strains. This decrease is not due to a reduction in neutral lipid mass, but instead appears to be due to a subcellular mislocalization of neutral lipids, with an accumulation of lipid droplet-like structures in the vacuole of the *get3Δ dga1Δ* double mutant. We also demonstrate that *get3Δ* mutants have a reduction in autophagic flux, as measured by GFP-ATG8 cleavage and decreased survival under nitrogen starvation condition, indicating defective autophagosome flux. This defect is likely due to abnormal vacuolar lipolysis, as protease activity and vacuolar pH were both normal in these mutants. *GET3* is also a guanine nucleotide exchange factor (GEF), extending its role beyond tail anchored protein insertion. As a GEF, *GET3* activates an endosomal signaling cascade which has been implicated in endosomal maturation and trafficking. We suggest that a deletion in *GET3* results in decreased trafficking of a vacuolar lipase through a block in endosomal maturation, causing reduced vacuolar lipid recycling and defective neutral lipid turnover.

INTRODUCTION

Baker's yeast (*Saccharomyces cerevisiae*) is an excellent tool for the identification and characterization of novel pathways involved in mammalian lipotoxicity and lipid droplet biogenesis due to the evolutionary conservation of lipid metabolic mechanisms. Yeast neutral lipid enzymes and many lipid droplet associated proteins have been conserved in both sequence and function to their mammalian counterparts [8, 13, 20]. The ACAT related enzymes Are1p and Are2p are responsible for all sterol esterification [245] whereas diacylglycerol esterification is mediated by *LRO1* (a lecticin-acyl-CoA acyltransferase (LCAT) ortholog) during logarithmic growth [246]and *DGA1* (the sole DGAT2 ortholog) during stationary phase [14]. Ablation of all four yeast neutral lipid synthesis genes (*ARE1, ARE2, DGA1* and *LRO1*) results in a complete loss of cytosolic lipid droplets and a pronounced sensitivity to unsaturated fatty acids (UFA) [22, 23]. Quadruple mutations are unlikely to occur in nature, and thus a yeast screen for single mutants conferring sensitivity to the UFA palmitoleate (C16:1) was completed in order to identify genes involved in the mechanisms of lipotoxicity. From this screen, we identified 156 gene deletions with increased sensitivity to the UFA (chapter 2). Of these deletions, several genes are known to encode proteins involved in vesicular trafficking were identified, particularly the GARP endosomal tethering complex and the GET complex. The three primary members of the GET complex (GET1-3) were identified as conferring sensitivity to palmitoleate upon deletion, and thus function in an important mechanism involved in fatty acid tolerance.

The GET complex was initially identified in an epistatic miniarray profile (E-MAP) method designed to identify gene clusters likely involved in the same biological pathway. This group showed that the three GET complex members (Get1-3) are functionally related and act together in an integral ER/Golgi trafficking process [215]. Subsequently the GET complex was

found to be essential in mediating the post-translational insertion of tail-anchored (TA) proteins into the ER membrane [216]. TA protein insertion is independent and distinct from the classical signal recognition particle (SRP)-dependent pathway which is the primary mode of insertion for the majority of ER membrane proteins. TA proteins are characterized by a single 30 residue C-terminal transmembrane domain (TMD) and an N-terminal cytosolic domain and make up 3-5% of all membrane proteins [247]. The cytosolic member of the complex, Get3p, binds the TA protein TMDs through a large, hydrophobic, composite groove and subsequently tethers to the N-terminus of the ER resident protein Get2 [248, 249]. Get1, which is found tightly associated to Get2 at the ER membrane, mediates TA protein release into the membrane by forcing the transition of Get3 from a closed to an open conformation [250] (Fig 3-1).

More recently, two additional GET complex members were identified, Get4p and Get5p [197]. Together with the scaffolding protein, Sgt2p, these proteins form the TMD recognition complex (TRC), and are able to differentiate between the mitochondrial and the ER TA-protein TMD sequences. The C-terminal domain of Sgt2 recognizes TA proteins, and following this recognition, Get4 and Get5 facilitate the transfer of ER TA proteins to Get3 [251] (Fig 3-1). Knockout of either *GET4* or *GET5* caused mislocalization of the TA proteins Sed5p-GFP from Golgi to a diffuse pattern as well as a relocalization of Pex15 to the mitochondria [248].

Our palmitoleate sensitivity screen indicated a link between the GET complex members and lipid homeostasis. We chose to specifically focus on the role of Get3p in lipid metabolism due to its high evolutionary conservation, with orthologs in all eukaryotes [252]. The goal of this study was to determine by what means mutations in *GET3* alter lipotoxicity and lipid droplet homeostasis using the yeast model organism, *S. cerevisiae*. We propose that defects in lipid

droplet homeostasis resulting from a *GET3* deletion are due to slowed vacuole turnover and are independent of tail anchored protein misinsertion.

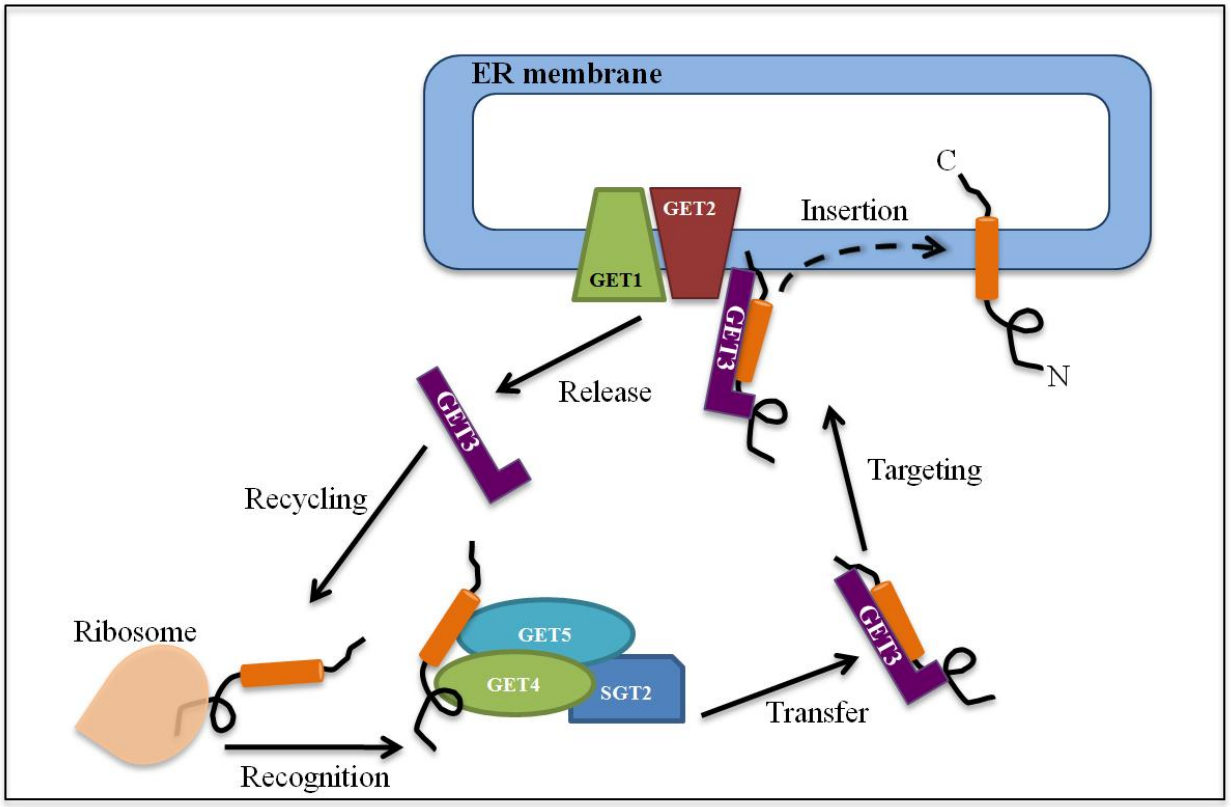

Figure 3-1: Tail anchored protein insertion into the endoplasmic reticulum by the GET complex machinery. The transmembrane domain recognition complex (TRC) made up of Get4p, Get5p and Sgt2p recognizes newly synthesized tail anchored proteins and directs them to Get3p which subsequently localizes to the ER membrane. Get3p then docks to the membrane bound Get1p and Get2p and together these proteins insert the protein into the membrane and Get3p is released for further binding capabilities. See introduction for details [247].

.

MATERIALS AND METHODS

Yeast General. Molecular biology and yeast procedures were performed according to conventional methods. Complete (YPD; yeast extract, peptone, dextrose), synthetic complete (SC), selective media and 5-fluoroorotic acid (5-FOA) were prepared as described previously [177]. All yeast strains (Table 3-1) used in this study were derived from s288C (Open Biosystems), with the exception of SCY2021 (*are1::HIS3 are2::LEU2 dga1::URA3 lro1::URA3*) which is derived from W303[178]. All single mutants were obtained from Open Biosystems Yeast Knock Out Strain collection (Cat # YSC1053). Double mutants were generated using the one-step PCR-mediated gene disruption protocol [253] in which PCR products containing 20 nucleotides of the selection cassette (*Kluyveromyces lactis URA3* or Nourseothricin resistance cassette) and 50 nucleotides of the gene specific sequence were generated prior to transformation. PCR products and plasmids were introduced into the host strain via lithium acetate transformation [254] followed by selection and PCR confirmation. ATG8-GFP [255] and SEC63-RFP [256] plasmids were a kind gift of Dr. Elizabeth Miller. When indicated, fatty acids were added to media in 0.6% ethanol:tyloxapol (5:1, v/v) with the designated quantity of fatty acid (Sigma; Palmitoleate and Oleate as a 10% w/v stock in ethanol).

Table 3-1: Yeast strains used in these studies. All Strains except for SCY325 and SCY3256 have a BY4741 background

Yeast Strain	**Genotype**
BY7471 Wild Type	Normal MATa *his3Δ1 leu2Δ0 met15Δ0 ura3Δ0*
get1Δ (ygl020cΔ)	*get1Δ::KANMX*
get2Δ (ygl083cΔ)	*get2Δ::KANMX*
get3Δ (ydl100cΔ)	*get3Δ::KANMX*
dga1Δ (yor425cΔ)	*dga1Δ::KANMX*
lro1Δ (ynr008wΔ)	*lro1Δ::KANMX*
arv1Δ (ylr242cΔ)	*arv1Δ::KANMX*
ybl100cΔ	*ybl100cΔ::KANMX*
gos1Δ (yhl031cΔ)	*gos1Δ::KANMX*
SCY 3370	*dga1Δ::URA3 get3Δ::KANMX*
SCY 3384	*dga1Δ::KANMX get2Δ::URA3*
SCY 3391	*dga1Δ::KANMX get1Δ::URA3*
SCY 3416	*dga1Δ::URA3 get3Δ::KANMX lro1Δ::NAT*
SCY 3411	*dga1Δ::KANMX get2Δ::URA3 lro1Δ::NAT*
SCY 3408	*dga1Δ::KANMX get1Δ::URA3 lro1Δ::NAT*
SCY 3407	*lro1Δ::NAT get3Δ::KANMX*
SCY 3405	*lro1Δ::NAT get2Δ::KANMX*
SCY 3402	*lro1Δ::NAT get1Δ::KANMX*
SCY 3421	*dga1Δ::KANMX lro1Δ::NAT*
SCY 3423	*dga1Δ get3Δ::KANMX* (5-FOA URA3 disruption of SCY 3370)
SCY 3427	*dga1Δ get3Δ::KANMX lro1Δ::NAT* (5-FOA URA3 disruption of SCY 3416)
SCY 325	W-303normal
SCY 3256	*W-303 are1Δ::HIS3 are2Δ::LEU2 dga1Δ::URA3 lro1Δ::URA3*

Growth Assays. Yeast strains were plated in serial dilutions from overnight cultures and grown at 30°C for 3 days. For liquid growth assays, overnight cultures were used to inoculate liquid media such that the starting optical density was 0.1 (A600 nm) and growth curves were obtained using a Microbiology Workstation Bioscreen C (Thermo Electron Corp.) and Research Express Bioscreen C software (Transgalactic Ltd). Three isolates per genotype were normalized to an Absorbance (OD600) of 0.1 and 10 µl of each strain was added to 290 µl of media per well and grown at 30° for 4 days and averaged in order to produce the final growth curve.

Apoptosis Assays. Yeast apoptosis was assessed using Annexin V binding and propidium idodine staining using the FITC Annexin V/Dead Cell apoptosis kit (Molecular probes V13242). Cells were washed with sorbitol buffer (1.2 M Sorbitol, 0.5 mM Magnesium Cloride, 35 mM Potassium Acetate ph 6.8), digested with 5.5% gluculase and 15 U/ml lyticase in sorbitol buffer and resuspended in Annexin/PI for 20 minutes [257].

Fluorescence Microscopy. Yeast cells were grown in specified media overnight or to log phase growth (OD600= 0.4-0.8) when specified. For lipid droplet analysis, cells were stained with Nile Red (1 µg/ml) (Sigma-Aldrich N3013) and visualized with a long pass GFP filter (excitation 440 nm). For quantification, 10 frames 0.25 µm apart were captured and displayed as maximum intensity projections. Lipid droplets were counted for 6 frames per strain, with 15-30 cells in each frame. Statistical analysis was carried out by comparing variation within frames. C1-BODIPY 500/510-C12, BODIPY 493/503, FM4-64, and CMAC-Arg were all purchased from Molecular Probes (Invitrogen). Cells treated with the neutral lipid stain BODIPY 493/503 were grown overnight and stained with 1.25 µg/ml for 30 minutes at 30°C and washed 3 times with

PBS prior to visualization. The long-chain fatty acid analog C1-BODIPY 500/510-C12 was added from a 5 mM ethanolic stock to 1 ml of cells at a final concentration of 50 µM and incubated for 60 seconds followed by 3 washes in 50 µM fatty acid-free BSA (Sigma-Aldrich) in PBS [258]. Vacuolar staining was carried out using FM 4-64 (Molecular Probes) lipophic dye as previously described [259]. Briefly, cells were incubated for 2 hours in YPD with 0.03 µM FM4-64, washed once with ddH_2O and visualized using a Texas red filter. CMAC-Arg (7-amino-4-chloromethylcouramrin, L-arginine-amide) was used as a probe for veast vacuolar protease cleavage (Molecular Probes, Y-7531) as per the manufacturer's instructions. For Oil red O staining, cells were fixed in 4% formaldehyde in PBS for 20 minutes and washed twice in PBS. The cells were then stained with 0.2% Oil Red O (Sigma) in H_2O:isopropanol (1:1) for 15 minutes followed by fluorescent imaging. All microscopy was performed using a Zeiss Axiovert 200 M using a 63x oil immersion objective and images taken by a Hamamatsu Orca-ER camera.

Lipid Analysis and Metabolic Labeling. Yeast lipid labeling was performed using [9,10- ^{3}H] Oleic acid and [9,10- ^{3}H]palmitic acid (PerkinElmer Life Sciences) labeling by growth with 0.1 µCi/ml overnight at 30°C. Lipids were isolated by hexane/isopropyl alcohol (2:1) organic extraction of dried cell pellets and resolved by TLC in petroleum ether/diethyl ether/acetic acid (84:15:1). Lipids were then detected using iodine staining and quantified with scintillation counting [14]. Phospholipids were separated using a 2 solvent system. Lipids were extracted as described above, resolved first in ether:diethyl ether:acetic acid (84:15:1), followed by a second solvent system of chloroform:methanol:acetic acid:H_2O (60:50:1:4).

Subcellular fractionation. Membranes were prepared from cells grown for 18 hours in YPD with [9,10- ^{3}H] Oleic acid and organelle fractionation was completed as previously described [205]. 200 µl of each fractions was resuspended in H_2O:isopropanol (4:1) followed by extraction twice with hexane and analysis by TLC separation and scintillation counting. 15 µl of each fraction were used for western blot analysis of marker proteins. Protein extracts from yeast or mammalian samples were applied to 12% SDS-PAGE gels and transferred to nitrocellulose membranes. Membranes were then blotted with corresponding primary antibodies and secondary antibodies, and proteins bands were detected by ECL immunodetection system.

Electron microscopy. Cells were grown to mid-log phase, prefixed in glutaraldehyde and postfixed in potassium permanganate. They were then dehydrated by graded ethanol series and embedded in Spurr's resin [260]. Cells were thick sectioned and stained with Reynold's lead citrate followed by visualization on a transmission electron microscope [261].

Autophagy assay. A GFP-ATG8 plasmid was transformed into indicated strains and grown in SCD-URA to mid-log followed by 3 hours of starvation in nitrogen deficient SD-N medium (0.17% yeast nitrogen base without amino acids and ammonium sulfate, 2% glucose). Cells were visualized via fluorescent microscopy and protein was isolated as previously described [89]. Protein concentrations were determined by BCA assay (Bio-Rad) and 20 µg total protein was loaded onto a 12% SDS-PAGE gel and separated by electrophoresis. Proteins were transferred to nitrocellulose and analyzed by Western blotting techniques suing a mouse anti-GFP monoclonal antibody (Santa Cruz).

Nitrogen starvation growth. Log phase growth cultures grown in YPD were shifted to nitrogen deficient media (SD-N) and grown for 8 days. Viability was measured by plating aliquots on YPD and counting colonies every 2-3 days [262].

RESULTS

Mutations in GET complex members confer sensitivity to the unsaturated fatty acid palmitoleate. We previously identified single deletions in *GET1-3* in the genome-wide fatty acid sensitivity screen as being sensitive to the monounsaturated fatty acid palmitoleate (chapter 2). We validated these results on liquid and solid media and found that all three mutants were sensitive to 0.5 mM palmitoleate (C16:1) but were not sensitive to oleate (C18:1) or palmitate (C16:0) (Fig 3-2A-C). Two additional GET complex members, *GET4* and *GET5*, were not identified by our screen, but were tested for palmitoleate sensitivity through serial dilution growth on 0.5 mM palmitoleate. In contrast to the other complex member deletions, these mutants did not show any sign of sensitivity to any of the fatty acids tested (Fig 3-2C). Get4p and Get5p are members of the transmembrane domain recognition complex (TRC), along with the scaffolding protein, Sgt2p [247]. The lack of sensitivity of these mutants to palmitoleate treatment indicates that these genes are dispensable in the GET complex dependent lipid metabolism pathway.

GET3 has been exceptionally well conserved over evolutionary time, with orthologs existing in all eukartyotes and some prokaryotes [252]. For this reason, we chose to focus primarily on the role of *GET3* in eukaryotic pathways of lipotoxicity. Treatment of *get3Δ* with 0.5 mM palmitoleate for five hours resulted in increased cell death, as measured by Annexin V staining of externalized phosphatidylserine and internalization of propidium iodide (PI) (Fig 3-3A).

Quantification of Annexin V/PI positive cells found a significant increase in both Annexin V and PI staining in palmitoleate treated *GET3* mutants (7.9% Annexin + and 10.8% PI +) compared to palmitoleate treated wild type cells (3.2% Annexin + and 3.6% PI +) (Fig 3-

3A,B). Overnight treatment with valproic acid was used as a positive control for yeast apoptosis, causing death in 100% of cells within the collected frames (Fig 3-3A). Valproic acid is an inhibitor of histone deacetylases (HDACs) in mammalian cells [263] and induces yeast apoptosis dependent on the caspase-like protein Yca1p [264]. We observed a majority of dead cells (PI+) costained with Annexin V, indicating an apoptotic response (Fig 3-3). A similar apoptotic response was reported in NL-deficient mutants treated with unsaturated fatty acids [22].

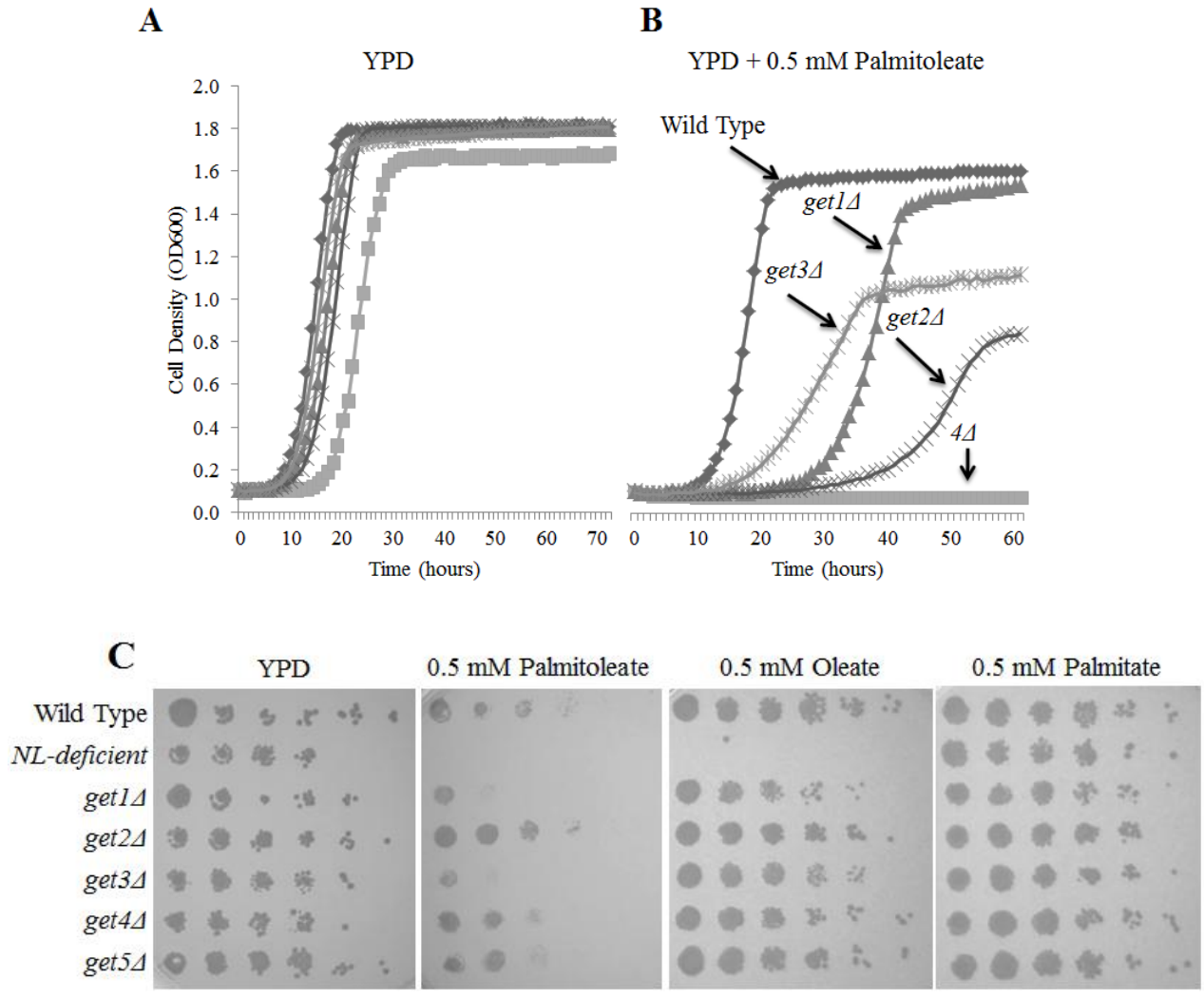

Figure 3-2: Mutations in GET1-3 result in sensitivity to palmitoleate in liquid and solid media. (A,B) Growth curve analysis using Bioscreen C workstation in YPD ± 0.5 mM palmitoleate (16:1). *4Δ* refers to the neutral lipid deficient *are1Δ are2Δ dga1Δ lro1* strain. (C) Growth on solid media (YPD ± 0.5 mM indicated fatty acid), plated at 5 fold serial dilutions and grown for 2 days at 30°

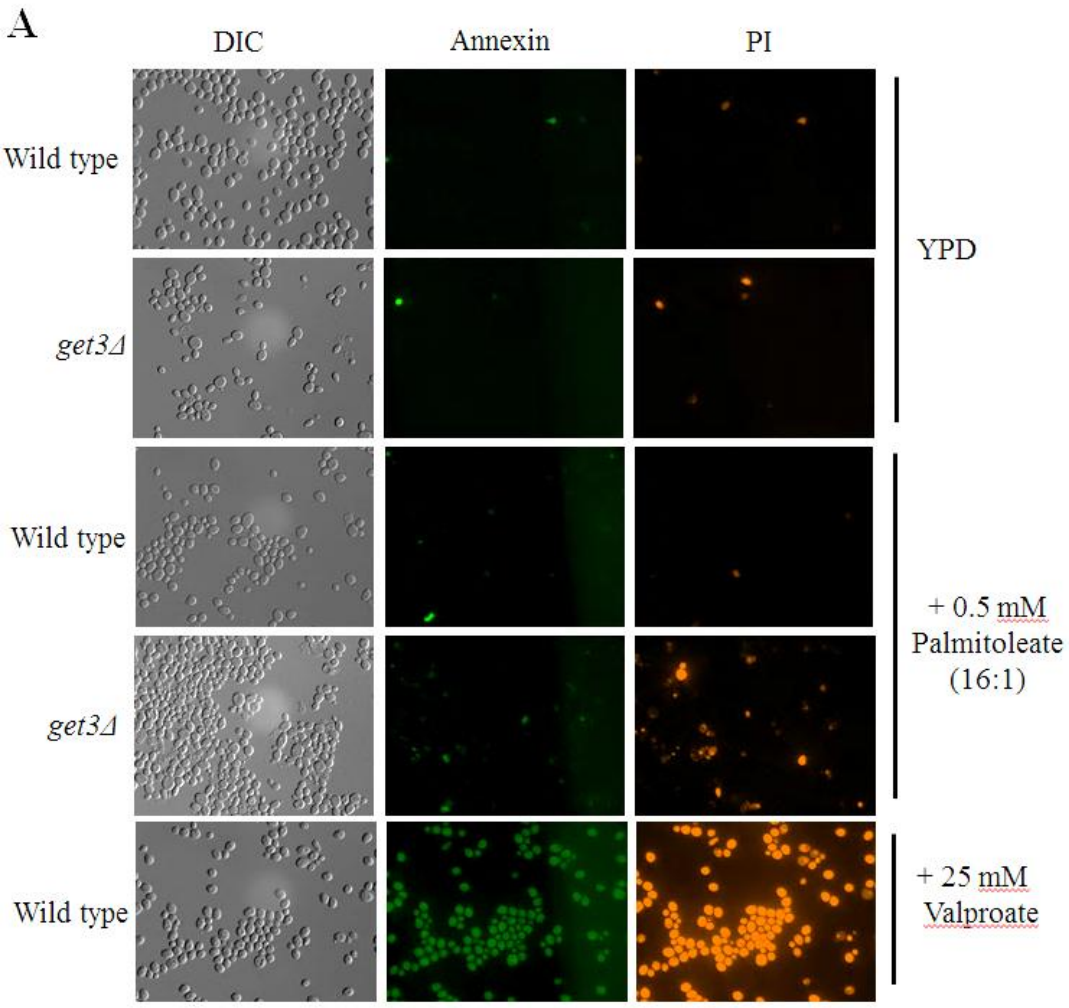

B

Condition	Annexin V	PI
Wild Type	2.1% (±0.31)	2.6% (±0.53)
get3Δ	2.3% (±0.62)	1.9% (±0.51)
Wild Type + Palmitoleate	3.2% (±0.93)	3.6% (±0.48)
get3Δ + Palmitoleate	7.9% (±1.11)*	10.8% (±1.05)*

Figure 3-3: Palmitoleate treatment causes increased apoptosis and cell death in get3Δ. (A) Annexin/PI staining of yeast grown overnight in YPD or YPD + 0.5 mM palmiolteate. Control cells incubated overnight with 25 μM Valproate was used as a positive control for apoptosis [264]. (B) Quantification of Annexin and PI positive cells as a percent of total cells (>500 cells per strain). Asterisks indicates statistical significance ($p<0.05$) compared to control in the same treatment condition.

Knockout of GET3 results in a reduction in lipid droplets. Lipid droplet formation and storage plays an integral role in the cells ability to survive conditions of fatty acid accumulation [7, 22, 23]. In order to determine if increased fatty acid sensitivity in *GET3* mutants was due to defects in LD formation or stability, cytosolic lipid droplets were stained using the lipophilic dye, Nile Red (Fig 3-4A). The number of lipid droplets per cell after overnight growth in rich media were counted and we found that a deletion in *GET3* resulted in a 31% decrease in lipid droplet number (3.83 ± 0.15) compared to a normal control (5.55 ± 0.47) (Fig 3-4B).

Synthetic lethality screens focusing on genes encoding proteins involved in the early secretory pathway identified an interaction between the gene encoding the diacylglycerol acyltransferase enzyme, Dga1p , and *GET2* [22, 215]. This interaction indicates a potential link between TG synthesis and GET complex dependent mechanisms. We validated this, and found that the double deletion of *get2*Δ *dga1*Δ did result in a growth defect under normal growth conditions (data not shown). For this reason, we hypothesized that knockout of both *DGA1* and members of the GET complex may exacerbate the lipid phenotypes in these strains. Consequently, a double deletion of *get3*Δ *dga1*Δ resulted in a 75% reduction in the number cytoplasmic lipid droplets (1.38 ± 0.12 per cell), which was not associated with an increase in lipid droplet size (Fig 3-4A,B). The lipid droplet deficiency in *get3Δ dga1Δ* was significantly worse than that seen in the *dga1*Δ (3.02 ± 0.25) or *get3*Δ (3.83 ± 0.15) single deletion (Fig 3-4B).

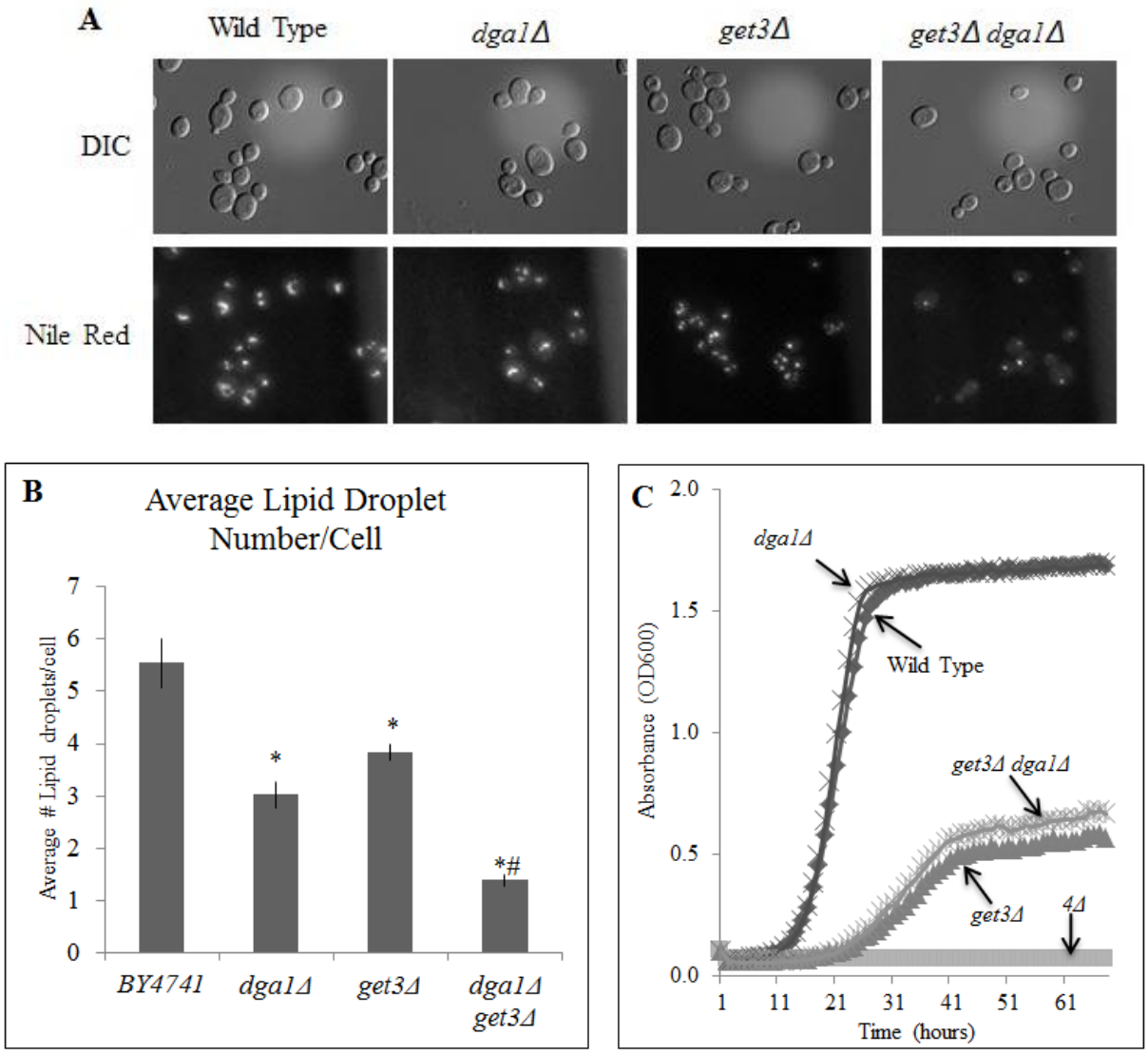

Figure 3-4: The *get3*Δ *dga1*Δ double mutant has a significant reduction lipid droplet number (A) Neutral lipid staining of *GET3* and *DGA1* mutants using Nile Red dye (B) Average number of lipid droplets per cell, >50 cells counted in at least 7 frames per strain * p-value < 0.01 compared to wild type, # p-value <0.05 compared to *dga1Δ* and *get3Δ* (C) Growth of *GET3* and *DGA1* mutants in YPD + 0.5 mM palmitoleate for 3 days. The *4Δ* neutral lipid deficient strain (*are1Δ are2Δ dga1Δ lro1Δ*) was used as a positive control for palmitoleate sensitivity.

Since all three members of the GET complex are involved in the same process of tail anchored protein insertion into the ER membrane, single deletions of each gene often cause similar cellular defects and phenotypes [216]. Furthermore, in addition to *DGA1*, there is an alternate yeast TG synthesis enzyme, LRO1 [14, 246]. Knockout of either *DGA1* or *LRO1* decreases triglyceride synthesis and could potentially affect lipid droplet morphology similarly. In order to assess if the reduction in LDs is specific to the *GET3 DGA1* double mutation, we made all 6 mutant combinations of a single TG synthesis gene knockout on a *GET* mutant background (*get1Δ dga1Δ, get1Δ lro1Δ, get2Δ dga1Δ, get2Δ lro1Δ, get3Δ dga1Δ* and *get3Δ lro1Δ*). We then stained each strain for lipid droplets in order to determine if any other knockout combinations caused a similar phenotype to that seen in *get3Δ dga1Δ* strains. The *get3Δ dga1Δ* double mutant was the only mutant combination causing a significant decrease in LD number, demonstrating that the defect is specific to these genes and not a general consequence of a GET complex or TG synthesis deficiency (Fig 3-5).

The triple deletion of *get3Δ dga1Δ lro1Δ* had an even more striking reduction in LD number compared to both *get3Δ* and *dga1Δ lro1Δ* with many cells having no visible lipid droplets (Fig 3-5). This does not occur however, in either *get1Δ dga1Δ lro1Δ* or *get2Δ dga1Δ lro1Δ* (Fig 3-5). The double deletion of *DGA1* and *LRO1* is essentially TG deficient, with a greater than 95% reduction in TG synthesis, though a low level of TG synthesis remains through Are1p and Are2p activity [14]. In this strain sterol esterification is still intact. Therefore, the almost complete lack of LD in *get3Δ dga1Δ lro1Δ* indicates that the additional deletion of *GET3* in the TG "deficient" background is due to either decreased in lipid droplet biogenesis or an increase in LD catabolism. This effect is specific to *GET3* and the removal of other neutral lipid synthesis pathways isolates the role of Get3p in this process.

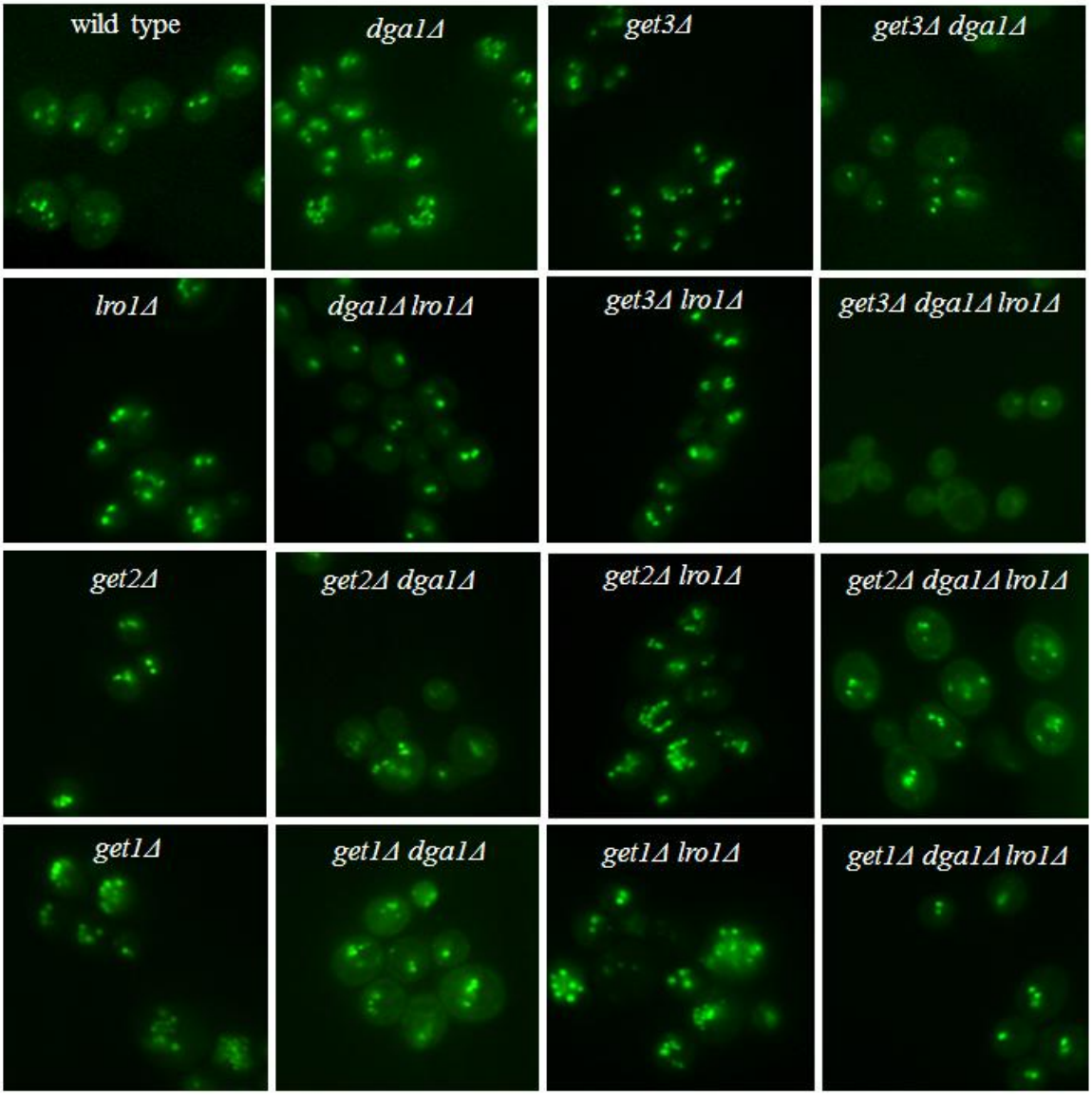

Figure 3-5: The lipid droplet defect seen in a GET3 mutant does not occur in GET1 or GET2 knockout strains. The *GET3* mutants with additional *DGA1* deletion has a severe lipid droplet phenotype, which is not seen with other GET complex/DAG acyltransferase double mutants Neutral lipid staining using Nile Red of all GET complex and TG synthesis enzyme knockout combinations, after overnight growth at 30° in YPD.

Despite the significant loss in lipid droplets in *get3Δ dga1Δ*, sensitivity to palmitoleate treatment was not further increased compared to the *GET3* single deletion (Fig 3-4C). In fact, double mutants of *LRO1* or *DGA1* in any *GET* mutant background did not exacerbate the palmitoleate sensitivity (Fig S3-1). From this, we determined that the *GET3* deletion causes major aberrations in lipid metabolism, which manifests as a defect in neutral lipid storage and increased palmitoleate sensitivity. Though an additional mutation in *DGA1* does not exacerbate the palmitoleate sensitivity, the further reduction in lipid droplets in the double deletion emphasizes the role of GET3 in lipid droplet homeostasis. This finding also highlights the concept that though important in the protection against lipotoxicity, a reduction in lipid droplet number does not always predict an increase in fatty acid sensitivity.

***GET3* induced lipid droplet defect is not due to decreased cellular neutral lipid levels.** As the primary location of NL storage, decreased LD number is typically associated with lower levels of NLs. Therefore, the severe lack of lipid droplets in *get3Δ dga1Δ* may occur through a decrease in cellular triglyceride or sterol ester. Lipid levels were measured using lipid extraction techniques followed by densitometry of thin layer chromatography (TLC) separated lipid species. There was no significant decrease in TG or SE mass in any of the mutants (Fig 3-6). Consequently, despite their lack in LD storage, these cells did not have decreased NL mass compared to control. This result is consistent with the growth curve data (Fig 3-4) which demonstrates that decreased lipid droplet number in *get3Δ dga1Δ* did not result in an increase in vulnerability of this strain to exogenous fatty acids compared to either single deletion (*get3Δ* or *dga1Δ*). If neutral lipid synthesis was significantly decreased in the double mutant compared to either single, we would predict an even more severe UFA sensitivity phenotype. These results

demonstrate that the FA-sensitivity in the GET mutants may not be related to the lipid droplet phenotype occurring upon deletion of *GET3*.

Regardless of normal NL mass, the levels of SE and TG synthesis were decreased in *get3Δ dga1Δ* as measured by average percent of [^{3}H]oleate and [^{3}H]palmitate incorporation into neutral lipids (Fig 3-7). Cells were grown in rich media overnight with fatty acid label, and following lipid extraction each fatty acid species (phospholipid, diacylglycerol, free fatty acid, triglyceride and sterol ester) was quantified by scintillation counting. The average percent of radiolabeled oleate incorporated into either SE or TG was decreased for both *get3Δ dga1Δ* and *get3Δ* during steady state overnight growth (Fig 3-7A). Palmitate incorporation was also decreased in all three mutants when grown with label overnight (Fig 3-7B). Alternatively, a three hour pulse at saturation phase with radiolabeled oleate showed a decrease in TG synthesis for *dga1Δ* and *get3Δ dga1Δ,* but not for the *GET3* single deletion (Fig 3-7C). This is likely due to the role of Dga1p in TG synthesis during the saturation growth phase [14]. A deletion in *GET3* results in decreased NL synthesis during log growth phase growth [22], whereas a mutation in *DGA1* results in decreased TG synthesis during saturation (Fig 3-7C). Together, these results indicate that TG and SE synthesis is decreased throughout growth in the *GET3 DGA1* double mutant. The concurrent decrease in TG and SE synthesis with normal NL mass occurring in *GET3* mutants indicates that there is a likely reduction in NL turnover.

Analysis of [^{3}H]oleate incorporation into other lipid species separated by TLC (diacylglycerol, free fatty acids and phospholipid) found that phospholipid (PL) synthesis levels were significantly increased in both *get3Δ* and *get1Δ dga1Δ* (Fig 3-7 D). The PL species separated out by this method of TLC contains multiple phospholipid types, characterized by their diglyceride group, including phosphatidylcholine (PC), phosphatidylethanolamine (PE),

phosphatidylserine (PS), phosphatidylinositol (PI) and diphosphatidylglycerol (DPG). To dissect out if a specific phospholipid type was responsible for the rise in total PL synthesis, we further separated the phospholipid species using a two solvent system followed by quantification of radiolabeled oleate incorporation into each PL type. This quantification indicated that the rise in PL synthesis seen in *GET3* mutants is due to a general increase in fatty acid flux through the phospholipid synthesis pathway, with increases in four phospholipid types; diphosphatidyl glycerol (DPG), phosphatidylinositol (PI), phosphatidylserine (PS) and phosphatidylcholine (PC) (Fig 3-8).

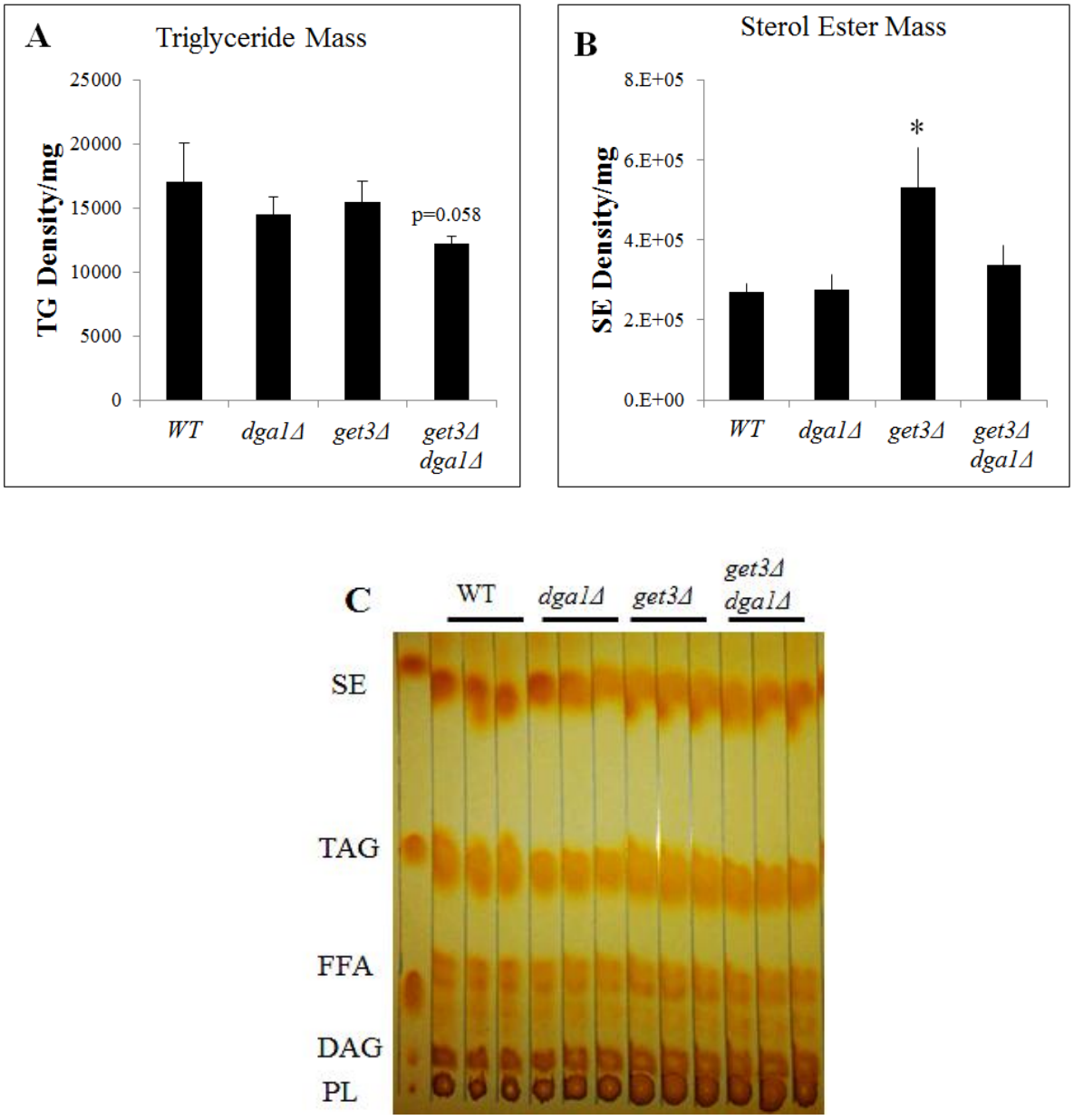

Figure 3-6: The get3Δ dga1Δ double mutant does not cause a decrease in neutral lipid mass. Lipid mass, as measured by species density of iodine stained TLC plate separation of extracted lipids. Iodine binds to double bonds in fatty acids. 'p' indicates p value of statistical significance compared to wild type (WT) obtained using an unpaired t-test.

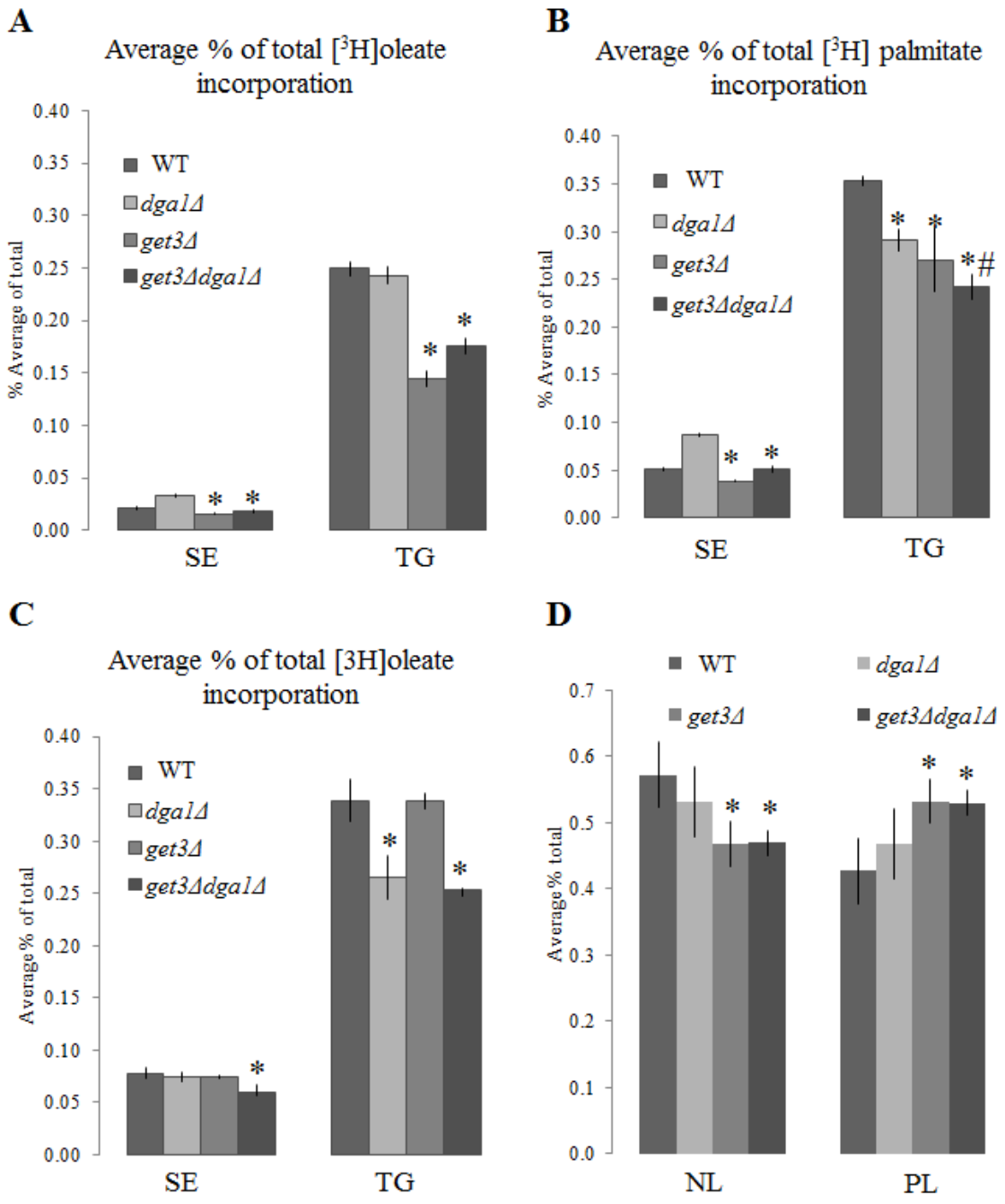

Figure 3-7: get3Δ mutants have decreased neutral lipid synthesis levels. Levels of sterol ester (SE) and triglyceride (TG) synthesis as measured by [^{3}H]oleate (A) and [^{3}H]palmitate (B) incorporation into neutral lipids after overnight growth with labeling media.(C) [^{3}H]oleate incorporation during 3 hour pulse at saturation. (D) Increased [^{3}H]oleate into phospholipids (PL) occurs with decreased [^{3}H]oleate incorporation into neutral lipids (NL= sterol ester + triglyceride) in both *GET3* mutants. (*) indicates significance ($p<0.05$) compared to wild type, (#) indicates significance ($p<0.05$) compared to *dga1*

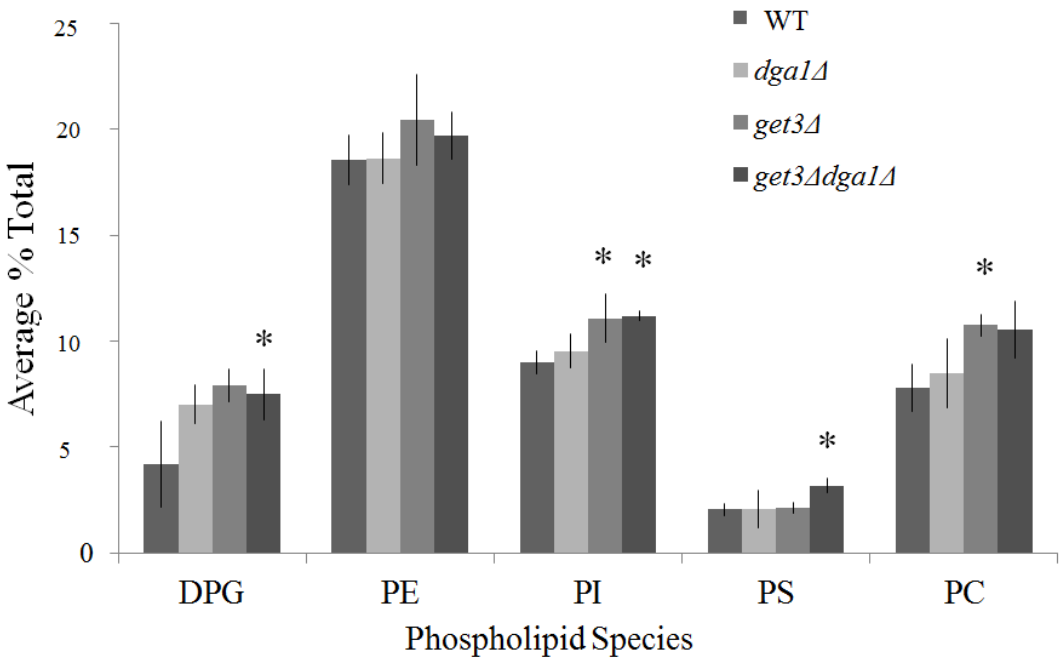

Figure 3-8: get3Δ mutants have increased oleate incorporation into phospholipids. The decrease in oleate incorporation into neutral lipid synthesis seen in *GET3* mutants is counterbalanced by increased incorporation into phospholipid species. Asterisks indicate significance ($p<0.05$) compared to wild type (WT). Phospholipid species; DPG: diphosphatidylglycerol PE: phosphatidylethanolamine, PI: phosphatidylinositol, PS: phosphatidylserine, PC: phosphatidylcholine.

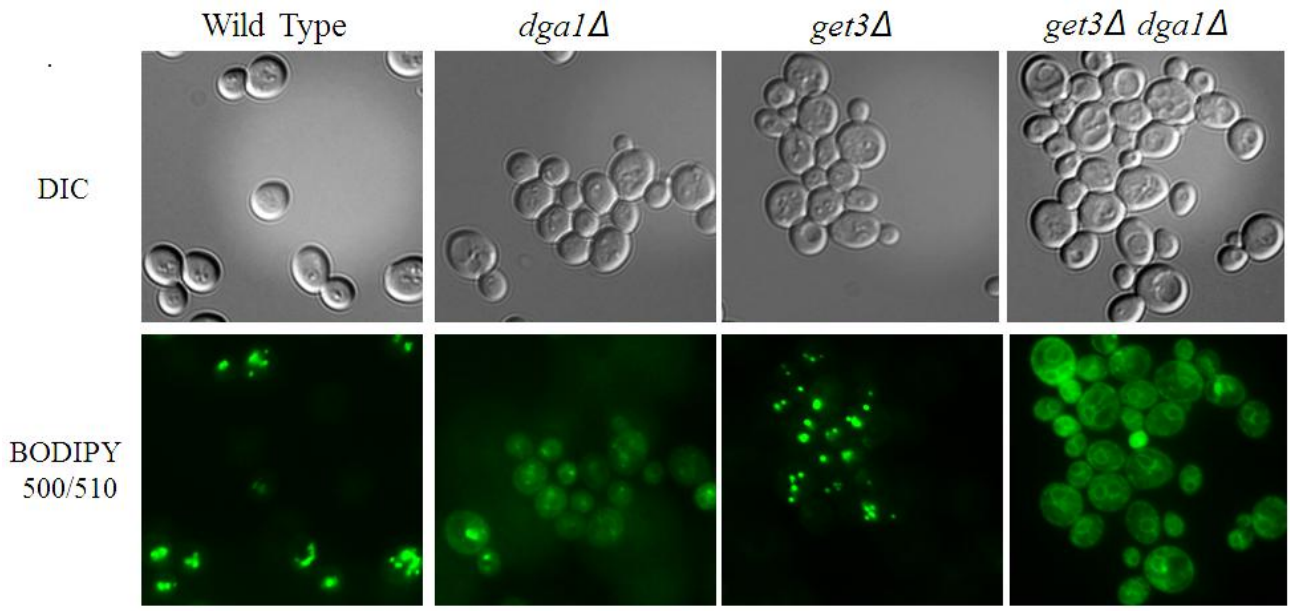

Figure 3-9: Use of BODIPY fatty acid analog indicates lipid localization changes in get3*Δ **and** *dga1*Δ *mutants. BODIPY fatty acid analog (C1-BODIPY 500/510-C12) shows decreased incorporation of fatty acids into lipid droplets in *get3Δ dga1Δ.* Cells were treated with BODIPY 500/510 for 1 minute followed by 3 washes in 50 µM fatty acid free BSA in PBS.

For visualization of fatty acid uptake, incorporation and localization in live cells, we used a fluorescent BODIPY conjugated long chain fatty acid (C1-BODIPY 500/510-C12). The fatty acid conjugate, dodecanoic acid, is a precursor for PL and NL biosynthesis and long term labeling (>1 hour) stains lipid droplets in yeast [265]. Additionally, short term incubation (~2 minute) with this analog has been used to monitor FA uptake and localization in mammalian cells [266]. Incubation of *GET3* and *DGA1* mutants with C1-BODIPY 500/510-C12 for 1 minute followed by fluorescent microscopy results in lipid droplet staining in wild type and *get3Δ*. Alternatively, lipid droplet and membrane staining occurred in *dga1Δ* and only membrane staining was seen in *get3Δ dga1Δ* (Fig 3-9).

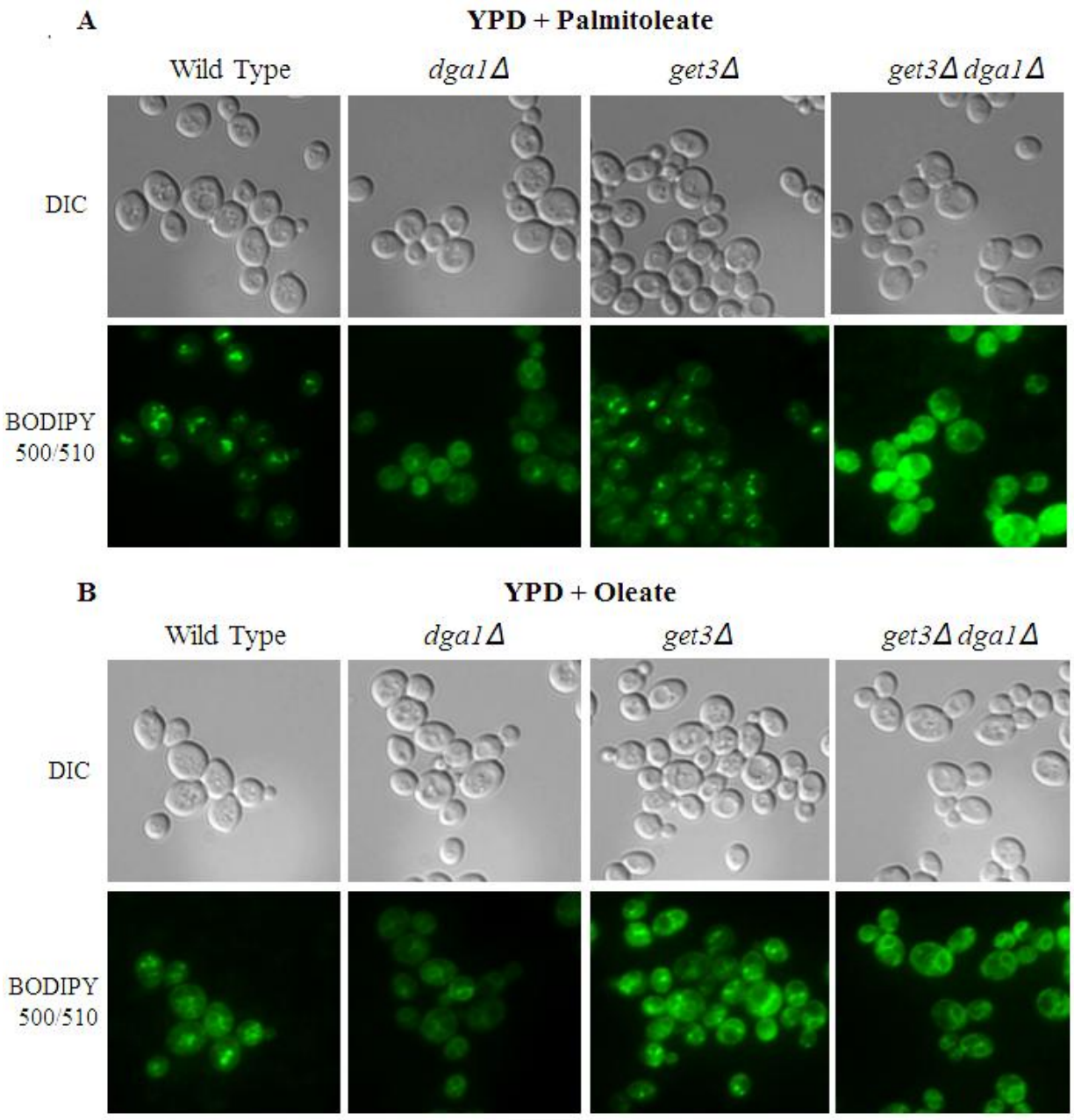

***Figure 3-10: get3*Δ **and** *dga1*Δ *mutants have increased BODIPY fatty acid membrane staining after preincubation with monounsaturated fatty acids*.**
BODIPY fatty acid analog (C1-BODIPY 500/510-C12) staining for 1 minute after 3 hour incubation in (A) 0.1 mM palmitoleate or (B) 0.5 mM oleate.

Pretreatment of cells with 0.1 mM palmitoleate or oleate for 3 hours resulted in increased membrane and cytosolic staining in both *dga1Δ* and *get3Δ dga1Δ* likely due to the *DGA1* dependent defect in TG synthesis (Fig 3-10). Increased membrane staining by BODIPY 500/510

also occurs in the palmitoleate treated *GET3* mutant, while wild type has mainly LD staining under all treatment conditions, with some membrane staining following oleate incubation (Fig 3-10). These results show that fatty acid incorporation into the LD is slowed in *GET3* and *DGA1* mutants when pretreated with monounsaturated fatty acids (MUFA) oleate or palmitoleate. The fluorescent membrane staining seen in these mutants could be due to either incorporation of the BODIPY-FA into phospholipid acyl chains or through synthesis into TG. In either case, [^{3}H]oleate incorporation and C1-BODIPY 500/510-C1 demonstrates that fatty acid flux into LD storage is slowed with deletions in *GET3* and/or *DGA1*.

GET3 mutants have altered triglyceride subcellular localization. The 75% decrease in LD number accompanied by normal NL levels suggests a defect in LD formation in *get3Δ dga1Δ*. The current model of lipid droplet biogenesis posits that NL synthesis occurs in specific regions the ER bilayer and buds off of the ER to form an independent organelle [30]. A similar phenotype of normal NL mass with reduced LD number occurs with deletion of the phosphatidic acid hydrolase, *PAH1*. This mutation results in a buildup of TG in the ER bilayer due to defective channeling of TG into the budding lipid droplet structure. The TG accumulation in the ER was visualized by both BODIPY 493/503 fluorescence and electron microscopy (EM) as lipid filled ER rings [187]. In order to determine if a similar mechanism of defective LD budding was occurring in our *GET3* mutants, we analyzed electron micrographs of these strains and looked for fatty buildup within the ER membrane. We saw no such accumulation in any of our mutants, demonstrating that the decrease in LD seen in *get3Δ dga1Δ* is likely not due to an accumulation of NL within the ER bilayer (Fig 3-11).

Further analysis of the electron microscopy (EM) images indicate an increase in structures resembling lipid droplets, based on their electron light staining, within the vacuole in

both *dga1Δ* and *get3Δ dga1Δ* (Fig 3-11 and 3-12A, black arrows). Vacuoles with associated lipid droplets were counted for each genotype and we found that over 40% of cells had vacuolar lipids in both *DGA1* deletion strains, while wild type and *get3Δ* had less than 20% (Fig 3-12B). The increased number of lipid droplet-like structures in the *dga1Δ* single mutant was surprising, and indicate a preferential movement of lipid to the vacuole in this strain. Lipid droplets located within or in tight association with the yeast vacuole and mammalian lysosome have been reported in lysosomal hydrolase inhibited hepatocytes [91], in yeast mutants of the trafficking genes *ARF1* [267]and *SEC13* [268], and in a mutant of the yeast lipid phosphatase, *SAC1* [269].

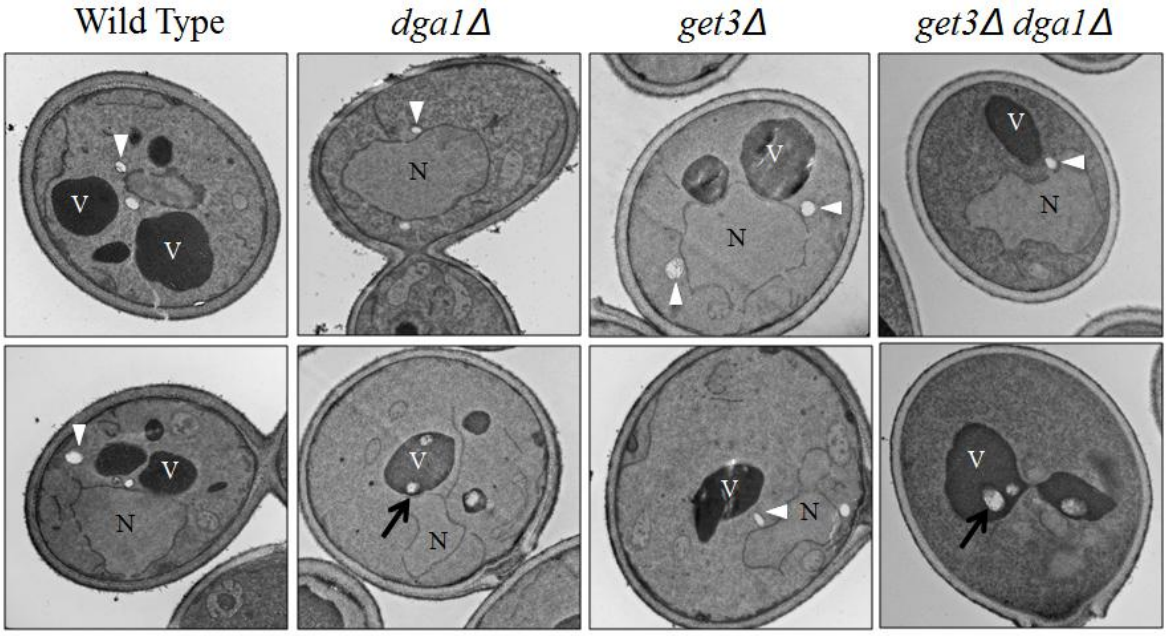

Figure 3-11: Electron Microscopy of *get3*Δ and *dga1*Δ mutants. Thin section EM of control, *dga1Δ, get3Δ,* and *get3Δ dga1Δ.* Two images shown per strain. N, nucleus; V, vacuole; white arrowheads indicate lipid droplets and black arrows indicate lipid droplet-like structures within the vacuole.

In addition to vacuolar associated lipid droplets, membrane-like structures were found within a portion (16%) of the vacuolar lipid only in the *GET3 DGA1* double mutant and not in either single mutant or normal cells. These structures are reminiscent of those formed during

membrane recycling through autophagy [89]. Autophagy is a process involved in the degradation of cellular products and organelles through lysosomal hydrolysis and plays a particularly important role under starvation conditions. There are three modes of autophagy, macroautophagy, microautophagy and chaperone mediates autophagy. Microautopahgy occurs through nonspecific cytoplasmic invagination by the autophagosome while chaperone mediated autophagy targets only specific peptide sequences for degradation. Macroautophagy, from here on referred to simply as "autophagy" is a selective process in which particular organelles, such as the mitochondria or lipid droplet, are targeted and sequestered by the autophagosome [90]. This mode of autophagy has been recently implicated in the degradation of hepatic lipids [91] and in adipocyte differentiation [87].

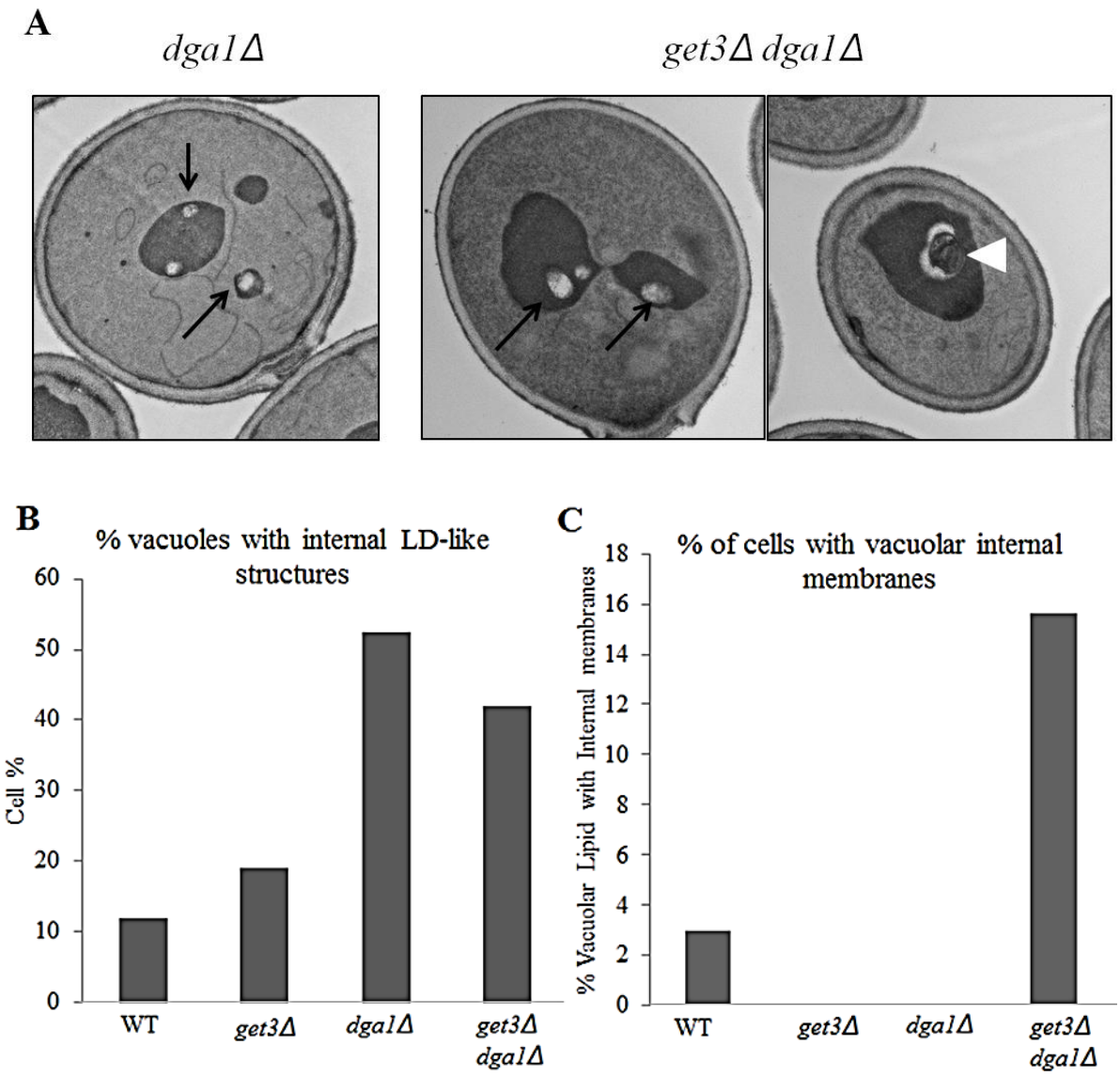

Figure 3-12: Electron Microscopy of get3*Δ **and** *dga1*Δ *mutants indicates increased lipid droplet association with the vacuole and internal membrane structures in the GET3 DGA1 double mutant. (A) Abnormal structures in the *get3Δ dga1Δ* include increased lipid droplets in vacuoles (black arrows) and the presence of membranes structures inside vacuolar lipid droplets (white arrowheads). (B,C) Quantification of these structures in all four genotypes. (B) Percent of cells imaged with vacuolar associated internal lipids. (C) Percent of vacuolar lipids which have the internal membrane structures (white arrowhead).

Since the *GET3 DGA1*double mutant has membrane accumulation within the vacuole, we went on to assess the vacuolar structure and lipid association using fluorescent probes. Staining of the vacuolar membrane with, FM4-64 did not indicate any obvious vacuolar phenotypes in any of the *GET3*, or *DGA1* mutants (Fig 3-13). Co-staining with the neutral lipid stain BODIPY 493/503 showed a close interaction between vacuoles and lipid droplets in all strains (Fig 3-13), but the localization of droplets within the vacuole could not be deciphered using this method.

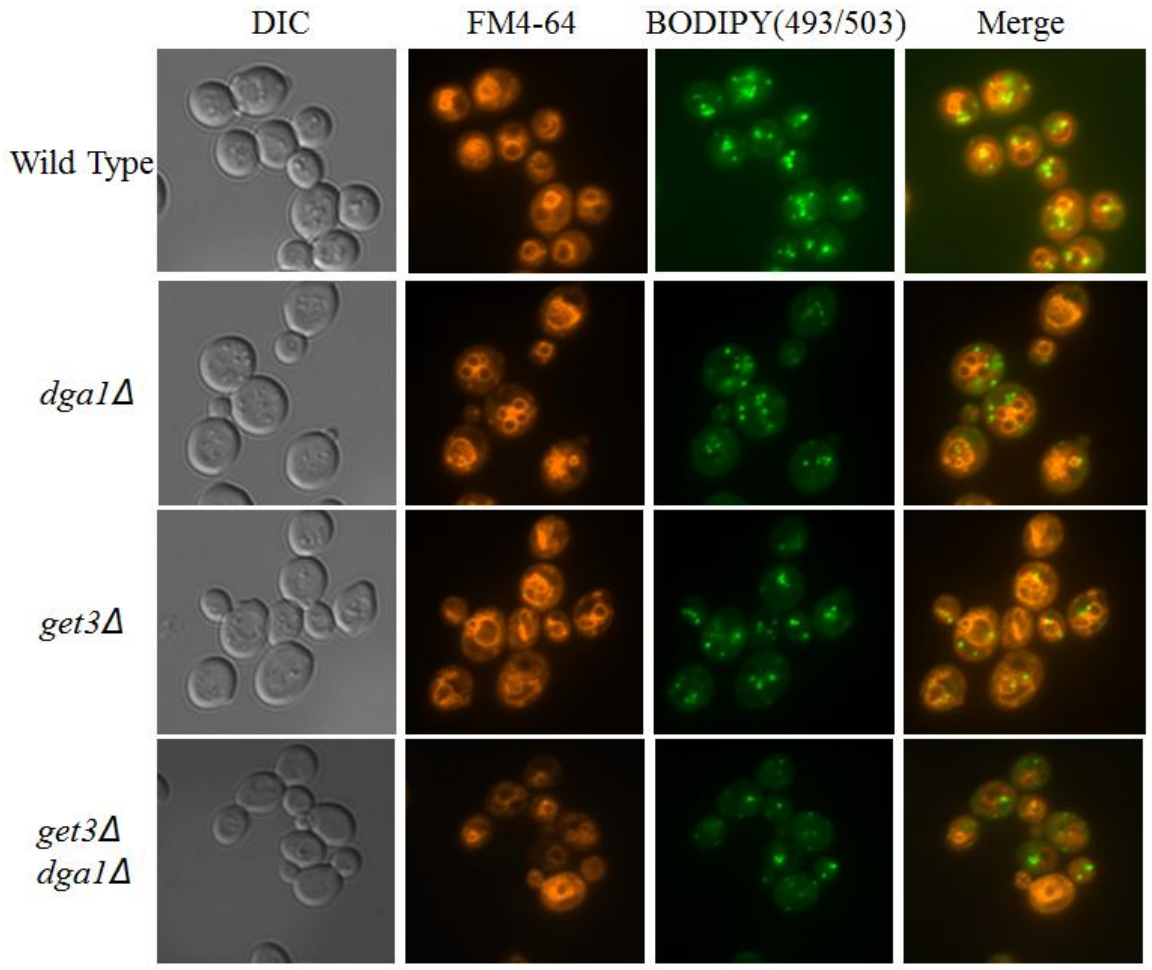

Figure 3-13: Vacuolar membrane marker FM4-64 demonstrates normal vacuolar morphology in *get3*Δ and *dga1*Δ mutants. Log phase (OD600~ 0.4-0.8) cells were labeled for 90 minutes with 0.03 mM FM4-64 in YPD and for 30 minutes with neutral lipid stain BODIPY 493/503.

To further rule out an accumulation of NL within the ER membrane, we transformed cells with a plasmid containing the fluorescent ER marker Sec63-RFP and co-stained with the neutral lipid stain BODIPY 493/503 (Fig 3-14). In agreement with the EM results, we saw no obvious accumulation of lipids within the ER bilayer in any strain. Consistent with previous work [55] lipid droplets were found in frequent association with the ER membrane in all strains. Additionally, all mutants had normal Sec63-RFP localization and ER structure (Fig 3-14), despite known vesicular trafficking defects characteristic of *GET* mutants [215].

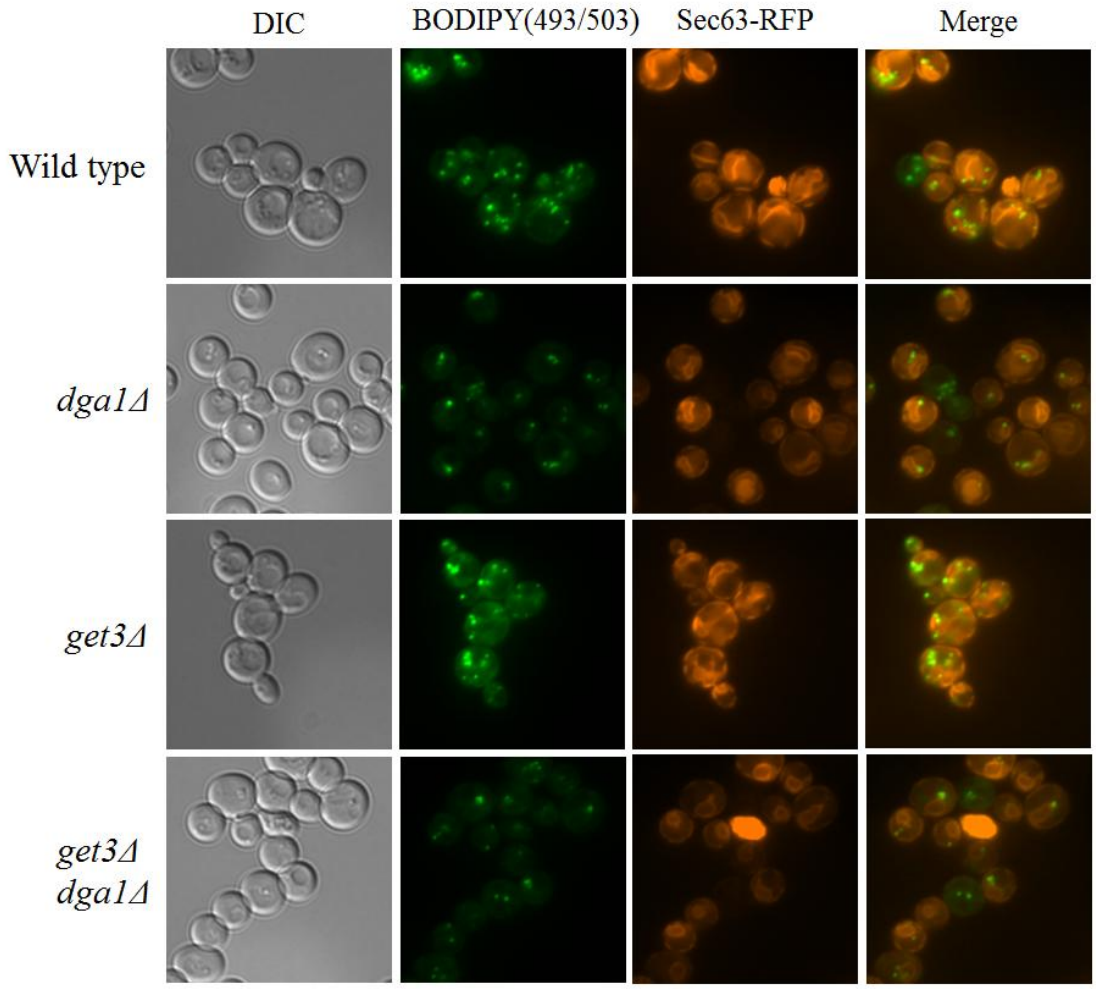

Figure 3-14: Neutral lipids do not colocalize with the ER membrane in get3Δ and dga1Δ mutants. Co-localization of neutral lipids and the ER membrane using the neutral lipid dye BODIPY 493/503 and the fluorescent ER marker protein Sec63-RFP. Cells grown overnight in SCD-URA at 30°C.

As an alternate method for the determination of subcellular TG localization, we labeled all four strains overnight with [^{3}H]oleate and completed a whole cell membrane fractionation. The thirteen fractions were grouped into their associated organelles, based on organelle specific marker proteins (Fig 3-14). As expected from Nile Red staining, levels of TG in the lipid droplet fractions were significantly decreased in both *get3Δ* and *get3Δ dga1Δ* compared to wild type and *dga1Δ*. The TG levels were increased throughout several other membrane fractions, including those associated with the golgi, vacuole and cortical ER/plasma membrane marker proteins (Fig 3-15). The TG within these mutants is dispersed throughout several membrane fractions in the cell, but the exact localization of this storage is still unclear. What is clear from these results is that TG in the *GET3* mutants is localized to non-LD structures within the cell. Based on the EM data (Fig 3-11 and Fig 3-12), it appears that this localization likely occurs within the vacuole.

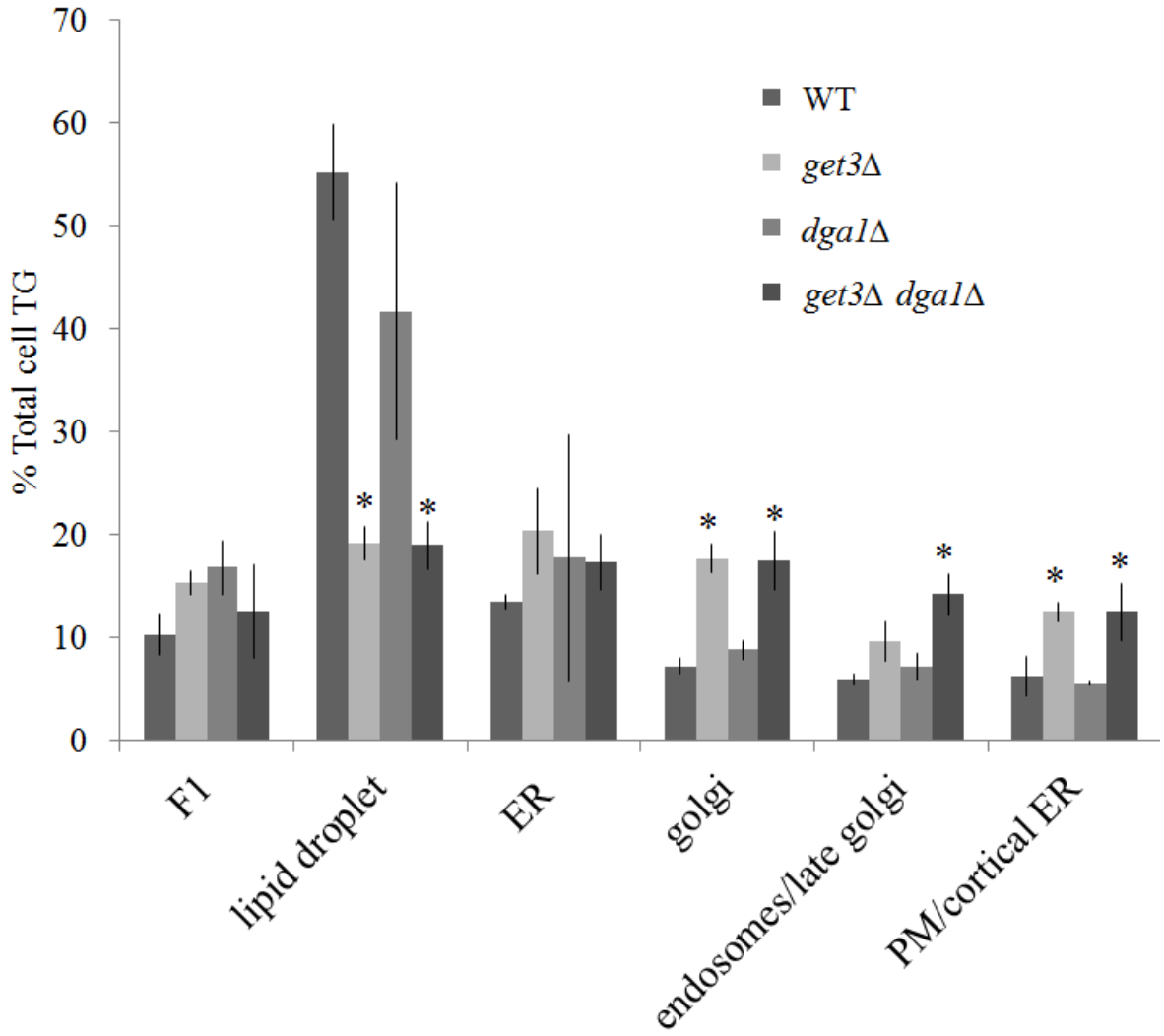

Figure 3-15: get3Δ causes mislocalization of cellular triglyceride Total cell fractionation using renograffin and grouped based on associated organelle. Cells were labeled for 16 hours with [H]oleate. Western blots of all strains for organelle specific proteins Sec61 (ER), Sec22 (ER and Golgi), Pma1 (Plasma Membrane). Lipid droplet fractions were based on wild type neutral lipid levels. Fraction 1 (F1) was not associated with any tested organelle.

Lipid structures within the GET3 DGA1 double mutant can be explained by decreased vacuolar lipid turnover. The yeast vacuole is the primary site of degradation and cellular recycling. An accumulation of vacuolar lipid could occur through either an increase in vacuolar directed lipid droplet trafficking, or by a decrease in vacuolar lipid degradation, likely through a

defect in vacuolar hydrolase activity [270]. Vacuolar directed trafficking occurs through either macroautophgy or the biosynthetic Cvt pathway (Fig 3-22). These pathways share many mechanistic similarities. Both form at the phagophore assembly site (PAS), after which the membrane expands to form a vesicle, taking up vacuolar specific hydrolases in Cvt trafficking or targeting whole organelles as seen in macroautophagy. These vesicles fuse with the vacuole through use of the autophagy machinery leading to whole organelle degradation and nutrient recycling. The accumulation of internal membranes within the vacuole seen in the EM images of *get3Δ dga1Δ* (Fig 3-12) could potentially occur through increased autophagy resulting in a rise in LD associated autophagosome transport to the vacuole.

A commonly used method for the determination of yeast autophagy is through the transformation of a GFP-Atg8 fusion plasmid [255]. Atg8p, the yeast ortholog of mammalian LC3, is an early mediator of autophagosome formation and its expression increases in response to autophagy induction [271, 272]. ATG8p exists as a cytosolic protein until lipidation, after which it accumulates in pre-autophagosomal structures (PASs). These structures can be visualized by fluorescence microscopy in cells expressing the GFP-ATG8 plasmid (Fig 3-14 b). In addition to PAS visualization, the GFP-Atg8p fusion protein can be used as a marker for vacuolar processing. When autophagosomes lyse to vacuoles, GFP is released from Atg8 through proteolytic cleavage, which can be detected by Western blot. Figure 3-16 shows that autophagy induced by nitrogen starvation (SD-N) increases GFP-ATG8 cleavage in both wild type and *dga1Δ* while starvation induced proteolytic cleavage was not detected in either *get3Δ* or *get3Δ dga1Δ* (Fig 3-16A). In agreement with these results fluorescence microscopy under nitrogen starvation conditions also shows an accumulation of GFP-Atg8 bodies in *get3Δ dga1* (Fig 3-16C), indicating slowed autophagosome degradation.

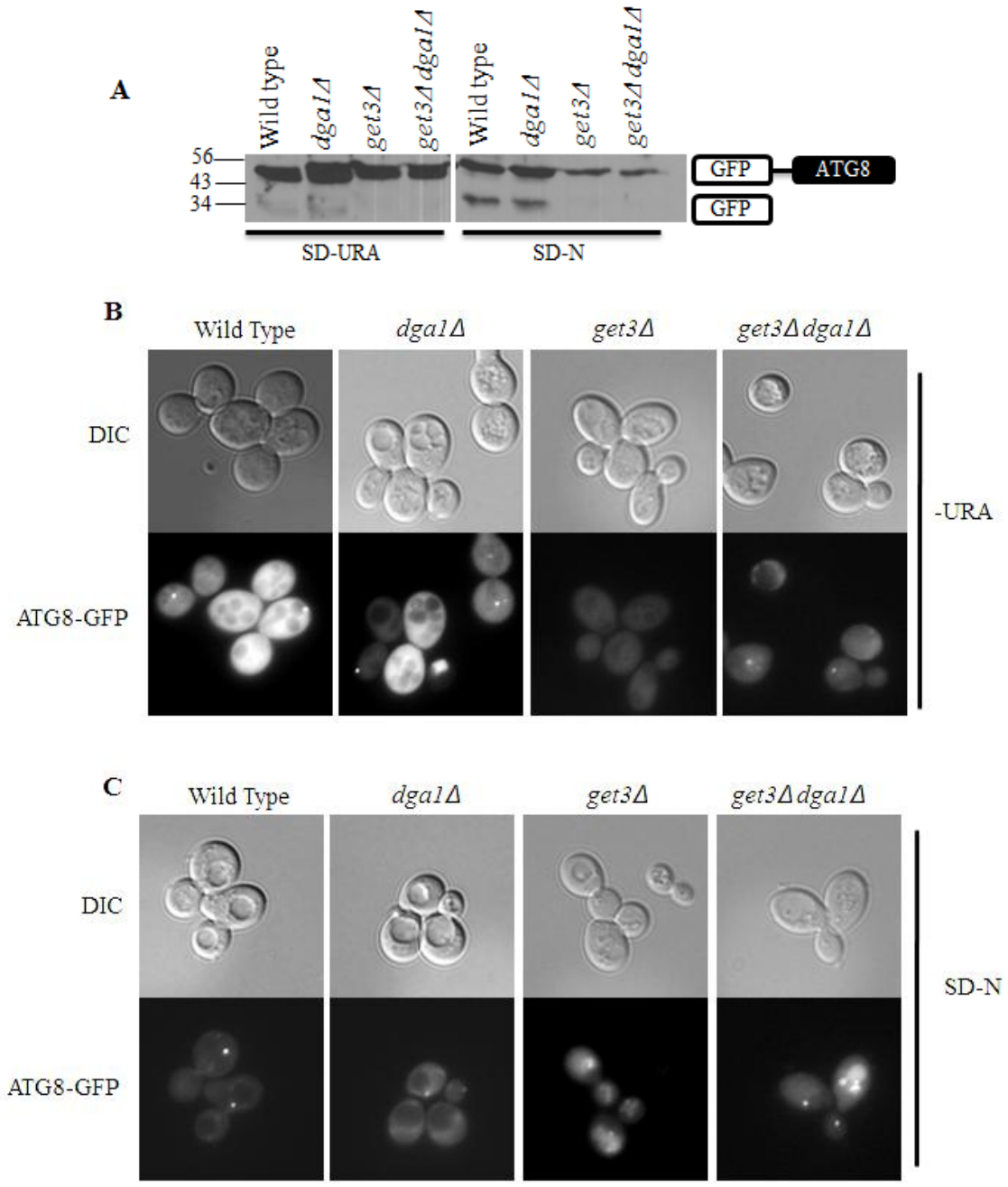

Figure 3-16: Mutation in GET3 results in decreased GFP-ATG8 vacuolar processing under conditions of nitrogen starvation. Strains were transformed with a plasmid containing GFP-ATG8 protein and grown to log phase in SCD media followed by 3 hours incubation in nitrogen starvation media (SD-N). Cells were harvested for protein preparation and protein extract was analyzed by Western blot using antibodies specific against GFP. Equal protein concentrations were loaded into each lane. (B,C) Cells grown in the conditions described above were visualized by fluorescence microscopy.

Similar defects in proteolytic cleavage have been reported in the vacuolar protease deficient, *vps4Δ pep4Δ* and in the vacuolar lipase mutant *atg15Δ* resulting in an accumulation of autophagic bodies within the vacuole [89, 262]. Therefore, it is possible that the *GET3* mutants are defective in vacuolar hydrolysis resulting in decreased autophagosome breakdown.

The hydrolytic defects occurring in both vacuolar protease deficient (*vps4Δ pep4Δ*) and vacuolar lipase deficient (*atg15Δ*) strains results in a block in autophagy due to a failure in autophagosome breakdown. The inability to breakdown autophagic bodies results in an inviability under conditions that require nutrient recycling for survival. Therefore both of these vacuolar hydrolysis mutant strains have decreased percent survival in nitrogen deficient (SD-N) media compared to control [89, 262]. In order to determine if the *GET3* mutants also had decreased survival due to defects in vacuolar hydrolysis, we grew all four strains in YPD media to log phase (OD ~ 0.5) and transferred the cells to SD-N media for 8 days. Every 2-3 days we plated an aliquot of cells on solid YPD media to assess survival during starvation. Consistent with the defect in GFP-ATG8 processing, both *get3Δ* and *get3Δ dga1Δ*had a significant reduction in percent survival under nitrogen deficient conditions compared to both wild type and *dga1Δ.* Decreased survival in SD-N indicates that mutations in *GET3* result in a defect in nutrient recycling, which could occur through a decrease in autophagic induction or reduced breakdown of autophagosomes.

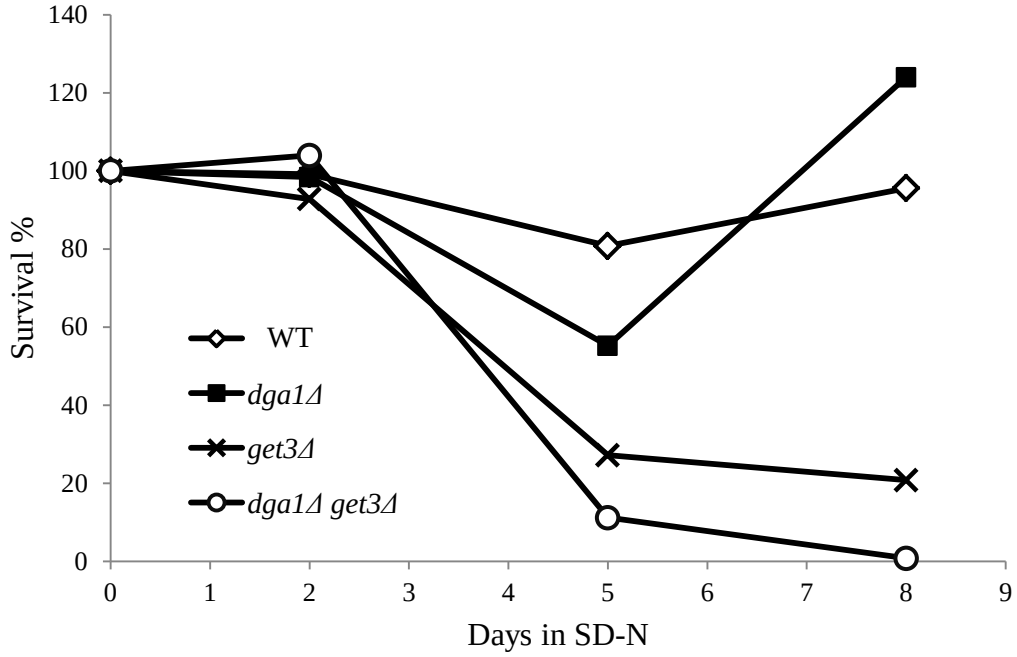

Figure 3-17: *GET3* mutants have reduced survival rates under nitrogen starvation conditions. Cells were grown to log-phase (OD ~ 0.5) and transferred to SD-N media for 8 days. Plating of cell aliquots on YPD plates were completed every 2-3 days and grown for 2 days at 30°C. Colonies were counted in order to assess culture viability and percent survival. WT indicates wild type control.

Breakdown of the autophagosomes is necessary for survival under starvation conditions because it allows vacuolar hydrolases access to its internal contents for nutrient recycling. The breakdown of autophagosomes depends on action of proteinase A (yeast Pep4p) [273] and B (yeast Prb1) [274] and vacuolar acidification [275]. To test for vacuolar protease activity, we used the vacuolar lumen specific marker, CMAC-Arg (7-amino-4-choloromethylcoumarin, L-arginine-amide). CMAC-Arg is a coumarin-based vacuolar marker conjugated to L-Arginine, and is nonfluorescent until cleaved by vacuolar proteases, after which it fluoresces a bright blue. Treatment of these cells with CMAC-Arg under normal (Fig 3-18) and nitrogen starvation conditions (Fig 3-19) demonstrates that the vacuoles of *GET3* and *DGA1* mutants have normal protease activity and normal CMAC-Arg cleavage. Cells lacking protease activity would not

have proper CMAC-Arg cleavage, which would be evident through a lack of vacuolar fluorescence. This also indicates that these mutants have normal vacuolar acidification.

In addition to vacuolar proteases, vacuolar lipases are known to degrade lipids and breakdown autophagic bodies in yeast [262] and mammalian cells [276]. The yeast vacuolar lipase Atg15p is a membrane bound lipase and knockout of *ATG15* results in an accumulation of autophagic bodies in the vacuole, but normal vacuolar pH [277]. Atg15p is transported to the vacuole from the ER through the multivescular body (MVB) pathway and is blocked in VPS Class E mutants [277]. Defective localization of Atg15p, due to deletion in *GET3*, could explain the vacuolar processing defects and decreased survival rate with starvation and thus must be tested in these strains.

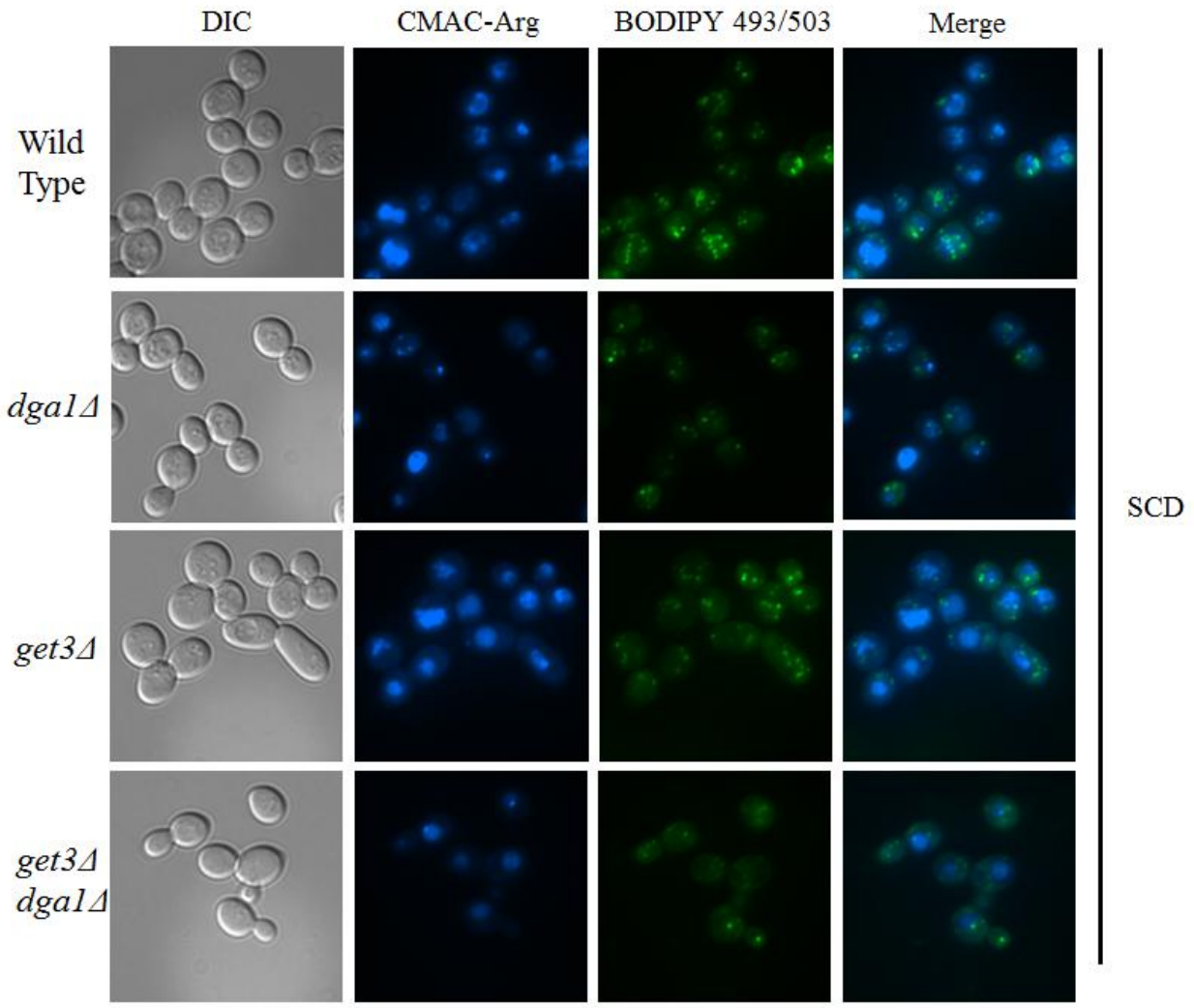

Figure 3-18: Probe for vacuole protease activity indicates that GET3 mutants properly hydrolyze proteins under normal conditions. Strains were grown in minimal media (SCD) and re-suspended in 10 mM HEPES (ph 7.4) with 5% glucose containing 100 µM CMAC-Arg for 30 minutes and visualized by fluorescence microscopy. Blue fluorescence indicates protease cleavage of Arginine conjugate and activation of the coumarin-based fluorescence. Lipid droplets were stained with BODIPY 493/503 neutral lipid dye.

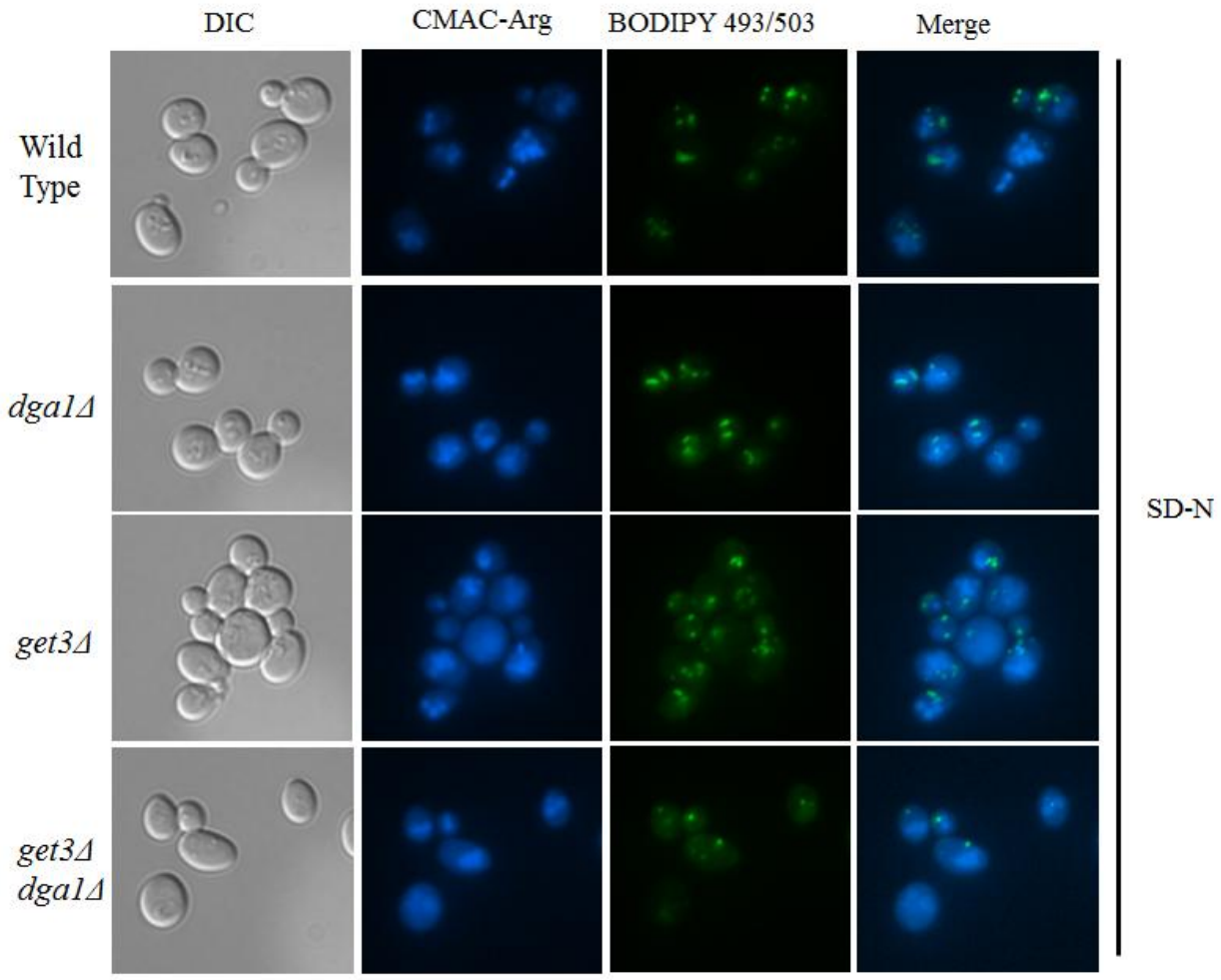

Figure 3-19: Probe for vacuole protease activity indicates that GET3 mutants properly hydrolyze proteins in nitrogen deficient conditions. Strains were grown for 2 hours in nitrogen deficient media and re-suspended in 10 mM HEPES (ph 7.4) with 5% glucose containing 100 µM CMAC-Arg for 30 minutes and visualized by fluorescence microscopy. Blue fluorescence indicates protease cleavage of Arginine conjugate and activation of the coumarin-based fluorescence. Lipid droplets were stained with BODIPY 493/503 neutral lipid dye.

Lipid droplets within the vacuolar are not shown through BODIPY or Nile Red staining.

Despite the increase in vacuolar associated lipid droplets seen by EM, we were unable to localize BODIPY or Nile Red stained lipid droplets to the vacuole in these strains (Fig 3-13 and 3-18).

The yeast vacuole has a pH of approximately 5.5 dependent on growth conditions [278] and some fluorescent probes, particularly green fluorescent proteins (GFPs), are known to have reduced signal in the vacuole due to the low pH conditions [279]. We first considered that was the lack of fluorescent staining was due to a similar acid-induced signal reduction. Studies determining pH effects on Nile Red fluorescence indicate that a pH between 4.5 and 8.5 causes little change in relative fluorescent intensity [280]. Additionally, in *C. elegans*, BODIPY and Nile Red probes are able to fluoresce in acidic lysosomal-related organelles (LROs), despite the low pH [281]. It is therefore unlikely that the acidic environment of yeast vacuoles is responsible for these contradictory results.

Although vacuolar lipid association and accumulation visualized by EM has been reported in yeast [267-269], to our knowledge, no study has demonstrated vacuolar lipid droplets through fluorescence staining in this organism. In order to decipher if we were not capturing all cellular neutral lipids using these fluorescent dyes, we also used the lypophilic dye Oil Red O following cell fixation. We did not see droplet-like structures in the vacuole by these methods, but did find increased fluorescence within a structure reminiscent of the vacuole in the *GET3 DGA1* double mutant, which was not seen in either single deletion strain (Fig 3-20). The staining was not localized within a punctate structure, but was instead a diffuse appearance. This diffuse pattern may explain we did not see vacuolar staining using either BODIPY or Nile Red, which may require a higher signal density for visualization. Alternatively, lipid staining in the vacuole may require cell fixation for visualization. These results confirm that there is an increase in neutral lipids in a "non-lipid droplet" structure in *get3*Δ *dga1*Δ, most likely within the vacuolar lumen, though a vacuolar co-stain is required with Oil Red O to determine exact localization.

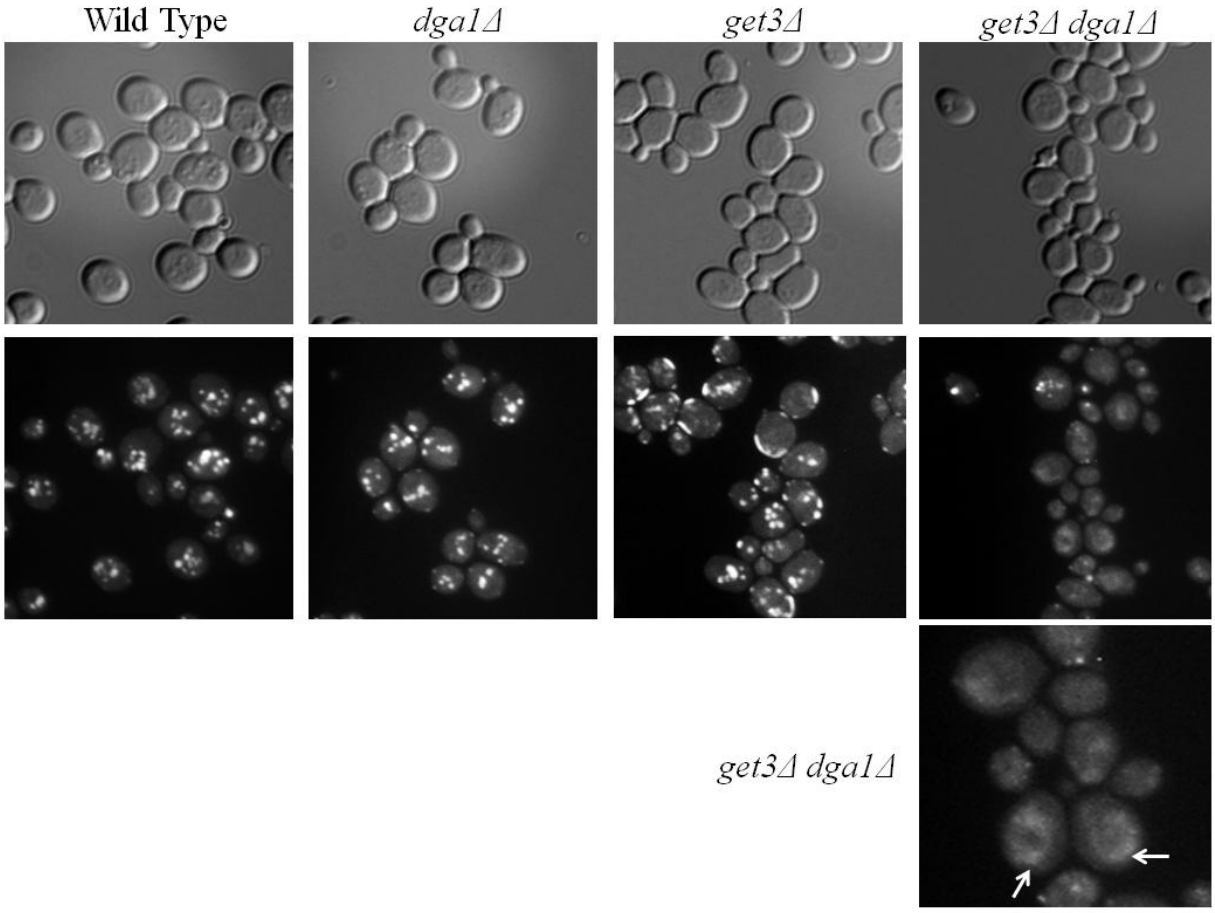

Figure 3-20: Oil red O staining demonstrates subcellular staining of non-lipid droplet structures in the get3Δ dga1Δ double mutant. Cells grown overnight in YPD and fixed after which they were incubated in Oil red O for 10 minutes followed by fluorescent imaging. Lower pane with *get3*Δ *dga1*Δ is a 2x enlargement of above image. Arrows indicate a diffuse non-LD staining.

Deletions in tail-anchored proteins does not recapitulate GET3 mutant lipid phenotypes. The GET complex is involved in protein localization of at least 50 different proteins, and therefore knockout mutations of these genes results in broad cellular defects. A deletion of the cytosolic *GET3* causes a mislocaliztion of tail-anchored proteins, which is exacerbated in both *get1Δ* and *get2Δ*. The more severe protein mislocalization in deletions of *GET1* and *GET2* compared to

get3Δ is due to the accumulation of cytosolic Get3-TA protein aggregates in *GET1/2* knockouts, leading to an extensive depletion of TA proteins. In the *GET3* deletion, these aggregates do not occur, though efficient insertion into the ER membrane is still somewhat impaired. Deficiency in *GET3* results in a less specific targeting of TA proteins and insertion into non-ER membranes. Get3p is therefore critical in accurate targeting of TA-proteins to the ER membrane, but lack of Get3p does not deplete the cell of these proteins like that seen in *get1Δ* and *get2Δ.*

Being that a major function of Get3p is its role in the movement of tail-anchored proteins from the ribosome to the ER for insertion into the ER membrane, we tested for palmitoleate sensitivity in all known non-mitochondrial yeast tail anchored gene mutants (44 knockouts or DaMP strains) to determine if the lipid phenotypes in the *GET3* mutants could be easily explained by altered tail anchored protein localization. Of the 44 genes, mutations in two resulted in increased sensitivity to palmitoleate, both of which had been already identified by our genome-wide screen (*gos1Δ* and *ybl100cΔ*) (Table 3-2, chapter 2). Both *gos1Δ* and *ybl100cΔ* had a similar growth defect as *get3Δ* in media containing 0.5 mM palmitoleate (Table S3-1 and Fig 3-21A) but neither have a defect in TG synthesis measured by [^{3}H] oleate incorporation (Fig 3-21B). Furthermore, ablation of *DGA1* in either *gos1Δ* or *ybl100cΔ* did not phenocopy the severe LD defect observed in *get3Δ dga1Δ* (Fig 3-22). Together, these results indicate that the lipid metabolism defects in *GET3* mutants are not explained by the mislocalization of a single known tail anchored protein, however we cannot rule out the possibility that inefficient targeting of an unknown tail-anchored protein or a combination of proteins are mediating these effects.

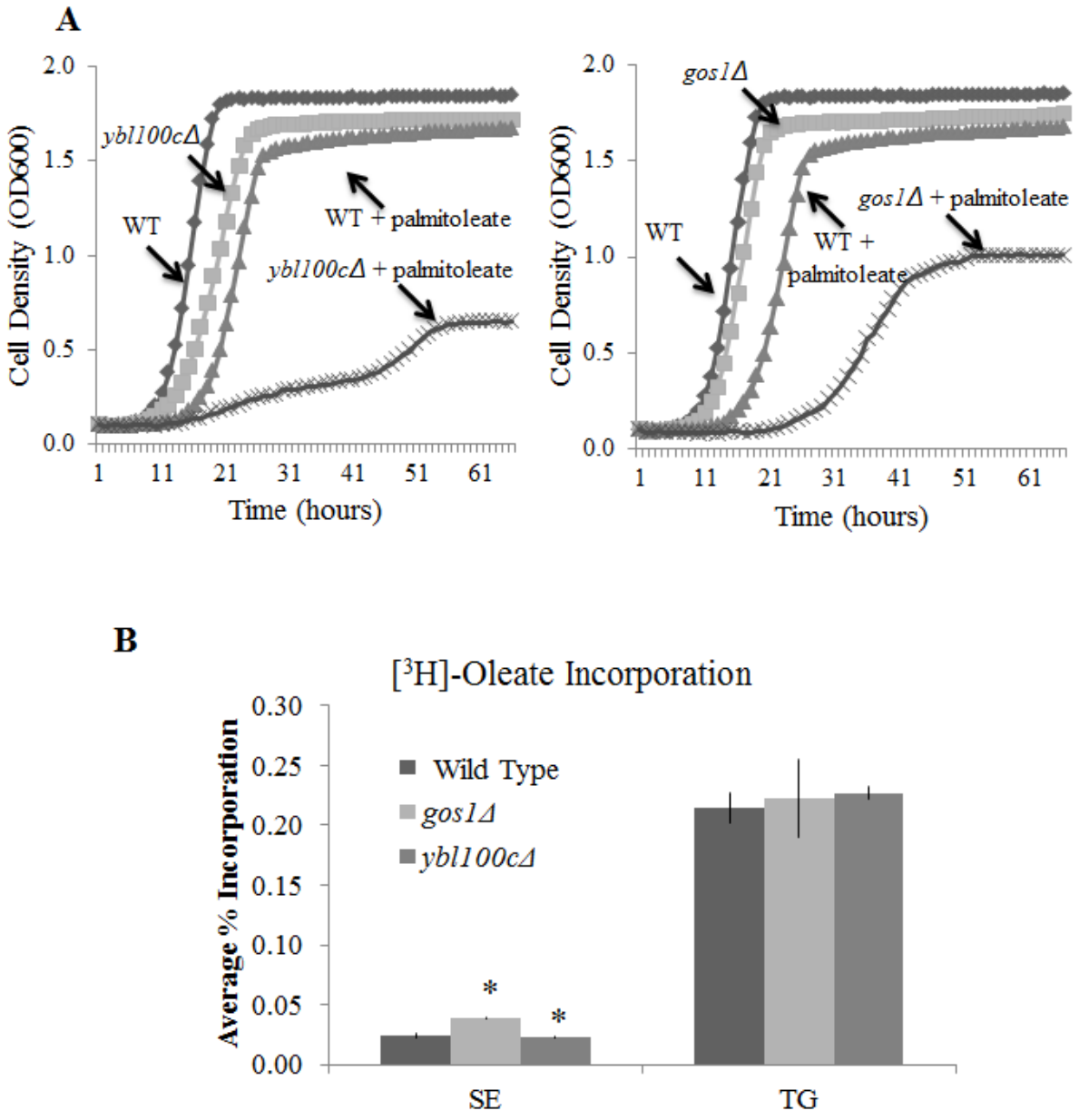

Figure 3-21: Two genes encoding tail anchored proteins, GOS1 and YBL100C, are sensitive to palmitoleate treatment (A) 44 known tail anchored proteins were tested for 16:1 sensitivity in liquid media and found that both *ybl100cΔ* and *gos1Δ* have sensitivity similar to GET family knockouts. (B) [^{3}H]-Oleate labeling of *ybl100cΔ* and *gos1Δ.* (C) Neutral lipid staining of *gos1Δ dga1Δ* and *ybl100cΔ dga1Δ.* *p<0.05

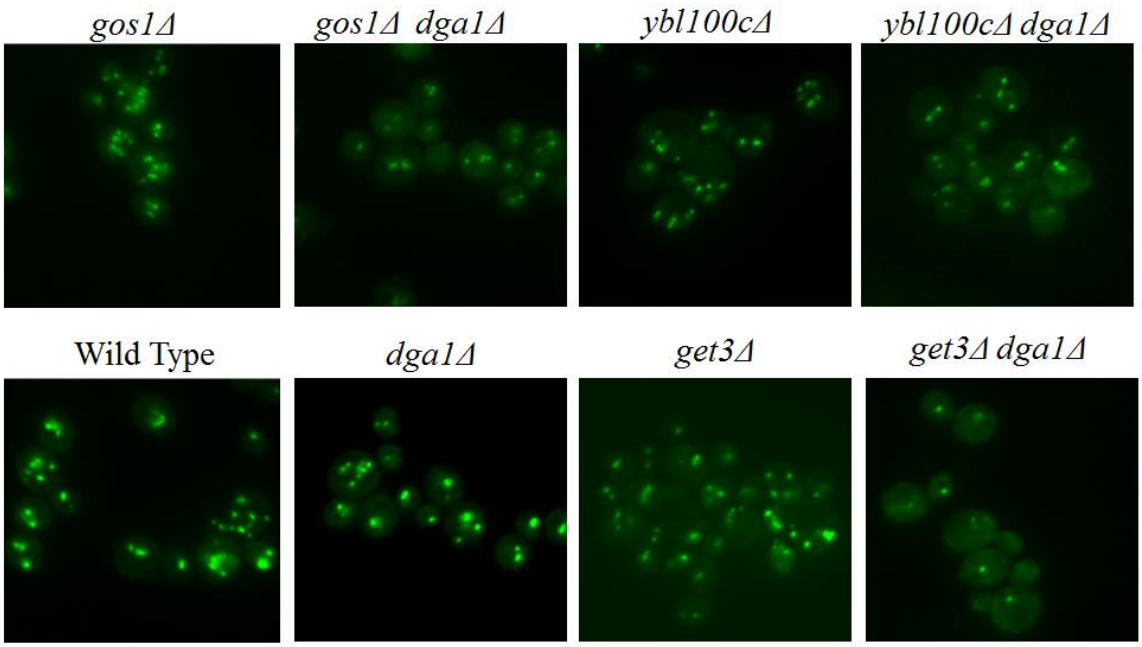

Figure 3-22: Knockout of DGA1 in a gos1Δ or ybl100cΔ background does not phenocopy the get3Δ dga1Δ double mutant lipid droplet defect. Double mutations *gos1Δ dga1Δ* and *ybl100cΔ dga1Δ* were stained for lipid droplets using Nile Red after overnight growth in rich media (YPD). Both double mutant strains did not exhibit the same defect in lipid droplet number seen in *get3Δ dga1Δ*.

DISCUSSION

In this study, we have identified a novel role for Get3p in lipid homeostasis, which appears to be independent of *GET3* mediated defects in tail-anchored protein insertion. We propose that this effect is not due to inefficient insertion of tail anchored proteins for two reasons; the contrasting lipid droplet phenotypes in *get3Δ* and *get1Δ* or *get2Δ* as well as the lack of overlap in lipid droplet morphology in double mutants of tail anchored protein genes in a *GET3* deletion background.

Results demonstrating that the lipid droplet defect occurring in the *get3Δ dga1Δ* double deletion is specific to *GET3*, and does not occur in deletions of either *GET1* or *GET2* (Fig 3-4) supports the idea that this phenotype is not due to TA protein misinsertion. Each GET complex member plays a different role in tail-anchored protein insertion; with cytosolic Get3p binding to newly synthesized TA-proteins and anchoring to ER localized Get1p and Get2p, which together insert the protein into the membrane (Fig 3-1). Ablation of either *GET1* or *GET2* results in a general loss in tail anchored proteins throughout the cell, due not only to improper insertion but also to an aggregation of TA proteins bound to cytosolic Get3p. A *GET3* deletion does not have protein aggregate build up, but does have an inefficient insertion of ER tail anchored proteins, resulting in protein insertion into multiple membranes. Studies of *GET* complex deletions have focused on the pleiotropic phenotypes caused by deletions in either *GET1* or *GET2*, due to their marked sensitivities to multiple growth conditions. Knockout of *GET3* has less growth sensitivities compared to knockouts in the other two complex members, due to the continued insertion of TA proteins [216], thus phenotypes which are dependent on GET complex function should occur in all GET mutants, but especially in *get1*Δ and *get2*Δ. For example, Schuldiner *et al.*, showed that a subset of TA protein mutants are sensitive to copper, tunicamycin and high

temperatures. Both *get1*Δ and *get2*Δ have these same sensitivity phenotypes, but *get3Δ* was shown to have either no growth defect or a less severe phenotype under all conditions [216]. Therefore, because we do not see the same deficiency in lipid droplets in *get1*Δ *dga1*Δ or *get2*Δ *dga1*Δ, it is unlikely that the defect is due to GET complex dysfunction.

Furthermore, the two tail anchored protein gene deletions found to be palmitoleate sensitive, *GOS1* and *YBL100C,* did not cause a significant reduction in LD number with an additional deletion of *DGA1*. If these proteins were responsible for the LD defect characteristic of *get3Δ dga1Δ*, we would expect double deletions of *DGA1* and *YBL100C* or *GOS1* to phenocopy the 75% reduction in LD number (Fig 3-22). As previously mentioned, many of the phenotypes resulting from a deletion in *GET1* or *GET2* can be easily explained by the extensive defects in TA protein insertion including sensitivity to copper, tunicamycin, heat and hydroxyurea [216]. Therefore, we originally assumed that the lipid metabolism defects occurring in *get3Δ* were due to TA protein misinsertion into membranes of other organelles, such as the mitochondria and Golgi. Our analysis of lipid phenotypes in TA protein mutants does not support this explanation and therefore, it is unlikely that the lipid phenotype can be explained by protein misinsertion. Nonetheless, at this point we cannot conclude that the *GET3* lipid phenotypes are unrelated to mislocalization of a combination of TA proteins (ie *gos1Δ ybl100cΔ)*.

If the lipid droplet defects resulting from a deletion in *GET3* are not due to TA protein misinsertion, then Get3p must play an alternate role in cellular homeostasis. In addition to protein insertion pathways, Get3p has been identified as a guanine nucleotide exchange factor (GEF) for the guanine nucleotide binding protein (G protein), Gpa1p [217]. G proteins are membrane bound proteins that respond to a broad range of environmental stimuli by activating

downstream signal transduction pathways. Typically, receptor activated G-proteins consist of three complex members the G_α, G_β and G_γ which are localized to the plasma membrane where they respond to external stimuli. In addition to plasma membrane localized G proteins, G proteins are also found on intracellular compartments where they play a role in trafficking [282]. Activation of a G protein-coupled receptor (GPCR) occurs through guanine nucleotide exchange (GDP for a GTP) by GEF proteins at the G_α subunit. This exchange triggers $G_{\beta\gamma}$ activation and the stimulation of downstream signaling cascades. Yeast Gpa1p is localized to both the plasma membrane and endosome, where it functions in external pheromone response and endosomal phosphatidylinositide-3-phosphate (PtdIns-3-P) production [218]. Gpa1p co-localizes with Vps34p and Vps15p at the endosome, which have been proposed to function as the G_γ and G_β, respectively [283]. Consistent with G protein function, Gpa1p localizes with Vps34p/Vps1p5 in a guanine nucleotide dependent manner and GTP bound Gpa1p leads to increased PtdIns-3-P production by the yeast phosphoinositide-3-kinase, Vps34p [284] (Fig 3-23). Get3p is a non-receptor GEF which binds to Gpa1p directly and accelerates the exchange of guanine for signal activation [217]. Therefore a deletion in *GET3* would result in decreased nucleotide exchange, causing a reduction in endosomal PtdIns-3-P production.

Levels of PtdIns-3-P at the endosome are involved in the recruitment of proteins to the membrane [285] and have been implicated in the multivesicular body (MVB) formation and vesicular trafficking [286]. A role for phosphatidylinositides in endosomal trafficking, has been shown through PtdIns-3-Kinase inhibition in human melanoma cells and selective modification of PtdIns-3-P in endosomes of HeLa cells causing slowed endosome maturation and reduced protein flux through the endosome [287, 288]. Protein sorting from the Golgi to the vacuole occurs through 3 different pathways; the “CPY” pathway, which transports proteins through the

late endosomes and MVB; the "ALP" pathway, which bypasses the endosome completely; and trafficking through the early endosome requiring maturation into the late endosome and MVB for vacuolar transport (Fig 3-23). An appealing explanation for the nutrient recycling and lipid droplet defect occurring in *get3Δ* can be inferred from the role of Get3p in guanine nucleotide exchange and activation of the Gap1p/Vps15p/Vps34p G protein complex leading to PtdIns-3-P synthesis. The deletion in *GET3* likely result in defective endosomal maturation, from the early endosome to the late endosome, due to reduced PtdIns-3-P production and a subsequent decrease in protein trafficking from the early endosome to the vacuole (Fig 3-23). This defect in protein trafficking may contribute to the lipid droplet phenotypes characterized by a *GET3* mutant.

Of the three complex members, *GET3* has been the most highly conserved compared to either *GET1* or *GET2* [289]. As all three proteins play an integral role in tail anchored protein insertion, the high level of conservation in *GET3* may be due to its dual role in tail anchored protein insertion and endosomal trafficking, though a role for the mammalian ortholog of *GET3, ASNA1*, in guanine nucleotide exchange has not yet been reported. Since these proteins contain similar structures and domains, this additional protein function cannot be ruled out and further research regarding the role of *GET3* and *ASNA1* in endosomal trafficking and maturation is required.

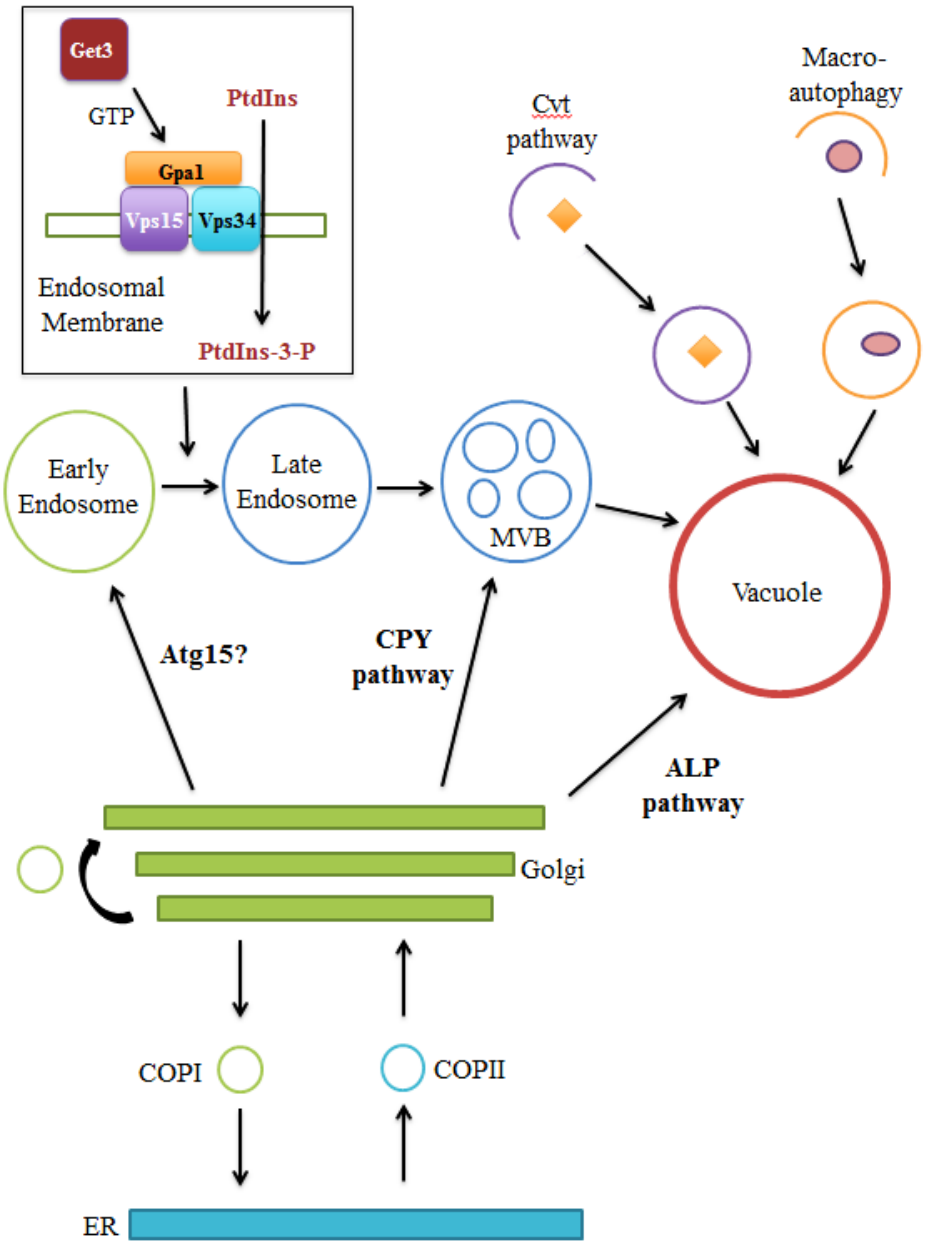

Figure 3-23: Role of GET3 in endosomal maturation and vesicular trafficking. Protein trafficking pathways from the late golgi include (1) the ALP pathway, which sorts proteins including ALP and Vam3p to the vacuole independent to MVB sorting (2) the CPY pathway which moves proteins from the golgi through the late endosome or MVB to the vacuole (the vacuolar hydrolase, CPS, and proteins destined for vacuolar degradation such as Ste2p), (3) movement from the golgi to the early endosome [223]. Additional pathways for vacuolar targeting include the cytoplasm to vacuole targeting (Cvt) pathway, which delivers the hydrolase Ape1 to the vacuole and pathways of autophagy, including microautophagy, chaperone mediated autophagy and macroautophagy. Adapted from Li *et al.*, 2009 [278]

The reduction in neutral lipid turnover (Fig 3-6, Fig 3-7), decreased autophagosome body processing (Fig 3-16) and reduced survival under starvation conditions (Fig 3-17) indicate that *GET3* mutants are unable to properly recycle nutrients through pathways of vacuolar hydrolysis. Protein hydrolysis of CMAC-Arg was functional in both *GET3* and *DGA1* mutants (Fig 3-18 and Fig 3-19) indicating efficient localization and function of vacuolar proteases and normal vacuolar pH. Despite normal proteolysis, targeting of a vacuolar lipase, such as Atg15p, may be altered in *GET3* mutants. Proteins which traffic through the early endosome to the vacuole are appealing targets to explain the slowed nutrient turnover in a *GET3* mutant due to its role in endosomal PtdIns-3-P production. Soluble vacuolar proteases and vacuolar ATPases are sorted through the MVB to the vacuole through the CPY pathway. It has been suggested that a group of proteins are first trafficked to early endosomes and through endosomal maturation enter the same MVB pathway for vacuolar targeting (Fig 3-23). We suggest that it is this latter pathway which requires the transition from early to late endosomes that is targeted by Get3p. The only identified yeast vacuolar lipase, Atg15p, requires the MVB pathway for vacuolar targeting and may utilize this early endosome trafficking pathway [277]. In summary, we propose that the decrease in endosomal PtdIns-3-P production resulting from ablation of *GET3* may cause decreased vacuolar lipase (Atg15p) trafficking to the vacuole and reduced autophagic body turnover. A role for Get3p/Gpa1p in vacuolar turnover is further supported by a genome-wide screen identifying gene deletions with reduced viability in conditions of nutrient deprivation. This screen found that deletions in *GET3, GPA1, VPS15* and *VPS34,* have decreased survival in low nutrient conditions but did not identify any other *GET* mutants with this phenotype [290].

Furthermore, increased vacuolar lipid droplet association and internalization was found in both *dga1Δ* and *get3Δ dga1Δ* (Fig 3-7). There are several possible pathways for protein and

lipid vacuolar targeting, including vesicular trafficking and autophagy (Fig 3-22). Autophagy serves as a mechanism for protein and lipid recycling during periods of starvation and has been shown to function in mammalian lipid droplet homeostasis through regulating levels of lipolysis [91]. In many cases, autophagy is specific in targeting whole organelles for degradation, as seen in mitophagy (mitochondria), reticulophagy (endoplasmic reticulum) and lipophagy (lipid droplets) [91]. During lipophagy, LDs are taken up into the autophagosomes for lysosomal (vacuolar) degradation and lipid lipolysis. In the *get3Δ dga1Δ* double mutant, internalized membranes were observed within the vacuole (Fig 3-7) reminiscent to that seen in autophagic conditions [89, 291]. As taken with the defects in vacuolar hydrolysis characteristic of *GET3* mutants, these results indicate that the reduction in LDs characteristic of the *GET3 DGA1* double mutant could occur through a combination of decreased vacuolar lipid turnover with increased basal lipophagy.

So why would lipophagy increase in this double mutant? Interestingly, the *DGA1* single mutant also showed increased vacuolar lipid association similar to that in *get3Δ dga1Δ*. Furthermore, it was only with a *DGA1* deletion that we saw a significant reduction in lipid droplet number in the *get3Δ* background. Perhaps, the increased vacuolar lipid droplet levels are due to mechanistic differences in the two diacylglycerol acyltransferase genes *DGA1* and *LRO1*. Dga1p is an acyl-coA dependent diacylglycerol acyltransferase and is most active during the stationary phase of growth [14]. Lro1p, on the other hand, has the highest enzymatic activity during the log phase and esterifies diacylglycerol from a phospholipid acyl donor [246]. The catalytic site of Dga1p faces the cytosol [292] where it synthesizes lipid droplet bound TG. In contrast, topological analysis of the yeast Lro1p predicts that the active site of Lro1p may be facing the luminal leaflet of the ER membrane [293]. This is analogous to the mechanisms of

lipoprotein particle formation, in which VLDL particles are lipidated in the ER lumen through the addition of neutral lipids to Apolipoprotein B. Moreover, similar results have been shown in hepatocytes, with DGAT1 having a "dual toplogy" where it is able to synthesize triglyceride in the lumen or cytosol based on nutrient availability [294]. We propose that synthesis of luminal TG by Lro1p is packaged separately from that formed by Dga1p. Increased vacuolar lipids in *DGA1* mutants may be due to preferential movement of Lro1p synthesized luminal TG to the vacuole, through the autophagic machinery (Fig 3-24). This would explain the normal lipid droplet number occurring in the *get3*Δ *lro1*Δ double mutant, since DGA1 synthesized TG would channel directly to the lipid droplet and would not require vacuolar lipid turnover. We predict that unlike *dga1*Δ, a knockout of *LRO1* would not have any lipid accumulation in the vacuole.

The reason for vacuolar turnover targeting of Lro1p synthesized TG is unclear, but may be related to the changing needs of the cell throughout the growth cycle. During the initial phase of growth, TG degradation is high in order to release lipid precursors for rapid membrane growth [188]. Lro1p is most active during this growth phase, and may synthesize a more accessible TG pool for cellular growth in the form of membrane building blocks. In contrast, during saturated growth, LD numbers rise and cells presumably use FA released from TG for energy and not for cellular proliferation. As the primary TG synthesis gene during saturated growth, DGA1 likely synthesizes a more stable lipid droplet pool in the cytosol for energy storage.

In summary, a double deletion in *GET3 DGA1* results in a 75% reduction in lipid droplet number, without a significant decrease in neutral lipid mass. We propose that this is due to *GET3* dependent defects in vacuolar hydrolysis, potentially through slowed Atg15p trafficking to the vacuole, and *DGA1* dependent increases in vacuolar lipid trafficking. This combination results in an accumulation of autophagic bodies and decreased nutrient and lipid turnover with a

GET3 DGA1 double deletion (Fig 3-23 and Fig 3-24). In light of the palmitoleate sensitivity occurring in *GET3* mutants, decreased neutral lipid synthesis [7, 22, 23, 151, 187] and defects in vacuolar lipolysis [91] and lipophagy [184] have both been shown to cause major impacts on cellular function during lipid load. It is therefore not surprising that loss of Get3p sensitizes these cells to fatty acid mediated cell death.

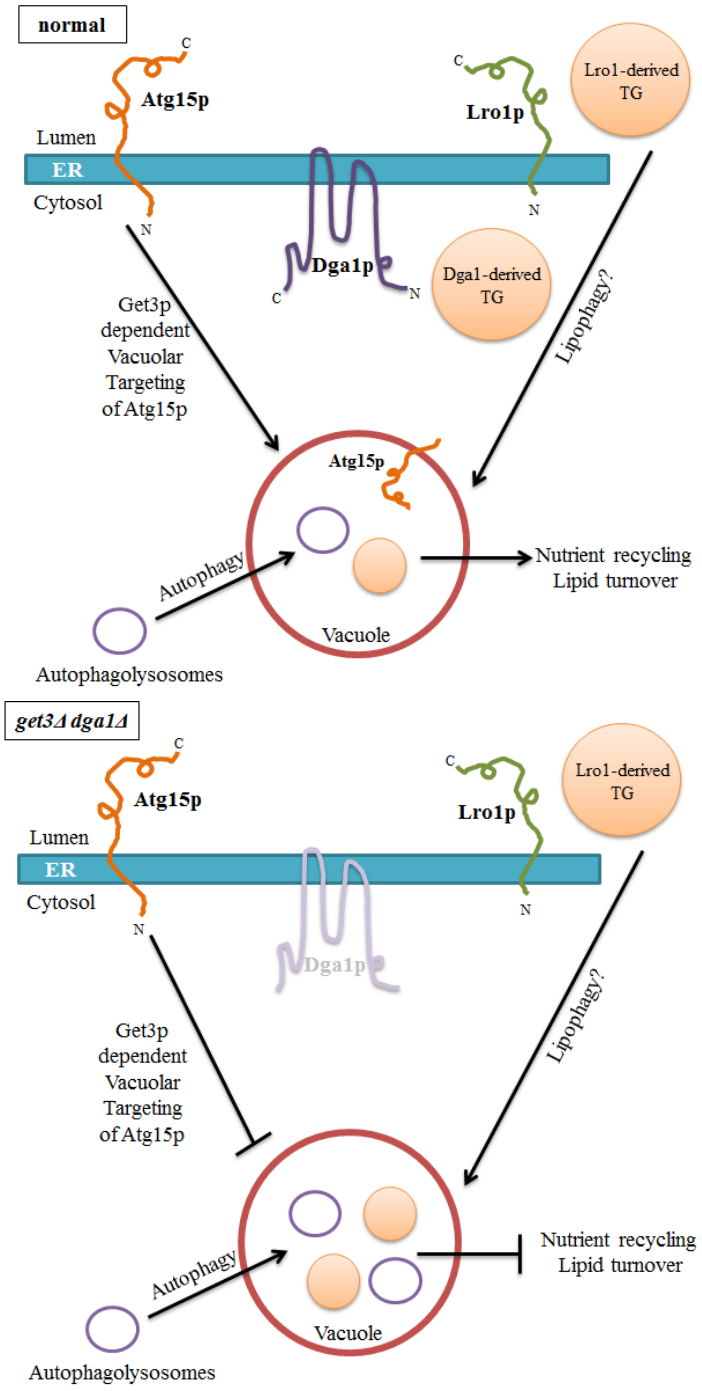

Figure 3-24: Role of GET3 and DGA1 in lipid droplet homeostasis under normal conditions and with deletions in DGA1 and GET3. Under normal conditions, nutrient recycling of vacuolar proteins and lipids continues under basal conditions and with nutrient deprivation. Lro1p derived triglyceride is more likely to target to the vacuole for lipolysis. In a *GET3 DGA1* double deletion, inefficient targeting of Atg15p may decrease vacuolar hydrolysis and autophagosome breakdown, resulting in decreased lipid droplets and reduced survival under conditions of nutrient deprivation.

CHAPTER 4

Mammalian ASNA1 is involved in palmitate-induced apoptosis and nutrient amplification of insulin release in the MIN6 pancreatic β-cell line

ABSTRACT

Lipotoxicity is a major contributor to obesity related disorders such as type 2 diabetes and nonalcoholic fatty liver disease. We completed a yeast palmitoleate sensitivity screen to identify new pathways important in mammalian lipotoxicity. Identification of Get3p as an important regulator of lipid metabolism and fatty acid sensitivity in yeast led us to its mammalian ortholog, *ASNA1*. We hypothesized that knockdown of *ASNA1* in mammalian cells would result in increased fatty acid induced apoptosis similar to that seen in the yeast *GET3* deletion. Consistent with our prediction, we found that apoptosis in the MIN6 pancreatic β-cell line following palmitate treatment was significantly increased upon *ASNA1* knockdown compared to control. Furthermore, knockdown of ASNA1 has been shown to cause a defect in insulin secretion in pancreatic β-cells, though the mechanism of this defect is still unclear. We determined that the defect in insulin secretion characteristic of *ASNA1* knockdown cells could be normalized by palmitate or amino acid supplementation. As a mediator of tail anchored protein insertion, knockdown of *ASNA1* causes a mislocalization of proteins, such as SNARES, which can affect insulin granule docking and fusion. Therefore, we propose that the defect in glucose stimulated insulin secretion resulting from reduced *ASNA1* expression is due to the mislocalization of SNAREs necessary for insulin granule fusion. The amplification of insulin secretion pathways by fatty acids and amino acids are likely to compensate for this defect by increasing the insulin granule flux and fusion of these vesicles through an *ASNA1* independent pathway.

INTRODUCTION

Chronically high levels of circulating free fatty acids (FFA) can occur through the combination of nutrient overload and insulin resistance, typically associated with obesity [105, 106, 295-297]. In the context of pancreatic β-cells, excess intracellular lipids are associated with a reduction in insulin secretion and β-cell mass through increased apoptosis [298, 299] leading to the onset of type 2 diabetes (T2D) [300-303]. Though there is a clear association between obesity and T2D, a subset of the population is more vulnerable to T2D progression, likely due to genetic variation. In order to determine gene polymorphisms responsible for this susceptibility, genome-wide association studies have been employed, and several novel genes identified [134, 135, 304]. The known genes associated with T2D still only account for a small proportion of disease pathology, and additional research is needed to understand the details of disease progression.

In order to identify genes involved in eukaryotic lipotoxicity, we carried out a genome-wide fatty acid sensitivity screen in yeast (chapter 2). Of the 156 gene mutants identified, we found that a knockout of yeast *GET3* caused increased sensitivity to the unsaturated fatty acid palmitoleate and a decrease in lipid droplet storage (chapter 3). A major goal of our yeast FA sensitivity screen was to identify conserved genes that are involved in both yeast and mammalian lipotoxic pathways (chapter 2). The high sequence conservation between yeast *GET3* and human *ASNA1* (46% identity) suggests a role for *ASNA1* in cellular lipotoxicity.

Like *GET3*, *ASNA1* is a member of the transmembrane domain recognition complex (TRC) that targets tail anchored (TA) proteins for ER protein insertion [305]. As seen with Get3p, the cytosolic ASNA1 recognizes transmembrane domains of TA proteins and delivers them to the ER (Fig 4-1). Yeast Get3p interacts with two ER resident proteins, Get1p and Get2p,

which are necessary for protein insertion. Through sequence similarity, a mammalian *GET1* ortholog, *CHD5* (congenital heart disease 5 protein) was recently identified, which has a similar topology to GET1, with 3 predicted transmembrane domains and an exposed cytosolic coiled-coil domain. CHD5 binds to ASNA1 in this coiled-coil domain and provides a docking site at the ER membrane [306] (Fig 4-1).

ASNA1 requires several other factors for efficient protein insertion. The three protein complex consisting of the *GET4* and *GET5* orthologs, TRC35 and UBL4A, and the functional Sgt2 ortholog BAT3, were found to increase TA protein insertion efficiency through TA protein loading. The TRC35-UBL4A-BAT3 complex provides a scaffold, bringing ASNA1 and the TA protein substrate in close proximity for transfer (Fig 4-1). Only those proteins which have ER-destined TA protein motifs actively bind to ASNA1, providing a key sorting step in this process [247].

Human *ASNA1* is highly expressed in pancreatic beta cells and increased *ASNA1* expression promotes insulin secretion in the mouse insulinoma cell line, NIT-1, though the mechanism of this increase is still unclear. Likewise, insulinoma clones with reduced *ASNA1* expression showed decreased insulin secretion with no change in the total cell content of proinsulin or insulin protein [233]. This data demonstrates that *ASNA1* is not involved in the insulin synthesis pathway but instead likely promotes one of the steps leading to insulin release from β-cells, possibly ion channel regulation or the docking and fusion of insulin containing vesicles.

The role of *ASNA1* in insulin secretion indicates that it may be an innovative target for the two contributors of type 2 diabetes; defects in pancreatic β-cell insulin secretion and lipid-induced apoptosis. A whole body knockout of *ASNA1* is embryonic lethal in mice [307], and

therefore we do not expect that loss of function mutations exist in the population. Instead polymorphisms reducing function may sensitize cells to lipotoxicity. For this reason, we chose to study the role of *ASNA1* in lipotoxic disease using siRNA-induced knockdown of *ASNA1* expression in the MIN6 insulin secreting pancreatic β-cell line.

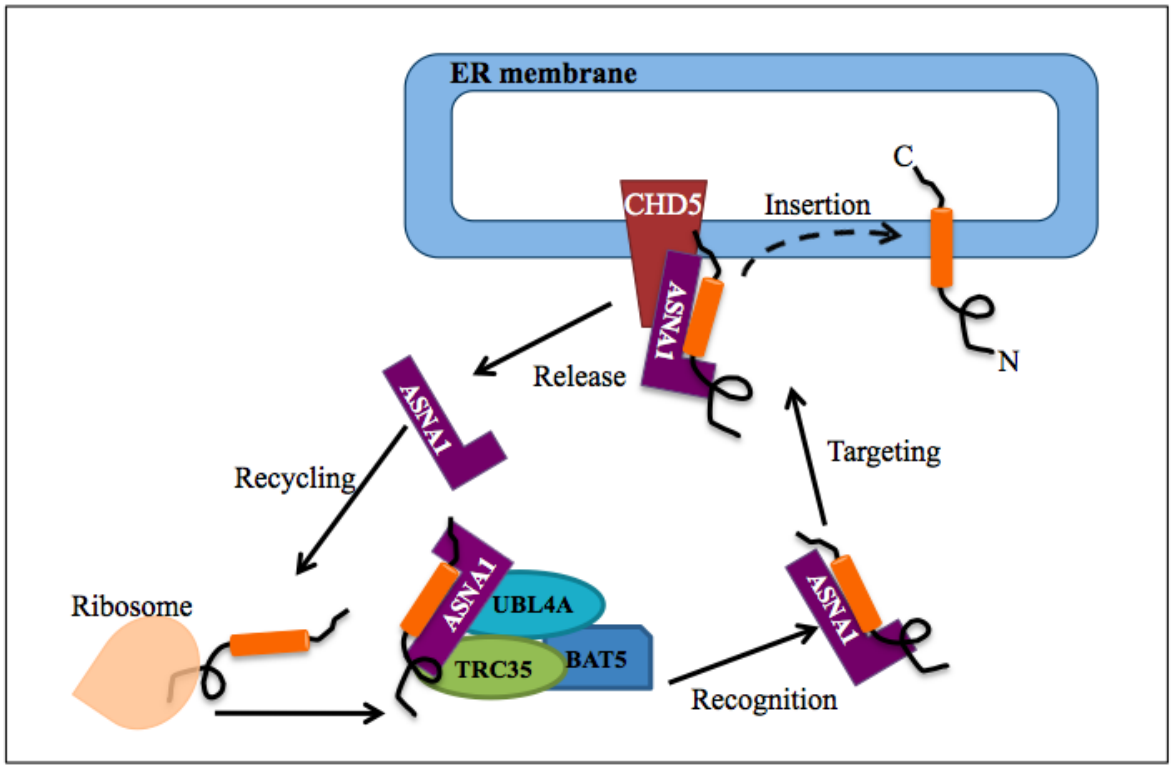

Figure 4-1: Role of ASNA1 in tail anchored protein insertion. ASNA1 recognizes newly synthesized tail anchored proteins and directs them to the ER membrane. The putative docking site for ASNA1 is the GET1 ortholog WRB. Together these proteins insert the TA protein into the membrane and ASNA1 is then released for further binding capabilities. See introduction for details.

METHODS

Cell Culture. The MIN6 mouse insulinoma cell line was a kind gift of Alan Attie. MIN6 cells were maintained in Dulbecco's modified Eagles Medium (DMEM) containing 25 mM glucose, 15% heat-inactivated fetal bovine serum (FBS), 100 units/ml penicillin, 100 μg/ml streptomycin, 100 μg/ml L-glutamine and 5 100 μl/L β-mercaptoethanol [308]. Cells between passages of 25-40 were used for knockdown. McArdle RH7777 cells were obtained from ATCC and were maintained in DMEM with 10% FBS, 10 % Horse Serum, 100 units/ml penicillin, and 100 μg/ml streptomycin. Cells were grown in humidified 5% CO_2, 95% air at 37°C. For fatty acid studies, cells were incubated for 0-20 hours in DMEM with 10% FBS containing oleate palmitate or palmitoleate (Sigma-Aldrich) bound to 1% fatty acid free BSA (Sigma-Aldrich). Control incubations contained only BSA.

siRNA knockdown. ASNA1 expression was specifically silenced using prevalidated duplexes (Stealth™ Select RNAi, Invitrogen) directed against mouse *ASNA1* (siRNA 92: sense 5'-GGACGUGAGAGUGUUCUGAUCAUUU , siRNA 94: sense 5'-CCUGGACCAGAUGGAAGACCUAUA). Stealth™ Select RNAi negative control duplexes based on GC content (Invitrogen) were used as a non-specific control. Transfection was completed using Lipofectamine 2000 according to the manufacturers protocol. Cells were treated with a final concentration of 100 pM siRNA in a total of 2 mL media per dish for 24 hours in normal culture conditions. When specified fatty acids were added to culture 24 hours after knockdown.

Lipid Analysis and Metabolic Labeling. For lipid labeling, cells were pulse labeled with 0.5 μCi/ml [9,10-^{3}H] Oleic acid (Perkin Elmer) for 6 hours in serum free DMEM with 1% fatty acid free BSA plus 0.25 mM cold oleate. Glycerol labeling was completed with 20 μCi/ml of [^{3}H] Glycerol (PerkinElmer) in 1.5% fatty acid free BSA in serum free DMEM. Cells were pulse labeled for 2 hours at 37°C followed by a 4 hour chase (serum free DMEM with 1.5% BSA, no label). Lipid were extracted with 2 ml of hexane:isopropanol (3:2) was added to each well of a 6 well plate and incubated at room temperature for 1 hour, after which the supernatant was removed and the extraction repeated. Supernatant was dried with nitrogen, resuspended in chloroform:methanol (2:1) and lipids were separated on a TLC plate [309].

Quantitative PCR. RNA was isolated using the Qiagen RNAeasy kit as specified by the manufacturer and used to generate first strand cDNA (SuperScript first strand synthesis system, Invitrogen). Quantitative real time PCR was performed with the MyiQ single color real time PCR detection system (Bio-Rad), SYBR Green 2X supermix (Bio-Rad) and the indicated primers (Table 4-1). Expression levels were calculated relative to mouse GAPDH.

Immunoblotting. Cells were washed twice with PBS and lysed using SDS buffer (2% SDS, 62.5 mM Tris-HCL (pH 6.8), 10% glycerol, 10% β-mercaptoethanol, and 0.01% bromophenol blue) and boiled for 5 minutes. Protein extracts were prepared in a lysis buffer containing 25 mM Tris-HCL (pH 7.4), 2 mM Na_3VO_4, 10 mM NaF, 10 mM $Na_4P_2O_7$, 1 mM EGTA, 1 mM EDTA, 1% NP-40, 5 μg/ml leupeptin, 5 μg/ml aprotinin, 10 nM okaidic acid and 1 mM phenylmethylsulfonylfluoride. Equal amounts of protein extract were separated on a 12% SDS-PAGE gel and electrotransferred to a 0.45 μm nitrocellulose membrane using a Bio-Rad

laboratories mini-transfer tank. Membranes were blocked for 1 hour at room temperature with 5% non-fat milk in Tris-Buffered Saline with 0.1% Tween 20 (TBST) and incubated with primary antibodies overnight at 4°C. Protein bands were detected with HRP-conjugated secondary antibodies and SuperSignal West Pico enhanced chemiluminescent solution (Pierce). Membranes were stripped with Restore Western blot stripping buffer (Pierce) for 10 minutes at room temperature and reprobed with β-actin primary antibodies to control for loading differences. Primary antibodies used were anti-GRP78, anti-phospho-eIF2α (Stressgen, Victoria, British Columbia) and anti-β-actin (Sigma). Immunoblots were quantified by densitometry.

Oil Red O staining. Cells were fixation was carried out in 10% neutral-buffered formalin for 1 hour at room temperature followed by 5 minute incubation in 60% isopropanol. Cells were stained in 0.5% Oil Red O solution in isopropanol:water (3:2) for 30 minutes followed by several washes with distilled water. Cells were dried overnight and visualized using light microscopy.

Apoptosis Assays. Apoptosis levels were quantified using Invitrogen Vibrant Apoptosis Assay Kit #5 (V13244) by manufacturer's directions. Briefly, cells were incubated with 5 μg/ml Hoechst 33342 and 1 μg/ml propidium iodide (PI) for 30 minutes on ice. Apoptotic cells are characterized as having condensed chromatin, which is stained by blue-fluorescent Hoechst 3342, and stains the nuclei of apoptotic cells more brightly than that seen in normal cells. Dead cells were identified as having internalization of PI, and apoptotic cells were considered as cell stained positive for Hoechst-33342 and negative for PI. Ten frames per condition were captured and cells within these frames were counted in order to obtain a percentage of apoptotic cells within the population.

Insulin Secretion. Cells (5 x 10^5 cells/well, 12 well plate) were seeded and cultured as described. The cells were preincubated for 1 hour in HEPES-balanced Krebs-Ringer bicarbonate buffer (119 mM NaCl, 4.74 mM KCL, 2.54 mM $CaCl_2$, 1.19 mM $MgCl_2$, 1.19 mM KH_2PO_4, 25 mM $NaHCO_3$ and 10 mM HEPES, pH 7.4) containing 0.5% BSA with 5 mM glucose and incubated for 1 hour with various concentrations of glucose or KCL. Released insulin was measured by rat insulin radioimmunoassay (Millipore) and the cellular DNA content was used to normalize the amount of insulin secretion.

ApoB immunoprecipitation. Cells were incubated in methionine/cysteine-free DMEM with 1.5% fatty acid free BSA for 2 hours followed by [^{35}S] methionine labeling for 2 hours. After labeling, media was transferred into eppendorf tubes and a mixture of protease inhibitors (30µl/ml protease inhibitors, 1 mM benzamidine, 5 mM EDTA, 100 units/ml aprotinin, 50 µg/ml leupeptin, 50 µg/ml pepstatin A and 10 mM Hepes, pH 8.0) and 0.86 mM freshly added phenylmethylsulfonyl fluoride. Immunoprecipitation of apoB in medium and cells was carried out according to the method described by Dixon et al [310] Antibodies against apoB (Calbiochem, San Diego, CA) and rProtein G Agarose (Invitrogen) was added to the reactive solution to precipitate apoB. ApoB was precipitated by boiling for 5 minutes in sample buffer (0.125 M Tris-HCl, pH 6.8, 4% SDS, 20% glycerol and 10% β-mercaptoethanol). Proteins were separated by SDS-PAGE and gels were then treated with autofluor (Natioal Diagnostics, Atlanta GA) and after drying exposed to X-ray film (Kodak, X Omat AR) at -80°C for 1-3 days. Incorporation of [^{35}S] into apoB48 and apoB100 was quantified by autoradiography and bands were cut and radioactive incorporation was quantified by liquid scintillation counting [311].

RESULTS

In order to determine the role of *ASNA1* in pancreatic β-cell lipotoxicity, we used the MIN6 insulin secreting mouse pancreatic β-cell line [308]. *ASNA1* expression is known to be particularly high in mouse and human pancreatic islet cells [233, 312], which we validated by real time PCR compared to expression levels in the mouse liver (Fig 4-2). We also found significant levels of ASNA1 expression in the MIN6 and McA-RH7777 rat hepatoma cell line (Fig 4-2).

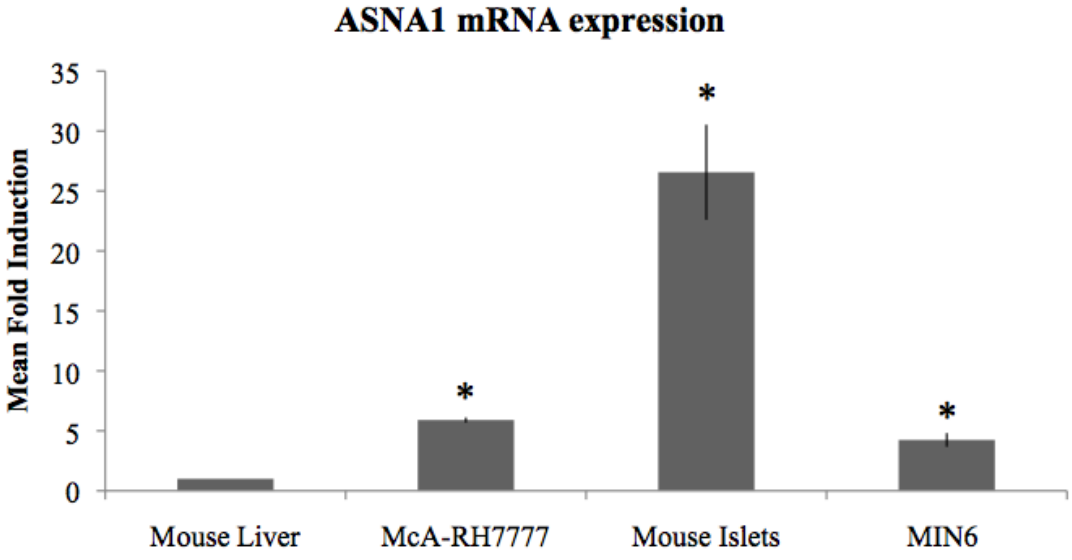

Figure 4-2: Tissue specific mRNA expression of ASNA1. Real time PCR measurements of *ASNA1* mRNA in mouse pancreatic islet cells, the mouse pancreatic β-cell line MIN6 , the rat hepatoma cell line McA-RH7777 and mouse liver. Differences of mean fold induction (ΔΔCt) relative to mouse liver (mean ± s.d., n=3). Asterisks denote statistical significance (*$p<0.05$) compared to liver by unpaired t-test.

For gene knockdown, MIN6 cells were transfected with *ASNA1* specific or control siRNA oligonucleotides and grown at 37°C for 48 hours. Treatment with *ASNA1* siRNA resulted in an approximate 70% reduction in mRNA expression compared to control (Fig 4-3).

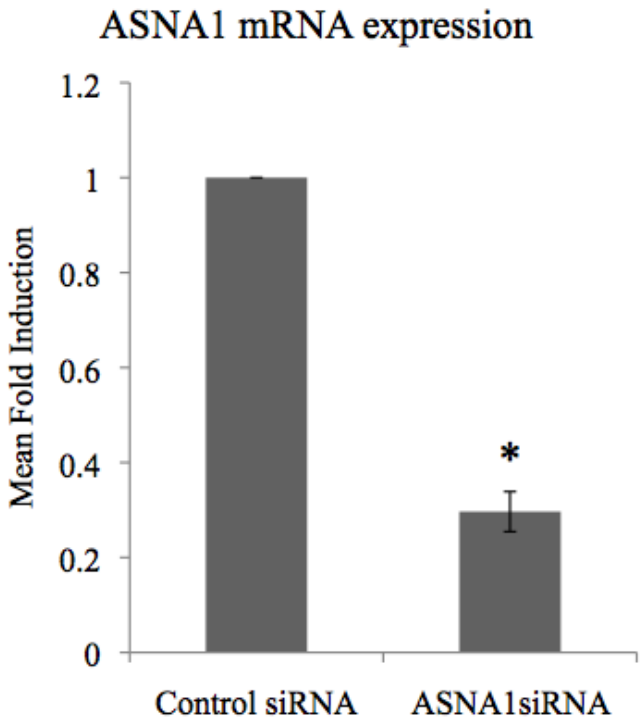

Figure 4-3: ASNA1 knockdown in MIN6 mouse pancreatic β-cells. MIN6 cells were treated with 100 pM ASNA1 or control siRNA for 48 hours after which our follow up studies were completed. Total RNA was isolated and quantitative RT-PCR was performed to assess mRNA levels of ASNA1 (mean ± s.d., n=3). Asterisks denote statistical significance (*$p<0.001$) compared to liver by unpaired t-test.

Levels of lipid-induced apoptosis are significantly altered in MIN6 cells with ASNA1 knockdown. Treatment of yeast *get3Δ* with 0.5 mM palmitoleate causes a significant increase in apoptosis compared to the control strain (chapter 3). Due to the conservation of both sequence and function between yeast *GET3* and mammalian *ASNA1* we expected that knockdown of *ASNA1* would also increase sensitivity of cells to fatty acid induced apoptosis. We grew control and *ASNA1* siRNA treated MIN6 cells with media containing palmitate (0.5 mM and 1.0 mM),

palmitoleate (0.5 mM and 1.0 mM) or 0.5 mM oleate for 20 hours and assayed apoptosis by Hoechst 33342 and propidium iodide (PI) staining (Fig 4-4 A,B).

We quantified percentage of cells undergoing apoptosis, including both early apoptotic (Hoechst +/PI -) and late apoptotic (Hoechst +/ PI +), and necrotic (Hoechst -/ PI +) cells as a percentage of the total cells within each frame (Fig 4-4 C). Knockdown of *ASNA1* resulted in a significant increase in the percent of apoptotic cells at 1.0 mM palmitate, which was not seen at lower concentrations of palmitate (0.5 mM) or with treatment with the unsaturated fatty acids palmitoleate and oleate (Fig 4-4 B). In fact, cells treated with 0.5 mM palmitoleate had reduced apoptosis in the *ASNA1* knockdown cells compared to control. The differential sensitivity of MIN6 cells with reduced *ASNA1* expression to UFA versus SFA is interesting. UFA and SFA induced β-cell lipotoxicity are known to occur through independent pathways, with SFA causing cellular dysfunction through increased ceramide biosynthesis [110, 111] and increased reactive oxygen species [125], and UFA induced lipotoxicity involving the phosphorylation/dephosphorylation of protein phosphatase type 2C proteins [116, 130]. Both UFA and SFA mediated cell dysfunction can occur through altered ER stress activation [129, 182]. Therefore, ASNA1 may alter these pathways conversely, leading to the contrasting lipoapoptosis results (Fig 4-4B).

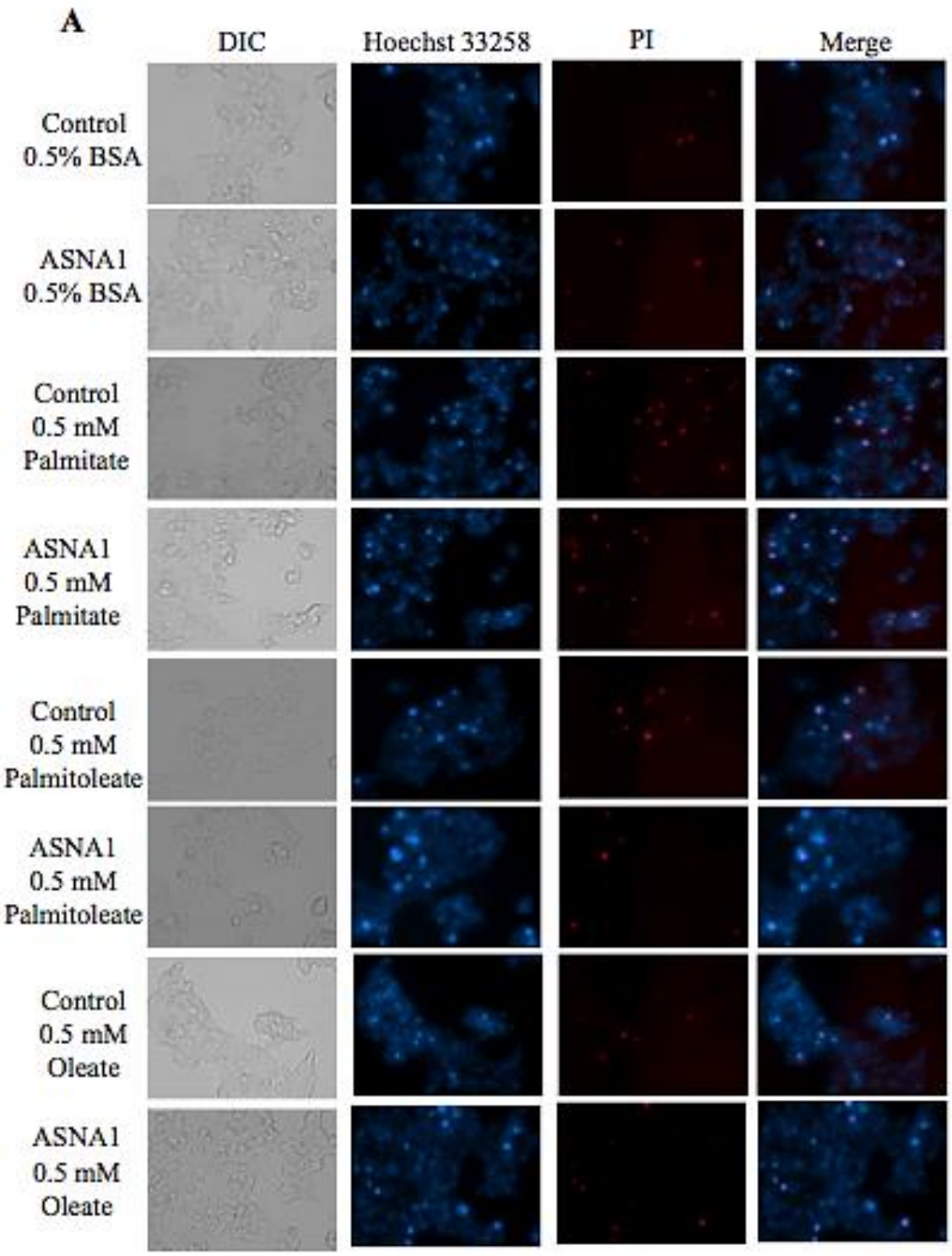
A
DIC
Hoechst 33258
PI
Merge
Control
0.5% BSA
ASNA1
0.5% BSA
Control
0.5 mM
Palmitate
ASNA1
0.5 mM
Palmitate
Control
0.5 mM
Palmitoleate
ASNA1
0.5 mM
Palmitoleate
Control
0.5 mM
Oleate
ASNA1
0.5 mM
Oleate

Figure 4-4

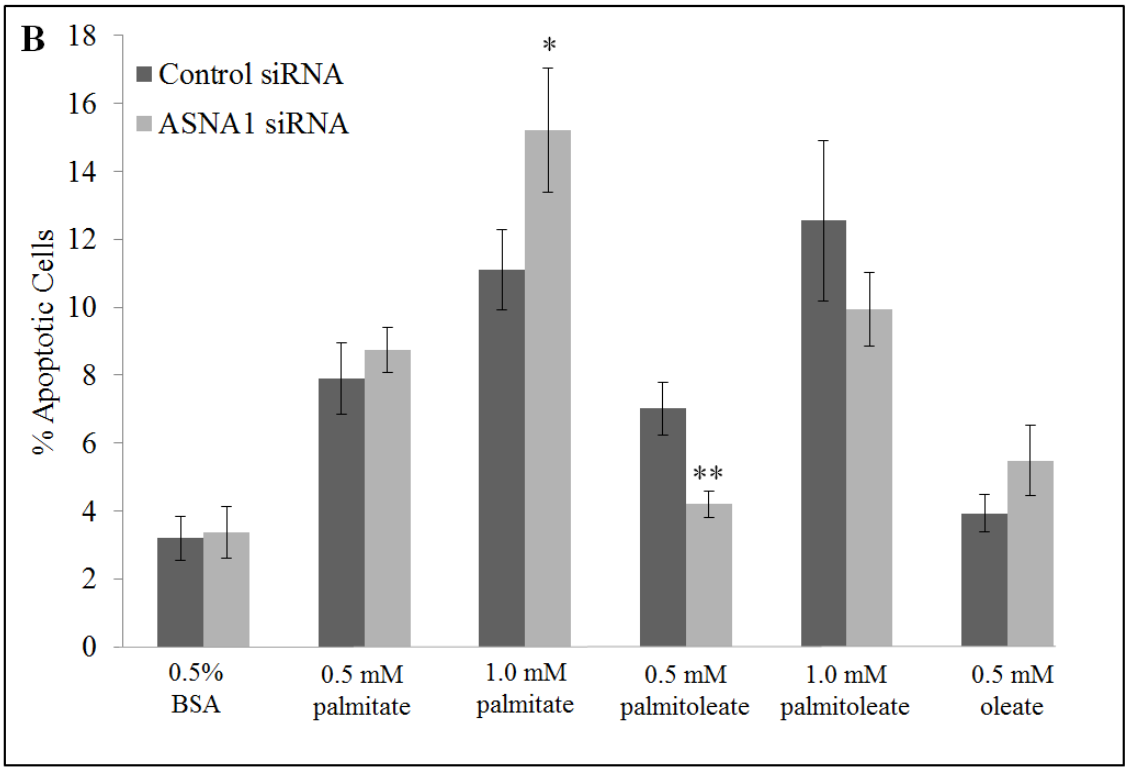

Figure 4-4: Knockdown of ASNA1 in MIN6 cells increases sensitivity to palmitate-induced apoptosis. Apoptosis rate of MIN6 cells was measured by Hoechst 33342 and propidium iodide staining after 16 hours of fatty acid treatment in DMEM + 10% FBS with 0.5 mM fatty acid free BSA (A) Fluorescent microscopy images of Hoechst 33342 and propidium iodide (PI) staining of fatty acid treated cells. (B) Quantification of apoptotic (Hoechst +) cells as a percentage of total cells. (mean ± s.e., 7 frames with at least 150 cells per frame) Asterisks indicate statistical significance (*$p<0.05$, **$p<0.01$) compared to control siRNA by two tailed t-test. (C) Example of early apoptotic (Hoecsht +), late apoptotic (Hoechst +/PI +) and necrotic (PI +) cells.

Knockdown of ASNA1 in mouse pancreatic β-cells does not alter levels of lipid synthesis. Neutral lipid synthesis serves not only as a mechanism for energy storage during periods of nutrient deprivation, but also as a protective mechanism against an accumulation of intracellular fatty acids [114]. As such, ablation of neutral lipid storage capacity results in sensitivity of eukaryotic cells to fatty acid induced apoptosis [7, 22, 23].

As described in chapter 3, knockout of *GET3* in yeast results in decreased neutral lipid synthesis and a significant reduction in lipid droplet number per cell. For this reason, and because lipoapoptosis was significantly increased with *ASNA1* knockdown, we predicted that a reduction in *ASNA1* expression would result in a decrease in neutral lipid storage capacity. In order to measure neutral lipid levels in these strains, we used radiolabeled oleate incorporation and Oil Red O, which stains the neutral lipids, cholesterol ester and triglyceride.

In contrast to the decreased neutral lipid levels occurring in yeast *get3Δ* there was no change in lipid synthesis detected in the *ASNA1* knockdown, as measured by [^{3}H]oleate incorporation in mammalian cells. We separated several lipid species (sterol ester (SE), triglyceride (TAG), free fatty acid (FFA), diacylglycerol (DAG) and phospholipids (PL)) by thin layer chromatography followed by scintillation counting in order to determine the synthesis of each during a 4 hour growth period (Fig 4-5). Consistent with the lipid labeling results, Oil Red O staining indicated no change in lipid droplet morphology in *ASNA1* siRNA treated cell compared to control (Fig 4-6).

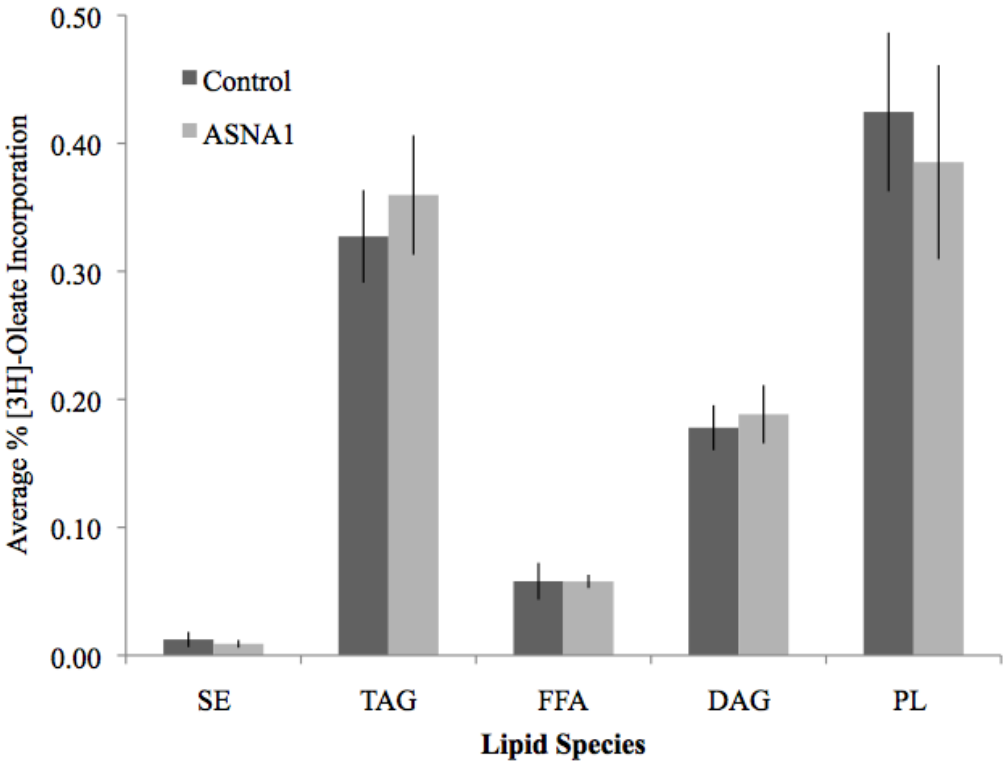

Figure 4-5: A reduction in ASNA1 expression in MIN6 cells does not alter levels of lipid synthesis. Lipid extraction and species separation through thin layer chromatography (TLC) was completed on MIN6 cells after 4 hours pulse with [^{3}H]-Oleate incorporation after 4 hour pulse.

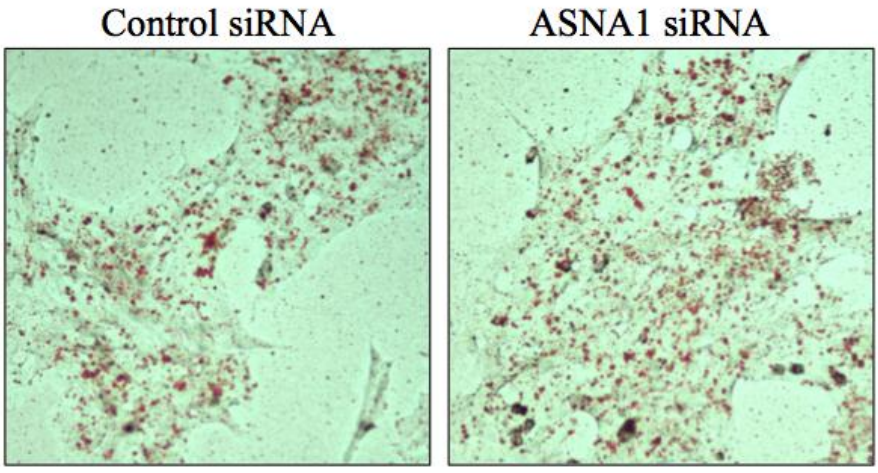

Figure 4-6: ASNA1 knockdown in MIN6 mouse pancreatic β-cellsdoes not change lipid droplet number or size. Oil Red O staining of neutral lipids in MIN6 cells treated for 20 hours with 0.5 mM oleate in DMEM + 10% FBS.

ASNA1 knockdown has increased basal ER stress, as measured by GRP78 protein expression. Increased levels of ER stress are commonly associated with lipoapoptosis [129, 131] and pancreatic β-cells are particularly vulnerable to lipid induced ER stress due to the protein load associated with their role in insulin secretion [313]. We went on to determine if the differences in lipotoxicity with *ASNA1* knockdown could be explained by altered ER stress response by measuring mRNA and protein levels of the ER stress marker, GRP78 [314]. Gene expression levels of *GRP78* were increased in response to 0.5 mM palmitate in both control and *ASNA1* siRNA treated cells, consistent with the known role of palmitate in ER stress activation [128, 142]. Oleate treatment did not cause any increase in GRP78 mRNA expression in either siRNA condition (Fig 4-7C).

In line with the mRNA expression levels, incubation of MIN6 control cells with palmitate resulted in an increase in GRP78 protein levels (Fig 4-7B). GRP78 protein expression in the control was also increased when treated with 1.0 mM oleate (Fig 4-7B), a result which was not seen in the mRNA expression but one which has been previously reported in other studies [124, 128]. As protein levels are more relevant to ER stress induction, we used the protein expression as the more accurate readout of ER stress.

Interestingly, GRP78 protein expression in *ASNA1* knockdown was significantly increased under no treatment conditions (0.5% BSA) compared to control, at levels similar to that seen following palmitate treatment in the control condition (Fig 4-7B). Growth of *ASNA1* knockdown cells with fatty acids did not induce a further elevation in GRP78 expression compared to the high basal levels, and the GRP78 protein levels remained constant regardless of the media type (Fig 4-7 A,B). In other words, knockdown of *ASNA1* causes a rise in GRP78

protein expression and this expression level is not further increased upon fatty acid treatment in the *ASNA1* knockdown (Fig 4-7B). The significant increase in GRP78 expression under normal conditions (0.5% BSA) indicates that cells with reduced ASNA1 expression have elevated basal ER stress, a condition that may influence the cells ability to handle exogenous fatty acids.

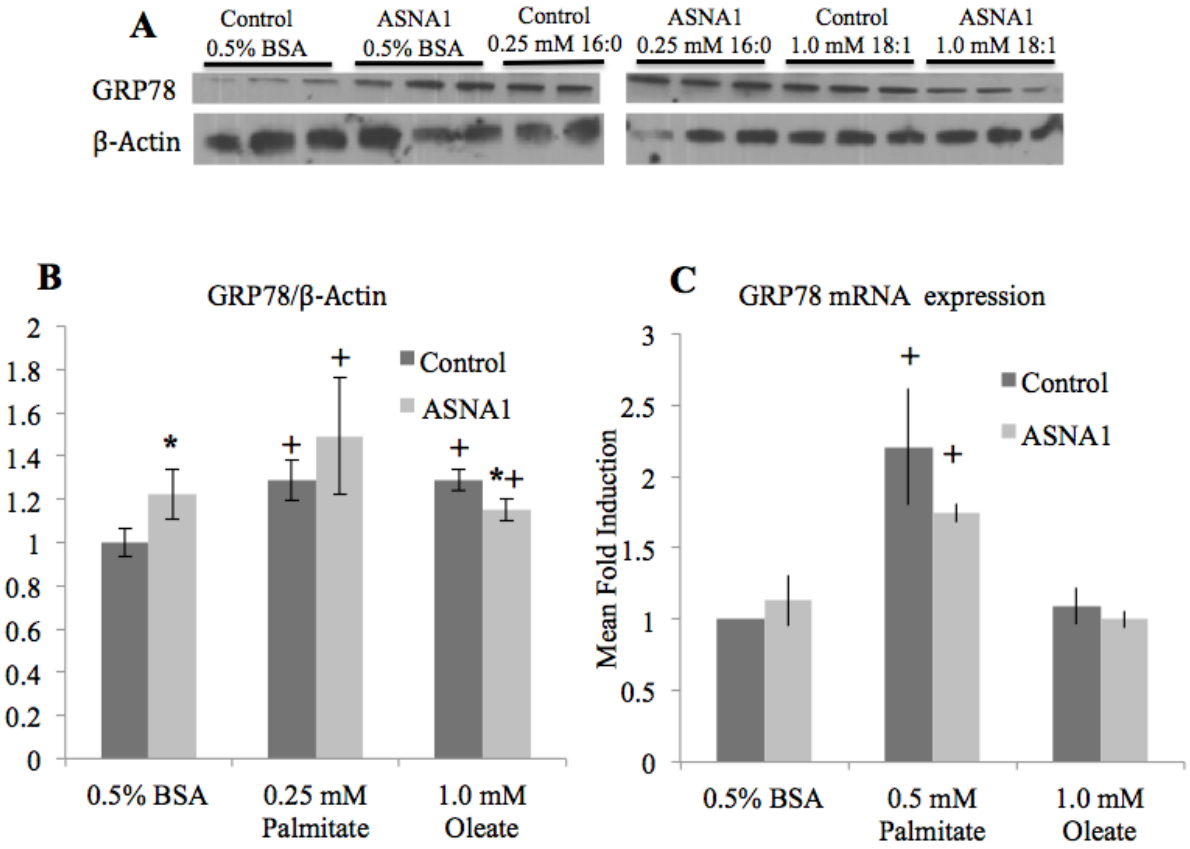

Figure 4-7: Altered GRP78 levels in ASNA1 knockdown indicates increased ER stress activation under basal conditions. In order to determine ER stress levels, protein and mRNA was isolated from MIN6 cells treated with fatty acids for 16 hours. Protein levels of GRP78 were determined through Western blotting (A) and quantified relative to the housekeeping gene β-Actin (B). Gene expression of GRP78 was quantified through real time PCR relative to 0.5 % BSA control. Statistical significance was determined through unpaired t-test (mean ± s.d., n=3). Asterisks indicate statistical significance (*$p<0.05$) compared to control within the same treatment condition, + indicates statistical significance (+$p<0.05$) compared to 0.5% BSA for the same siRNA treatment.

ASNA1 is required for insulin secretion in response to glucose. Kao *et al,* described a defect in insulin release and glucose stimulated insulin secretion in clones of the mouse insulinoma cell line NIT-1 with decreased *ASNA1* expression. This was not due to decreased pro-insulin or insulin production [233] and therefore, *ASNA1* likely affects the fusion of insulin granules with the membrane.

Acute exposure of pancreatic β-cells to long chain fatty acids promotes insulin secretion through several potential mechanisms, including increased insulin granule fusion with the membrane [315] and activation of the G-protein coupled receptor (GRP40) which stimulates insulin secretion through increased cytosolic Ca^{2+} [316] (Fig 4-8). In order to determine if the *ASNA1* dependent defect in insulin secretion also occur in response to acute free fatty acid treatment, we challenged MIN6 cells in buffer containing glucose with and without the fatty acid palmitoleate or palmitate for 1 hour and measured insulin secretion (Fig 4-9A).

Consistent with the previously reported results [233], we found a reduction in insulin release in *ASNA1* siRNA treated cells in both low (2.8 mM) and high (20 mM) glucose conditions compared to the siRNA control. We also measured insulin secretion in these cells when challenged with buffer containing both fatty acids and glucose. Co-supplementation of glucose at low levels (2.8 mM) with 0.5 mM palmitate resulted in an increase in insulin secretion in MIN6 cells in both the control and *ASNA1* siRNA groups, to an equal extent. In other words, challenge of *ASNA1* cells with an acute palmitate treatment resulted in an amplification of insulin release to the same level of the control (Fig 4-10). Therefore, palmitate amplification of glucose stimulated insulin secretion (GSIS) was able to compensate for the *ASNA1* dependent secretion defect.

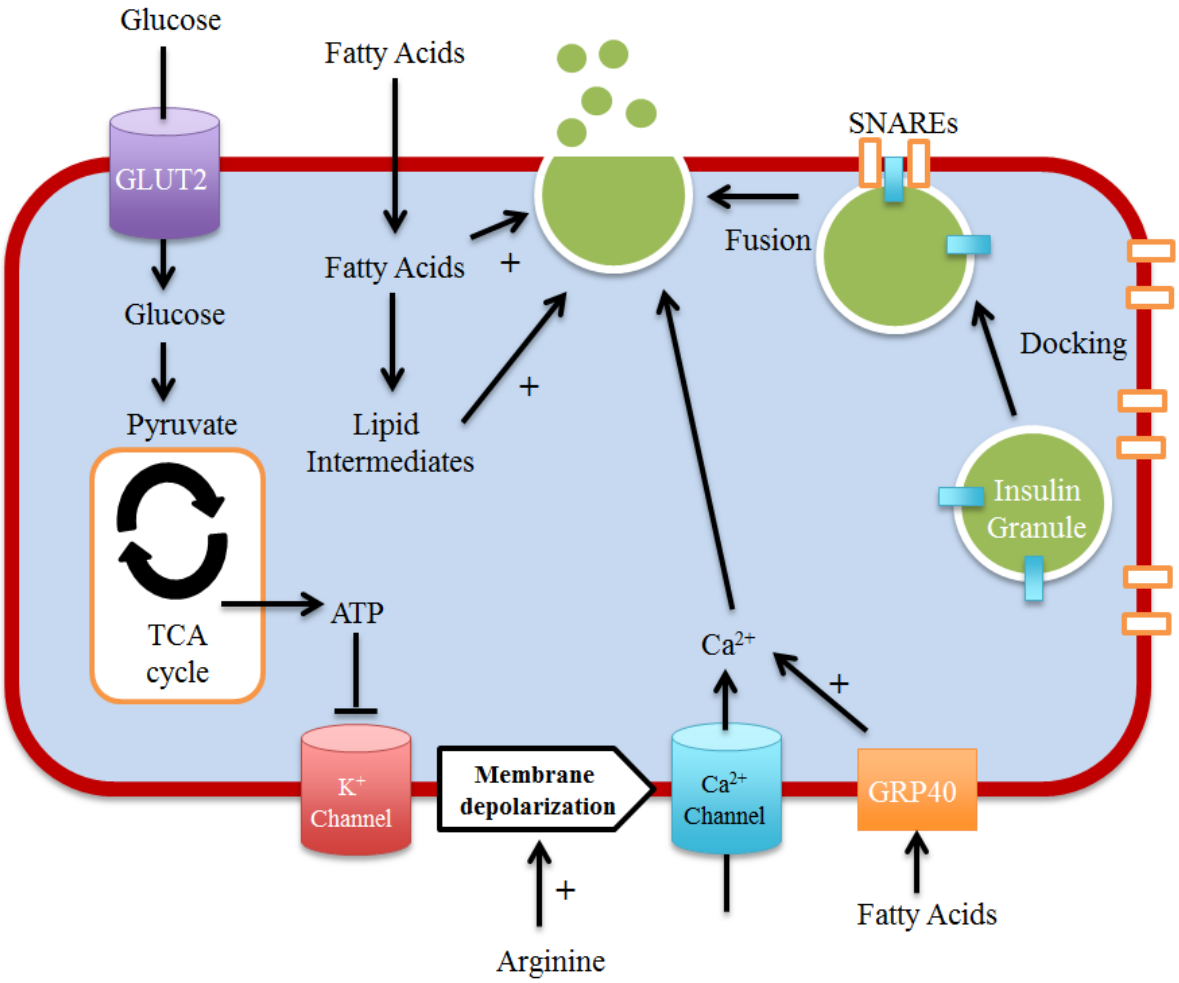

Figure 4-8: Nutrient modulation of insulin secretion in pancreatic β-cells. Interaction of glucose, fatty acids and amino acids (arginine) in stimulation and potentiation of the insulin release. Glucose uptake through the GLUT2 insulin independent glucose transporter increases glycolysis and ATP synthesis. Increased intracellular ATP inhibits potassium channel, causing a subsequent membrane depolarization and the opening of voltage gated calcium channels. Increased intracellular calcium resulting in insulin secretion. Fatty acids and amino acids, such as Arginine, are able to amplify these pathways through increased fusion (fatty acids and lipid intermediates), increased intracellular calcium through FA binding to GRP40 and increased membrane polarization (through arginine stimulation).

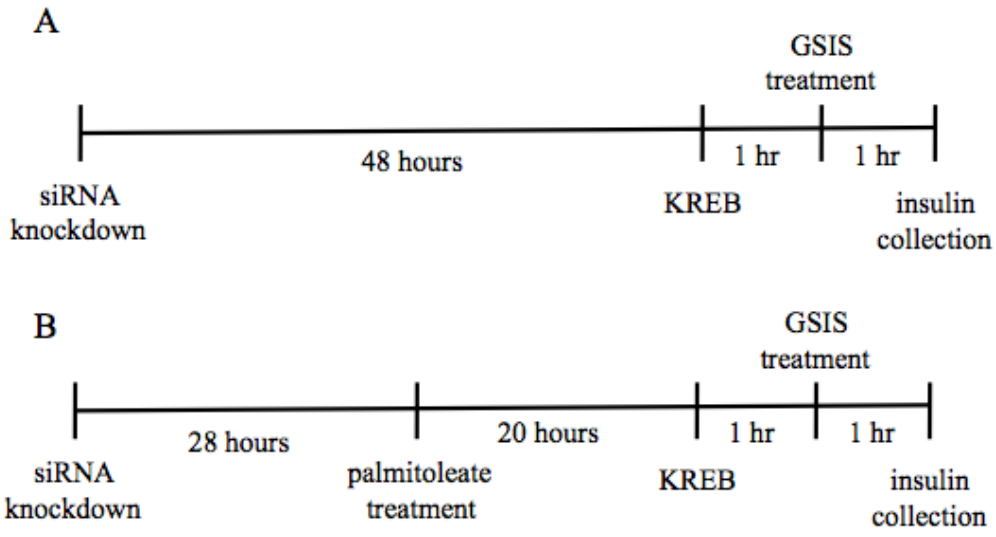

Figure 4-9: Schematic of glucose stimulated insulin secretion methods. (A) Tests for acute fatty acid exposure or amino acid treatment were completed after 48 hour knockdown with 1 hour of Krebs-Ringer bicarbonate buffer (KREB) pre-incubation followed by 1 hour GSIS treatment with indicated concentration of glucose ±fatty acid or amino acid in the same buffer. (B) Tests for chronic fatty acid exposure were completed following 28 hours of incubation and 20 hours of 0.5 mM palmitoleate treatment. One hour of Krebs-Ringer bicarbonate buffer (KREB) pre-incubation and 1 hour of GSIS treatment with indicated concentration of glucose in the same buffer. Insulin was collected from the media and quantified using the insulin RIA kit to determine secretion levels.

Acute palmitoleate treatment with low (2.8 mM glucose) and high (20 mM glucose) treatment resulted in a robust increase of insulin secretion in both control and *ASNA1* knockdown cells. In contrast to that seen with palmitate treatment, the levels of insulin secretion after a 1-hour stimulation with buffer containing both palmitoleate and glucose were significantly reduced in *ASNA1* knockdown cells compared to control in the same treatment conditions (Fig 4-10). Therefore, the insulin secretion defect occurring with decreased *ASNA1* expression continues even with palmitoleate stimulation of GSIS, but is completely normalized with acute palmitate exposure (Fig 4-10).

Generally, fatty acids are unable to stimulate insulin secretion alone, and instead amplify glucose stimulation of insulin release [317]. Since palmitate was able to normalize insulin secretion in the *ASNA1* knockdown cell line, this fatty acid is likely involved in a compensatory pathway to that blocked by *ASNA1* knockdown. Unlike palmitate, palmitoleate was unable to completely normalize the insulin secretion levels in the *ASNA1* knockdown to levels of the control, but did cause a significant amplification of insulin release in these cells. In summary, fatty acid treatment was able to amplify the GSIS in the *ASNA1* knockdown, with a 2 fold increase insulin release following palmitate exposure and a 3 fold increase in insulin release following palmitoleate treatment compared to the glucose treatment alone. This suggests that the fatty acid potentiation of GSIS is not entirely through an *ASNA1* dependent pathway.

Amino acid and glucose stimulated insulin secretion. In addition to fatty acids, amino acids such as L-arginine are also able to amplify the glucose stimulation of insulin release from pancreatic β- cells through alteration of plasma membrane permeability [317] (Fig 4-8). Since palmitate treatment was able to offset the insulin secretion defects upon *ASNA1* knockdown, we treated cells with L-Arginine to determine if amino acid treatment would have a comparable effect (Fig 4-9A). Similar to that seen with palmitate supplementation, treatment of MIN6 cells with L-Arginine resulted in a significant increase in GSIS in both *ASNA1* and control siRNA treatments. The level of insulin secretion was equal for both control and *ASNA1* knockdown under these conditions (Fig 4-10). Therefore, amino acid supplementation was also able to compensate for the loss in *ASNA1* expression. From this study and others [233], it is clear that *ASNA1* plays a central role in insulin secretion, but the effect of *ASNA1* changes depending on

the nutrient challenge conditions. Supplementation of *ASNA1* knockdown cells with fatty acids and amino acids is able to amplify and in some cases normalize insulin secretion.

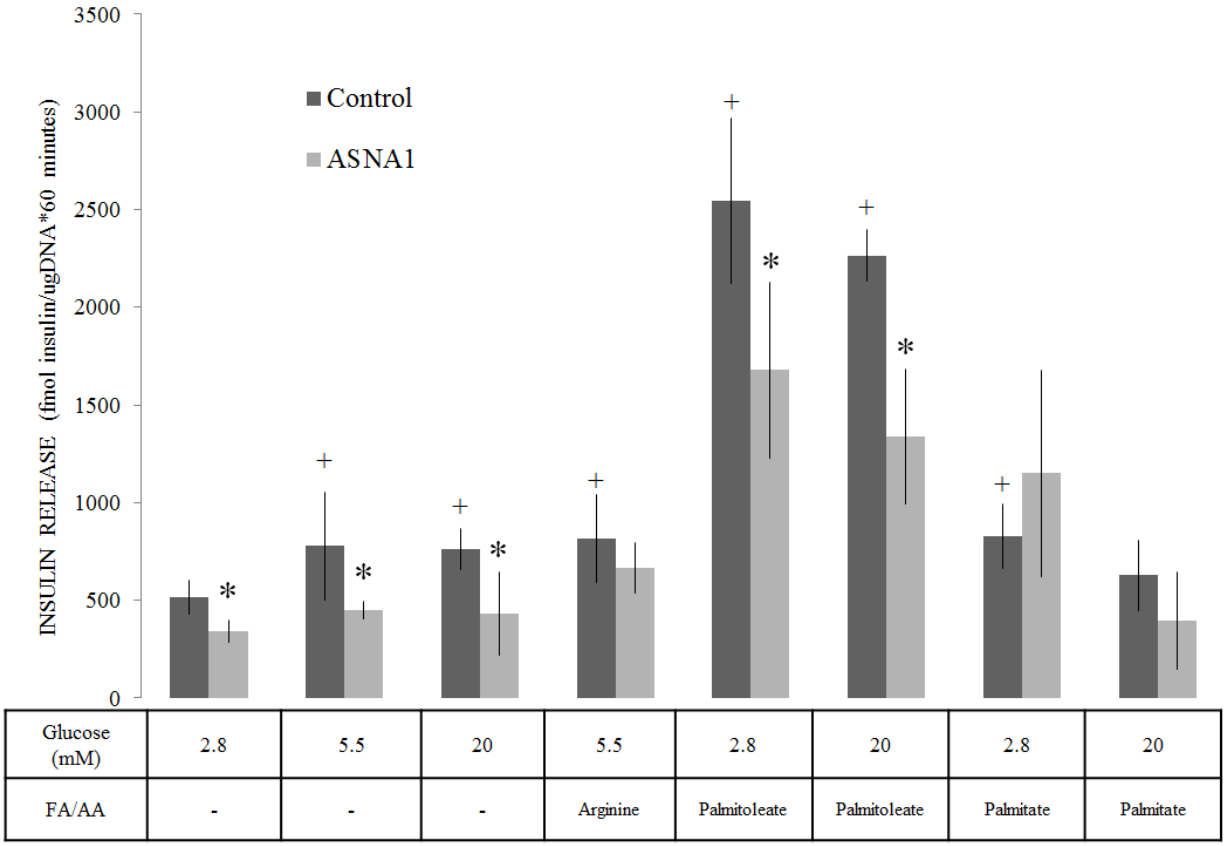

Figure 4-10: ASNA1 knockdown decreases glucose stimulated insulin secretion. ASNA1 knockdown was carried out in MIN6 cells using ASNA1 specific siRNA oligos and a control siRNA. Insulin secretion was assayed after pretreatment with KREBS Insulin secretion was measured using an insulin radioimmunoassay (RIA) and normalized to total cellular DNA. Glucose-stimulated insulin secretion (GSIS), amino acid-stimulated insulin secretion (AASIS), and fatty acid stimulated insulin secretion (FASIS) were assayed in MIN6 cells after 48 hours of knockdown challenged with 2.8 to 20 mM glucose, 10 mM arginine or a combination of glucose and 0.5 mM palmitoleate. Fatty acid (FA), amino acid (AA).

Chronic fatty acid exposure in ASNA1 siRNA treated MIN6 cells. Though acute treatment (1-3 hours) of pancreatic β-cells with fatty acids is able to increase GSIS, chronic exposure (>20

hours) causes cellular dysfunction through pathways of lipotoxicity [142]. Long-term fatty acid exposure not only increases levels of β-cell apoptosis, but also causes cellular dysfunction, particularly in the cells insulin secretion capacity. Diabetic subjects have increased levels of intracellular fatty acids [318], which have been shown to cause major defects in sensitization of pancreatic beta cells to glucose stimulated insulin secretion (GSIS) [319]. ASNA1 is involved in both sensitization of pancreatic β-cells to exogenous lipids as well as insulin release, and thus may be involved in glucose responsiveness under chronic fatty acid conditions.

In order to assess the role of ASNA1 in glucose stimulation of pancreatic β-cells grown in the presence of fatty acids, we treated MIN6 *ASNA1* knockdown and control cells with 0.5 mM palmitoleate overnight and tested insulin secretion with low (2.8 mM) and high (20 mM) glucose (Fig 4-9B). As expected, the overnight fatty acid treatment resulted in a significant reduction in insulin release in both high and low glucose compared to the untreated condition (Fig 4-11A). The insulin secreted following overnight FA exposure was equivalent in both control and *ASNA1* siRNA treated MIN6 cells. Therefore the defect in glucose stimulation due to chronic FA exposure was not exacerbated in the ASNA1 knockdown, with equally low secretion levels for both siRNA conditions (Fig 4-11). This data suggests that more than one pathway is involved in fatty acid amplification of GSIS, and ASNA1 plays a role in at least one of these pathways.

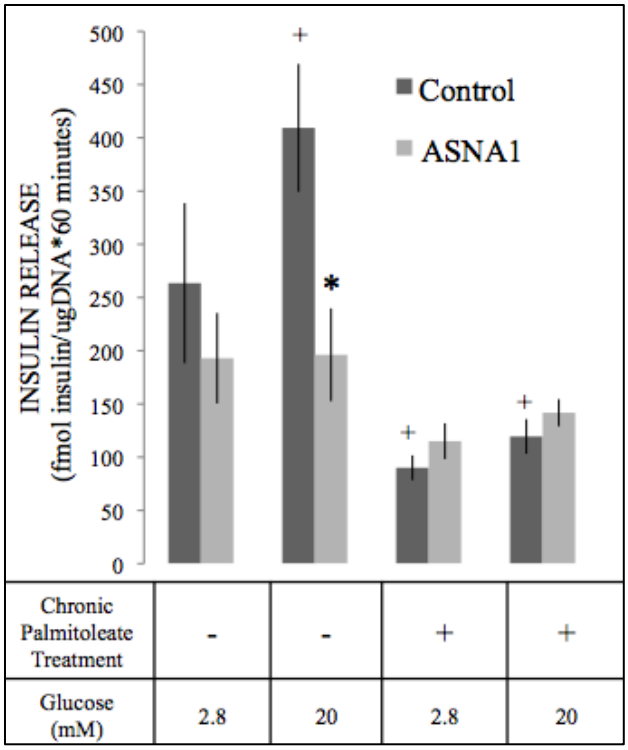

Figure 4-11: Effect of overnight fatty acid exposure on insulin secretion in ASNA1 knockdown cells. GSIS of knockdown cells grown overnight (20 hours) in 0.5 mM palmitoleate and challenged with glucose stimulation with and without 0.5 mM palmitoleate. Values are mean ± SD from 2 separate experiments, each in triplicate. * indicates significant difference from control values in the same condition ($p<0.05$) and + indicates statistical significance compared to control siRNA in 2.8 mM glucose challenge with no fatty acids.

Knockdown of ASNA1 in rat hepatoma cells does not alter lipid metabolism or ApoB secretion. Since knockdown of ASNA1 caused significant defects in insulin secretion, we questioned whether ASNA1 played a role in other secretion pathways, particularly those involved in the progression of lipotoxic disease. Defects in very low density lipoprotein (VLDL) secretion from the liver are associated with nonalcoholic fatty liver disease (NAFLD) characterized by a hepatic lipid accumulation. To study the effects of *ASNA1* knockdown on hepatocytes, we used the rat hepatoma cell line McA-RH7777, treated with *ASNA1* specific siRNAs. This hepatoma cell line expresses comparable *ASNA1* mRNA levels to that seen in the

MIN6 cell line (Fig 4-2B). Treatment of McA cells with *ASNA1* siRNA resulted in a greater than 95% reduction in *ASNA1* expression compared to control (Fig 4-12A). As seen with *ASNA1* knockdown in MIN6 cells, this reduction was not associated with any change in fatty acid synthesis levels, as measured by [^{14}C]oleate incorporation (Fig 4-112B).

VLDL is necessary for the transport of TG out of the liver to peripheral tissues for energy and storage [320, 321]. VLDL assembly and secretion are stimulated by increases in hepatic TG [322] and this assembly occurs through lipidation of apoB100 in the ER lumen followed by secretion into the circulation [321]. ApoB48 is a truncated product of the *APOB* gene found only in human intestine for chylomicron assembly (though ApoB48 is synthesized in murine and rat liver) [322]. Defects in VLDL secretion result in an accumulation of TG in hepatocytes [323-325] , a disorder which can progress into the more inflammatory steatosis and cirrhosis. We tested ApoB secretion levels by labeling cells with [^{35}S]methinone and monitoring radiolabeled ApoB. We found no change in ApoB-100 or Apo-48 levels in either the media or cells for ASNA1 knockdown compared to control siRNA (Fig 4-13). Consistent with normal levels of ApoB secretion, we see no change in TG (Fig 4-12C) or PL (Fig 4-12D) in the hepatoma cells, after a 2-hour pulse or after a 4 hour chase. This demonstrates that ASNA1 knockdown in the McA –RH7777 hepatoma cell line does not alter lipid synthesis or VLDL secretion.

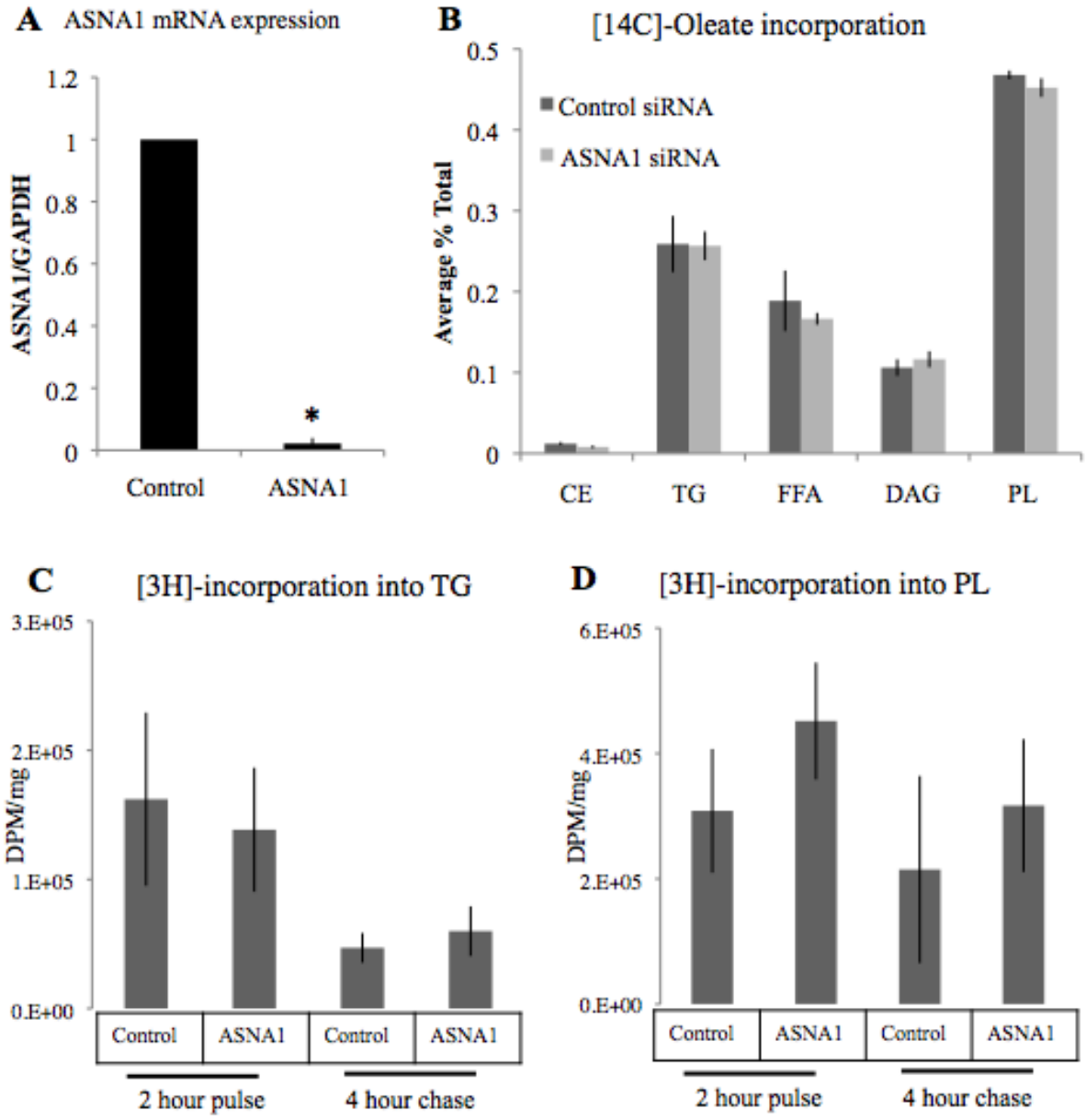

Figure 4-12: ASNA1 knockdown in McA-RH7777 rat hepatoma cells does not alter radiolabeled oleate or glycerol incorporation. All studies were completed following 48 hour knockdown of ASNA1 in McA-RH7777 cells. (A) Total RNA was isolated and quantitative RT-PCR was performed to assess mRNA levels of ASNA1 relative to housekeeping gene GAPDH. Lipid extraction and species separation through thin layer chromatography (TLC) was completed on McA-RH7777 cells after either (B) 4 hour pulse with [^{14}C]-Oleate incorporation or [^{3}H]-Glycerol incorporation into TAG (C) and PL (D) after 4 hour pulse (T = 0 hr) and 4 hour chase (T = 4 hr). Asterisks denote statistical significance ($p<0.05$) compared to control siRNA condition.

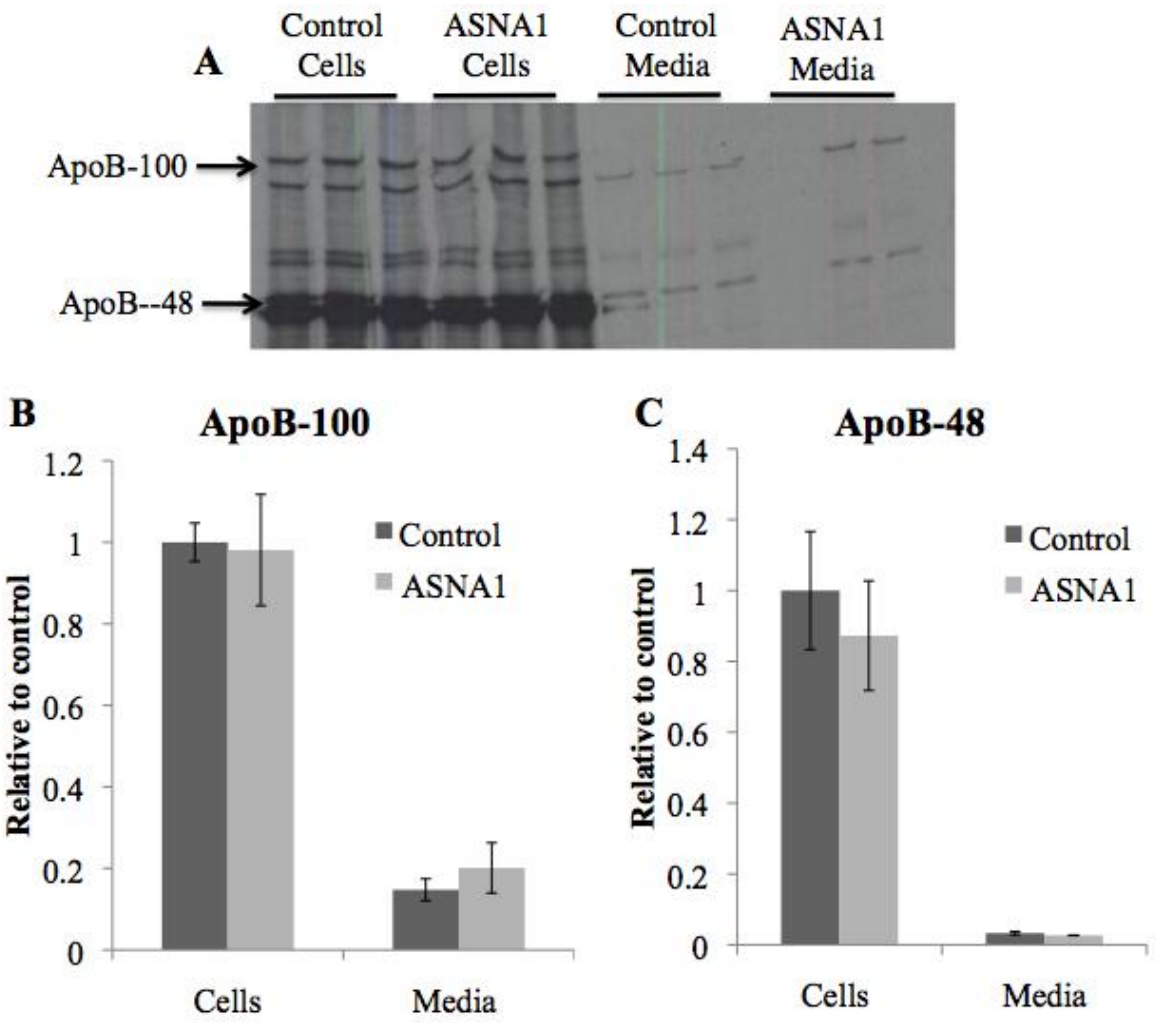

Figure 4-13: ApoB secretion in McA-RH7777 with ASNA1 knockdown. To determine levels of ApoB secretion, cells were labeled with [^{35}S]methionine for 2 hours with. Cells and media were collected, apoB immunoprecipitated and run on an SDS-PAGE gel followed by development via autoradiography (A). Quantification of [^{35}S]methionine incorporation into ApoB100 (B) and ApoB48 (C) relative to control.

DISCUSSION

Insulin resistance is a common consequence of obesity, due in part to high levels of circulating free fatty acids and ectopic fat deposition. In order to compensate for peripheral insulin resistance and the resulting hyperglycemia, pancreatic β-cell mass and insulin production capacity increase. Speculation from T2D subject autopsies indicates that those predisposed to type 2 diabetes are unable to increase β-cell expansion in response to these conditions. A major reason for the deficient compensation is due to the negative impacts of chronically high circulating free fatty acids on β-cell health. Exposure of pancreatic β-cells to free fatty acids results in lipotoxicity, characterized by defects in insulin secretion, increased ER stress and apoptosis. Consistent with these known FA-mediated effects, we found that treatment of the MIN6 pancreatic β-cell line with palmitate and palmitoleate induced lipotoxicity, with increased levels of apoptosis (Fig 4-4), ER stress (Fig 4-7) and decreased glucose stimulated insulin secretion (Fig 4-11). In this study, we identified *ASNA1* as an important protein affecting both fatty acid mediated cell death and insulin secretion.

ASNA1 is involved in two compensatory pathways associated with T2D progression, β-cell expansion and increased insulin release and is therefore, a compelling target in diabetes prevention. *In vitro* studies have shown that exposure of cultured β-cells to long chain saturated fatty acids (SFAs) decreases viability within only a few hours due to cytochrome c release and caspase activation [326]. Treatment of MIN6 cells with palmitate significantly increased apoptosis in both control and *ASNA1* siRNA treated conditions but the percentage of apoptotic cells was markedly higher for *ASNA1* knockdown cells following 1.0 mM palmitate treatment

(Fig 4-4) demonstrating that decreased *ASNA1* expression sensitizes MIN6 cells to SFA induced apoptosis.

For many years, only SFAs were believed to be toxic and unsaturated fatty acids were considered protective against pancreatic β-cell dysfunction and death. This idea is based on *in vitro* studies, in which treatment of cultured β-cells with monounsaturated fatty acids (MUFAs) such as oleate and palmitoleate have minimal signs of dysfunction [130, 327, 328] and could protect against SFA induced apoptosis [329]. Higher levels of UFA (>0.8 mM) induce ER stress response and apoptosis in mammalian cells [128, 182, 311] and we found 1.0 mM palmitoleate was able to activate apoptosis in both control and *ASNA1* siRNA treated cells. In contrast to that seen with palmitate treatment, knockdown of ASNA1 did not sensitize cells to palmitoleate induced cell death (Fig 4-4). The differential effect of palmitate versus palmitoleate on β-cell survival with *ASNA1* knockdown can be explained through alternative pathways for saturated and unsaturated fatty acid metabolism. After cellular uptake, UFAs are preferentially incorporated into pathways of triglyceride storage [7] whereas SFAs are more likely to enter into other metabolic pathways including ceramide and phospholipid biosynthesis [111]. As a result of the independent channeling, SFA induced lipotoxicity occurs through pathways separate from UFAs. Our studies indicate that *ASNA1* has alternate effects on these pathways, though the mechanism of this interaction is unclear.

Pancreatic β-cells are particularly vulnerable to lipid induced ER stress due to the role of these cells in insulin secretion. Insulin synthesis accounts for more than half of the total protein synthesis in the pancreatic β-cell, and the subsequently high protein load at the ER is balanced with an increase in ER folding capacity [128, 142, 330]. For this reason, lipid induced ER stress can have major effects on cellular dysfunction and insulin secretion defects. Using GRP78

expression as a marker for ER stress, we found an expected increase in GRP78 protein expression following overnight palmitate and oleate treatment in the control (Fig 4-7). Upon knockdown of *ASNA1* GRP78 levels were elevated in no treatment conditions and stayed at this level despite fatty acid treatment (Fig 4-7). This demonstrates that basal ER stress is increased in the *ASNA1* knockdown strain, and may be a potential mechanism for palmitate-sensitivity in these cells.

In addition to altering the vulnerability of pancreatic β-cells to lipid induced apoptosis, knockdown of *ASNA1* causes a major defect in glucose stimulated insulin secretion (GSIS) [233]. In order to clarify the role of *ASNA1* in GSIS, we challenged cells with glucose and either fatty acids (acute or chronic) or the amino acid, L-arginine, which have known effects on glucose stimulatory pathways [317]. Glucose is the only nutrient able to promote the release of insulin without additional stimulants, whereas amino acids and fatty acids, are able to amplify the glucose response but do not act independently from glucose in insulin stimulation [317]. Glucose stimulates the release of insulin through an increase in oxidation and a rise in the ATP/ADP ratio, which closes ATP-sensitive K^+ channels and depolarizes the membrane. Membrane depolarization opens voltage-gated Ca^{2+} channels, increasing intracellular calcium and triggering the exocytosis of insulin granules into circulation [331, 332] (Fig 4-9).

Fatty acids are able to potentiate this response through several mechanisms. The first is through an increase in intracellular long chain-CoA (LC-CoA) levels due to a glucose stimulated inhibition of carnitine palmitoyl-transferase (CPT1) dependent fatty acid oxidation. The defect in FA oxidation results in a rise in LC-CoA within the cell which can act on insulin granules and increase levels of exocytosis [333]. The second mechanism occurs through increased TG/FFA cycling causing a rise in lipid intermediates, such as DAG, which can act as lipid signaling

molecules and effect insulin granule release [333]. The last pathway acts through stimulation of the G-protein coupled receptor, GRP40, by fatty acid binding. This binding leads to phospholipase C (PLC) activity at the plasma membrane resulting in hydrolysis of phosphatidylinositol 4-5 biphosphate (PIP_2) to inositol 4,5-triphosphate (IP_3) and diacylglycerol (DAG). The stimulation of insulin release after GRP40-FA binding occurs through IP_3 movement to the ER where it stimulates Ca^{2+} release, and activation of insulin secretion through DAG signaling cascades [334]. In addition to fatty acids, proteins and amino acids are also to regulate insulin secretion [335-337]. For instance, L-Arginine, a cationic-charged amino acid, enhances insulin secretion by depolarization of the plasma membrane [335] (Fig 4-9) .

Knockdown of *ASNA1* caused decreased glucose stimulated insulin release (Fig 4-10), consistent with previously published results [233]. Amplification of the insulin secretion pathway with acute fatty acid or protein treatment increased insulin secretion in both siRNA groups, with a significant secretion defect remaining following palmitoleate treatment in the *ASNA1* knockdown (Fig 4-10). Despite this defect, insulin secretion levels were three times that seen with glucose alone in cells with reduced *ASNA1* expression. From these results we propose that fatty acid and protein amplification pathways do not rely on *ASNA1* mediated insulin secretion mechanisms. If these pathways were driven through *ASNA1*, a knockdown in this gene would block the associated amplification.

Defects in insulin secretion resulting from reduced *ASNA1* are not due to decreased insulin or proinsulin production [233]. Therefore, a likely explanation for the reduced insulin secretion occurring with *ASNA1* knockdown is a defect in insulin granule docking and/or fusion. Like *GET3, ASNA1* mediates tail anchored protein insertion into the ER membrane and a knockdown in A*SNA1* results in inefficient insertion and altered localization of the SNARE

protein, Sed5 [338]. Therefore, it is possible that that several other SNARE proteins are mislocalized in the *ASNA1* knockdown, which would result in slowed insulin granule docking and fusion (Figure 4-14). Currently, there are eight SNARE proteins and 11 accessory factors which have been implicated in β-cell insulin secretion, specifically in insulin vesicle targeting and fusion [339]. Moreover, numerous studies have linked T2D and insulin resistance with decreased SNARE protein levels in rodents and humans [340-342]. We propose that increased levels of exocytosis through fatty acid or L-arginine supplementation compensates for the SNARE insertion defect occurring with *ASNA1* knockdown by increasing docking and fusion efficiency despite decreased SNARE protein levels (Figure 4-14).

The inability of palmitoleate to completely rescue the *ASNA1* dependent insulin secretion defect may be due to differences in palmitate and palmitoleate mediated GSIS amplification. For example, activation of GRP40 depends on the fatty acid type, with the highest induction of Ca^{2+} occurring with the SFA between 12-16 carbons and a lower activation following oleate treatment [343]. Though palmitoleate was not tested by these methods, it is possible that the difference in insulin secretion following palmitoleate challenge in *ASNA1* knockdown cells is due to the differential stimulation of GRP40 by palmitate versus palmitoleate.

In conclusion, this study has shown that the lipid sensitivity phenotype occurring in a *GET3* deletion in yeast has been conserved in mammals, with decreased *ASNA1* expression resulting in increased palmitate induced apoptosis. Not only is this a proof of principle for our yeast genome-wide screen, but it also indicates that many other genes identified by our screen may have similar lipotoxicity phenotypes. Therefore additional yeast to human translational research is required to determine if the other 67 mammalian orthologs identified by our screen (chapter 2) are also involved in pathways of mammalian lipotoxicity. Furthermore, these studies

demonstrate that fatty acid and amino acid amplification of GSIS is able to partially rescue the insulin secretion defects due to reduced ASNA1 expression and provides insight into the role of ASNA1 in insulin granule release.

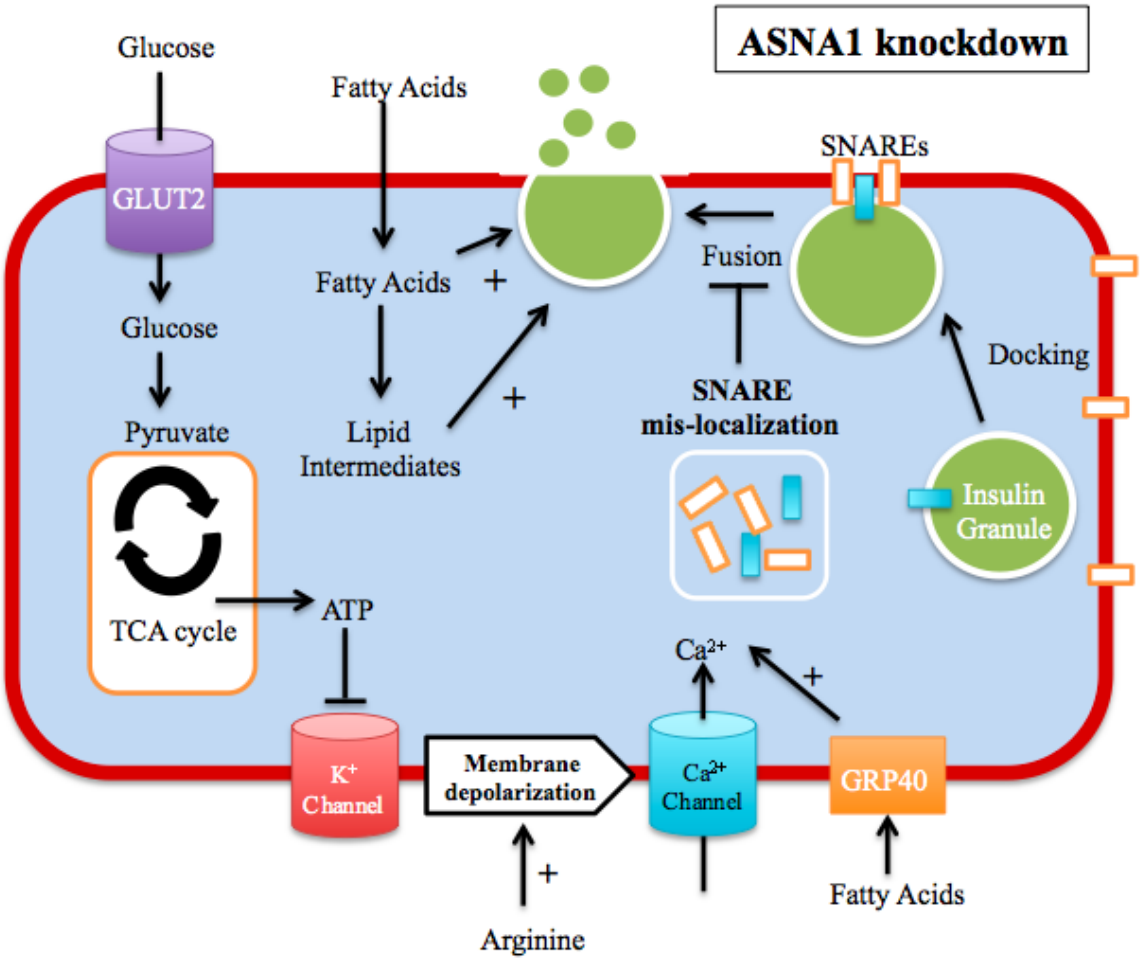

Figure 4-14: Model for ASNA1 mediated insulin secretion defects in pancreatic β-cells. ASNA1 functions in tail anchored protein insertion into the ER membrane. The membrane fusion SNARE proteins are all tail anchored proteins, and loss of *ASNA1* results in reduced insertion and misolicalzation these SNARE proteins. Insulin grandule docking and fusion requires SNARE proteins. Therefore the SNARE protein mislocalization characteristic of reduced *ASNA1* expression likely reduces insulin granule docking and fusion efficiency.

CHAPTER 5

The role of ARV1 in lipotoxicity of the pancreatic β- cell and nonalcoholic fatty liver disease.

FORWARD

A portion of this body of work was previously submitted by Ying Liu for his doctorate thesis in 2004 [156]. After our identification of *ARV1* in the yeast palmitoleate sensitivity screen (chapter 2) we continued his work in the context of lipotoxicity. Contributions by Dr. Liu include knockdown (Fig 5-6 and 5-7) and overexpression (Fig 5-10 and 5-11) of *ARV1* in HEK293 cells and *ARV1* overexpression studies in mice (Fig 5-12 and 5-13, Table 5-1 and 5-2). My work focused instead on the effect of decreased *ARV1* expression with respect to lipid synthesis and lipid induced apoptosis in yeast (Fig 5-1, 5-2 and 5-3) and mouse pancreatic β-cells (Fig 5-4, 5-5, 5-8 and 5-9). Human ARV1 overexpression studies in McA-RH7777 cells (Fig 5-14, Fig 5-15 and Fig 5-16) were also conducted as follow up to the mouse *hARV1* overexpression studies.

ABSTRACT

The most sensitive strain identified by our yeast palmitoleate sensitivity screen was in the deletion of *ARE2* Required for Viability gene, *ARV1*. *ARV1* is a putative sterol transporter which localizes to the ER membrane, deletion of which results in an accumulation of sterols at the ER and constitutively active unfolded protein response (UPR), likely due to the sterol buildup. Orthologs of *ARV1* exist in all eukaryotic systems queried, and expression of human *ARV1* is able to rescue lipid related phenotypes in the yeast *ARV1* deletion, demonstrating functional homology. We found that knockdown of *ARV1* in the MIN6 pancreatic β-cell line caused a similar fatty acid sensitivity phenotype to that in the yeast *arv1Δ,* with increased apoptosis in response to both palmitate and palmitoleate. In addition, reduced *ARV1* expression in MIN6 and HEK293 cells resulted in decreased neutral lipid synthesis. In order to determine the role of *ARV1 in vivo*, we used a human ARV1 adenovirus (AdhARV1) to induce hepatic *ARV1* overexpression. Mice injected with the AdhARV1 saw a significant increase in triglyceride mass and an accumulation of lipid droplets within the liver, with no change in plasma lipid levels. Gene expression levels of the triglyceride synthesis enzyme, *DGAT1*, were significantly increased in these livers compared to control, with no significant changes in other lipid synthesis enzymes. These results suggest that mammalian *ARV1* is involved in the regulation of neutral lipid synthesis in both pancreatic β-cells and in the liver, and therefore may be a factor in genetic predisposition to lipotoxic disease.

INTRODUCTION

In order to identify gene deletions resulting in increased sensitivity to exogenous free fatty acids, we completed a genome-wide fatty acid sensitivity screen in yeast (chapter 2). The goal of this screen was to find novel genes required for protection against the negative effects of lipid accumulation in eukaryotic cells, focusing primarily on those which have been conserved across evolution. A deletion in *ARV1* resulted in the most severe growth defect in response to the unsaturated fatty acid palmitoleate compared to all other single deletions tested (chapter 2), making it an appealing gene for follow up studies.

The *ARE2* Required for Viability gene, *ARV1,* was first identified in yeast as essential in cells lacking all sterol esterification capacity due to deletions in the two ACAT related enzymes, *ARE1* and *ARE2*. In yeast *ARV1* deletion strains, free sterol levels in the ER dramatically rise at the expense of the plasma membrane (PM). Thus, *ARV1* has been proposed to act as a sterol transporter, involved in free sterols export out of the ER membrane. Yeast *arv1Δ* has a robust induction of the UPR under basal conditions, likely due to the sterol accumulation in the ER [206]. These sterol localization defects characteristic of yeast *ARV1* mutants are complemented by expression of human *ARV1,* indicating a functional conservation throughout evolution [205].

ARV1 has been identified in all eukaryotic organisms queried thus far [239, 344, 345], with sequence conservation occurring primarily in a 61-residue *ARV1* homology domain (AHD) at the N-terminal region of the protein. This region is made up of a putative zinc binding motif and a block of 33 conserved residues [205]. Human *ARV1* is expressed in most tissues, but is highest in the liver and adipose tissue. Mice also have ubiquitous expression of *ARV1,* with

maximum expression levels in the lung [239]. Similar to the yeast *ARV1* deletion, knockdown of *ARV1* in mouse liver using antisense oligonucleotides results in an accumulation of free sterol in the liver resulting in a 2-4 fold increase in hepatic and plasma bile acid levels through an increase in FXR activation [239].

Despite the recognized role of *ARV1* in sterol metabolism, no known phenotypes connecting *ARV1* and fatty acid homeostasis have been reported [344]. Due to its high evolutionary conservation, we predict that decreased mammalian *ARV1* expression will sensitize cells to lipid-induced apoptosis, similar to that seen in yeast. Furthermore, we propose that *ARV1* is integral in the progression of the lipotoxic diseases, type 2 diabetes (T2D) and nonalcoholic fatty liver disease (NAFLD), due to its role in lipotoxicity.

Overall, our results show that *ARV1* expression is positively correlated with triglyceride synthesis in mouse pancreatic β cells and mouse liver, due, at least in part, to increased *DGAT1* levels. Additionally, *ARV1* is protective against lipid induced pancreatic β-cell lipotoxicity and may be an important factor in type 2 diabetes susceptibility.

MATERIALS AND METHODS

Yeast General. Molecular biology and yeast procedures were performed according to conventional methods [177]. Complete (YPD; yeast extract, peptone, dextrose), synthetic complete (SC) and selective media were prepared as described previously [177]. All yeast strains used in this study were derived from s288C (Open Biosystems), with the exception of SCY2021 (*are1::HIS3 are2::LEU2 dga1::URA3 lro1::URA3*) which is derived from W303[178]. All single mutants were obtained from the Open Biosystems Yeast Knock Out Strain collection (Cat # YSC1053). When indicated, fatty acids (Sigma) were added to media in 0.6% ethanol:tyloxapol (5:1, v/v) with the designated quantity of fatty acid (palmitoleate and oleate as a 10% w/v stock in ethanol). For liquid growth assays, overnight cultures were used to inoculate liquid media such that the starting optical density was 0.1 (OD600 nm) and growth curves were obtained using a Microbiology Workstation Bioscreen C (Thermo Electron Corp.) and Research Express Bioscreen C software (Transgalactic Ltd). Three isolates per genotype were normalized to an absorbance (OD600) of 0.1 and 10 µl of each strain was added to 290 µl of media per well and grown at 30° for 4 days and averaged in order to produce the final growth curve.

Cell Culture. The MIN6 mouse insulinoma cell line [346] was a kind gift of Dr. Alan Attie (Madison, WI). MIN6 cells were maintained in Dulbecco's modified Eagles medium DMEM) containing 25 mM glucose, 15% heat-inactivated fetal bovine serum (FBS), 100 units/mL penicillin, 100 ug/ml streptomycin, 100 ug/ml L-glutamine and 5 ul/L β-mercaptoethanol. Human Embryotic Kidney 293 (HEK293) cells were purchased from American Type Culture

Collection (ATCC, Manassas, VA) and cultured in Dulbecco's modified Eagle's Medium (DMEM) medium containing 10% fetal bovine serum (FBS), L-glutamine and antibiotics. McArdle RH7777 cells were obtained from ATCC. McA-RH7777 cells were maintained in DMEM with 10% FBS, 10 % Horse Serum, 100 units/ml penicillin, and 100 μg/ml streptomycin. Cells were grown in humidified 5% CO2, 95% air at 37°C. Fatty acids were prepared using fatty acid free bovine serum albumin (BSA) (Invitrogen). Cells were incubated for 0-20 hours in DMEM with 10% FBS containing oleate, palmitate or palmitoleate (Sigma-Aldrich) bound to 1% fatty acid free BSA (Sigma-Aldrich). Control incubations contained only BSA.

Lipid Analysis and Metabolic Labeling. Mammalian lipid labeling was performed on cells seeded overnight in a 6 well plate. For oleate labeling, cells were pulse labeled with 0.5 μCi/ml [9,10- ^{3}H] Oleic acid for 6 hours in serum free DMEM with 1% essentially fatty acid free BSA + 0.25 mM cold oleate. Labeling with 0.5 μCi/ml [^{3}H]acetate and 3μCi/ml [^{3}H] glycerol was done with cells grown to 95% confluence for 8 hours at 37°C [156]. For lipid extraction, 2 ml of hexane:isopropanol (3:2) was added to each well and incubated at room temperature for 1 hour, after which the supernatant was removed and the extraction repeated. Samples were dried with nitrogen gas, resuspended in chloroform:methanol (2:1) and lipids were separated on a TLC plate [309]. Total cholesterol levels were measured by Gas Liquid Chromatography (GLC) as described [309]. TG content was determined by enzymatic assay using Trig/GB from Roche. Lipid levels were quantified as described previously and normalized to protein level using a Bradford protein quantification assay (BioRad).

Fluorescence Microscopy. Yeast cells were grown in specified media to saturation. For lipid droplet analysis, cells were stained with Nile Red (1 μg/ml) (Sigma-Aldrich) and visualized with a long pass GFP filter (excitation 440 nm). For quantification, 10 confocal frames 0.25 μm apart were captured and displayed as maximum intensity projections. Lipid droplets were counted for 6 frames per strain, with 15-30 cells per frame. Statistical analysis was carried out by comparing variation within frames. All microscopy was performed using a Zeiss Axiovert 200 M using a 63x oil immersion objective and images taken using a Hamamatsu Orca-ER camera.

Apoptosis Assays. Yeast apoptosis was assessed using Annexin V binding and propidium idodide staining using the FITC Annexin V/Dead Cell apoptosis kit (Molecular probes V13242). Cells were washed with sorbitol buffer (1.2 M Sorbitol, 0.5 mM Magnesium Cloride, 35 mM Potassium Acetate ph 6.8), digested with 5.5% glusulase and 15 U/ml lyticase in sorbitol buffer and resuspended in Annexin/PI for 20 minutes [257]. MIN6 apoptosis levels were quantified using Invitrogen Vibrant Apoptosis Assay Kit #5 (V13244) as described by manufacturer. 10 frames per condition were captured and cells within these frames were counted in order to obtain a percentage of apoptotic and dead cells within the population.

***siRNA and ASO transfection*.** Murine *ARV1* specific and negative control ASOs were provided by Isis Pharmaceuticals, Inc (Carlsbad, CA). The ASOs are chimeric 20-mer phosphorothioate oligonucleotides with 2'-O-Methoxyethyl (MOE) groups at positions 1-3 and 17-20. ASOs were prepared as a 200 uM concentration in dH2O. Transient transfection experiments were conducted using Lipofectamine 2000 with 250 nM *ARV1* ASO in OptiMem for 6 hours after

which media was changed to DMEM with 10% FBS for 24-48 hours. When specified, fatty acids were added to culture 24 hours after knockdown.

Immunoblots. Cells were washed twice with PBS and lysed using SDS buffer (2% SDS, 62.5 mM Tris-HCL (pH 6.8), 10% glycerol, 10% β-mercaptoethanol, and 0.01% bromophenol blue) and boiled for 5 minutes. Protein extracts were prepared in a lysis buffer containing 25 mM Tris-HCL (pH 7.4), 2 mM Na_3VO_4, 10 mM NaF, 10 mM $Na_4P_2O_7$, 1 mM EGTA, 1 mM EDTA, 1% NP-40, 5 μg/ml leupeptin, 5 μg/ml aprotinin, 10 nM okaidic acid and 1 mM phenylmethylsulfonylfluoride. Equal amounts of protein extract were separated on a 12% SDS-PAGE gel and electrotransferred to a 0.45 μm nitrocellulose membrane using a Bio-Rad laboratories mini-transfer tank. Membranes were blocked for 1 hour at room temperature with 5% non-fat milk in Tris-Buffered Saline with 0.1% Tween 20 (TBST) and incubated with primary antibodies overnight at 4°C. Protein bands were detected with HRP-conjugated secondary antibodies and SuperSignal West Pico enhanced chemiluminescent solution (Pierce).

ApoB immunoprecipitation. Cells were incubated in methionine/cysteine-free DMEM with 1.5% fatty acid free BSA for 2 hours followed by [^{35}S] methionine labeling for 2 hours. After labeling, media was transferred into eppendorf tubes and a mixture of protease inhibitors (30μl/ml protease inhibitors, 1 mM benzamidine, 5 mM EDTA, 100 units/ml aprotinin, 50 μg/ml leupeptin, 50 μg/ml pepstatin A and 10 mM Hepes, pH 8.0) and 0.86 mM freshly added phenylmethylsulfonyl fluoride. Immunoprecipitation of apoB in medium and cells was carried out according to the method described by Dixon et al [310]. Antibodies against apoB (Calbiochem, San Diego, CA) and rProtein G Agarose (Invitrogen) were added to the reactive

solution to precipitate apoB. ApoB was precipitated by boiling for 5 minutes in sample buffer (0.125 M Tris-HCl, pH 6.8, 4% SDS, 20% glycerol and 10% β-mercaptoethanol). Proteins were separated by SDS-PAGE and gels were then treated with autofluor (National Diagnostics, Atlanta GA) and after drying exposed to X-ray film (Kodak, X Omat AR) at -80°C for 1-3 days. Incorporation of [^{35}S]methionine into apoB48 and apoB100 was quantified by autoradiography and bands were cut and radioactive incorporation was quantified by liquid scintillation counting [311].

Miscellaneous. The following methods were completed as described by Dr. Ying Liu [156]: SRE-luciferase Activity Assay, Recombinant Adenovirus Construction, Gene Expression Analysis, Animal Studies and Affymetrix Oligonucleotide Array Hybridization.

RESULTS

Deletion in ARV1 results in robust palmitoleate sensitivity. Of the 156 deletion strains identified in the palmitoleate sensitivity screen (chapter 2), the most sensitive based on growth curve analysis and colony density was *arv1Δ*. This gene mutant was the only deletion tested having similar levels of sensitivity to that of the *are1Δ are2Δ dga1Δ lro1Δ* neutral lipid deficient yeast strain, and is similarly unable to grow in the presence of 0.05 mM palmitoleate (a concentration 10 fold lower than used in the screen) (Fig 5-1).

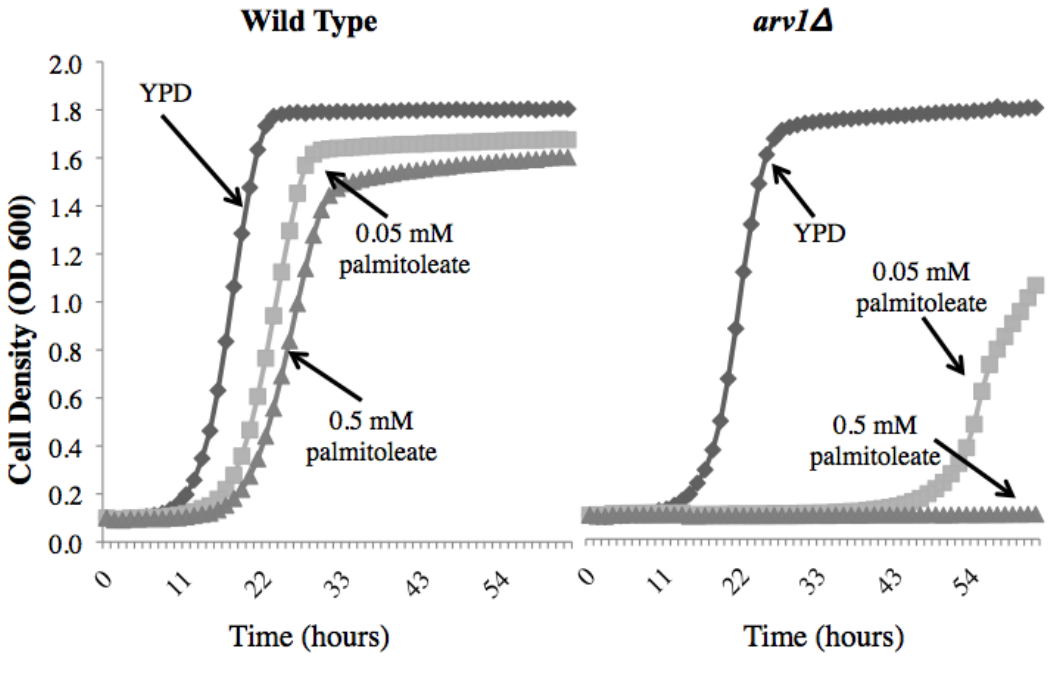

Figure 5-1: Deletion of ARV1 results in severe fatty acid sensitivity and increased lipid droplet number. Wild Type and *arv1Δ* growth in YPD liquid media with indicated concentrations of palmitoleate. n=3 for each condition

In order to determine if this sensitivity was due to fatty acid induced apoptosis or necrosis, we treated wild type and the *ARV1* deletion with 0.1 mM palmitoleate for 16 hours, after which we stained for apoptosis and cell death with Annexin V and propidium iodide (PI),

respectively. We considered any cells staining positive for Annexin V to be undergoing apoptosis, either as late stage apoptosis (Annexin+/ PI+) or early stage apoptosis (Annexin +/PI) [257]. Consistent with its growth sensitivity phenotype (Fig 5-1), we saw a significant increase in apoptotic cells in the *ARV1* deletion after palmitoleate treatment, which did not occur in the wild type strain (Fig 5-2). Even in YPD media alone, *arv1Δ* had significantly higher levels of Annexin V and PI staining compared to the control, indicating that ablation of *ARV1* results in increased apoptosis under basal conditions (Fig 5-2). Since the cell death percentage in the *ARV1* deletion was increased even under normal growth conditions, we also compared the apoptotic cell percentage of *arv1Δ* in YPD versus the palmitoleate treatment condition and found that fatty acid supplement significantly increased apoptosis levels (Fig 5-2B). Therefore, knockout of *ARV1* results in increased cell death under basal conditions and a further increase in apoptotic induction when treated with palmitoleate, compared to control (Fig 5-2).

Since neutral lipid (NL) synthesis is a cell's primary defense against lipotoxicity, we considered if the increased fatty acid (FA)-sensitivity was due to insufficient lipid storage. Images of lipid droplets, stained with Nile Red, were captured and quantified in the wild type and *ARV1* mutant in YPD +/- 0.1 mM palmitoleate to obtain the average number of droplets per cell (Fig 5-3A). We saw no significant difference in lipid droplet number between strains when grown in YPD, but in the presence of palmitoleate there was a significant increase in lipid droplet number in *arv1Δ* (8.06 droplets/cell) compared to wild type (5.23 droplets/cell) (Figure 5-3 A-B). A similar increase in lipid droplet number was seen in cholesterol treated *ARV1* mutants [205, 206]. Interestingly, activation of ER stress in yeast through tunicamycin or Brefeldin A treatment results in lipid droplet accumulation [347]. Since *ARV1* mutant strains have a constitutively active UPR [206], the lipid challenge occurring with palmitoleate treatment

may result in increased LD number through a similar ER stress induction and/or altered ER architecture.

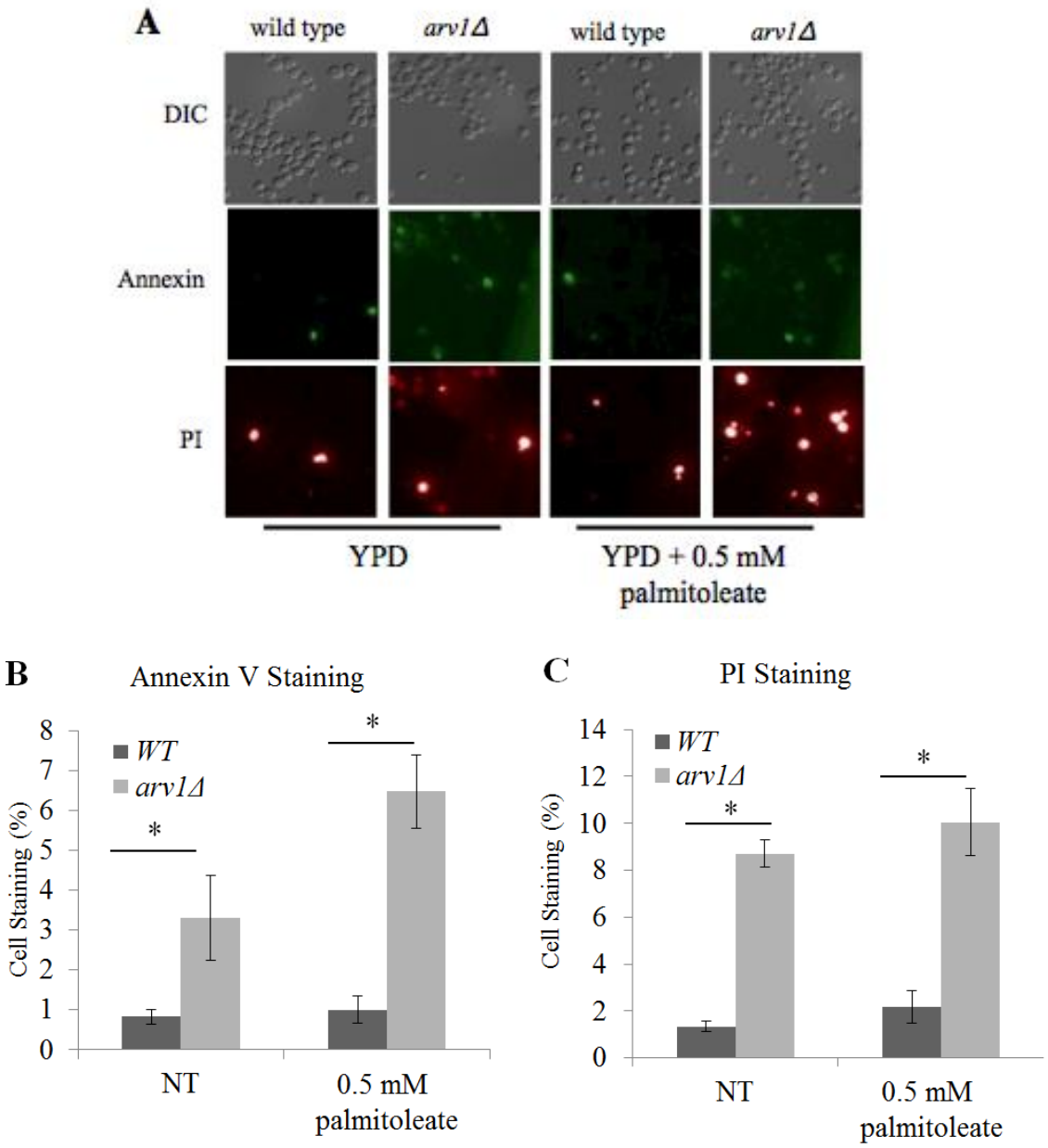

Figure 5-2: Mutation in ARV1 increases levels of fatty acid induced apoptosis. (A) Annexin/Propidium iodide staining of wild type and *arv1Δ* cells after incubation in YPD ± 0.1 mM palmitoleate for 16 hours (B-C) and quantified based on proportion of total cells stained for externalization of phosphatidylserine (Annexin V +) and propidium idodide (PI) internalization. (mean ±s.e, 10 fields of cells, at least 60 cells per field). Asterisks denote statistical significance compared to the wild type control in the same condition (*p<0.05).

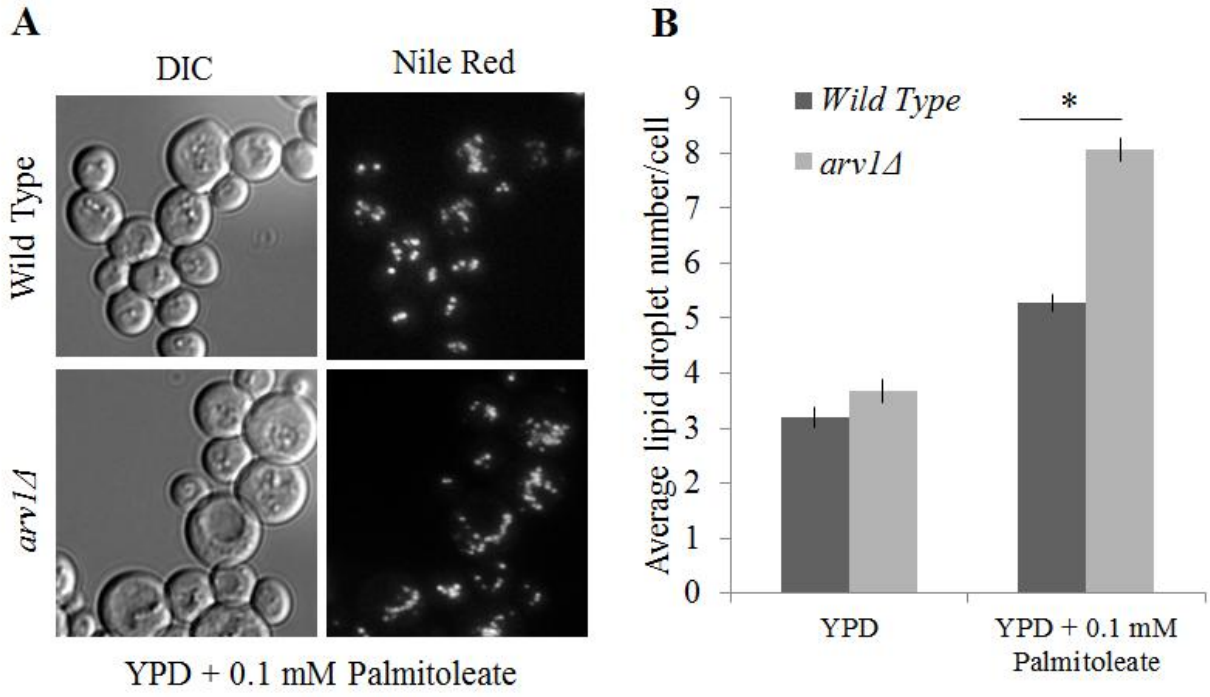

Figure 5-3: Deletion of ARV1 results in increased lipid droplet number with palmitoleate treatment. (A) Strains grown for 24 hours in YPD ± 0.1 mM Palmitoleate and stained for lipid droplets with Nile Red (1µg/ml). (B) Lipid droplets per cell quantified for each strain and condition, (mean ±s.e., 10 fields of cells, at least 60 cells per field). Asterisks denote statistical significance compared to the wild type control in the same condition (*$p<0.05$).

Decreased expression of mammalian ARV1 increases fatty acid induced lipotoxicity of pancreatic β-cells. Human *ARV1* is a functional ortholog of yeast *ARV1*, and as such is able to rescue sensitivity and lipid phenotypes associated with yeast *arv1Δ*. Due to this conservation, we hypothesized that altering expression levels of *ARV1* in mammalian systems would affect lipid homeostasis and FA-sensitivity similarly to that seen in yeast. The identification of *ARV1* in the yeast lipotoxicity screen indicates that mammalian *ARV1* may also play an integral role in lipid induced cell death and lipotoxic disease progression. Therefore, the goal of this study was

to focus on *ARV1* in the context of TG homeostasis and obesity related diseases, such as type 2 diabetes and nonalcoholic fatty liver disease.

As a deletion in yeast *ARV1* results in robust apoptosis in response to FA treatment, we predicted that knockdown of mammalian *ARV1* would confer a similar sensitivity. Lipid induced apoptosis of pancreatic β-cells is associated with altered glucose metabolism and T2D progression [126, 348-350]. In order to elucidate the role of *ARV1* in β-cell health, we used the MIN6 mouse pancreatic β-cell line to test for levels of lipoapoptosis upon specific gene knockdown. Cells were treated with murine *ARV1* specific antisense oligonucleotides (ASOs) for 48 hours to induce a significant reduction in gene expression. This treatment caused an approximate 40% decrease in *ARV1* expression compared to control ASO treatment (Fig 5-4).

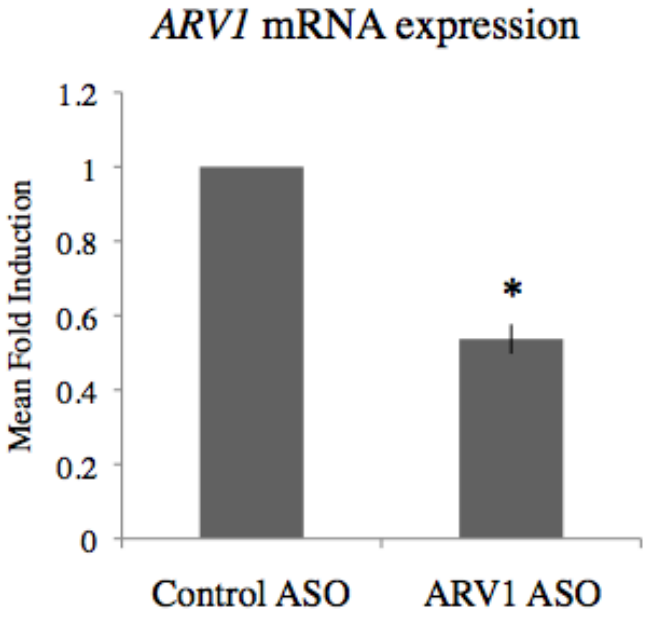

Figure 5-4: ARV1 knockdown in MIN6 pancreatic β-cells. Mouse *ARV1* mRNA expression levels with 0.25 μM ASO treatment for 48 hours measured by quantitative RT-PCR. Asterisks denote statistical significance compared to the

wild type control in the same condition (*$p<0.05$) by unpaired t-test of differences of the mean fold induction ($\Delta\Delta Ct$) ±s.d. (n=3).

Levels of apoptosis were measured after 24 hours of fatty acid treatment by the fluorescent apoptotic marker stain, Hoechst 33342, and the cell death marker, propidium iodide (PI) (Fig 5-5). Condensing chromatin, characteristic of apoptotic cells, is stained brightly with blue-fluorescent Hoechst 33342 dye compared with a dim nuclear stain of normal cells. Apoptotic cells were identified as cells staining positive for Hoechst 33342 and negative for PI [351].

Treatment of MIN6 cells with the saturated fatty acid (SFA) palmitate (at both 0.1 and 0.5 mM) and the unsaturated fatty acid (UFA) palmitoleate (at 0.5 mM), induced a significant increase in apoptosis in both control and *ARV1* siRNA groups compared to the apoptosis percentage under no treatment conditions (Fig 5-5). Similar levels of apoptosis have been demonstrated in pancreatic β-cell models following chronic fatty acid exposure [202, 352].

When comparing control and *ARV1* siRNA treatments, we saw a significant increase in apoptosis in *ARV1* knockdown following the addition of both palmitate (at 0.1 and 0.5 mM) and palmitoleate (Fig 5-5). Incubation of either control or *ARV1* siRNA treated cells with oleate or low levels of palmitoleate (0.1 mM) did not increase apoptosis in either group. However, in the no treatment condition (0.5% BSA), *ARV1* knockdown caused a significant increase in the apoptotic cell percentage compared to the no treatment control (Fig 5-5B). This mirrors the increase in basal apoptosis occurring with yeast *arv1Δ* grown in rich media (YPD) and indicates that knockdown of *ARV1* in either model results in a decrease in cellular viability (Fig 5-2). Furthermore, these results demonstrate that knockdown of *ARV1* sensitizes MIN6 cells to both

palmitate and palmitoleate induced apoptosis, which is consistent with the FA-sensitivity phenotype in yeast and congruent with our original prediction.

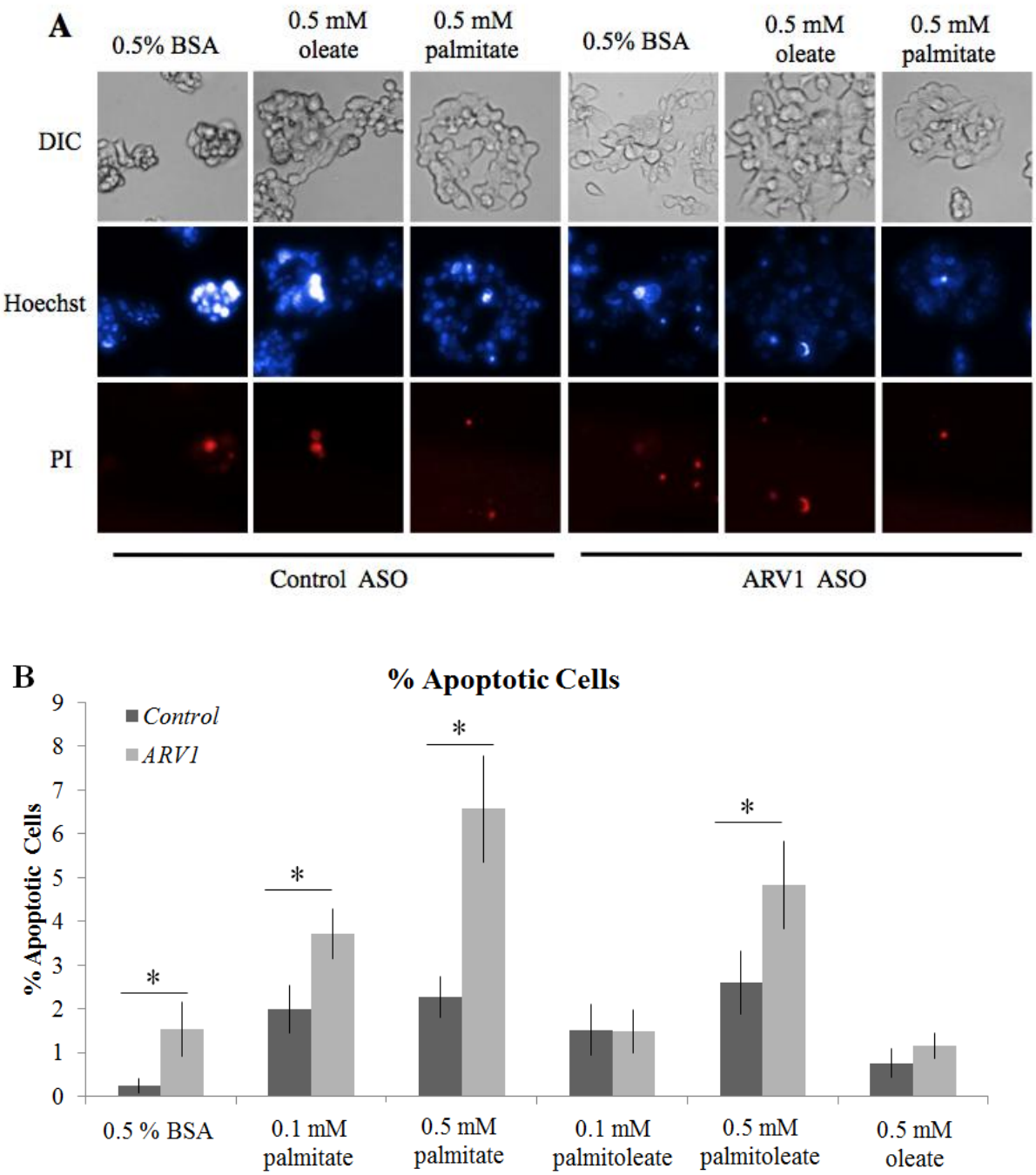

Figure 5-5: Decreased ARV1 expression in MIN6 cells increases sensitivity to fatty acid induced apoptosis. (A) Hoechst/PI staining and of MIN6 cells treated with 0.5 mM Oleate, Palmitoleate and Palmitate for 16 hours. (B) Quantification of the average number of apoptotic cells. (mean ±s.e., 7 fields with 70-200 cells per field). Asterisks denote statistical significance (*$p<0.05$) compared to Control ASO under the same condition.

Neutral lipid synthesis is directly correlated to ARV1 expression levels. A reduction in neutral lipid (NL) synthesis and storage in both yeast and mammalian systems is associated with increased levels of fatty acid induced apoptosis, ER-stress and cellular dysfunction [22, 186]. Obesity related diseases such as type 2 diabetes (T2D) are due in part to these lipid-induced cellular defects [353, 354]. In order to test for alterations in NL synthesis resulting from *ARV1* knockdown, we used two model systems, human embryonic kidney (HEK293) cells and MIN6 cells. HEK293 cells were chosen due to their minimal level of TG mass under normal growth conditions, making any small increase in TG and lipid droplets easier to detect. Stable HEK293 cell lines with suppressed *ARV1* expression were constructed using *ARV1* specific siRNA followed by clone selection. A stable cell line with a >85% reduction in *ARV1* expression was chosen for the subsequent experiments (Fig 5-6).

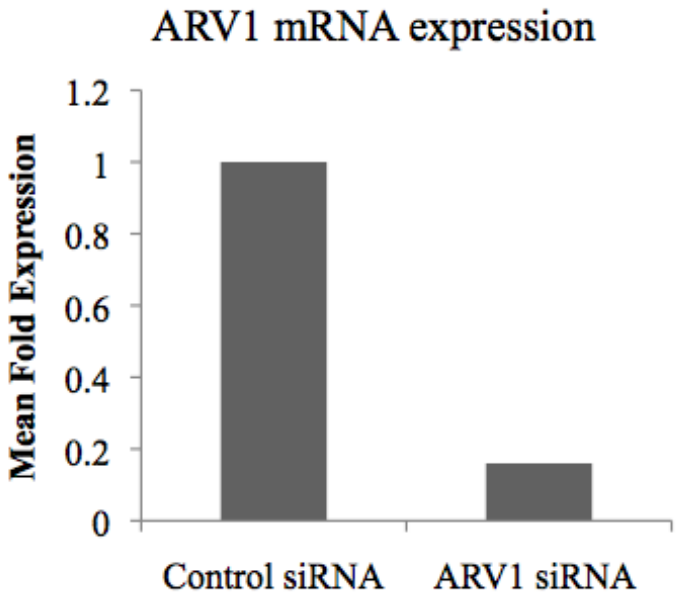

Figure 5-6: Knockdown of ARV1 in HEK293 cells. (A) Selection of HEK293 stable cells with suppressed hARV1 expression. After antibiotic selections, monoclonal cell lines were assessed for hARV1 mRNA level by Northern blot.

Signals were measured by phospho-imaging. Relative abundance of ARV1 mRNA was expressed as a ratio to housekeeping gene G3PDH. Control (CT) stably transfected with pSilencer-scrambled

Triglyceride synthesis in HEK293 cells were determined by [^{3}H]acetate incorporation and expressed in terms of radioactivity incorporation (DPM) per milligram (mg) of protein. Knockdown of human *ARV1* in HEK293 cells resulted in a 55% decrease in [^{3}H]acetate incorporation into triglyceride and a 70% reduction in cholesteryl ester (Fig 5-7 A-B), implicating *ARV1* in the regulation of NL synthesis. Consistent with these results, Tong et al., demonstrated that liver TG was significantly reduced in mice with decreased hepatic *ARV1* expression [239].

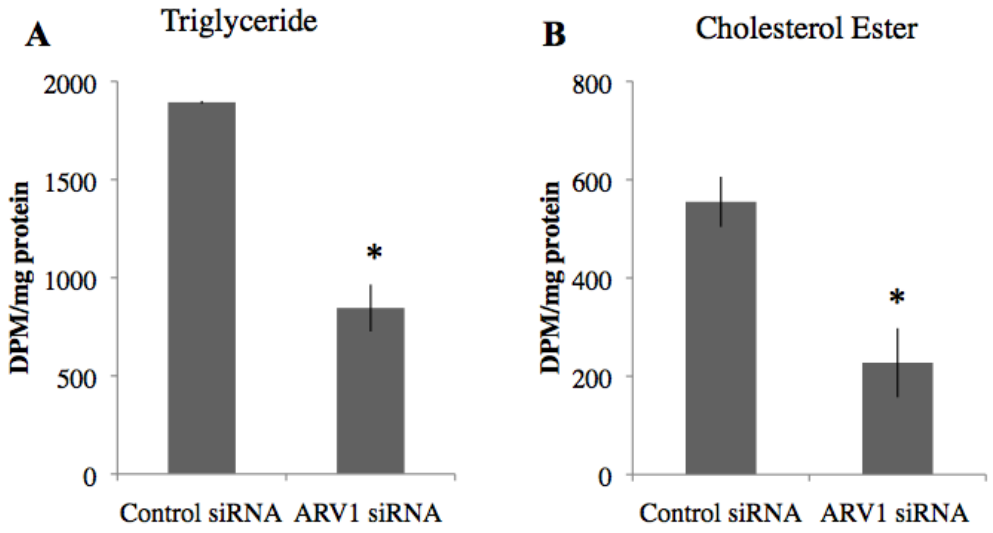

Figure 5-7: Knockdown of ARV1 in HEK293 cells results in a reduction in neutral lipid levels. Lipid labeling in ARV1 siRNA cells has reduced levels of (A) triglyceride and (B) cholesterol ester synthesis. There was no change in [^{3}H]acetate incorporation into free cholesterol (FC) or phospholipid between control and ARV1 knockdown cells (data not shown). Astrisks demotes statistical significance (*$p<0.05$) as determined by unpaired t-test (Mean ±s.d., n=3)

As knockdown of *ARV1* in MIN6 cells resulted in a robust sensitivity to fatty acid induced apoptosis, we also measured NL synthesis levels in this pancreatic β-cell line. Lipid synthesis levels in MIN6 cells were measured by average percent [^{3}H]oleate incorporation into lipid species following 4 hour label. Like that seen in HEK293 cells, triglyceride synthesis was decreased with *ARV1* knockdown compared to control (Fig 5-8A). All other lipid species measured (free fatty acid, diacylglycerol and cholesterol ester) had normal incorporation with the exception of phospholipids, which showed a significant increase (Fig 5-8 B).

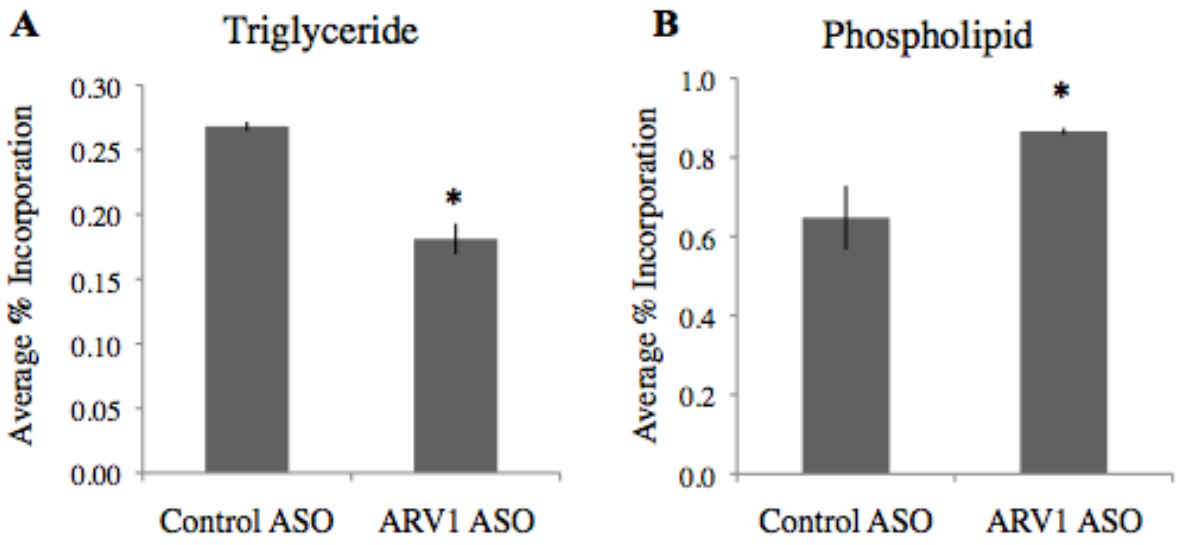

Figure 5-8: ARV1 knockdown in MIN6 pancreatic β-cells results in decreased triglyceride and increased phospholipid synthesis. Lipid synthesis measured by [^{3}H]oleate incorporation into triglyceride (A) and phospholipid (B) as a percentage of total lipid species. No changes were seen in any other species synthesis (SE, FFA, DAG). Astrisks demotes statistical significance (*$p<0.05$) as determined by unpaired t-test (Mean ±s.d., n=3)

The neutral lipids, triglyceride and cholesterol ester, are stored in the core of the lipid droplet, where they can be used as membrane building blocks or as a source of energy [30]. Since NL synthesis levels were significantly reduced in HEK293 and MIN6 cells following *ARV1* knockdown, we expected a similar decrease in lipid droplet number and/or size following decreased *ARV1* expression. In order to determine if this was the case, we grew siRNA treated cells overnight in 0.5 mM oleate, and stained for lipid droplets with Oil Red O. Despite the reduction in NL synthesis, we saw no obvious change in LD morphology upon *ARV1* knockdown in MIN6 cells (Fig 5-9). Moreover, in contrast to yeast *arv1Δ*, which had an increase in lipid droplets following palmitoleate treatment (Fig 5-3), knockdown of *ARV1* in MIN6 cells with overnight FA treatment had no effect on lipid droplet number or morphology (Fig 5-9). This may be due to differences in lipid droplet homeostasis in yeast and MIN6 cells, or perhaps to the differences in a full deletion versus a gene knockdown, which still has ~60% residual *ARV1* levels (Fig 5-4).

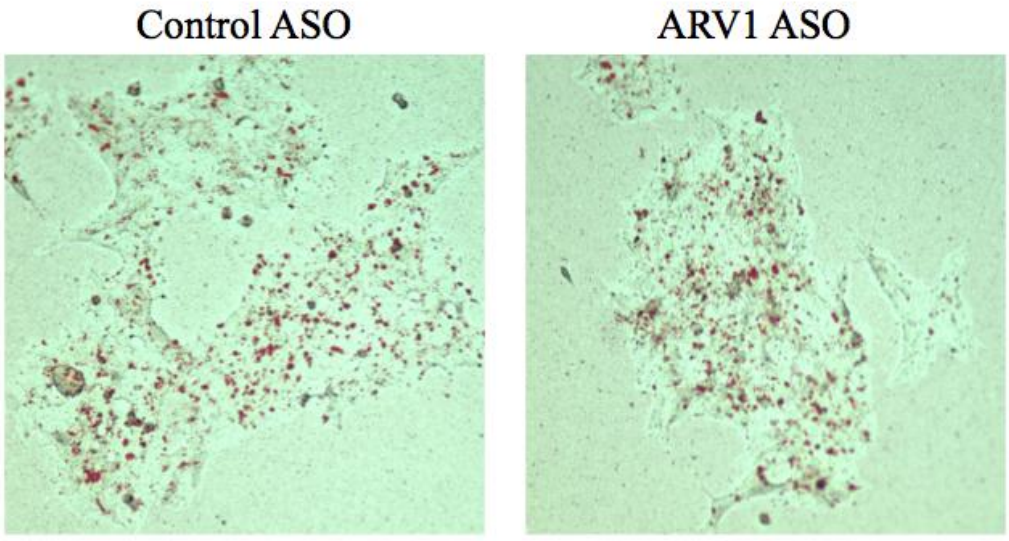

Figure 5-9. Reduced ARV1 expression in MIN6 cells does not alter lipid droplet morphology. Cells were grown overnight in oleate for 20 hours followed by Oil Red O staining.

Human ARV1 overexpression alters lipid levels independent of SREBP. In order to further elucidate the role of *ARV1* in mammalian lipid metabolism, we used a constitutively active human *ARV1* vector to determine the effects of *ARV1* overexpression in lipid synthesis. Stable HEK293 monoclonal cell lines transfected with human *ARV1* (hARV1-EGFP) were selected using fluorescent microscopy and western blot analysis to identify clones with the highest levels of hARV1-EGFP expression (Fig 5-10 A-C). Since decreased *ARV1* expression resulted in a reduction in TG synthesis, we tested for altered TG synthesis levels with increased *ARV1* expression. Corresponding to that seen with *ARV1* knockdown, *ARV1* overexpression resulted in a dramatic increase in [^{3}H]glycerol labeling of both triglyceride (TG) (163%) and phospholipid (109%) in hARV1-EGFP cells compared to control (Fig. 5-10 D-E). Taken together with *ARV1* knockdown data, these results indicate that *ARV1* expression directly correlates with levels of triglyceride synthesis.

In mammals, levels of cholesterol and fatty acids within the cell are controlled, in part, by the sterol regulatory element-binding protein (SREBP) family of transcription factors [355]. These proteins are localized at the ER membrane and are cleaved in response to intracellular lipid levels, releasing mature forms of the SREBPs that bind to the sterol regulatory elements (SRE) of genes involved in cholesterol and fatty acid synthesis [356]. Mice with hepatic *ARV1* knockdown showed increased ER cholesterol and a downregulation of SREBP cleavage and activation in the liver. We therefore reasoned that the increased TG synthesis in hARV1-EGFP transfected HEK293 cells could be explained by a rise in SRE-mediated gene expression. To test for a potential role for SREBP in hARV1-EGFP cells we used a pSyn-SRE vector to measure luciferase activity. In all conditions tested, there were no significant changes in SRE-mediated gene expression between control and hARV1-EGFP cells (Fig 5-11), suggesting that increased levels of TG synthesis by *ARV1* are via a SREBP independent pathway.

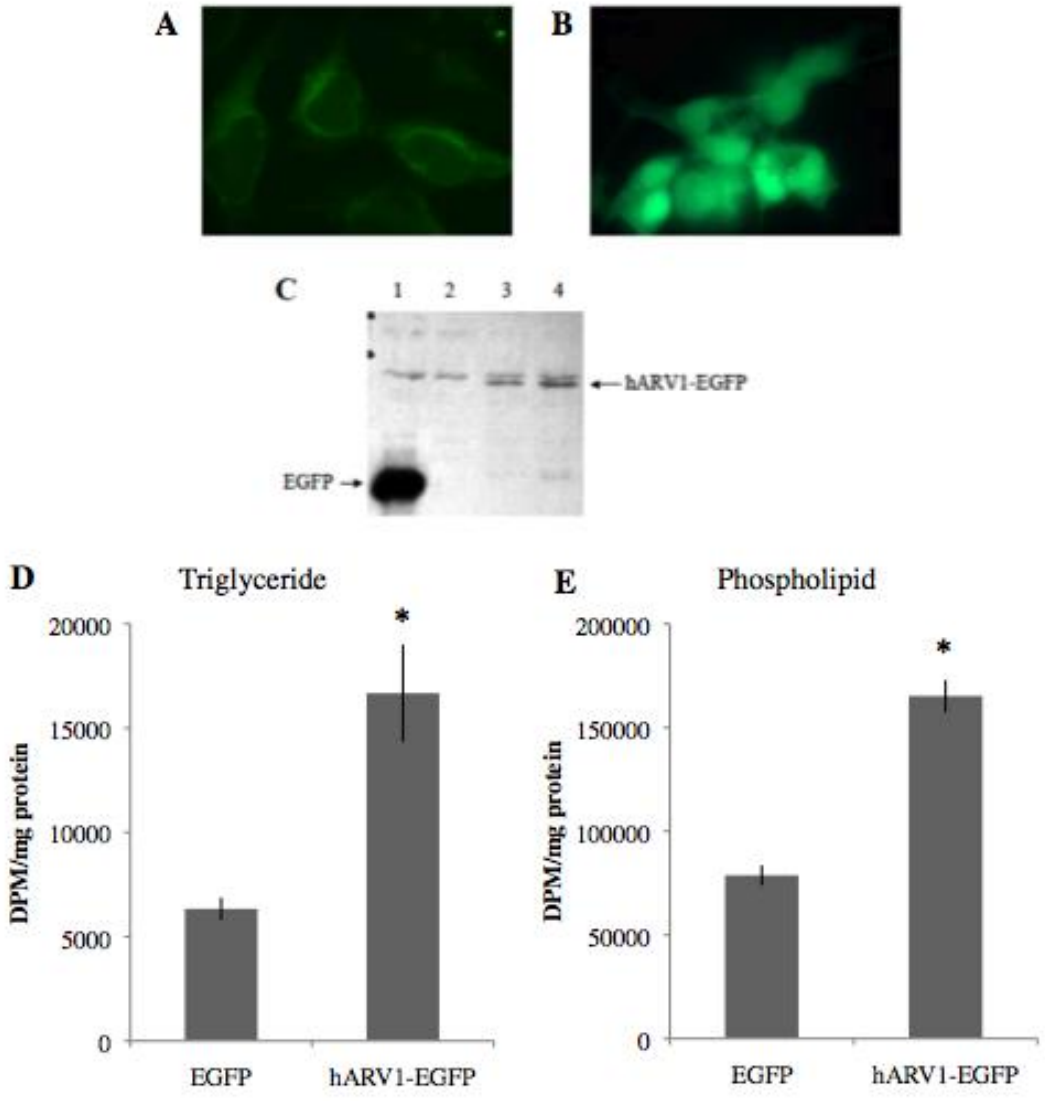

Figure 5-10: Overexpression of ARV1 in HEK293 cells causes increases triglyceride and phospholipid synthesis[156] (A-B) Stable transfection of HEK293 cells with hARV1-EGP and control EGFP. hARV1-EGFP cells were labeled for 8 hours with [3H]glycerol and lipid species were separated by TLC. TG (D) and PL (E) are expressed as DPM/mg of protein. Asterisks denote statistical significance ($p<0.05$)compared to EGFP control cells

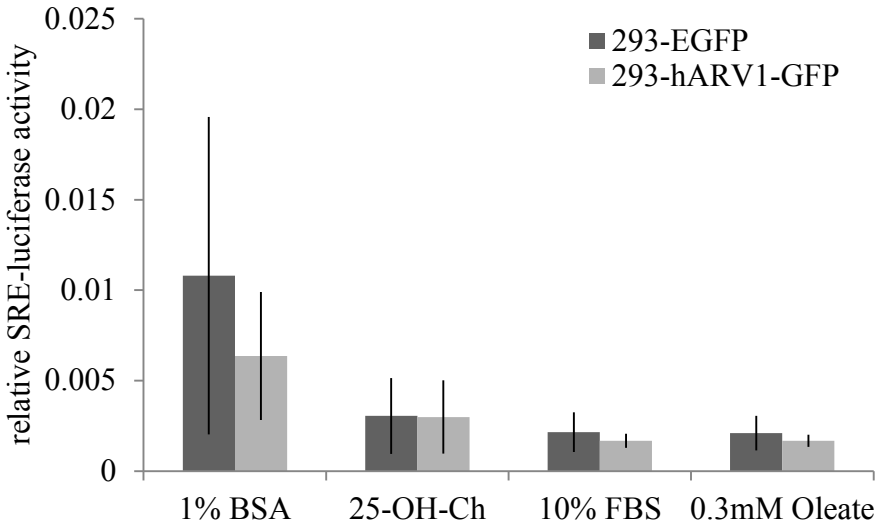

Figure 5-11. Increased lipid synthesis levels in HEK293 cells with ARV1 overexpression is independent of the sterol regulatory element binding protein (SREBP) [156]. SRE-mediate gene expression measured by transfection with pSyn-SRE and pRL-CMV and treated for 16 hours with serum free (SF) DMEM + 1% BSA, SF DMEM + 1% BSA with 10 µg/ml cholesterol and 1 µg/ml 25-OH-cholesterol, DMEM with 10% fetal bovine serum (FBS) and SF DMEM + 1% BSA with 0.3 mM oleate. Relative SRE activity expressed as a ratio of firefly to *Renilla* luciferase activity.

Overexpression of Human ARV1 in Mice Increases Heptatic Triglyceride Levels. Altered NL synthesis can have profound effects on cellular health in the face of caloric excess. For instance, ablation of the TG synthesis enzyme, *DGAT1*, results in increased UFA induced toxicity in mouse fibroblasts [7] and overexpression of TG synthesis enzymes is able to decrease lipotoxic phenotypes *in vivo* [25]. In agreement with these studies, we demonstrate that decreased NL synthesis in MIN6 cells following *ARV1* knockdown is associated with increased FA-induced apoptosis. In addition to a reduction in NL synthesis, lipid deposition in the liver, which can occur through increased TG synthesis, is associated with cellular dysfunction categorized as nonalcoholic fatty liver disease. Therefore, altered lipid synthesis to either extreme is associated

with obesity related disorders. A protein like *ARV1*, which has obvious effects on TG synthesis, may be an important regulator of lipotoxic pathways.

In order to assess the role of *ARV1* in mammalian physiology, we induced *ARV1* overexpression in mouse liver and monitored hepatic and plasma lipid levels. In order to increase hepatic *ARV1* expression we injected C57BL/6 female mice with a human *ARV1* specific adenovirus (AdhARV1) or a control adenovirus (AdNull) for 4 days, after which serum was collected and tested for total cholesterol, triglyceride and HDL and mice were sacrificed for hepatic lipid analysis [357, 358]. As expected, mRNA expression levels of hepatic hARV1 were consistently increased in ARV1 adenovirus injected mice (AdhARV1) compared to control (AdNull) (Fig 5-12A). This did not cause any change in the serum lipid profile between the two groups (data not shown) but did result in a significant increase in hepatic TG compared to control (Fig 5-12C). This is consistent with our *in vitro* studies showing increased TG synthesis with higher *ARV1* expression (Fig 5-10D). Both free cholesterol and phospholipids also showed a significant increase in the livers of the AdhARV1 injected mice compared to control, with a 33% and 21% increase respectively (Fig 5-12C). To confirm the hepatic lipid accumulation, we stained the livers with Oil Red O and observed large neutral lipid droplets in AdhARV1 infected livers in which was not seen in the AdNull control mice (Fig 5-12 D) [359].

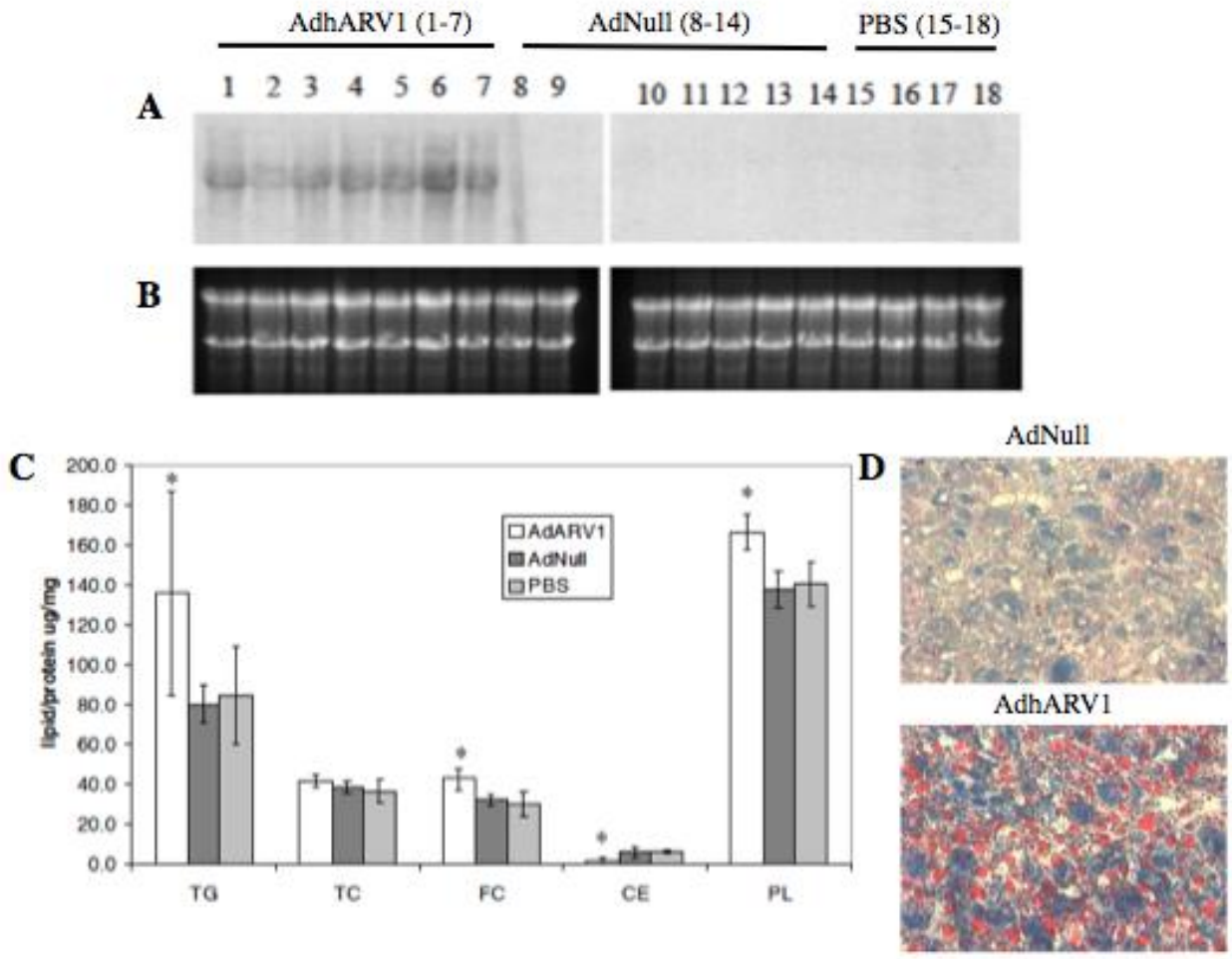

Figure 5-12: Overexpression of human ARV1 in mice causes fatty liver [156]. Mice injected with AdhARV1 or AdNull for 4 days, sacrificed and livers were perfused and homologized (A) mRNA levels of hARV1 gene expression in mouse livers (B) Ethidium bromide staining of 18s and 18s rRNA to show equal loading of RNA samples. Samples 1-7, RNA from livers of AdhARV1 infected mice; 8-14, RNA from lives of AdNull Infected mice; 15-18 RNA samples from livers of PBS injected mice (C) Liver lipids were measured enzymatically (D) Neutral lipid staining in livers with Oil-red-O stain.

Increased liver TG can be associated with hepatic insulin resistance and ER stress and occurs due to an imbalance between TG liver influx (*de novo* biosynthesis, diet or adipose tissue) and removal (secretion or oxidation) [360]. In order to determine potential mechanisms for the

lipid changes observed in AdhARV1 infected mice, we used gene expression profiling with an Affymetrix GeneChip. Using high stringent criteria (student t test $P<0.001$ between AdhARV1 and AdNull, fold changes either >1.5 or <0.5) we identified 27 upregulated (Table 5-1) and 9 downregulated genes in the AdhARV1 livers (Table 5-2). The triglyceride synthesis gene, *DGAT1*, was found to be upregulated 1.6 fold in and this increase was confirmed by real-time PCR (Fig 5-13). There is little known about the regulation of *DGAT1* transcription, but *DGAT1* contains a Peroxisomal Proliferator-Activated Receptor (PPAR) binding site and its mRNA expression increases in response to the PPARγ activators, thiazolidinediones, in adipose tissue [361]. Furthermore, gene expression analysis of biopsy samples taken from patients with nonalcoholic fatty liver disease (NAFLD) have a significant increase in expression of both DGAT1 and PPARγ [362]. Other enzymes involved in triglyceride or sterol ester synthesis did not have altered gene expression in these livers including downstream targets of SREBP. This result is consistent with our previous observation in the HEK293 cell model, showing no major role for SRE-mediated gene expression in ARV1 driven lipid metabolism.

Table 5-1. Genes with increased expression in AdhARV1 treated mice [156].
Genes upregulated (fold change 1.5 or more P<0.001) in livers with hARV1 overexpression. Results calculated based on data of 6 sets of Affymetrix oligonuclotide arrays

Process	Gene ID	Fold Change	Gene	Gene Symbol
Lipid metabolism	13350	1.6	Diacylglycerol O-acyltransferase 1	Dgat1
DNA replication and repair	18974	2.2	DNA polymerase II subunit 2	Pole2
	17217	2.2	Minichromosome maintenance deficient 4 homolog	Mcm4
	22256	2.2	Uracil-DNA glycosylase	Ung
Protein modification and metabolism	12236	2.6	Budding uninhibited by benzimidazoles 1 homolog, beta	Bub1b
	14864	2.3	Glutathione S-transferase, mu 3	Gstm3
	17387	2.2	Matrix metalloproteinase 14 (membrane-inserted)	Mmp14
	52033	1.8	Pbk PDZ binding kinase	Pbk
	20873	1.6	Polo-like kinase 4	Plk4
	53892	1.5	Protein phosphatase 1D magnesium-dependent, delta isoform	Ppm1d
	30841	1.7	Lysine (K)-specific demethylase 2B	Kdm2b
Miscellaneous	333182	4.6	Cytochrome c oxidase subunit VIb polypeptide 2	Cox6b2
	110789	3.3	G protein-coupled receptor 98	Gpr98
	66929	2.7	ASF1 anti-silencing function 1 homolog B	Asf1b
	20888	2.2	Sulfotransferase family, cytosolic, 1C, member 1	Sult1c1
	57261	1.8	Bromodomain containing 4	Brd4
	68087	1.8	Dephospho-CoA kinase domain containing	Dcakd
	69482	1.8	Nucleoporin 35	Nup35
	50927	1.7	Nuclear autoantigenic sperm protein (histone-binding	Nasp
	14265	1.7	Fragile X mental retardation syndrome 1 homolog	Fmr1
	70021	1.6	5'-nucleotidase domain containing 2	Nt5dc2
	213012	1.6	Abhydrolase domain containing 10	Abhd10
	69860	1.5	Eukaryotic translation initiation factor 1A domain containing	Eifad
	76375	9.9	De-etiolated homolog 1	Det1
	209378	2.1	Inter-alpha (globulin) inhibitor H5	Itih5
Uncharacterized	74476	6.2	4933439C10Rik	----
	13957	5.7	EST X83313	X83313

Table 5-2. Genes with decreased expression in AdhARV1 treated mice[156].
Genes downregulated (fold change 0.5 or less, P<0.001) in livers with hARV1 overexpression. Results calculated based on data of 6 sets of Affymetrix oligonuclotide arrays

Gene ID	Fold Change	Gene	Gene Symbol
227627	0.369	Lipocalin 13	Lcn13
59041	0.391	Serine/threonine kinase 25	Stk25
72747	0.409	Tetratricopeptide repeat domain 39C	Ttc39c
12352	0.412	Carbonic anhydrase 5a, mitochondrial	Car5a
106064	0.422	Expressed sequence AW549877	AW549877
70524	0.441	RIKEN cDNA 5730414N17 gene	5730414N17Rik
69066	0.479	RIKEN cDNA 1810010H24 gene	1810010H24Rik
208292	0.486	Zinc finger protein 871	Zfp871

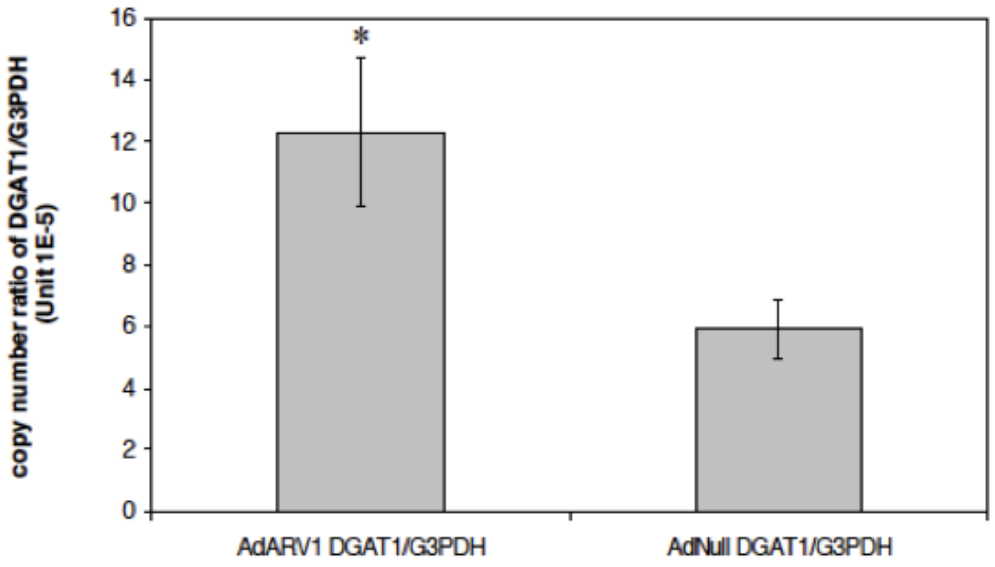

Figure 5-13: DGAT1 expression levels are significantly increased in AdhARV1 treated mice [156]. DGAT1 mRNA expression levels from AdhARV1 injected mouse livers compared to AdNull control. Asterisks denotes statistical significance as determined by unpaired t-test (*$p<0.05$) compared to control.

ARV1 overexpression in rat hepatoma cell line McA-RH7777. There are several mechanisms in which hepatic lipid accumulation can occur. In addition to increased TG synthesis, increased

fatty acid uptake from circulation, decreased fatty acid oxidation or a reduction in very low density lipoprotein (VLDL) secretion can all result in a rise in hepatic TG mass. These mechanisms can occur simultaneously or independent from one another [68] and therefore, in addition to the increase in hepatic TG synthesis seen with *ARV1* overexpression, any of these defects could exacerbate the fatty liver phenotype.

In order to test for altered TG secretion we transfected rat hepatoma McA-RH77777 cells with the same control (AdNull) and human ARV1 (AdhARV1) adenoviral constructs used in our mouse study and assessed TG clearance using [^{3}H]glycerol labeling. McA-RH7777 cells were treated with the adenovirus constructs for 48 hours to induce *ARV1* overexpression (Fig 5-14A) and pulse labeled with [^{3}H]glycerol for 2 hours. In contrast to the mouse studies, there was no difference in triglyceride levels in AdhARV1 infected cells compared to control (Fig 5-14B). Following the 2 hour pulse, fresh media without label was added to a subset of cells for 4 hours, after which lipids were extracted. An accumulation of lipids due to defects in TG secretion would result in increased [^{3}H]glycerol labeled intracellular TG after this 4 hour chase. We did not see any difference in TG levels post-chase with human *ARV1* overexpression compared to control (Fig 5-14C), indicating that it is unlikely that VLDL secretion is affected by altered *ARV1* expression.

In order to be certain, we went on to quantify VLDL synthesis and secretion levels in adenoviral treated McA-RH7777 cells. VLDL is assembled in the liver through lipidation of apolipoprotein B (ApoB) and secreted into the circulation where it delivers lipids to peripheral tissues [68]. ApoB synthesis and secretion were quantified by protein labeling of McA cells with [^{35}S] methionine in serum free DMEM ± oleate for 2 hours. Media and cells were collected and the two forms of apoB (apoB100 and apoB48) were immunoprecipitated with an apoB specific

antibody (Fig 5-15) [311]. Oleate was included in this study because short term incubation of McA cells with oleate induces an increase in apoB100 secretion compared to secretion in without oleate [124]. We found that overexpression of human *ARV1* in McA-RH7777 cells did not change apoB100 or apoB48 secretion in either treatment condition (Fig 5-15). Together with the [^{3}H]glycerol studies, these results indicate that there is no change in TG synthesis or TG secretion in McA-RH7777 cells overexpressing human *ARV1*.

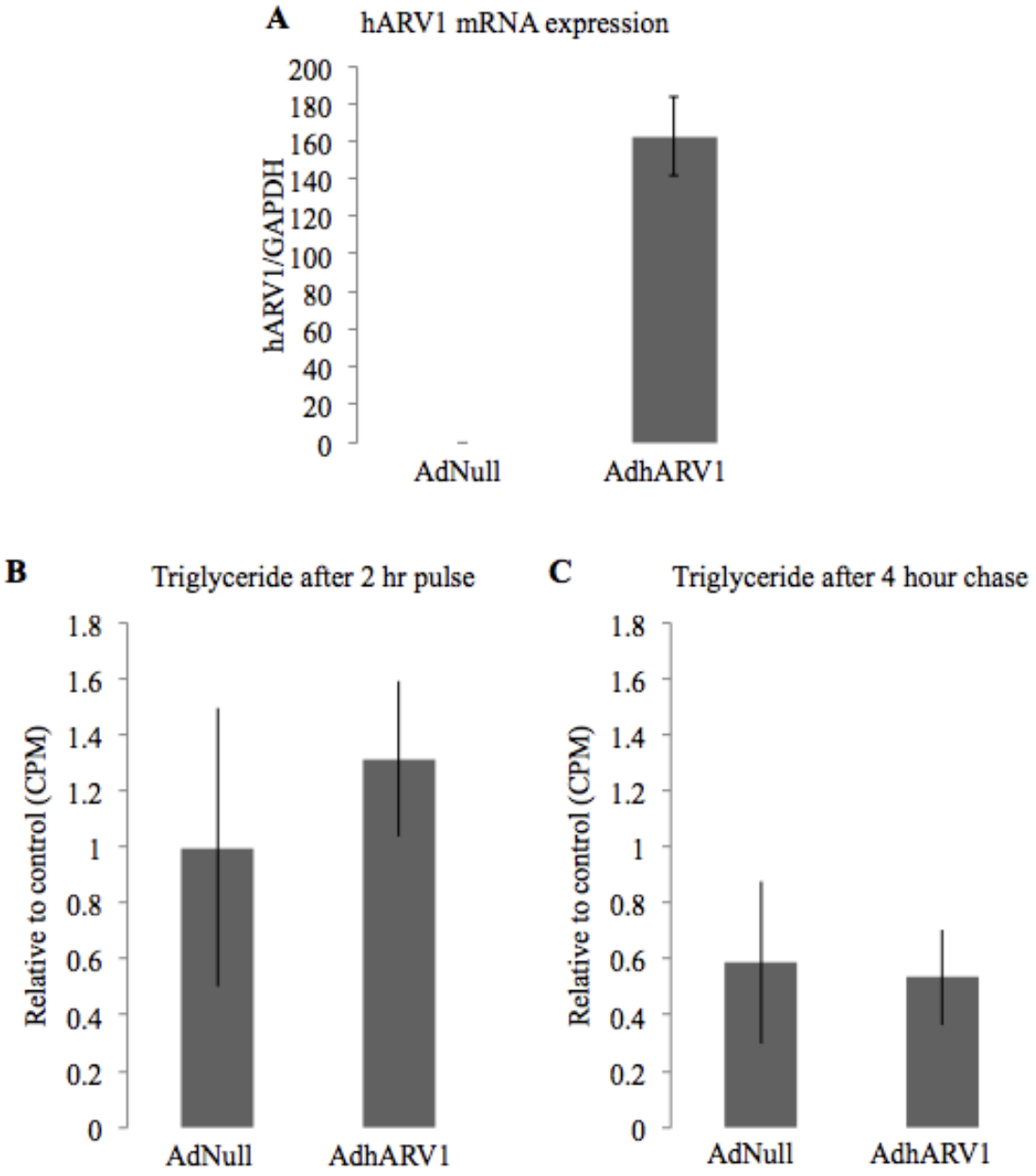

Figure 5-14: ARV1 overexpression in McA-RH7777 cells does not change levels of lipid synthesis (A) human ARV1 expression levels as measured by quantitative RT-PCR relative to GAPDH internal control (B)[3H]glycerol labeling of triglyceride in adenoviral treated McA-RH7777 cells after 2 hour pulse with label in serum free (SF) DMEM + 1.5% BSA and after 4 hour pulse in SF-DMEM + 1.5% BSA and no label.

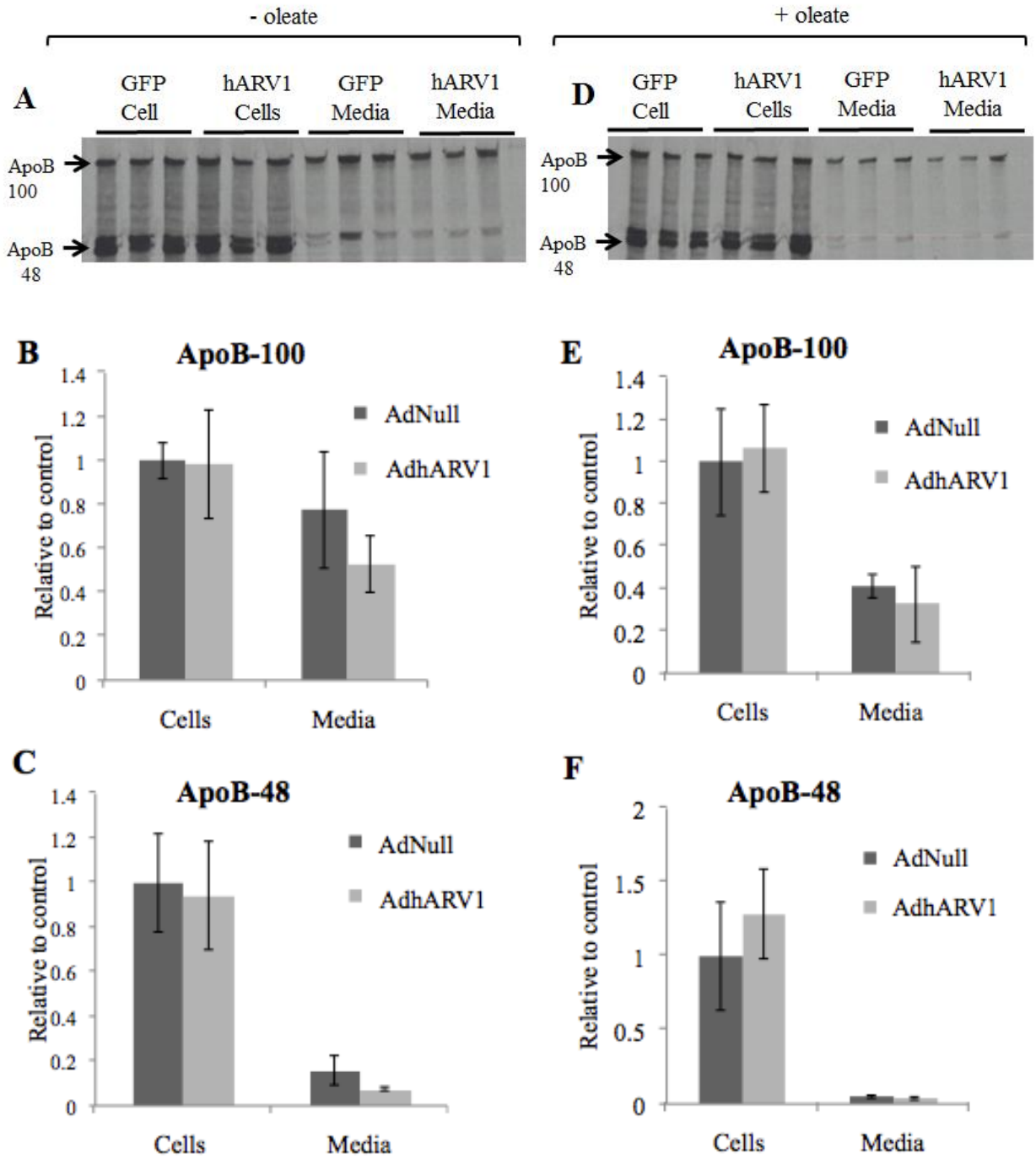

Figure 5-15: ApoB secretion is unchanged with human ARV1 overexpression in McA-RH7777 cells. To determine levels of ApoB secretion, cells were labeled with [^{35}S]methionine for 2 hours with (D-F) and without (A-C) oleate. Cells and media were collected, apoB immunoprecipitated and run on an SDS-PAGE gel followed by development via autoradiography (B and D). Quantification of

[^{35}S]methionine incorporation into ApoB100 (B and E) and ApoB48 (C and F) relative to AdNull control.

The significant increase in TG synthesis occurring in AdhARV1 injected mice was not recapitulated in the McA-RH7777 cell line. We measured mRNA expression levels of basal *ARV1* in mouse liver and McA-RH7777 cells to determine if the contradictory results were due to a difference in *ARV1* expression in untreated cells. Using quantitative RT-PCR we found that mRNA expression of *ARV1* was significantly elevated, by more than 50 fold, in McA-RH7777 cells compared to levels in mouse liver (Fig 5-16). *ARV1* expression in pancreatic islets and MIN6 cells were also significantly lower than those in McA-RH7777 cells by more than 15 fold (Fig 5-16). Therefore, the contradictory results between rat hepatoma cells and the mouse liver could be due to the naturally higher *ARV1* expression levels in McA-RH7777 cells compared to mouse liver, which would confound any further increase in *ARV1*.

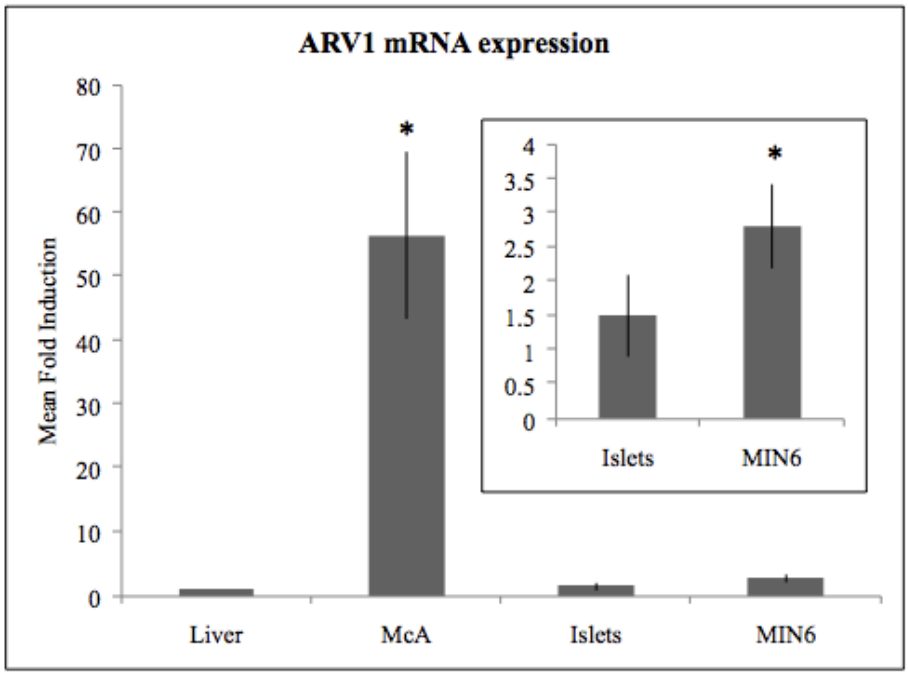

Figure 5-16: ARV1 mRNA expression is increased in MIN6 and McA-RH7777 cell lines compared to mouse liver and pancreatic islet cells. Real-time PCR measurements of ARV1 expression in mouse liver and pancreatic islet cells, the rat hepatoma cell line McA-RH-7777 (McA) and the mouse pancreatic β-cell line,

MIN6. Mean fold induction relative to mouse liver expression. Asterisks denote statistically significant ($p<0.05$) differences in the mean fold induction ($\Delta\Delta Ct$) compared to liver by unpaired t-test (n =3).

DISCUSSION

In these studies, we demonstrate a role for eukaryotic *ARV1* in triglyceride synthesis and lipotoxic pathways in both yeast and mammalian cells. Our major finding was that the role of *ARV1* in lipotoxicity has been conserved between yeast and mammalian systems, with decreased expression resulting in increased fatty acid sensitivity. Additionally, mammalian *ARV1* expression is directly correlated with levels of TG synthesis in several mammalian models, including MIN6 pancreatic β-cells, HEK-293 embryonic kidney cells and mouse liver. In AdhARV1 injected mice, hepatic *ARV1* overexpression resulted in lipid droplet accumulation (Fig 5-12D) and upregulation of the TG synthesis gene *DGAT1* (Table 5-1). Lipid accumulation in nonadipose tissue, such as the liver, is associated with fatty acid induced cellular dysfunction, through increased toxic fatty acid metabolites (ie, ceramides, FFA, DAG) [68, 161, 184, 354, 363].

DGAT1 expression has been implicated in fatty liver phenotypes in both rodent models and human subjects. Gene expression analysis of biopsy samples taken from patients with nonalcoholic fatty liver disease (NAFLD) have a significant increase in *DGAT1* expression [362]. Furthermore, *DGAT1* deficient hepatocytes are protected against hepatic steatosis and inhibition of *DGAT1* protects against high fat diet induced fatty liver in mice [364]. Our findings indicate that overexpression of human *ARV1* in mouse liver is able to induce DGAT1 dependent fatty liver implicating *ARV1* as a central regulator of hepatic TG metabolism.

The mechanism by which *ARV1* overexpression drives DGAT1 mediated TG synthesis is still unclear. Gene expression analysis of AdhARV1 injected mice (Table 5-1 and 5-2) and SRE-

driven luciferase promoter activity in HEK-293 *ARV1* overexpressing cell lines (Fig 5-11) demonstrate that the lipid accumulation is independent of SREBP activity. Previous *ARV1 in vivo* studies have focused on sterol phenotypes resulting from a reduction in hepatic *ARV1* expression. The *ARV1* liver knockdown results in increased bile acid production in response to an accumulation of intracellular cholesterol [239]. In yeast, a deletion in *ARV1* also causes sterol accumulation, which activates ER stress and UPR induction [206]. In both cases, *ARV1* functions to detoxify the ER of sterol accumulation, though a precise mechanism for sterol movement remains elusive. As a result of these studies, and others, the proposed function for *ARV1* is as a sterol transporter, lack of which results in free sterol accumulation in the ER membrane [205, 206, 239].

Multiple studies have shown that *ARV1* is integrally involved in general lipid trafficking and homeostasis [58, 205, 344, 365]. The pleiotropic phenotypes exhibited in *arv1Δ* have made it difficult to assess primary and secondary response to the lipid transport defects and have made the determination of *ARV1* function challenging. We propose that the defects in TG homeostasis resulting from altered *ARV1* expression can be explained as a secondary effect to its function as a sterol transporter.

As a mediator of sterol detoxification from the ER, overexpression of *ARV1* would likely result in free sterol deficiency in the ER membrane and a subsequent increase in plasma membrane (PM) cholesterol (Fig 5-17 (1)). Plasma membrane localized cholesterol causes an increase in the lateral ordering of the membrane, decreasing membrane fluidity [366]. This fluidity is integral in cellular health, and extreme membrane fluidity or rigidity can result in broad cellular defects [367-369]. For example, high levels of cholesterol at the membrane cause an overly ordered structure resulting in decreased membrane protein diffusion and reduced

membrane-binding capabilities [370]. The accumulation of free cholesterol in the plasma membrane due to increased *ARV1* expression would result in a rigid membrane architecture and require cellular maintenance in order to regain normal membrane structure (Fig 5-17 (2)).

A cell is able to balance decreased fluidity through alterations in phospholipid acyl chain composition. The ratio of saturated to unsaturated fatty acyl chains in membrane phospholipids has a major impact on membrane fluidity, with increased unsaturated fatty acyl chains increasing membrane fluidity. Feedback mechanisms likely exist to increase unsaturated fatty acid production and normalize membrane fluidity in instances of increased free cholesterol. Fatty acid biosynthesis genes, acetyl-CoA carboxylase (ACC), fatty acid synthase (FAS) and stearoyl-CoA desaturase (SCD), contain sequences which indicate that they may be regulated by sterols and likely explain the coupling of sterol-FA levels at the membrane [371, 372]. We propose that following hepatic *ARV1* overexpression, increased plasma membrane cholesterol upregulates UFA biosynthesis in order to maintain membrane architecture (Fig 5-17 (3) and (4)). The increase in intracellular UFA could channel not only into PL acyl chains but also into other pathways, particularly triglyceride synthesis (Fig 5-17(5)). Therefore, the continuous biosynthesis of unsaturated fatty acids through a membrane fluidity feedback mechanism could explain the increase in TG synthesis with *ARV1* overexpression.

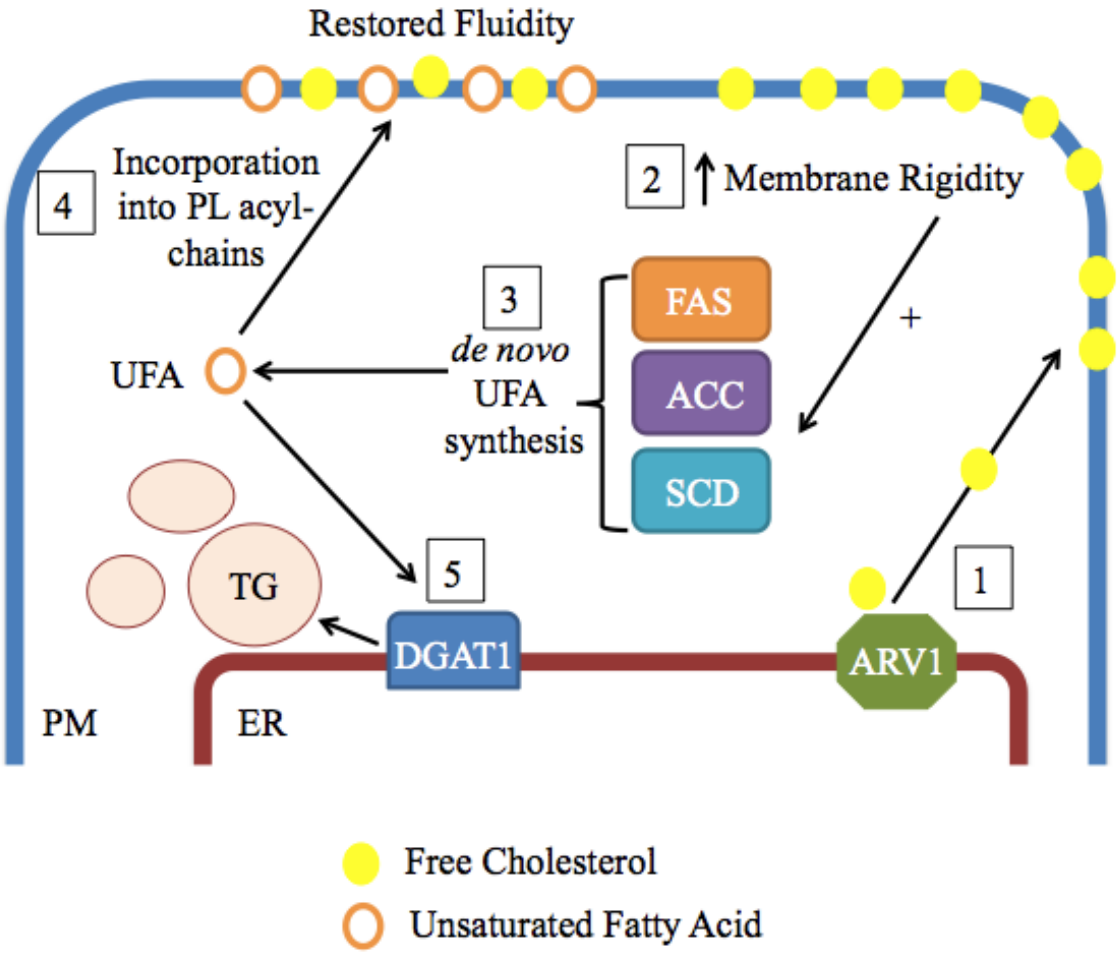

Figure 5-17: Model for increased DGAT1 driven triglyceride synthesis with ARV1 overexpression. (1) As an ER sterol transporter, overexpression of *ARV1* would result in increased transport of free cholesterol from the ER to the plasma membrane (PM) causing a cholesterol deficient ER and an accumulation of sterols at the PM. (2) Increased cholesterol levels within the membrane changes membrane properties and increases rigidity. A large change in membrane fluidity affects protein movement within the membrane and is involved in general cellular health. (3) In order to restore normal fluidity, *de novo* FA synthesis is upregulated, particularly UFA synthesis. (4) Increased UFA incorporation into phospholipid (PL) acyl chains increases membrane fluidity to preserve membrane structure and function. (5) The increase in cellular UFA can also channel into TG synthesis through DGAT1 dependent esterification, resulting in lipid droplet accumulation (steatosis).

Our study not only identified a novel pathway involved in lipotoxic disease, but also further demonstrates the power of yeast genetics in the identification of human disease modifiers. A primary goal of our UFA sensitivity screen in yeast (chapter 2) was to find conserved genes that are involved in lipotoxicity in both yeast and mammals. As expected from the screen, we found a significant increase in apoptosis in response to fatty acid treatment in the yeast *ARV1* deletion compared to control (Fig 5-2). We also demonstrate that knockdown of *ARV1* in MIN6 cells increases vulnerability of pancreatic β-cells to lipoapoptosis. Therefore, our screen was successful in the identification of a currently unreported mammalian lipotoxicity pathway through sequence and functional homology.

The role of neutral lipid synthesis as a protective mechanism against the formation of toxic lipid metabolites has been well established [7, 22, 23, 373]. It is therefore not surprising that decreased TG synthesis in MIN6 cells upon *ARV1* knockdown increases cell sensitivity to FA-induced apoptosis (Fig 5-5). The reduction in TG synthesis occurring with decreased *ARV1* expression may occur through a mechanism similar to that described in its overexpression (Fig 5-17), with feedback mechanisms attempting to correct for changes in membrane properties and having secondary lipid homeostatic consequences.

Yeast *ARV1* mutants have a multitude of lipid related phenotypes, many of which involve defects in sterol and ceramide metabolism [205, 344]. Strains lacking *ARV1* have increased sensitivity to the polyene antibiotic nystatin, a decrease in sterol uptake, and an increase in the propapoptotic sphingolipid, ceramide [205, 344]. In addition, deletion of *ARV1* results in a significant increase in ER stress and unfolded protein response (UPR) under basal conditions [206]. Within the past ten years studies have identified ceramide production [374-377] and ER

stress response [378, 379] as playing an integral role in pathways of lipotoxicity and insulin resistance. The accumulation of ceramide and the constitutively active UPR characteristic of *ARV1* mutants are two potential mechanisms explaining FA sensitivity in yeast *arv1Δ*.

Alternatively *ARV1* knockdown in the mouse liver did not result in increased UPR activation, due to the hepatocytes ability to channel excess cholesterol into bile acid production [239]. Pancreatic β-cells lack this detoxification pathway, and likely deal with sterol accumulation in a mechanism more similar to yeast. Therefore, the increase in lipotoxicity in MIN6 cells with knockdown of *ARV1* likely occurs through UPR induction and increased ceramide synthesis driven by ER sterol accumulation, though further research is needed to substantiate this claim.

In conclusion, we have demonstrated a role for mammalian *ARV1* in the progression of two major lipotoxic disorders, nonalcoholic fatty liver disease and lipid-induced pancreatic β-cell failure. Altered expression of *ARV1* causes major changes in neutral lipid synthesis and overall lipid homeostasis. Though no known *ARV1* gene polymorphisms have been associated with disease states, it is possible that slight changes in *ARV1* expression in humans contributes to a predisposition to obesity related disorders and thus, future research is necessary to understand the role of this lipid metabolism regulator in human health.

CHAPTER 6: CONCLUSIONS AND FUTURE DIRECTIONS

SUMMARY

The aim of this thesis was to identify new pathways of lipotoxicity in eukaryotic cells using the model organism *S. cerevisiae.* Lipotoxicity occurs through lipid accumulation in cells, inducing cellular dysfunction associated with increases in reactive oxygen species [125, 139, 211, 380, 381], ceramide biosynthesis [111, 382], ER stress [129, 164, 182] and altered membrane fluidity [23, 113]. Loss of all neutral lipid synthesis in yeast (*are1Δ are2Δ dga1Δ lro1Δ*) results in robust sensitivity to unsaturated fatty acid (UFA) treatment [22, 23]. In order to identify single deletions inducing similar lipotoxicity, we completed a genome-wide sensitivity screen with the unsaturated fatty acid, palmitoleate. This screen identified 156 gene deletions resulting in significant sensitivity to growth on fatty acid containing media.

Of these genes, many are involved in vesicular trafficking defects, mitochondrial respiration, and translational regulation. In addition to palmitoleate sensitivity, we found the majority of these gene deletions to be sensitive to the sterol targeting polyene antibiotic, nystatin and growth in cold temperature (16°C). Over forty percent of the genes identified by our screen have mammalian orthologs and several have been previously reported to be involved in phenotypes associated with type 2 diabetes.

Three members of the vesicular trafficking, Golgi to ER Transport (GET) complex, were found to be sensitive to palmitoleate upon deletion. In order to gain insight into the role of the GET complex in UFA metabolism, we focused on the well-conserved member of the complex, *GET3*, and its role in lipotoxicity and lipid homeostasis. Deletion of *GET3* results in a decrease in lipid droplet number which was further reduced with an additional knockout of the triglyceride

synthesis gene, *DGA1*. This LD defect was not due to decreased neutral lipid mass, but NL synthesis in *GET3* mutants was significantly lower than control. Additionally, electron microscopy of the *GET3 DGA1* double deletion shows increased vacuolar lipid accumulation and membrane invaginations reminiscent of autophagic bodies.

In order to determine if the increase in vacuolar associated lipids was due to defects in hydrolysis, we tested for vacuolar proteinase activity, autophagic flux and survival rates under conditions of nitrogen starvation (SD-N). Autophagic flux, as measured by GFP-Atg8p cleavage, and survival in SD-N media were decreased in both *get3Δ* and *get3Δ dga1Δ*, indicating a *GET3* dependent defect in vacuolar nutrient turnover. Protease activity and vacuolar pH were both normal, as measured by cleavage of the fluorescent marker protein conjugate, CMAC-Arg. The increased vacuolar-lipid association is found in the *DGA1* single deletion as well, and thus is likely due to differences in trafficking of *LRO1* versus *DGA1* produced triglyceride. From this data we hypothesize that defects in *GET3* cause decreased vacuolar lipolysis, potentially through defective trafficking of the vacuolar lipase, Atg15p, from the endosome through the MVB pathway. This appears to be independent of mis-insertion of tail-anchored proteins characterized by mutations in the GET complex, and we propose that these defects can be explained by the role of Get3p in phophatidylinositol-3-phosphate production at the endosomal membrane and early endosome maturation.

Since a main goal of the original screen was in the identification of genes involved in lipotoxic disease, we followed up two mammalian orthologs of yeast genes found by our screen. The two orthologs we chose to focus on were the *GET3* ortholog, mammalian *ASNA1* and mammalian *ARV1*. We studied the effect of knockdown or overexpression of these genes on

lipid induced apoptosis and lipoid homeostasis in the mouse pancreatic β-cell line, MIN6, and the rat hepatoma cell line, McA-RH7777.

Due to the major effects of *GET3* deletion in lipid droplet homeostasis and lipotoxicity, we hypothesized that knockdown of *ASNA1* in MIN6 cells would increase susceptibility of these cells to fatty acid induced cell death. Apoptosis levels in *ASNA1* knockdown cells were significantly increased after palmitate treatment at 1.0 mM but palmitoleate, oleate and lower levels of palmitate (0.5 mM), did not result in a higher apoptotic level in *ASNA1* knockdown cells compared to control. Basal levels of ER stress were also significantly elevated in the *ASNA1* knockdown cells compared to control, a condition which may sensitize these cells to both lipoapoptosis [142] and defects in insulin secretion [128, 313].

In addition to β-cell apoptosis, cellular dysfunction following chronic fatty acid treatment is a major contributor in the progression of type 2 diabetes [142, 383, 384]. Previous work identified *ASNA1* as a regulator of glucose stimulated insulin resistance, with decreased *ASNA1* levels resulting in reduced insulin secretion [289]. In order to gain insight into the mechanisms of this secretion defect, we supplemented cells with fatty acids and amino acids, and tested for *ASNA1* dependent defects in glucose stimulated insulin secretion. From this study, we found that acute exposure of MIN6 cells to palmitate or L-Arginine was able to normalize the insulin secretion defects characteristic of cells with reduced *ASNA1* expression. These studies demonstrate that amplification of glucose stimulated insulin secretion by palmitate and L-arginine are able to compensate for the insulin secretion defect with knockdown of *ASNA1*, and likely operate within a parallel cellular pathway. We propose the defects in insulin secretion resulting from reduced *ASNA1* expression are due to decreased insertion of SNARE proteins through the tail anchored protein insertion pathway, resulting in a defect in insulin granule

docking and fusion. Fatty acids supplementation was able to increase insulin secretion, potentially through GRP40 binding, despite the ASNA1 dependent defects.

The second ortholog we examined was mammalian *ARV1*, which is homologous to the yeast *ARV1*, particularly in a 61 residue ARV1-homology domain. We chose *ARV1* for several reasons. Deletions in yeast *ARV1* caused the most dramatic palmitoleate sensitivity of all single mutants tested. Additionally, unpublished work in the Sturley Lab demonstrated a role for *ARV1* in lipid biosynthesis and the progression of nonalcoholic fatty liver disease in mice [156]. We used rat hepatoma McA-RH7777 cells with adenoviral vectors containing human ARV1 to study the effects of *ARV1* overexpression in very low density lipoprotein (VLDL) secretion and found no change in VLDL secretion in these cells compared to a GFP control. We predict that the increase in neutral lipid synthesis with *ARV1* overexpression is a secondary effect based on its role as an ER resident sterol transporter. Upregulation of *ARV1* likely result in cholesterol accumulation at the plasma membrane, and a subsequent increase in membrane ridgity. Increased unsaturated fatty acid synthesis for incorporation into phospholipid acyl chains is a primary cellular response to increased membrane fluidity [371], and thus a rise in intracellular UFA could channel not only into phospholipid synthesis but also into the DGAT1 triglyceride synthesis pathway.

Additionally, knockdown of *ARV1* in MIN6 pancreatic sensitized cells to apoptosis under basal conditions and with palmitoleate or palmitate treatment. Neutral lipid synthesis was decreased in with reduced ARV1 expression, which is consistent with increased lipoapoptosis. Deletion of *ARV1* in yeast results in an accumulation of the toxic lipid metabolite, ceramide, and a constituitely active unfolded protein response (UPR)[205, 206, 344]. Both ceramide and UPR induction are two major contributors to lipotoxicity, and we propose that sensitization of MIN6

cells with a knockdown in *ARV1* occurs through these mechanisms. Together, these results indicate that ARV1 is involved in disease progression of two lipotoxic disease, type 2 diabetes and nonalcoholic fatty liver disease, through its role in fatty acid biosynthesis.

CONCLUDING REMARKS

Genetic make-up is well recognized as an important variable determining susceptibility to lipotoxic disease in the face of nutrient overload. Genome-wide lipid droplet morphology screens and genome-wide association studies have identified several genes involved in cellular lipid metabolism [56-60] or polymorphisms associated with disease phenotypes [65, 134, 235, 236, 304, 342, 385], but there is much to be determined in terms of the cellular mechanisms of lipotoxicity. The goal of our screen was to identify genes involved in not only yeast lipotoxicity, but also potential targets for mammalian lipotoxic disease treatment. We found 68 new mammalian genes, which may confer sensitivity to fatty acids in mammalian cells, based on their sequence homology to yeast genes identified by our palmitoleate sensitivity screen.

We demonstrate that knockdown of two of these orthologs, *ASNA1* and *ARV1*, in MIN6 pancreatic β-cells increases levels of fatty acid induced apoptosis and demonstrate a role for both of both genes in lipotoxic pathways leading to T2D. These studies demonstrate that our yeast sensitivity screen was successful in the identification of mammalian lipotoxicity genes based on gene sequence identity. Therefore, it is likely that our list of 66 unstudied human orthologs contains more genes that are integrally involved in the pathways of lipotoxicity, and these genes require additional exploration.

FUTURE DIRECTIONS

In order to further characterize the role of yeast Get3p and mammalian ASNA1 and ARV1 in lipotoxicity, we can continue to utilize both yeast and mammalian model systems. Future studies complementing this work include additional studies on *GET3* in lipid lipase activity and lipid droplet homeostasis, the unique effects of a *DGA1* deletion on TG localization, and the function of mammalian *ARV1* and *ASNA1* in pancreatic β-cell health *in vivo*.

1. Determine the role of yeast vacuolar lipase activity in whole cell lipid homeostasis.

We propose that the decreased lipid droplet number occurring in *GET3* mutants is due to defects in vacuolar lipase activity and decreased TG turnover. Likewise, studies in hepatocytes have shown that lipid stores can be mobilized by lysosomal lipases and an inhibition of autophagy results in lipid droplet accumulation [91]. In order to decipher the role of vacuolar lipase activity in yeast lipid metabolism, we could block autophagy, either chemically or genetically, and look for a neutral lipid accumulation and alterations in other pathways of lipid metabolism.

Further study in the *GET* mutant may also provide insight into the role of the yeast vacuolar lipase, Atg15p, in lipid recycling. Localization of Atg15, using a fluorescent tag such as GFP, in a *GET3* deletion would determine if the localization of this protein was in fact altered due to protein sorting defects. Additionally, we would expect specific blockage of PtdIns-3-P synthesis at the endosome would result in a similar defect in vacuolar lipase localization and activity. Together these studies would clarify the role of lipophagy and vacuolar lipid recycling in cellular lipid homeostasis.

2. Further elucidate the role of Get3p in lipid metabolism. In order to determine if the lipid phenotypes characteristic of Get3p are due to its role in G protein activation or TA protein insertion, these mechanisms must be isolated. Structural analysis studies of Get3p have determined protein domains integral for tail anchored protein insertion, particularly the nucleotide hydrolase domain (NDH) and a hydrophobic patch, which binds TA proteins [386]. One approach to separate out the two Get3p pathways is to mutate specific amino acids within the TA binding domain of Get3p. This would hypothetically block TA protein insertion without affecting its guanine exchange function. Lipid metabolism studies similar to those completed in this thesis could then be repeated in strains containing these TA protein point mutants, in order to determine if the decrease in LD number and neutral lipid synthesis are dependent on TA protein misinsertion.

Get3p strains with targeted mutations in the guanine nucleotide exchange domain would also be useful in clarification of the connection between Get3p and lipid metabolism. Unfortunately, no known signature sequence or domain exists that is able to predict activity of nonreceptor exchange factors, like Get3p [217]. Thus, additional research into the interaction between Get3p and Gpa1 is necessary to determine the protein domains important in nucleotide exchange.

3. **Identify if pools of triglyceride synthesized by Dga1p or Lro1p are differentially localized within the cell.** The diverse phenotypes seen with deletion of *LRO1* and *DGA1* in a strain lacking *GET3*, indicates that the TG synthesized by these enzymes exists in separate pools at the ER membrane. Topographical studies of Lro1p have indicated that the active enzymatic site is facing the ER lumen, whereas Dga1p activity occurs at the cytosolic face of the ER [293].

Similar results have been demonstrated in hepatocytes, which demonstrate that DGAT2 activity occurs in the cyosol whereas DGAT1 is able to synthesize TG in the lumenal compartment [294].

Furthermore, clarification of the differential metabolism of cytosolic and lumenally synthesized TG in yeast may explain the increased vacuolar lipid association occurring in *DGA1* mutants. Electron microscopy of single deletions in *LRO1* or *DGA1*, and triple deletions lacking all sterol ester synthesis (*are1Δ are2Δ*) with an additional deletion in one of the TG synthesis genes could provide valuable insight into TG localization and flux based on enzymatic origin.

3. **Selective knockdown of ASNA1 and ARV1 in mouse pancreatic β-cells and liver.** In order to determine the role of *ARV1* and *ASNA1* in pancreatic β-cell lipotoxicity and type 2 diabetes progression, conditional knockouts of either gene in mouse pancreatic β-cells would provide insight into cellular function and phenotypes related to type 2 diabetes and obesity related disease. Loss of *ARV1* in nematodes is embryonic lethal [387], and it is likely that a knockout of *ARV1* in a germ line would be inviable. Similarly, knockout of *ASNA1* in mice is embryonic lethal [307]. Therefore, use of the Cre/LoxP system [388] for tissue specific knockout of *ARV1* and *ASNA1* is a useful alternative to the whole body knockout model. Studies of pancreatic β-cell function in these mice, particularly when maintained on a high fat diet, would clarify the increased lipoapoptosis and altered glucose stimulated insulin release demonstrated in our tissue culture studies.

4. Complete an ARV1 overexpression and knockdown study in mice fed a high fat diet. *ARV1* overexpression in mouse liver through adenoviral infection resulted in hepatic lipid

accumulation through increased TG synthesis [156]. These mice were maintained on a normal diet, and additional studies of hepatic ARV1 overexpression in the face of high fat diet (HFD) challenge may uncover additional lipid related phenotypes. It would be particularly interesting to see if HFD in ARV1 overexpressing mice resulted in the progression of noninflammatory nonalcoholic fatty liver disease (NAFLD) to more advanced nonalcoholic steatohepatitis (NASH) and cirrhosis.

LITERATURE CITED

1. Wadd, W., *Cursory Remarks on Corpulence of Obesity*, in *Callow* 1816: London. p. 75.

2. Cheyne, G., *An Essay of Health and Long Life* 1724: London.

3. Buchan, N., *Domestic Medicine (American Edition)*, ed. Dobson. 1795, Philiadelphia, PA.

4. Thomas, R., *The Modern Practive of Physic.* , ed. C. Co. 1811, New York

5. *World Health Organization: Obesity* 2012; Available from: http://www.who.int/topics/obesity/en/.

6. Unger, R.H. and L. Orci, *Lipoapoptosis: its mechanism and its diseases*, in *Biochim Biophys Acta*2002. p. 202-12.

7. Listenberger, L.L., et al., *Triglyceride accumulation protects against fatty acid-induced lipotoxicity*, in *Proc Natl Acad Sci USA*2003. p. 3077-82.

8. Buhman, K.K., H.C. Chen, and R.V. Farese, Jr., *The enzymes of neutral lipid synthesis.* J Biol Chem, 2001. **276**(44): p. 40369-72.

9. Yen, C.L., et al., *Thematic review series: glycerolipids. DGAT enzymes and triacylglycerol biosynthesis.* J Lipid Res, 2008. **49**(11): p. 2283-301.

10. Ayciriex, S., et al., *YPR139c/LOA1 encodes a novel lysophosphatidic acid acyltransferase associated with lipid droplets and involved in TAG homeostasis.* Mol Biol Cell, 2012. **23**(2): p. 233-246.

11. Coleman, R.A. and D.P. Lee, *Enzymes of triacylglycerol synthesis and their regulation.* Prog Lipid Res, 2004. **43**(2): p. 134-76.

12. Rajakumari, S., K. Grillitsch, and G. Daum, *Synthesis and turnover of non-polar lipids in yeast.* Prog Lipid Res, 2008. **47**(3): p. 157-71.

13. Turkish, A. and S.L. Sturley, *Regulation of triglyceride metabolism. I. Eukaryotic neutral lipid synthesis: "Many ways to skin ACAT or a DGAT".* Am J Physiol Gastrointest Liver Physiol, 2007. **292**(4): p. G953-7.

14. Oelkers, P., et al., *The DGA1 gene determines a second triglyceride synthetic pathway in yeast.* J Biol Chem, 2002. **277**(11): p. 8877-81.

15. Oelkers, P., et al., *Characterization of two human genes encoding acyl coenzyme A:cholesterol acyltransferase-related enzymes.* J Biol Chem, 1998. **273**(41): p. 26765-71.

16. Cases, S., et al., *Cloning of DGAT2, a second mammalian diacylglycerol acyltransferase, and related family members.* J Biol Chem, 2001. **276**(42): p. 38870-6.

17. Stone, S.J., et al., *Lipopenia and skin barrier abnormalities in DGAT2-deficient mice.* J Biol Chem, 2004. **279**(12): p. 11767-76.

18. Smith, S.J., et al., *Obesity resistance and multiple mechanisms of triglyceride synthesis in mice lacking Dgat.* Nat Genet, 2000. **25**(1): p. 87-90.

19. Oelkers, P., et al., *The DGA1 gene determines a second triglyceride synthetic pathway in yeast*, in *J Biol Chem*2002. p. 8877-81.

20. Turkish, A.R. and S.L. Sturley, *The genetics of neutral lipid biosynthesis: an evolutionary perspective.* Am J Physiol Endocrinol Metab, 2009. **297**(1): p. E19-27.

21. Daum, G., et al., *Dynamics of neutral lipid storage and mobilization in yeast*, in *Biochimie*2007. p. 243-8.

22. Garbarino, J., et al., *Sterol and diacylglycerol acyltransferase deficiency triggers fatty acid-mediated cell death.* J Biol Chem, 2009. **284**(45): p. 30994-1005.

23. Petschnigg, J., et al., *Good fat - essential cellular requirements for triacylglycerol synthesis to maintain membrane homeostasis in yeast*, in *J Biol Chem*2009.

24. Chen, H.C., Z. Ladha, and R.V. Farese, Jr., *Deficiency of acyl coenzyme a:diacylglycerol acyltransferase 1 increases leptin sensitivity in murine obesity models.* Endocrinology, 2002. **143**(8): p. 2893-8.

25. Monetti, M., et al., *Dissociation of hepatic steatosis and insulin resistance in mice overexpressing DGAT in the liver.* Cell Metab, 2007. **6**(1): p. 69-78.

26. WIlson, E.B., *The Cell in Development and Inheritance* 1896, Macmillan New York

27. Altmann, R., *Die Elementarorganisem und ihre Bezlehungen zu den Zellen*, 1890: Leipzig.

28. Fujimoto, T., et al., *Lipid droplets: a classic organelle with new outfits*, in *Histochem Cell Biol*2008. p. 263-79.

29. Goodman, J.M., *The gregarious lipid droplet*, in *J Biol Chem*2008. p. 28005-9.

30. Walther, T.C. and R.V. Farese, *The life of lipid droplets*, in *Biochim Biophys Acta*2009. p. 459-66.

31. Kalantari, F., J.J. Bergeron, and T. Nilsson, *Biogenesis of lipid droplets--how cells get fatter.* Mol Membr Biol, 2010. **27**(8): p. 462-8.

32. Farese, R.V., Jr. and T.C. Walther, *Lipid droplets finally get a little R-E-S-P-E-C-T.* Cell, 2009. **139**(5): p. 855-60.

33. Prattes, S., et al., *Intracellular distribution and mobilization of unesterified cholesterol in adipocytes: triglyceride droplets are surrounded by cholesterol-rich ER-like surface layer structures.* J Cell Sci, 2000. **113 (Pt 17)**: p. 2977-89.

34. Cole, N.B., et al., *Lipid droplet binding and oligomerization properties of the Parkinson's disease protein alpha-synuclein.* J Biol Chem, 2002. **277**(8): p. 6344-52.

35. Herker, E. and M. Ott, *Unique ties between hepatitis C virus replication and intracellular lipids.* Trends Endocrinol Metab, 2011. **22**(6): p. 241-8.

36. Athenstaedt, K., et al., *Identification and characterization of major lipid particle proteins of the yeast Saccharomyces cerevisiae,* in *J Bacteriol*1999. p. 6441-8.

37. Beller, M., et al., *Characterization of the Drosophila lipid droplet subproteome*, in *Mol Cell Proteomics*2006. p. 1082-94.

38. Cermelli, S., et al., *The lipid-droplet proteome reveals that droplets are a protein-storage depot*, in *Curr Biol*2006. p. 1783-95.

39. Liu, P., et al., *Chinese hamster ovary K2 cell lipid droplets appear to be metabolic organelles involved in membrane traffic*, in *J Biol Chem*2004. p. 3787-92.

40. Wu, C.C., et al., *Proteomics reveal a link between the endoplasmic reticulum and lipid secretory mechanisms in mammary epithelial cells*, in *Electrophoresis*2000. p. 3470-82.

41. Larsson, S., et al., *Characterization of the lipid droplet proteome of a clonal insulin-producing beta-cell line (INS-1 832/13).* J Proteome Res, 2012. **11**(2): p. 1264-73.

42. Zhang, H., et al., *Proteome of skeletal muscle lipid droplet reveals association with mitochondria and apolipoprotein a-I.* J Proteome Res, 2011. **10**(10): p. 4757-68.

43. Brasaemle, D.L., et al., *Proteomic analysis of proteins associated with lipid droplets of basal and lipolytically stimulated 3T3-L1 adipocytes*, in *J Biol Chem*2004. p. 46835-42.

44. Hickenbottom, S.J., et al., *Structure of a lipid droplet protein; the PAT family member TIP47.* Structure, 2004. **12**(7): p. 1199-207.

45. Ting, J.T., et al., *Oleosin genes in maize kernels having diverse oil contents are constitutively expressed independent of oil contents. Size and shape of intracellular oil bodies are determined by the oleosins/oils ratio.* Planta, 1996. **199**(1): p. 158-65.

46. Grillitsch, K., et al., *Lipid particles/droplets of the yeast Saccharomyces cerevisiae revisited: lipidome meets proteome.* Biochim Biophys Acta, 2011. **1811**(12): p. 1165-76.

47. Sorger, D., et al., *A yeast strain lacking lipid particles bears a defect in ergosterol formation.* J Biol Chem, 2004. **279**(30): p. 31190-6.

48. Kuerschner, L., C. Moessinger, and C. Thiele, *Imaging of lipid biosynthesis: how a neutral lipid enters lipid droplets*, in *Traffic*2008. p. 338-52.

49. Smirnova, E., et al., *ATGL has a key role in lipid droplet/adiposome degradation in mammalian cells.* EMBO Rep, 2006. **7**(1): p. 106-13.

50. Martin, S., et al., *Regulated localization of Rab18 to lipid droplets: effects of lipolytic stimulation and inhibition of lipid droplet catabolism.* J Biol Chem, 2005. **280**(51): p. 42325-35.

51. Nakamura, N., et al., *ADRP is dissociated from lipid droplets by ARF1-dependent mechanism.* Biochem Biophys Res Commun, 2004. **322**(3): p. 957-65.

52. Bostrom, P., et al., *SNARE proteins mediate fusion between cytosolic lipid droplets and are implicated in insulin sensitivity.* Nat Cell Biol, 2007. **9**(11): p. 1286-93.

53. Yonezawa, T., et al., *Which CIDE are you on? Apoptosis and energy metabolism.* Mol Biosyst, 2011. **7**(1): p. 91-100.

54. Leber, R., et al., *Characterization of lipid particles of the yeast, Saccharomyces cerevisiae.* Yeast, 1994. **10**(11): p. 1421-8.

55. Jacquier, N., et al., *Lipid droplets are functionally connected to the endoplasmic reticulum in Saccharomyces cerevisiae.* J Cell Sci, 2011. **124**(Pt 14): p. 2424-37.

56. Guo, Y., et al., *Functional genomic screen reveals genes involved in lipid-droplet formation and utilization*, in *Nature*2008. p. 657-61.

57. Beller, M., et al., *COPI complex is a regulator of lipid homeostasis*, in *PLoS Biol*2008. p. e292.

58. Fei, W., et al., *Genome-wide analysis of sterol-lipid storage and trafficking in Saccharomyces cerevisiae*, in *Eukaryotic Cell*2008. p. 401-14.

59. Szymanski, K.M., et al., *The lipodystrophy protein seipin is found at endoplasmic reticulum lipid droplet junctions and is important for droplet morphology.* Proc Natl Acad Sci U S A, 2007. **104**(52): p. 20890-5.

60. Fei, W., et al., *Fld1p, a functional homologue of human seipin, regulates the size of lipid droplets in yeast.* J Cell Biol, 2008. **180**(3): p. 473-82.

61. Wolinski, H., et al., *A role for seipin in lipid droplet dynamics and inheritance in yeast.* J Cell Sci, 2011. **124**(Pt 22): p. 3894-904.

62. Watt, M.J. and L.L. Spriet, *Triacylglycerol lipases and metabolic control: implications for health and disease.* Am J Physiol Endocrinol Metab, 2010. **299**(2): p. E162-8.

63. Winzell, M.S., et al., *Pancreatic beta-cell lipotoxicity induced by overexpression of hormone-sensitive lipase,* in *Diabetes*2003. p. 2057-65.

64. Klannemark, M., et al., *The putative role of the hormone-sensitive lipase gene in the pathogenesis of Type II diabetes mellitus and abdominal obesity.* Diabetologia, 1998. **41**(12): p. 1516-22.

65. Magre, J., et al., *Human hormone-sensitive lipase: genetic mapping, identification of a new dinucleotide repeat, and association with obesity and NIDDM.* Diabetes, 1998. **47**(2): p. 284-6.

66. Stumvoll, M., et al., *Two novel prevalent polymorphisms in the hormone-sensitive lipase gene have no effect on insulin sensitivity of lipolysis and glucose disposal.* J Lipid Res, 2001. **42**(11): p. 1782-8.

67. Pihlajamaki, J., et al., *The hormone sensitive lipase gene in familial combined hyperlipidemia and insulin resistance.* Eur J Clin Invest, 2001. **31**(4): p. 302-8.

68. Anderson, N. and J. Borlak, *Molecular mechanisms and therapeutic targets in steatosis and steatohepatitis.* Pharmacol Rev, 2008. **60**(3): p. 311-57.

69. Schweiger, M., et al., *Adipose triglyceride lipase and hormone-sensitive lipase are the major enzymes in adipose tissue triacylglycerol catabolism.* J Biol Chem, 2006. **281**(52): p. 40236-41.

70. Haemmerle, G., et al., *Defective lipolysis and altered energy metabolism in mice lacking adipose triglyceride lipase.* Science, 2006. **312**(5774): p. 734-7.

71. Gronke, S., et al., *Brummer lipase is an evolutionary conserved fat storage regulator in Drosophila.* Cell Metab, 2005. **1**(5): p. 323-30.

72. Ahmadian, M., et al., *Adipose overexpression of desnutrin promotes fatty acid use and attenuates diet-induced obesity.* Diabetes, 2009. **58**(4): p. 855-66.

73. Zimmermann, R., et al., *Fate of fat: the role of adipose triglyceride lipase in lipolysis.* Biochim Biophys Acta, 2009. **1791**(6): p. 494-500.

74. Lass, A., et al., *Adipose triglyceride lipase-mediated lipolysis of cellular fat stores is activated by CGI-58 and defective in Chanarin-Dorfman Syndrome.* Cell Metab, 2006. **3**(5): p. 309-19.

75. Haemmerle, G., et al., *Hormone-sensitive lipase deficiency in mice causes diglyceride accumulation in adipose tissue, muscle, and testis.* J Biol Chem, 2002. **277**(7): p. 4806-15.

76. Holm, C., P. Belfrage, and G. Fredrikson, *Immunological evidence for the presence of hormone-sensitive lipase in rat tissues other than adipose tissue.* Biochem Biophys Res Commun, 1987. **148**(1): p. 99-105.

77. Egan, J.J., et al., *Mechanism of hormone-stimulated lipolysis in adipocytes: translocation of hormone-sensitive lipase to the lipid storage droplet.* Proc Natl Acad Sci U S A, 1992. **89**(18): p. 8537-41.

78. Osuga, J., et al., *Targeted disruption of hormone-sensitive lipase results in male sterility and adipocyte hypertrophy, but not in obesity.* Proc Natl Acad Sci U S A, 2000. **97**(2): p. 787-92.

79. Kurat, C.F., et al., *Cdk1/Cdc28-dependent activation of the major triacylglycerol lipase Tgl4 in yeast links lipolysis to cell-cycle progression.* Mol Cell, 2009. **33**(1): p. 53-63.

80. Athenstaedt, K. and G. Daum, *YMR313c/TGL3 encodes a novel triacylglycerol lipase located in lipid particles of Saccharomyces cerevisiae.* J Biol Chem, 2003. **278**(26): p. 23317-23.

81. Kurat, C.F., et al., *Obese yeast: triglyceride lipolysis is functionally conserved from mammals to yeast.* J Biol Chem, 2006. **281**(1): p. 491-500.

82. Athenstaedt, K. and G. Daum, *Tgl4p and Tgl5p, two triacylglycerol lipases of the yeast Saccharomyces cerevisiae are localized to lipid particles.* J Biol Chem, 2005. **280**(45): p. 37301-9.

83. Rajakumari, S., R. Rajasekharan, and G. Daum, *Triacylglycerol lipolysis is linked to sphingolipid and phospholipid metabolism of the yeast Saccharomyces cerevisiae.* Biochim Biophys Acta, 2010. **1801**(12): p. 1314-22.

84. Sekiya, M., et al., *The role of neutral cholesterol ester hydrolysis in macrophage foam cells.* J Atheroscler Thromb, 2011. **18**(5): p. 359-64.

85. Yang, L., et al., *Defective hepatic autophagy in obesity promotes ER stress and causes insulin resistance.* Cell Metab, 2010. **11**(6): p. 467-78.

86. Hur, K.Y., H.S. Jung, and M.S. Lee, *Role of autophagy in beta-cell function and mass.* Diabetes Obes Metab, 2010. **12 Suppl 2**: p. 20-6.

87. Singh, R., et al., *Autophagy regulates adipose mass and differentiation in mice.* J Clin Invest, 2009. **119**(11): p. 3329-39.

88. Priault, M., et al., *Impairing the bioenergetic status and the biogenesis of mitochondria triggers mitophagy in yeast.* Cell Death Differ, 2005. **12**(12): p. 1613-21.

89. Bernales, S., K.L. McDonald, and P. Walter, *Autophagy counterbalances endoplasmic reticulum expansion during the unfolded protein response.* PLoS Biol, 2006. **4**(12): p. e423.

90. Dong, H. and M.J. Czaja, *Regulation of lipid droplets by autophagy.* Trends Endocrinol Metab, 2011. **22**(6): p. 234-40.

91. Singh, R., et al., *Autophagy regulates lipid metabolism.* Nature, 2009. **458**(7242): p. 1131-5.

92. Poirier, Y., et al., *Peroxisomal beta-oxidation--a metabolic pathway with multiple functions.* Biochim Biophys Acta, 2006. **1763**(12): p. 1413-26.

93. Lelliott, C. and A.J. Vidal-Puig, *Lipotoxicity, an imbalance between lipogenesis de novo and fatty acid oxidation*, in *Int J Obes Relat Metab Disord*2004. p. S22-8.

94. Tehlivets, O., K. Scheuringer, and S.D. Kohlwein, *Fatty acid synthesis and elongation in yeast.* Biochim Biophys Acta, 2007. **1771**(3): p. 255-70.

95. Kamp, F. and J.A. Hamilton, *pH gradients across phospholipid membranes caused by fast flip-flop of un-ionized fatty acids.* Proc Natl Acad Sci U S A, 1992. **89**(23): p. 11367-70.

96. Schwenk, R.W., et al., *Fatty acid transport across the cell membrane: regulation by fatty acid transporters.* Prostaglandins Leukot Essent Fatty Acids, 2010. **82**(4-6): p. 149-54.

97. Schaffer, J.E. and H.F. Lodish, *Expression cloning and characterization of a novel adipocyte long chain fatty acid transport protein.* Cell, 1994. **79**(3): p. 427-36.

98. DiRusso, C.C. and P.N. Black, *Long-chain fatty acid transport in bacteria and yeast. Paradigms for defining the mechanism underlying this protein-mediated process.* Mol Cell Biochem, 1999. **192**(1-2): p. 41-52.

99. Zou, Z., et al., *Vectorial acylation in Saccharomyces cerevisiae. Fat1p and fatty acyl-CoA synthetase are interacting components of a fatty acid import complex.* J Biol Chem, 2003. **278**(18): p. 16414-22.

100. Ginsberg, H.N., Y.L. Zhang, and A. Hernandez-Ono, *Regulation of plasma triglycerides in insulin resistance and diabetes.* Arch Med Res, 2005. **36**(3): p. 232-40.

101. Lee, Y., et al., *Beta-cell lipotoxicity in the pathogenesis of non-insulin-dependent diabetes mellitus of obese rats: impairment in adipocyte-beta-cell relationships.* Proc Natl Acad Sci U S A, 1994. **91**(23): p. 10878-82.

102. Garg, A., *Lipodystrophies: genetic and acquired body fat disorders.* J Clin Endocrinol Metab, 2011. **96**(11): p. 3313-25.

103. Gaemers, I.C., et al., *Lipotoxicity and steatohepatitis in an overfed mouse model for non-alcoholic fatty liver disease.* Biochim Biophys Acta, 2011. **1812**(4): p. 447-58.

104. Unger, R.H. and L. Orci, *Lipotoxic diseases of nonadipose tissues in obesity*, in *Int J Obes Relat Metab Disord*2000. p. S28-32.

105. Ahmadian, M., R.E. Duncan, and H.S. Sul, *The skinny on fat: lipolysis and fatty acid utilization in adipocytes*, in *Trends Endocrinol Metab*2009. p. 424-8.

106. Blüher, M., *Adipose tissue dysfunction in obesity*, in *Exp Clin Endocrinol Diabetes*2009. p. 241-50.

107. Duncan, R.E., et al., *Regulation of lipolysis in adipocytes*, in *Annu Rev Nutr*2007. p. 79-101.

108. Unger, R.H., *Lipotoxic diseases*, in *Annu Rev Med*2002. p. 319-36.

109. Feldstein, A.E., et al., *Diet associated hepatic steatosis sensitizes to Fas mediated liver injury in mice.* J Hepatol, 2003. **39**(6): p. 978-83.

110. Listenberger, L.L., D.S. Ory, and J.E. Schaffer, *Palmitate-induced apoptosis can occur through a ceramide-independent pathway*, in *J Biol Chem*2001. p. 14890-5.

111. Summers, S.A., *Ceramides in insulin resistance and lipotoxicity*, in *Prog Lipid Res*2006. p. 42-72.

112. Wei, Y., et al., *Saturated fatty acids induce endoplasmic reticulum stress and apoptosis independently of ceramide in liver cells*, in *Am J Physiol Endocrinol Metab*2006. p. E275-81.

113. Koshkin, V., et al., *Limited mitochondrial permeabilization is an early manifestation of palmitate-induced lipotoxicity in pancreatic beta-cells*, in *J Biol Chem*2008. p. 7936-48.

114. Garbarino, J. and S.L. Sturley, *Saturated with fat: new perspectives on lipotoxicity*, in *Current opinion in clinical nutrition and metabolic care*2009. p. 110-6.

115. Reinbold, M., et al., *Unsaturated fatty acids liberated from VLDL cause apoptosis in endothelial cells.* Mol Nutr Food Res, 2008. **52**(5): p. 581-8.

116. Schwarz, S., et al., *Protein phosphatase type 2Calpha and 2Cbeta are involved in fatty acid-induced apoptosis of neuronal and endothelial cells*, in *Apoptosis*2006. p. 1111-9.

117. Zhu, Y., et al., *Oleic acid causes apoptosis and dephosphorylates Bad.* Neurochem Int, 2005. **46**(2): p. 127-35.

118. Klumpp, S., M.C. Thissen, and J. Krieglstein, *Protein phosphatases types 2Calpha and 2Cbeta in apoptosis.* Biochem Soc Trans, 2006. **34**(Pt 6): p. 1370-5.

119. Malhi, H., et al., *Free fatty acids sensitise hepatocytes to TRAIL mediated cytotoxicity.* Gut, 2007. **56**(8): p. 1124-31.

120. De Gottardi, A., et al., *Microarray analyses and molecular profiling of steatosis induction in immortalized human hepatocytes.* Lab Invest, 2007. **87**(8): p. 792-806.

121. Cury-Boaventura, M.F., et al., *Comparative toxicity of oleic and linoleic acid on human lymphocytes.* Life Sci, 2006. **78**(13): p. 1448-56.

122. Cury-Boaventura, M.F., C. Pompeia, and R. Curi, *Comparative toxicity of oleic acid and linoleic acid on Jurkat cells.* Clin Nutr, 2004. **23**(4): p. 721-32.

123. Kharroubi, I., et al., *Free fatty acids and cytokines induce pancreatic beta-cell apoptosis by different mechanisms: role of nuclear factor-kappaB and endoplasmic reticulum stress.* Endocrinology, 2004. **145**(11): p. 5087-96.

124. Ota, T., C. Gayet, and H.N. Ginsberg, *Inhibition of apolipoprotein B100 secretion by lipid-induced hepatic endoplasmic reticulum stress in rodents.* J Clin Invest, 2008. **118**(1): p. 316-32.

125. Schrauwen, P., et al., *Mitochondrial dysfunction and lipotoxicity,* in *Biochim Biophys Acta*2009.

126. Chavez, J.A. and S.A. Summers, *Lipid oversupply, selective insulin resistance, and lipotoxicity: Molecular mechanisms,* in *Biochim Biophys Acta*2009.

127. Colombini, M., *Ceramide channels and their role in mitochondria-mediated apoptosis.* Biochim Biophys Acta, 2010. **1797**(6-7): p. 1239-44.

128. Cnop, M., et al., *Causes and cures for endoplasmic reticulum stress in lipotoxic beta-cell dysfunction.* Diabetes Obes Metab, 2010. **12 Suppl 2**: p. 76-82.

129. Borradaile, N.M., et al., *Disruption of endoplasmic reticulum structure and integrity in lipotoxic cell death*, in *J Lipid Res*2006. p. 2726-37.

130. Diakogiannaki, E., H.J. Welters, and N.G. Morgan, *Differential regulation of the endoplasmic reticulum stress response in pancreatic beta-cells exposed to long-chain saturated and monounsaturated fatty acids.* J Endocrinol, 2008. **197**(3): p. 553-63.

131. Pineau, L., et al., *Lipid-induced ER stress: synergistic effects of sterols and saturated fatty acids.* Traffic, 2009. **10**(6): p. 673-90.

132. Moffitt, J.H., et al., *Adverse physicochemical properties of tripalmitin in beta cells lead to morphological changes and lipotoxicity in vitro.* Diabetologia, 2005. **48**(9): p. 1819-29.

133. Ozcan, L. and I. Tabas, *Role of endoplasmic reticulum stress in metabolic disease and other disorders.* Annu Rev Med, 2012. **63**: p. 317-28.

134. Marchetti, P., et al., *Insulin secretory function is impaired in isolated human islets carrying the Gly(972)-->Arg IRS-1 polymorphism.* Diabetes, 2002. **51**(5): p. 1419-24.

135. Sesti, G., et al., *The E23K variant of KCNJ11 encoding the pancreatic beta-cell adenosine 5'-triphosphate-sensitive potassium channel subunit Kir6.2 is associated with an increased risk of secondary failure to sulfonylurea in patients with type 2 diabetes.* J Clin Endocrinol Metab, 2006. **91**(6): p. 2334-9.

136. Cauchi, S. and P. Froguel, *TCF7L2 genetic defect and type 2 diabetes.* Curr Diab Rep, 2008. **8**(2): p. 149-55.

137. Henquin, J.C., *The dual control of insulin secretion by glucose involves triggering and amplifying pathways in beta-cells.* Diabetes Res Clin Pract, 2011. **93 Suppl 1**: p. S27-31.

138. Barg, S., et al., *A subset of 50 secretory granules in close contact with L-type Ca2+ channels accounts for first-phase insulin secretion in mouse beta-cells.* Diabetes, 2002. **51 Suppl 1**: p. S74-82.

139. Elsner, M., W. Gehrmann, and S. Lenzen, *Peroxisome-generated hydrogen peroxide as important mediator of lipotoxicity in insulin-producing cells.* Diabetes, 2011. **60**(1): p. 200-8.

140. Miranda, P.J., et al., *Metabolic syndrome: definition, pathophysiology, and mechanisms.* Am Heart J, 2005. **149**(1): p. 33-45.

141. Marchetti, P., et al., *The beta-cell in human type 2 diabetes.* Adv Exp Med Biol, 2010. **654**: p. 501-14.

142. Giacca, A., et al., *Lipid-induced pancreatic beta-cell dysfunction: focus on in vivo studies.* Am J Physiol Endocrinol Metab, 2011. **300**(2): p. E255-62.

143. Poitout, V., et al., *Glucolipotoxicity of the pancreatic beta cell.* Biochim Biophys Acta, 2010. **1801**(3): p. 289-98.

144. Anello, M., et al., *Functional and morphological alterations of mitochondria in pancreatic beta cells from type 2 diabetic patients.* Diabetologia, 2005. **48**(2): p. 282-9.

145. Cusi, K., *The role of adipose tissue and lipotoxicity in the pathogenesis of type 2 diabetes.* Curr Diab Rep, 2010. **10**(4): p. 306-15.

146. Browning, J.D., et al., *Prevalence of hepatic steatosis in an urban population in the United States: impact of ethnicity.* Hepatology, 2004. **40**(6): p. 1387-95.

147. Donnelly, K.L., et al., *Sources of fatty acids stored in liver and secreted via lipoproteins in patients with nonalcoholic fatty liver disease.* J Clin Invest, 2005. **115**(5): p. 1343-51.

148. Robertson, G., I. Leclercq, and G.C. Farrell, *Nonalcoholic steatosis and steatohepatitis. II. Cytochrome P-450 enzymes and oxidative stress.* Am J Physiol Gastrointest Liver Physiol, 2001. **281**(5): p. G1135-9.

149. Nielsen, J., *Systems biology of lipid metabolism: from yeast to human.* FEBS Lett, 2009. **583**(24): p. 3905-13.

150. Garbarino, J., et al., *Sterol and diacylglycerol acyltransferase deficiency triggers fatty acid-mediated cell death*, in *J Biol Chem*2009. p. 30994-1005.

151. Fakas, S., et al., *Phosphatidate phosphatase activity plays key role in protection against fatty acid-induced toxicity in yeast.* J Biol Chem, 2011. **286**(33): p. 29074-85.

152. Reue, K. and M. Peterfy, *Mouse models of lipodystrophy.* Curr Atheroscler Rep, 2000. **2**(5): p. 390-6.

153. Suviolahti, E., et al., *Cross-species analyses implicate Lipin 1 involvement in human glucose metabolism.* Hum Mol Genet, 2006. **15**(3): p. 377-86.

154. Petschnigg, J., et al., *Good fat, essential cellular requirements for triacylglycerol synthesis to maintain membrane homeostasis in yeast.* J Biol Chem, 2009. **284**(45): p. 30981-93.

155. Peter, A., et al., *Induction of stearoyl-CoA desaturase protects human arterial endothelial cells against lipotoxicity.* Am J Physiol Endocrinol Metab, 2008. **295**(2): p. E339-49.

156. Liu, Y., *Human ARV1- A New Modulator of Lipid Homeostasis*, in *Institue of Human Nutrition*2004, Columbia University: New York, NY.

157. Lee, Y., et al., *Beta-cell lipotoxicity in the pathogenesis of non-insulin-dependent diabetes mellitus of obese rats: impairment in adipocyte-beta-cell relationships*, in *Proc Natl Acad Sci USA*1994. p. 10878-82.

158. Briaud, I., et al., *Lipotoxicity of the pancreatic beta-cell is associated with glucose-dependent esterification of fatty acids into neutral lipids*, in *Diabetes*2001. p. 315-21.

159. Lencioni, C., R. Lupi, and S. Del Prato, *Beta-cell failure in type 2 diabetes mellitus*, in *Curr Diab Rep*2008. p. 179-84.

160. Wei, Y., et al., *Saturated fatty acids induce endoplasmic reticulum stress and apoptosis independently of ceramide in liver cells.* Am J Physiol Endocrinol Metab, 2006. **291**(2): p. E275-81.

161. Trauner, M., M. Arrese, and M. Wagner, *Fatty liver and lipotoxicity.* Biochim Biophys Acta, 2010. **1801**(3): p. 299-310.

162. Lim, H.Y. and R. Bodmer, *Phospholipid homeostasis and lipotoxic cardiomyopathy: a matter of balance.* Fly (Austin), 2011. **5**(3): p. 234-6.

163. Kohlwein, S.D. and J. Petschnigg, *Lipid-induced Cell Dysfunction and Cell Death: Lessons from Yeast*, in *Curr Hypertens Rep*2007. p. 455-461.

164. Gwiazda, K.S., et al., *Effects of palmitate on ER and cytosolic Ca2+ homeostasis in beta-cells*, in *Am J Physiol Endocrinol Metab*2009. p. E690-701.

165. Unger, R.H., et al., *Lipid homeostasis, lipotoxicity and the metabolic syndrome.* Biochim Biophys Acta, 2010. **1801**(3): p. 209-14.

166. Smith, J.J., et al., *Expression and functional profiling reveal distinct gene classes involved in fatty acid metabolism.* Mol Syst Biol, 2006. **2**: p. 2006 0009.

167. Giaever, G., et al., *Functional profiling of the Saccharomyces cerevisiae genome.* Nature, 2002. **418**(6896): p. 387-91.

168. Winzeler, E.A., et al., *Functional characterization of the S. cerevisiae genome by gene deletion and parallel analysis.* Science, 1999. **285**(5429): p. 901-6.

169. Matsufuji, Y., et al., *Acetaldehyde tolerance in Saccharomyces cerevisiae involves the pentose phosphate pathway and oleic acid biosynthesis.* Yeast, 2008. **25**(11): p. 825-33.

170. Fujita, K., et al., *The genome-wide screening of yeast deletion mutants to identify the genes required for tolerance to ethanol and other alcohols.* FEMS Yeast Res, 2006. **6**(5): p. 744-50.

171. Huang, R.Y., et al., *Genome-wide screen identifies genes whose inactivation confer resistance to cisplatin in Saccharomyces cerevisiae.* Cancer Res, 2005. **65**(13): p. 5890-7.

172. Dos Santos, S.C. and I. Sa-Correia, *A genome-wide screen identifies yeast genes required for protection against or enhanced cytotoxicity of the antimalarial drug quinine.* Mol Genet Genomics, 2011. **286**(5-6): p. 333-46.

173. Niu, W., et al., *Mechanisms of cell cycle control revealed by a systematic and quantitative overexpression screen in S. cerevisiae.* PLoS Genet, 2008. **4**(7): p. e1000120.

174. Barth, H. and M. Thumm, *A genomic screen identifies AUT8 as a novel gene essential for autophagy in the yeast Saccharomyces cerevisiae.* Gene, 2001. **274**(1-2): p. 151-6.

175. Schafer, A. and D.H. Wolf, *Endoplasmic reticulum-associated protein quality control and degradation: genome-wide screen for ERAD components.* Methods Mol Biol, 2005. **301**: p. 289-92.

176. Lockshon, D., et al., *The sensitivity of yeast mutants to oleic acid implicates the peroxisome and other processes in membrane function,* in *Genetics*2007. p. 77-91.

177. Ausubel FM, B.R., Kingston RE, Moore DD, Seidman JG, et al. , ed. *Current Protocols in Molecular Biology*. 1998, John Wiley & Sons: New York.

178. Orr-Weaver, T.L., J.W. Szostak, and R.J. Rothstein, *Yeast transformation: a model system for the study of recombination.* Proc Natl Acad Sci U S A, 1981. **78**(10): p. 6354-8.

179. Borradaile, N.M., et al., *A critical role for eukaryotic elongation factor 1A-1 in lipotoxic cell death,* in *Mol Biol Cell*2006. p. 770-8.

180. Michel, C.I., et al., *Small nucleolar RNAs U32a, U33, and U35a are critical mediators of metabolic stress.* Cell Metab, 2011. **14**(1): p. 33-44.

181. Lockshon, D., et al., *The sensitivity of yeast mutants to oleic acid implicates the peroxisome and other processes in membrane function.* Genetics, 2007. **175**(1): p. 77-91.

182. Deguil, J., et al., *Modulation of lipid-induced ER stress by fatty acid shape.* Traffic, 2011. **12**(3): p. 349-62.

183. Rockenfeller, P., et al., *Fatty acids trigger mitochondrion-dependent necrosis.* Cell Cycle, 2010. **9**(14): p. 2836-42.

184. Mei, S., et al., *Differential roles of unsaturated and saturated fatty acids on autophagy and apoptosis in hepatocytes.* J Pharmacol Exp Ther, 2011. **339**(2): p. 487-98.

185. Oh, C.S., et al., *ELO2 and ELO3, homologues of the Saccharomyces cerevisiae ELO1 gene, function in fatty acid elongation and are required for sphingolipid formation.* J Biol Chem, 1997. **272**(28): p. 17376-84.

186. Listenberger, L.L., et al., *Triglyceride accumulation protects against fatty acid-induced lipotoxicity.* Proc Natl Acad Sci U S A, 2003. **100**(6): p. 3077-82.

187. Adeyo, O., et al., *The yeast lipin orthologue Pah1p is important for biogenesis of lipid droplets.* J Cell Biol, 2011. **192**(6): p. 1043-55.

188. Kohlwein, S.D., *Obese and anorexic yeasts: experimental models to understand the metabolic syndrome and lipotoxicity.* Biochim Biophys Acta, 2010. **1801**(3): p. 222-9.

189. Connerth, M., et al., *Oleate inhibits steryl ester synthesis and causes liposensitivity in yeast.* J Biol Chem, 2010. **285**(35): p. 26832-41.

190. de Kruijff, B. and R.A. Demel, *Polyene antibiotic-sterol interactions in membranes of Acholeplasma laidlawii cells and lecithin liposomes. 3. Molecular structure of the polyene antibiotic-cholesterol complexes.* Biochim Biophys Acta, 1974. **339**(1): p. 57-70.

191. Koh, T.Y., et al., *Growth characteristics and polyene sensitivity of a fatty acid auxotroph of Candida albicans.* J Gen Microbiol, 1977. **102**(1): p. 105-10.

192. Okamoto, Y., S. Aoki, and I. Mataga, *Enhancement of amphotericin B activity against Candida albicans by superoxide radical.* Mycopathologia, 2004. **158**(1): p. 9-15.

193. Vallee, B. and H. Riezman, *Lip1p: a novel subunit of acyl-CoA ceramide synthase.* EMBO J, 2005. **24**(4): p. 730-41.

194. Sahara, T., T. Goda, and S. Ohgiya, *Comprehensive expression analysis of time-dependent genetic responses in yeast cells to low temperature.* J Biol Chem, 2002. **277**(51): p. 50015-21.

195. Schade, B., et al., *Cold adaptation in budding yeast.* Mol Biol Cell, 2004. **15**(12): p. 5492-502.

196. Nakagawa, Y., et al., *Mga2p is a putative sensor for low temperature and oxygen to induce OLE1 transcription in Saccharomyces cerevisiae.* Biochem Biophys Res Commun, 2002. **291**(3): p. 707-13.

197. Jonikas, M.C., et al., *Comprehensive characterization of genes required for protein folding in the endoplasmic reticulum.* Science, 2009. **323**(5922): p. 1693-7.

198. Piper, P.W., *The heat shock and ethanol stress responses of yeast exhibit extensive similarity and functional overlap.* FEMS Microbiol Lett, 1995. **134**(2-3): p. 121-7.

199. Ye, Y., et al., *Gaining insight into the response logic of Saccharomyces cerevisiae to heat shock by combining expression profiles with metabolic pathways.* Biochem Biophys Res Commun, 2009. **385**(3): p. 357-62.

200. Ron, D. and P. Walter, *Signal integration in the endoplasmic reticulum unfolded protein response.* Nat Rev Mol Cell Biol, 2007. **8**(7): p. 519-29.

201. Travers, K.J., et al., *Functional and genomic analyses reveal an essential coordination between the unfolded protein response and ER-associated degradation.* Cell, 2000. **101**(3): p. 249-58.

202. Green, C.D. and L.K. Olson, *Modulation of palmitate-induced endoplasmic reticulum stress and apoptosis in pancreatic beta-cells by stearoyl-CoA desaturase and Elovl6.* Am J Physiol Endocrinol Metab, 2011. **300**(4): p. E640-9.

203. Nguyen, L.N., A. Gacser, and J.D. Nosanchuk, *The stearoyl-coenzyme A desaturase 1 is essential for virulence and membrane stress in Candida parapsilosis through unsaturated fatty acid production.* Infect Immun, 2011. **79**(1): p. 136-45.

204. Li, Z.Z., et al., *Hepatic lipid partitioning and liver damage in nonalcoholic fatty liver disease: role of stearoyl-CoA desaturase.* J Biol Chem, 2009. **284**(9): p. 5637-44.

205. Tinkelenberg, A.H., et al., *Mutations in yeast ARV1 alter intracellular sterol distribution and are complemented by human ARV1.* J Biol Chem, 2000. **275**(52): p. 40667-70.

206. Shechtman, C.F., et al., *Loss of subcellular lipid transport due to ARV1 deficiency disrupts organelle homeostasis and activates the unfolded protein response.* J Biol Chem, 2011. **286**(14): p. 11951-9.

207. Uemura, S., et al., *Csg1p and newly identified Csh1p function in mannosylinositol phosphorylceramide synthesis by interacting with Csg2p.* J Biol Chem, 2003. **278**(46): p. 45049-55.

208. Ferreira, T.C., L.M. de Moraes, and E.G. Campos, *Cell density-dependent linoleic acid toxicity to Saccharomyces cerevisiae.* FEMS Yeast Res, 2011. **11**(5): p. 408-17.

209. Hiltunen, J.K., et al., *Mitochondrial fatty acid synthesis--an adopted set of enzymes making a pathway of major importance for the cellular metabolism.* Prog Lipid Res, 2010. **49**(1): p. 27-45.

210. Harington, A., et al., *Identification of a new nuclear gene (CEM1) encoding a protein homologous to a beta-keto-acyl synthase which is essential for mitochondrial respiration in Saccharomyces cerevisiae.* Mol Microbiol, 1993. **9**(3): p. 545-55.

211. Perrone, G.G., S.X. Tan, and I.W. Dawes, *Reactive oxygen species and yeast apoptosis.* Biochim Biophys Acta, 2008. **1783**(7): p. 1354-68.

212. Barros, M.H., L.E. Netto, and A.J. Kowaltowski, *H(2)O(2) generation in Saccharomyces cerevisiae respiratory pet mutants: effect of cytochrome c.* Free Radic Biol Med, 2003. **35**(2): p. 179-88.

213. Epp, N., et al., *Membrane dynamics and fusion at late endosomes and vacuoles--Rab regulation, multisubunit tethering complexes and SNAREs.* Eur J Cell Biol, 2011. **90**(9): p. 779-85.

214. Conibear, E., J.N. Cleck, and T.H. Stevens, *Vps51p mediates the association of the GARP (Vps52/53/54) complex with the late Golgi t-SNARE Tlg1p,* in *Mol Biol Cell*2003. p. 1610-23.

215. Schuldiner, M., et al., *Exploration of the function and organization of the yeast early secretory pathway through an epistatic miniarray profile.* Cell, 2005. **123**(3): p. 507-19.

216. Schuldiner, M., et al., *The GET complex mediates insertion of tail-anchored proteins into the ER membrane*, in *Cell*2008. p. 634-45.

217. Lee, M.J. and H.G. Dohlman, *Coactivation of G protein signaling by cell-surface receptors and an intracellular exchange factor.* Curr Biol, 2008. **18**(3): p. 211-5.

218. Slessareva, J.E., et al., *Activation of the phosphatidylinositol 3-kinase Vps34 by a G protein alpha subunit at the endosome.* Cell, 2006. **126**(1): p. 191-203.

219. Robinson, J.S., et al., *Protein sorting in Saccharomyces cerevisiae: isolation of mutants defective in the delivery and processing of multiple vacuolar hydrolases.* Mol Cell Biol, 1988. **8**(11): p. 4936-48.

220. Rothman, J.H., I. Howald, and T.H. Stevens, *Characterization of genes required for protein sorting and vacuolar function in the yeast Saccharomyces cerevisiae.* EMBO J, 1989. **8**(7): p. 2057-65.

221. Bolte, S., et al., *FM-dyes as experimental probes for dissecting vesicle trafficking in living plant cells.* J Microsc, 2004. **214**(Pt 2): p. 159-73.

222. Raymond, C.K., et al., *Morphological classification of the yeast vacuolar protein sorting mutants: evidence for a prevacuolar compartment in class E vps mutants.* Mol Biol Cell, 1992. **3**(12): p. 1389-402.

223. Bowers, K. and T.H. Stevens, *Protein transport from the late Golgi to the vacuole in the yeast Saccharomyces cerevisiae*, in *Biochim Biophys Acta*2005. p. 438-54.

224. Kohlwein, S.D., et al., *Tsc13p is required for fatty acid elongation and localizes to a novel structure at the nuclear-vacuolar interface in Saccharomyces cerevisiae.* Mol Cell Biol, 2001. **21**(1): p. 109-25.

225. Sasser, T., et al., *Yeast lipin 1 orthologue pah1p regulates vacuole homeostasis and membrane fusion.* J Biol Chem, 2012. **287**(3): p. 2221-36.

226. Jun, Y., R.A. Fratti, and W. Wickner, *Diacylglycerol and its formation by phospholipase C regulate Rab- and SNARE-dependent yeast vacuole fusion.* J Biol Chem, 2004. **279**(51): p. 53186-95.

227. Smith, J.J., et al., *Transcriptome profiling to identify genes involved in peroxisome assembly and function.* J Cell Biol, 2002. **158**(2): p. 259-71.

228. Koerkamp, M.G., et al., *Dissection of transient oxidative stress response in Saccharomyces cerevisiae by using DNA microarrays.* Mol Biol Cell, 2002. **13**(8): p. 2783-94.

229. Smith, J.J., et al., *Transcriptional responses to fatty acid are coordinated by combinatorial control.* Mol Syst Biol, 2007. **3**: p. 115.

230. Wan, Y., et al., *Role of the histone variant H2A.Z/Htz1p in TBP recruitment, chromatin dynamics, and regulated expression of oleate-responsive genes.* Mol Cell Biol, 2009. **29**(9): p. 2346-58.

231. Pray-Grant, M.G., et al., *The novel SLIK histone acetyltransferase complex functions in the yeast retrograde response pathway.* Mol Cell Biol, 2002. **22**(24): p. 8774-86.

232. Roden, M., et al., *Mechanism of free fatty acid-induced insulin resistance in humans.* J Clin Invest, 1996. **97**(12): p. 2859-65.

233. Kao, G., et al., *ASNA-1 positively regulates insulin secretion in C. elegans and mammalian cells,* in *Cell*2007. p. 577-87.

234. Guillam, M.T., et al., *Early diabetes and abnormal postnatal pancreatic islet development in mice lacking Glut-2.* Nat Genet, 1997. **17**(3): p. 327-30.

235. Hatunic, M., et al., *The Leu262Val polymorphism of presenilin associated rhomboid like protein (PARL) is associated with earlier onset of type 2 diabetes and increased urinary microalbumin creatinine ratio in an Irish case-control population.* Diabetes Res Clin Pract, 2009. **83**(3): p. 316-9.

236. Morcillo, S., et al., *ELOVL6 genetic variation is related to insulin sensitivity: a new candidate gene in energy metabolism.* PLoS One, 2011. **6**(6): p. e21198.

237. Kelly, T.J., et al., *GCN5-mediated transcriptional control of the metabolic coactivator PGC-1beta through lysine acetylation.* J Biol Chem, 2009. **284**(30): p. 19945-52.

238. Lerin, C., et al., *GCN5 acetyltransferase complex controls glucose metabolism through transcriptional repression of PGC-1alpha.* Cell Metab, 2006. **3**(6): p. 429-38.

239. Tong, F., et al., *Decreased expression of ARV1 results in cholesterol retention in the endoplasmic reticulum and abnormal bile acid metabolism.* J Biol Chem, 2010. **285**(44): p. 33632-41.

240. Miranda, M., et al., *Gene expression of paired abdominal adipose AQP7 and liver AQP9 in patients with morbid obesity: relationship with glucose abnormalities.* Metabolism, 2009. **58**(12): p. 1762-8.

241. Reiling, E., et al., *Genetic association analysis of 13 nuclear-encoded mitochondrial candidate genes with type II diabetes mellitus: the DAMAGE study.* Eur J Hum Genet, 2009. **17**(8): p. 1056-62.

242. Kurisu, J., et al., *MDG1/ERdj4, an ER-resident DnaJ family member, suppresses cell death induced by ER stress.* Genes Cells, 2003. **8**(2): p. 189-202.

243. Lee, S.B., et al., *Serum deprivation-induced reactive oxygen species production is mediated by Romo1.* Apoptosis, 2010. **15**(2): p. 204-18.

244. Chen, Z.J., et al., *Structural enzymological studies of 2-enoyl thioester reductase of the human mitochondrial FAS II pathway: new insights into its substrate recognition properties.* J Mol Biol, 2008. **379**(4): p. 830-44.

245. Yang, H., et al., *Sterol esterification in yeast: a two-gene process.* Science, 1996. **272**(5266): p. 1353-6.

246. Oelkers, P., et al., *A lecithin cholesterol acyltransferase-like gene mediates diacylglycerol esterification in yeast.* J Biol Chem, 2000. **275**(21): p. 15609-12.

247. Hegde, R.S. and R.J. Keenan, *Tail-anchored membrane protein insertion into the endoplasmic reticulum.* Nat Rev Mol Cell Biol, 2011. **12**(12): p. 787-98.

248. Simpson, P.J., et al., *Structures of Get3, Get4, and Get5 provide new models for TA membrane protein targeting.* Structure, 2010. **18**(8): p. 897-902.

249. Wang, F., et al., *The mechanism of tail-anchored protein insertion into the ER membrane.* Mol Cell, 2011. **43**(5): p. 738-50.

250. Stefer, S., et al., *Structural basis for tail-anchored membrane protein biogenesis by the Get3-receptor complex.* Science, 2011. **333**(6043): p. 758-62.

251. Wang, F., et al., *A chaperone cascade sorts proteins for posttranslational membrane insertion into the endoplasmic reticulum.* Mol Cell, 2010. **40**(1): p. 159-71.

252. Rosen, B.P., et al., *Mechanism of the ArsA ATPase.* Biochim Biophys Acta, 1999. **1461**(2): p. 207-15.

253. Erdeniz, N., U.H. Mortensen, and R. Rothstein, *Cloning-free PCR-based allele replacement methods.* Genome Res, 1997. **7**(12): p. 1174-83.

254. Ito, H., et al., *Transformation of intact yeast cells treated with alkali cations.* J Bacteriol, 1983. **153**(1): p. 163-8.

255. Nair, U., et al., *GFP-Atg8 protease protection as a tool to monitor autophagosome biogenesis.* Autophagy, 2011. **7**(12).

256. Shindiapina, P. and C. Barlowe, *Requirements for transitional endoplasmic reticulum site structure and function in Saccharomyces cerevisiae.* Mol Biol Cell, 2010. **21**(9): p. 1530-45.

257. Madeo, F., E. Frohlich, and K.U. Frohlich, *A yeast mutant showing diagnostic markers of early and late apoptosis.* J Cell Biol, 1997. **139**(3): p. 729-34.

258. Faergeman, N.J., et al., *Disruption of the Saccharomyces cerevisiae homologue to the murine fatty acid transport protein impairs uptake and growth on long-chain fatty acids.* J Biol Chem, 1997. **272**(13): p. 8531-8.

259. Vida, T.A. and S.D. Emr, *A new vital stain for visualizing vacuolar membrane dynamics and endocytosis in yeast.* J Cell Biol, 1995. **128**(5): p. 779-92.

260. Wright, R., *Transmission electron microscopy of yeast.* Microsc Res Tech, 2000. **51**(6): p. 496-510.

261. Reynolds, E.S., *The use of lead citrate at high pH as an electron-opaque stain in electron microscopy.* J Cell Biol, 1963. **17**: p. 208-12.

262. Teter, S.A., et al., *Degradation of lipid vesicles in the yeast vacuole requires function of Cvt17, a putative lipase.* J Biol Chem, 2001. **276**(3): p. 2083-7.

263. Medina, V., et al., *Induction of caspase-3 protease activity and apoptosis by butyrate and trichostatin A (inhibitors of histone deacetylase): dependence on protein synthesis and synergy with a mitochondrial/cytochrome c-dependent pathway.* Cancer Res, 1997. **57**(17): p. 3697-707.

264. Mitsui, K., et al., *Valproic acid induces apoptosis dependent of Yca1p at concentrations that mildly affect the proliferation of yeast.* FEBS Lett, 2005. **579**(3): p. 723-7.

265. Buttner, S., et al., *Synphilin-1 enhances alpha-synuclein aggregation in yeast and contributes to cellular stress and cell death in a Sir2-dependent manner.* PLoS One, 2010. **5**(10): p. e13700.

266. Milger, K., et al., *Cellular uptake of fatty acids driven by the ER-localized acyl-CoA synthetase FATP4.* J Cell Sci, 2006. **119**(Pt 22): p. 4678-88.

267. Gaynor, E.C., et al., *ARF is required for maintenance of yeast Golgi and endosome structure and function.* Mol Biol Cell, 1998. **9**(3): p. 653-70.

268. Gaspar, M.L., et al., *A block in endoplasmic reticulum-to-Golgi trafficking inhibits phospholipid synthesis and induces neutral lipid accumulation*, in *J Biol Chem*2008. p. 25735-51.

269. Foti, M., A. Audhya, and S.D. Emr, *Sac1 lipid phosphatase and Stt4 phosphatidylinositol 4-kinase regulate a pool of phosphatidylinositol 4-phosphate that functions in the control of the actin cytoskeleton and vacuole morphology.* Mol Biol Cell, 2001. **12**(8): p. 2396-411.

270. Harding, T.M., et al., *Isolation and characterization of yeast mutants in the cytoplasm to vacuole protein targeting pathway.* J Cell Biol, 1995. **131**(3): p. 591-602.

271. Kirisako, T., et al., *Formation process of autophagosome is traced with Apg8/Aut7p in yeast.* J Cell Biol, 1999. **147**(2): p. 435-46.

272. Huang, W.P., et al., *The itinerary of a vesicle component, Aut7p/Cvt5p, terminates in the yeast vacuole via the autophagy/Cvt pathways.* J Biol Chem, 2000. **275**(8): p. 5845-51.

273. Suriapranata, I., et al., *The breakdown of autophagic vesicles inside the vacuole depends on Aut4p.* J Cell Sci, 2000. **113 (Pt 22)**: p. 4025-33.

274. Thumm, M., et al., *Isolation of autophagocytosis mutants of Saccharomyces cerevisiae.* FEBS Lett, 1994. **349**(2): p. 275-80.

275. Nakamura, N., et al., *Acidification of vacuoles is required for autophagic degradation in the yeast, Saccharomyces cerevisiae.* J Biochem, 1997. **121**(2): p. 338-44.

276. Wu, X., et al., *Exogenous VLDL stimulates apolipoprotein B secretion from HepG2 cells by both pre- and post-translational mechanisms.* J Lipid Res, 1994. **35**(7): p. 1200-10.

277. Epple, U.D., et al., *Aut5/Cvt17p, a putative lipase essential for disintegration of autophagic bodies inside the vacuole.* J Bacteriol, 2001. **183**(20): p. 5942-55.

278. Li, S.C. and P.M. Kane, *The yeast lysosome-like vacuole: endpoint and crossroads.* Biochim Biophys Acta, 2009. **1793**(4): p. 650-63.

279. Patterson, G.H., et al., *Use of the green fluorescent protein and its mutants in quantitative fluorescence microscopy.* Biophys J, 1997. **73**(5): p. 2782-90.

280. Sackett, D.L. and J. Wolff, *Nile red as a polarity-sensitive fluorescent probe of hydrophobic protein surfaces.* Anal Biochem, 1987. **167**(2): p. 228-34.

281. O'Rourke, E.J., et al., *C. elegans major fats are stored in vesicles distinct from lysosome-related organelles.* Cell Metab, 2009. **10**(5): p. 430-5.

282. Helms, J.B., *Role of heterotrimeric GTP binding proteins in vesicular protein transport: indications for both classical and alternative G protein cycles.* FEBS Lett, 1995. **369**(1): p. 84-8.

283. Heenan, E.J., et al., *Structure and function of Vps15 in the endosomal G protein signaling pathway.* Biochemistry, 2009. **48**(27): p. 6390-401.

284. Sorkin, A. and M. von Zastrow, *Endocytosis and signalling: intertwining molecular networks.* Nat Rev Mol Cell Biol, 2009. **10**(9): p. 609-22.

285. Misra, S., G.J. Miller, and J.H. Hurley, *Recognizing phosphatidylinositol 3-phosphate.* Cell, 2001. **107**(5): p. 559-62.

286. Piper, R.C. and J.P. Luzio, *Late endosomes: sorting and partitioning in multivesicular bodies.* Traffic, 2001. **2**(9): p. 612-21.

287. Fili, N., et al., *Compartmental signal modulation: Endosomal phosphatidylinositol 3-phosphate controls endosome morphology and selective cargo sorting.* Proc Natl Acad Sci U S A, 2006. **103**(42): p. 15473-8.

288. Fernandez-Borja, M., et al., *Multivesicular body morphogenesis requires phosphatidyl-inositol 3-kinase activity.* Curr Biol, 1999. **9**(1): p. 55-8.

289. Kao, G., et al., *ASNA-1 positively regulates insulin secretion in C. elegans and mammalian cells.* Cell, 2007. **128**(3): p. 577-87.

290. Davey, H.M., et al., *Genome-wide analysis of longevity in nutrient-deprived Saccharomyces cerevisiae reveals importance of recycling in maintaining cell viability.* Environ Microbiol, 2012.

291. Wurmser, A.E. and S.D. Emr, *Novel PtdIns(3)P-binding protein Etf1 functions as an effector of the Vps34 PtdIns 3-kinase in autophagy.* J Cell Biol, 2002. **158**(4): p. 761-72.

292. Liu, Q., et al., *Functional and topological analysis of yeast acyl-CoA:diacylglycerol acyltransferase 2, an endoplasmic reticulum enzyme essential for triacylglycerol biosynthesis.* J Biol Chem, 2011. **286**(15): p. 13115-26.

293. Choundhary, V.J., N. and R. Schneiter, *The topology of the triacylglycerol synthesizing enzyme Lro1 indicates that neutral lipids can be produced within the luminal compartment of the endoplasmic reticulum.* Communicative & Integrative Biology, 2011. **4**(6): p. 781-784.

294. Wurie, H.R., L. Buckett, and V.A. Zammit, *Evidence that diacylglycerol acyltransferase 1 (DGAT1) has dual membrane topology in the endoplasmic reticulum of HepG2 cells.* J Biol Chem, 2011. **286**(42): p. 36238-47.

295. Chung, W.K. and R.L. Leibel, *Molecular physiology of syndromic obesities in humans*, in *Trends Endocrinol Metab*2005. p. 267-72.

296. Ginsberg, H.N., Y.L. Zhang, and A. Hernandez-Ono, *Metabolic syndrome: focus on dyslipidemia*, in *Obesity (Silver Spring)*2006. p. 41S-49S.

297. Goossens, G.H., *The role of adipose tissue dysfunction in the pathogenesis of obesity-related insulin resistance*, in *Physiol Behav*2008. p. 206-18.

298. Poitout, V. and R.P. Robertson, *Glucolipotoxicity: fuel excess and beta-cell dysfunction.* Endocr Rev, 2008. **29**(3): p. 351-66.

299. Unger, R.H., *Lipotoxicity in the pathogenesis of obesity-dependent NIDDM. Genetic and clinical implications.* Diabetes, 1995. **44**(8): p. 863-70.

300. Butler, A.E., et al., *Beta-cell deficit and increased beta-cell apoptosis in humans with type 2 diabetes.* Diabetes, 2003. **52**(1): p. 102-10.

301. Kloppel, G., et al., *Islet pathology and the pathogenesis of type 1 and type 2 diabetes mellitus revisited.* Surv Synth Pathol Res, 1985. **4**(2): p. 110-25.

302. Sakuraba, H., et al., *Reduced beta-cell mass and expression of oxidative stress-related DNA damage in the islet of Japanese Type II diabetic patients.* Diabetologia, 2002. **45**(1): p. 85-96.

303. Yoon, K.H., et al., *Selective beta-cell loss and alpha-cell expansion in patients with type 2 diabetes mellitus in Korea.* J Clin Endocrinol Metab, 2003. **88**(5): p. 2300-8.

304. Cauchi, S., et al., *Effects of TCF7L2 polymorphisms on obesity in European populations.* Obesity (Silver Spring), 2008. **16**(2): p. 476-82.

305. Stefanovic, S. and R.S. Hegde, *Identification of a targeting factor for posttranslational membrane protein insertion into the ER.* Cell, 2007. **128**(6): p. 1147-59.

306. Vilardi, F., H. Lorenz, and B. Dobberstein, *WRB is the receptor for TRC40/Asna1-mediated insertion of tail-anchored proteins into the ER membrane.* J Cell Sci, 2011. **124**(Pt 8): p. 1301-7.

307. Mukhopadhyay, R., et al., *Targeted disruption of the mouse Asna1 gene results in embryonic lethality.* FEBS Lett, 2006. **580**(16): p. 3889-94.

308. Ishihara, H., et al., *Pancreatic beta cell line MIN6 exhibits characteristics of glucose metabolism and glucose-stimulated insulin secretion similar to those of normal islets.* Diabetologia, 1993. **36**(11): p. 1139-45.

309. Seo, T., et al., *Differential modulation of ACAT1 and ACAT2 transcription and activity by long chain free fatty acids in cultured cells.* Biochemistry, 2001. **40**(15): p. 4756-62.

310. Dixon, J.L., S. Furukawa, and H.N. Ginsberg, *Oleate stimulates secretion of apolipoprotein B-containing lipoproteins from Hep G2 cells by inhibiting early intracellular degradation of apolipoprotein B.* J Biol Chem, 1991. **266**(8): p. 5080-6.

311. Caviglia, J.M., et al., *Different fatty acids inhibit apoB100 secretion by different pathways: unique roles for ER stress, ceramide, and autophagy.* J Lipid Res, 2011. **52**(9): p. 1636-51.

312. Kurdi-Haidar, B., et al., *Immunohistochemical analysis of the distribution of the human ATPase (hASNA-I) in normal tissues and its overexpression in breast adenomas and carcinomas.* J Histochem Cytochem, 1998. **46**(11): p. 1243-8.

313. Kim, M.K., et al., *Endoplasmic reticulum stress and insulin biosynthesis: a review.* Exp Diabetes Res, 2012. **2012**: p. 509437.

314. Rao, R.V., et al., *Coupling endoplasmic reticulum stress to the cell death program: role of the ER chaperone GRP78.* FEBS Lett, 2002. **514**(2-3): p. 122-8.

315. Kwan, E.P., et al., *Munc13-1 deficiency reduces insulin secretion and causes abnormal glucose tolerance.* Diabetes, 2006. **55**(5): p. 1421-9.

316. Latour, M.G., et al., *GPR40 is necessary but not sufficient for fatty acid stimulation of insulin secretion in vivo.* Diabetes, 2007. **56**(4): p. 1087-94.

317. Torres, N., L. Noriega, and A.R. Tovar, *Nutrient modulation of insulin secretion.* Vitam Horm, 2009. **80**: p. 217-44.

318. Shimabukuro, M., et al., *Fatty acid-induced beta cell apoptosis: a link between obesity and diabetes.* Proc Natl Acad Sci U S A, 1998. **95**(5): p. 2498-502.

319. Biden, T.J., et al., *Chronic effects of fatty acids on pancreatic beta-cell function: new insights from functional genomics*, in *Diabetes*2004. p. S159-65.

320. Fisher, E.A. and H.N. Ginsberg, *Complexity in the secretory pathway: the assembly and secretion of apolipoprotein B-containing lipoproteins.* J Biol Chem, 2002. **277**(20): p. 17377-80.

321. Fisher, E.A., et al., *The triple threat to nascent apolipoprotein B. Evidence for multiple, distinct degradative pathways.* J Biol Chem, 2001. **276**(30): p. 27855-63.

322. Choi, S.H. and H.N. Ginsberg, *Increased very low density lipoprotein (VLDL) secretion, hepatic steatosis, and insulin resistance.* Trends Endocrinol Metab, 2011. **22**(9): p. 353-63.

323. Shindo, N., et al., *Involvement of microsomal triglyceride transfer protein in nonalcoholic steatohepatitis in novel spontaneous mouse model.* J Hepatol, 2010. **52**(6): p. 903-12.

324. Cuchel, M., et al., *Inhibition of microsomal triglyceride transfer protein in familial hypercholesterolemia.* N Engl J Med, 2007. **356**(2): p. 148-56.

325. Wierzbicki, A.S., T. Hardman, and W.T. Prince, *Future challenges for microsomal transport protein inhibitors.* Curr Vasc Pharmacol, 2009. **7**(3): p. 277-86.

326. Maestre, I., et al., *Mitochondrial dysfunction is involved in apoptosis induced by serum withdrawal and fatty acids in the beta-cell line INS-1*, in *Endocrinology*2003. p. 335-45.

327. Welters, H.J., et al., *Mono-unsaturated fatty acids protect against beta-cell apoptosis induced by saturated fatty acids, serum withdrawal or cytokine exposure.* FEBS Lett, 2004. **560**(1-3): p. 103-8.

328. Maedler, K., et al., *Monounsaturated fatty acids prevent the deleterious effects of palmitate and high glucose on human pancreatic beta-cell turnover and function*, in *Diabetes*2003. p. 726-33.

329. Welters, H.J., et al., *Differential protective effects of palmitoleic acid and cAMP on caspase activation and cell viability in pancreatic beta-cells exposed to palmitate.* Apoptosis, 2006. **11**(7): p. 1231-8.

330. Eizirik, D.L., A.K. Cardozo, and M. Cnop, *The role for endoplasmic reticulum stress in diabetes mellitus.* Endocr Rev, 2008. **29**(1): p. 42-61.

331. Prentki, M., *New insights into pancreatic beta-cell metabolic signaling in insulin secretion.* Eur J Endocrinol, 1996. **134**(3): p. 272-86.

332. Ashcroft, F.M. and P. Rorsman, *ATP-sensitive K+ channels: a link between B-cell metabolism and insulin secretion.* Biochem Soc Trans, 1990. **18**(1): p. 109-11.

333. Nolan, C.J., et al., *Fatty acid signaling in the beta-cell and insulin secretion.* Diabetes, 2006. **55 Suppl 2**: p. S16-23.

334. Haber, E.P., et al., *New insights into fatty acid modulation of pancreatic beta-cell function.* Int Rev Cytol, 2006. **248**: p. 1-41.

335. Blachier, F., et al., *Stimulus-secretion coupling of arginine-induced insulin release. Functional response of islets to L-arginine and L-ornithine.* Biochim Biophys Acta, 1989. **1013**(2): p. 144-51.

336. Sener, A., et al., *Stimulus-secretion coupling of arginine-induced insulin release: comparison with lysine-induced insulin secretion.* Endocrinology, 1989. **124**(5): p. 2558-67.

337. Newsholme, P., C. Gaudel, and N.H. McClenaghan, *Nutrient regulation of insulin secretion and beta-cell functional integrity.* Adv Exp Med Biol, 2010. **654**: p. 91-114.

338. Leznicki, P., et al., *Bat3 promotes the membrane integration of tail-anchored proteins.* J Cell Sci, 2010. **123**(Pt 13): p. 2170-8.

339. Wang, Z. and D.C. Thurmond, *Mechanisms of biphasic insulin-granule exocytosis - roles of the cytoskeleton, small GTPases and SNARE proteins.* J Cell Sci, 2009. **122**(Pt 7): p. 893-903.

340. Ostenson, C.G., et al., *Impaired gene and protein expression of exocytotic soluble N-ethylmaleimide attachment protein receptor complex proteins in pancreatic islets of type 2 diabetic patients.* Diabetes, 2006. **55**(2): p. 435-40.

341. Romeo, S., et al., *Search for genetic variants of the SYNTAXIN 1A (STX1A) gene: the -352 A>T variant in the STX1A promoter associates with impaired glucose metabolism in an Italian obese population.* Int J Obes (Lond), 2008. **32**(3): p. 413-20.

342. Tsunoda, K., et al., *Single nucleotide polymorphism (D68D, T to C) in the syntaxin 1A gene correlates to age at onset and insulin requirement in Type II diabetic patients.* Diabetologia, 2001. **44**(11): p. 2092-7.

343. Itoh, Y., et al., *Free fatty acids regulate insulin secretion from pancreatic beta cells through GPR40.* Nature, 2003. **422**(6928): p. 173-6.

344. Swain, E., et al., *Yeast cells lacking the ARV1 gene harbor defects in sphingolipid metabolism. Complementation by human ARV1.* J Biol Chem, 2002. **277**(39): p. 36152-60.

345. Fores, O., et al., *Arabidopsis thaliana expresses two functional isoforms of Arvp, a protein involved in the regulation of cellular lipid homeostasis.* Biochim Biophys Acta, 2006. **1761**(7): p. 725-35.

346. Miyazaki, J., et al., *Establishment of a pancreatic beta cell line that retains glucose-inducible insulin secretion: special reference to expression of glucose transporter isoforms.* Endocrinology, 1990. **127**(1): p. 126-32.

347. Fei, W., et al., *Conditions of endoplasmic reticulum stress stimulate lipid droplet formation in Saccharomyces cerevisiae.* Biochem J, 2009. **424**(1): p. 61-7.

348. Kraegen, E.W., et al., *The role of lipids in the pathogenesis of muscle insulin resistance and beta cell failure in type II diabetes and obesity*, in *Exp Clin Endocrinol Diabetes*2001. p. S189-201.

349. Marchetti, P., et al., *The pancreatic beta-cell in human Type 2 diabetes*, in *Nutr Metab Cardiovasc Dis*2006. p. S3-6.

350. Robertson, R.P., et al., *Beta-cell glucose toxicity, lipotoxicity, and chronic oxidative stress in type 2 diabetes*, in *Diabetes*2004. p. S119-24.

351. Wrede, C.E., et al., *Protein kinase B/Akt prevents fatty acid-induced apoptosis in pancreatic beta-cells (INS-1).* J Biol Chem, 2002. **277**(51): p. 49676-84.

352. Sargsyan, E. and P. Bergsten, *Lipotoxicity is glucose-dependent in INS-1E cells but not in human islets and MIN6 cells.* Lipids Health Dis, 2011. **10**: p. 115.

353. Kusminski, C.M., et al., *Diabetes and apoptosis: lipotoxicity.* Apoptosis, 2009. **14**(12): p. 1484-95.

354. Cusi, K., *Role of insulin resistance and lipotoxicity in non-alcoholic steatohepatitis.* Clin Liver Dis, 2009. **13**(4): p. 545-63.

355. Ye, J. and R.A. Debose-Boyd, *Regulation of cholesterol and Fatty Acid synthesis.* Cold Spring Harb Perspect Biol, 2011. **3**(7).

356. Brown, M.S. and J.L. Goldstein, *The SREBP pathway: regulation of cholesterol metabolism by proteolysis of a membrane-bound transcription factor.* Cell, 1997. **89**(3): p. 331-40.

357. Jaye, M., et al., *A novel endothelial-derived lipase that modulates HDL metabolism.* Nat Genet, 1999. **21**(4): p. 424-8.

358. Tsukamoto, K., et al., *Hepatic expression of apolipoprotein E inhibits progression of atherosclerosis without reducing cholesterol levels in LDL receptor-deficient mice.* Mol Ther, 2000. **1**(2): p. 189-94.

359. Meiner, V.L., et al., *Disruption of the acyl-CoA:cholesterol acyltransferase gene in mice: evidence suggesting multiple cholesterol esterification enzymes in mammals.* Proc Natl Acad Sci U S A, 1996. **93**(24): p. 14041-6.

360. Cohen, J.C., J.D. Horton, and H.H. Hobbs, *Human fatty liver disease: old questions and new insights.* Science, 2011. **332**(6037): p. 1519-23.

361. Ranganathan, G., et al., *The lipogenic enzymes DGAT1, FAS, and LPL in adipose tissue: effects of obesity, insulin resistance, and TZD treatment*, in *J Lipid Res*2006. p. 2444-50.

362. Nakamuta, M., et al., *Evaluation of fatty acid metabolism-related gene expression in nonalcoholic fatty liver disease.* Int J Mol Med, 2005. **16**(4): p. 631-5.

363. van Herpen, N.A. and V.B. Schrauwen-Hinderling, *Lipid accumulation in non-adipose tissue and lipotoxicity*, in *Physiol Behav*2008. p. 231-41.

364. Villanueva, C.J., et al., *Specific role for acyl CoA:Diacylglycerol acyltransferase 1 (Dgat1) in hepatic steatosis due to exogenous fatty acids.* Hepatology, 2009. **50**(2): p. 434-42.

365. Kajiwara, K., et al., *Yeast ARV1 is required for efficient delivery of an early GPI intermediate to the first mannosyltransferase during GPI assembly and controls lipid flow from the endoplasmic reticulum.* Mol Biol Cell, 2008. **19**(5): p. 2069-82.

366. Mouritsen, O.G. and M.J. Zuckermann, *What's so special about cholesterol?* Lipids, 2004. **39**(11): p. 1101-13.

367. Los, D.A. and N. Murata, *Membrane fluidity and its roles in the perception of environmental signals.* Biochim Biophys Acta, 2004. **1666**(1-2): p. 142-57.

368. Konings, A.W. and A.C. Ruifrok, *Role of membrane lipids and membrane fluidity in thermosensitivity and thermotolerance of mammalian cells.* Radiat Res, 1985. **102**(1): p. 86-98.

369. Dolganiuc, A., *Role of lipid rafts in liver health and disease.* World J Gastroenterol, 2011. **17**(20): p. 2520-35.

370. Ikonen, E., *Cellular cholesterol trafficking and compartmentalization*, in *Nat Rev Mol Cell Biol*2008. p. 125-38.

371. Thewke, D., M. Kramer, and M.S. Sinensky, *Transcriptional homeostatic control of membrane lipid composition.* Biochem Biophys Res Commun, 2000. **273**(1): p. 1-4.

372. Ntambi, J.M., *Regulation of stearoyl-CoA desaturase by polyunsaturated fatty acids and cholesterol.* J Lipid Res, 1999. **40**(9): p. 1549-58.

373. Koliwad, S.K., et al., *DGAT1-dependent triacylglycerol storage by macrophages protects mice from diet-induced insulin resistance and inflammation.* J Clin Invest, 2010. **120**(3): p. 756-67.

374. Chavez, J.A. and S.A. Summers, *Characterizing the effects of saturated fatty acids on insulin signaling and ceramide and diacylglycerol accumulation in 3T3-L1 adipocytes and C2C12 myotubes.* Arch Biochem Biophys, 2003. **419**(2): p. 101-9.

375. Haus, J.M., et al., *Plasma ceramides are elevated in obese subjects with type 2 diabetes and correlate with the severity of insulin resistance.* Diabetes, 2009. **58**(2): p. 337-43.

376. Park, T.S., et al., *Ceramide is a cardiotoxin in lipotoxic cardiomyopathy.* J Lipid Res, 2008. **49**(10): p. 2101-12.

377. Holland, W.L., et al., *Inhibition of ceramide synthesis ameliorates glucocorticoid-, saturated-fat-, and obesity-induced insulin resistance.* Cell Metab, 2007. **5**(3): p. 167-79.

378. Wang, H., G. Kouri, and C.B. Wollheim, *ER stress and SREBP-1 activation are implicated in beta-cell glucolipotoxicity.* J Cell Sci, 2005. **118**(Pt 17): p. 3905-15.

379. Borradaile, N.M., et al., *Disruption of endoplasmic reticulum structure and integrity in lipotoxic cell death.* J Lipid Res, 2006. **47**(12): p. 2726-37.

380. Carlsson, C., L.A. Borg, and N. Welsh, *Sodium palmitate induces partial mitochondrial uncoupling and reactive oxygen species in rat pancreatic islets in vitro.* Endocrinology, 1999. **140**(8): p. 3422-8.

381. Joseph, J.W., et al., *Free fatty acid-induced beta-cell defects are dependent on uncoupling protein 2 expression*, in *J Biol Chem*2004. p. 51049-56.

382. Weinberg, J.M., *Lipotoxicity*, in *Kidney Int*2006. p. 1560-6.

383. Biden, T.J., et al., *Chronic effects of fatty acids on pancreatic beta-cell function: new insights from functional genomics.* Diabetes, 2004. **53 Suppl 1**: p. S159-65.

384. Chang-Chen, K.J., R. Mullur, and E. Bernal-Mizrachi, *Beta-cell failure as a complication of diabetes*, in *Rev Endocr Metab Disord*2008. p. 329-43.

385. Blakemore, A.I. and P. Froguel, *Is obesity our genetic legacy?*, in *J Clin Endocrinol Metab*2008. p. S51-6.

386. Chartron, J.W., W.M. Clemons, Jr., and C.J. Suloway, *The complex process of GETting tail-anchored membrane proteins to the ER.* Curr Opin Struct Biol, 2012. **22**(2): p. 217-24.

387. Kamath, R.S., et al., *Systematic functional analysis of the Caenorhabditis elegans genome using RNAi.* Nature, 2003. **421**(6920): p. 231-7.

388. Kos, C.H., *Cre/loxP system for generating tissue-specific knockout mouse models.* Nutr Rev, 2004. **62**(6 Pt 1): p. 243-6.

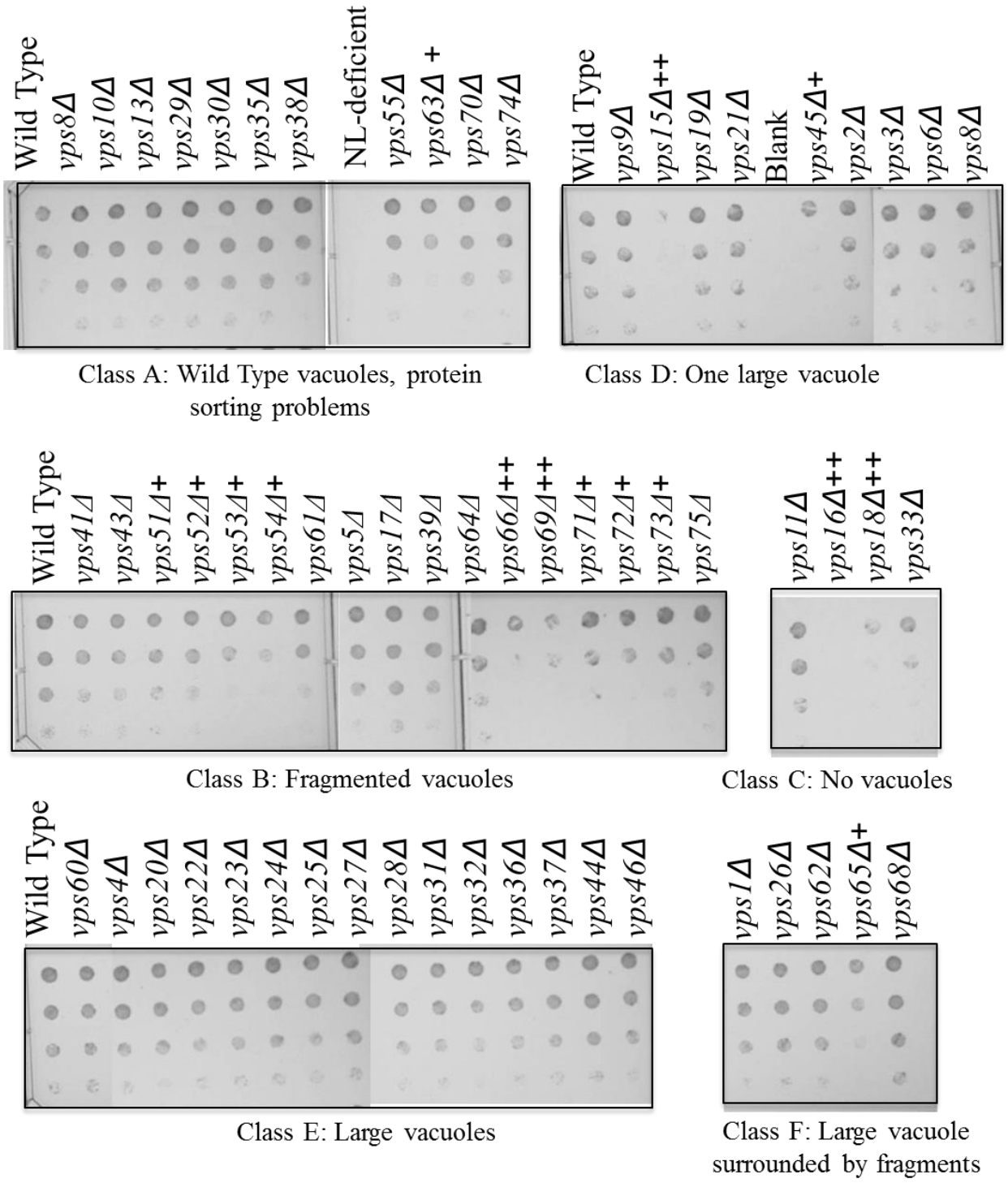

***Figure S2-1: Sensitivity of vacuolar protein sorting (VPS) mutants to palmitoleate*.** Serial dilution plating of 61 VPS mutants on 0.5 mM palmitoleate for 2 days at 30°C. + indicates sensitivity, ++ indicates inviability

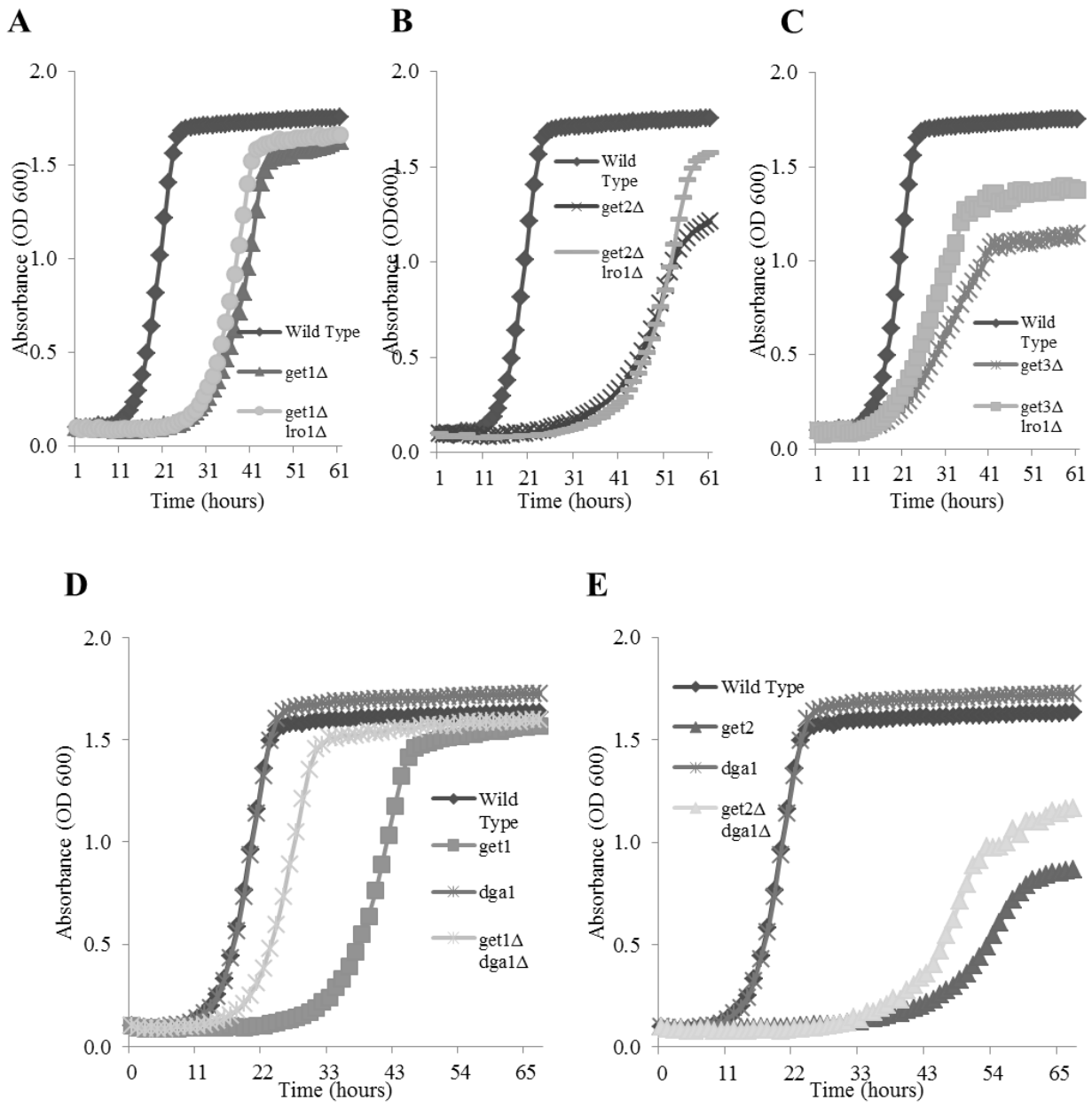

Figure S3-1: Growth curves of GET complex and triglyceride synthesis enzyme knockouts in palmitoleate. Strains grown in 0.5 mM palmitoleate for 3 days with cell density as measured by absorbance (OD600). (A) *GET1* and *LRO1* deletions (B) *GET2* and *LRO1* deletions (C) *GET3* and *LRO1* deletions (D) *GET1* and *DGA1* deletions (C) *GET2* and *DGA1* deletions

Table S2-1: Growth Curve Validation of significant palmitoleate sensitive screen hits.
Growth curve variables "Max Rate", "Time" and "Max OD" relative to wild type control. Strains are ranked first by the severity of their phenotype upon deletion. This severity was determined by summation of the three relative growth values ("Max Rate" + "Max OD" + "Time"). "Max Rate" and "Max OD" value is 1 for normal growth the higher the value to slower the growth. Normal growth for "Time" is 0 and .increased value indicates slow growth. p-values based on Student T-test analysis. Values in bold considered significant.

Rank	*Gene*	*ORF*	Max Rate	Time	Max OD	p-value Rate	p-value Time	p-value OD	Variable sum
1	*ARV1*	*YLR242C*	10.10	31.00	5.97	0.107	**0.001**	**0.003**	47.08
2	*RPB9*	*YGL070C*	37.00	2.00	0.91	0.568	**0.013**	0.090	39.91
3	*ARO1*	*YDR127W*	5.08	19.00	3.46	0.060	**0.000**	0.071	27.54
4	*GET1*	*YGL020C*	4.18	18.00	3.02	0.085	**0.000**	**0.012**	25.21
5	*VMA1*	*YDL185W*	5.74	12.00	4.28	**0.011**	**0.000**	**0.029**	22.01
6	*FEN1*	*YCR034W*	1.19	15.00	1.26	0.910	**0.000**	0.971	17.45
7	*YML095C-A*	*YML095C-A*	1.93	13.00	2.02	**0.007**	**0.003**	0.096	16.95
8	*VMA7*	*YGR020C*	1.58	14.00	1.21	0.123	**0.000**	0.831	16.80
9	*VPS69*	*YPR087W*	5.15	8.00	3.38	0.186	0.105	**0.044**	16.54
10	*IES6*	*YEL044W*	5.93	7.00	3.60	**0.022**	0.070	**0.044**	16.53

Rank	*Gene*	*ORF*	Max Rate	Time	Max OD	p-value Rate	p-value Time	p-value OD	Variable sum
11	*TRP5*	*YGL026C*	1.81	13.00	1.42	0.172	**0.000**	0.852	16.23
12	*FPS1*	*YLL043W*	2.16	12.00	1.63	0.074	**0.001**	0.106	15.78
13	*VPS71*	*YML041C*	1.31	13.00	1.04	0.817	**0.001**	0.297	15.35
14	*SCS7*	*YMR272C*	4.68	7.00	3.11	0.110	**0.001**	**0.030**	14.79
15	*ERV14*	*YGL054C*	1.34	12.00	1.10	0.172	**0.001**	0.460	14.44
16	*LOA1*	*YPR139C*	5.15	6.00	3.24	0.186	0.105	**0.041**	14.39
17	*HSL7*	*YBR133C*	1.19	12.00	1.01	0.925	**0.008**	0.292	14.21
18	*YOR331C*	*YOR331C*	2.01	10.00	1.77	**0.001**	**0.000**	**0.004**	13.77
19	*ITR1*	*YDR497C*	2.49	9.00	1.93	0.144	**0.027**	0.383	13.43
20	*MRP10*	*YDL045W-A*	3.10	8.00	2.23	0.194	**0.009**	0.217	13.34

Rank	*Gene*	*ORF*	Max Rate	Time	Max OD	p-value Rate	p-value Time	p-value OD	Variable sum
21	*YBL100C*	*YBL100C*	3.13	8.00	1.99	0.097	**0.024**	**0.049**	13.13
22	*CYT1*	*YOR065W*	1.21	10.00	1.35	0.289	**0.011**	0.053	12.56
23	*VPS61*	*YDR136C*	1.24	10.00	1.21	0.763	**0.000**	0.313	12.45
24	*GOS1*	*YHL031C*	1.96	9.00	1.47	0.243	**0.005**	0.477	12.43
25	*GFD2*	*YCL036W*	3.33	6.00	2.77	**0.000**	**0.008**	0.101	12.11
26	*YDL009C*	*YDL009C*	1.31	9.00	1.27	0.378	**0.000**	0.885	11.58
27	*CTF8*	*YHR191C*	1.78	8.00	1.73	0.090	**0.015**	0.335	11.52
28	*YDL041W*	*YDL041W*	2.63	7.00	1.83	0.121	**0.031**	0.316	11.45
29	*PGI1*	*YBR196C-A*	1.15	9.00	1.11	0.965	**0.002**	0.332	11.26
30	*IFM1*	*YOL023W*	2.34	7.00	1.84	**0.007**	**0.000**	**0.010**	11.18

Rank	*Gene*	*ORF*	Max Rate	Time	Max OD	p-value Rate	p-value Time	p-value OD	Variable sum
31	*VPS72*	*YDR485C*	2.29	7.00	1.79				11.07
32	*SAC1*	*YKL212W*	1.73	7.00	1.86	**0.039**	**0.020**	0.181	10.59
33	*FES1*	*YBR101C*	2.12	7.00	1.39	0.060	**0.000**	0.378	10.51
34	*STP2*	*YHR006W*	1.39	8.00	1.11	0.483	**0.002**	0.490	10.50
35	*TCO89*	*YPL180W*	2.19	6.00	2.26	**0.036**	**0.024**	0.115	10.45
36	*BUB1*	*YGR188C*	2.47	5.00	2.58	**0.001**	**0.035**	**0.000**	10.05
37	*ARO2*	*YGL148W*	1.59	7.00	1.37	**0.027**	**0.001**	0.963	9.97
38	*GET3*	*YDL100C*	1.67	7.00	1.29	0.388	**0.001**	0.777	9.96
39	*TPS1*	*YBR126C*	1.04	8.00	0.92	0.539	**0.002**	0.133	9.96
40	*SLX8*	*YER116C*	2.11	6.00	1.81	0.066	**0.000**	0.607	9.92

Rank	*Gene*	*ORF*	Max Rate	Time	Max OD	p-value Rate	p-value Time	p-value OD	Variable sum
41	*YER084W*	*YER084W*	1.90	6.00	1.57	0.251	**0.013**	0.527	9.47
42	*COX18*	*YGR062C*	1.83	6.00	1.62	**0.010**	**0.007**	0.087	9.45
43	*NPL6*	*YMR091C*	1.66	6.00	1.70	0.143	**0.001**	0.128	9.37
44	*YLR184W*	*YLR184W*	1.68	6.00	1.65	0.105	**0.000**	0.398	9.33
45	*EMP24*	*YGL200C*	3.01	4.00	2.12	**0.043**	**0.016**	**0.010**	9.13
46	*YAF9*	*YNL107W*	1.12	7.00	0.94	0.844	**0.018**	0.145	9.06
47	*RTG2*	*YGL252C*	3.35	3.00	2.69	**0.033**	**0.000**	**0.002**	9.03
48	*CEM1*	*YER061C*	1.44	6.00	1.45	0.204	**0.002**	0.705	8.89
49	*AIM10*	*YER087W*	1.40	6.00	1.36	0.453	**0.011**	0.657	8.77
50	*YBR144C*	*YBR144C*	3.25	3.00	2.49	**0.050**	0.131	**0.005**	8.75

Rank	*Gene*	*ORF*	Max Rate	Time	Max OD	p-value Rate	p-value Time	p-value OD	Variable sum
51	*YDR149C*	*YDR149C*	1.44	6.00	1.29	0.164	**0.027**	0.945	8.73
52	*GET2*	*YER083C*	1.29	6.00	1.06	0.358	**0.002**	0.601	8.35
53	*LDB7*	*YBL006C*	1.82	5.00	1.49	0.239	**0.007**	0.469	8.31
54	*MDM32*	*YOR147W*	1.17	6.00	1.13	0.667	**0.008**	0.388	8.30
55	*VPS63*	*YLR261C*	1.12	6.00	0.92	0.844	**0.004**	**0.010**	8.04
56	*CBP2*	*YHL038C*	1.47	5.00	1.44	0.103	**0.017**	0.697	7.91
57	*RPL8A*	*YHL033C*	2.12	4.00	1.75	0.059	**0.027**	**0.027**	7.87
58	*SSN3*	*YPL042C*	1.92	4.00	1.78	0.157	**0.014**	0.403	7.70
59	*YNL296W*	*YNL296W*	2.63	3.00	2.04	0.138	**0.029**	0.118	7.67
60	*VPS51*	*YKR020W*	1.92	4.00	1.74	0.220	**0.020**	0.792	7.66

Rank	*Gene*	*ORF*	Max Rate	Time	Max OD	p-value Rate	p-value Time	p-value OD	Variable sum
61	*MDJ1*	*YFL016C*	1.25	5.00	1.33	0.437	**0.046**	0.991	7.58
62	*HAP3*	*YBL021C*	1.22	5.00	1.17	0.151	**0.001**	0.221	7.39
63	*GGC1*	*YDL198C*	1.72	4.00	1.66	**0.000**	**0.000**	**0.022**	7.39
64	*LSM1*	*YJL124C*	1.79	4.00	1.59	**0.040**	**0.047**	0.183	7.38
65	*VPS52*	*YDR484W*	1.98	4.00	1.38	0.056	**0.007**	0.690	7.37
66	*PHO80*	*YOL001W*	1.07	5.00	1.27	0.808	**0.006**	0.985	7.34
67	*GCN5*	*YGR252W*	1.76	4.00	1.55	0.266	**0.023**	0.326	7.30
68	*CTF4*	*YPR135W*	1.08	5.00	1.20	0.896	**0.011**	0.791	7.29
69	*COQ3*	*YOL096C*	1.73	4.00	1.54	**0.002**	**0.026**	**0.016**	7.27
70	*PFD1*	*YJL179W*	3.11	2.00	2.16	**0.039**	0.266	**0.026**	7.27

Rank	*Gene*	*ORF*	Max Rate	Time	Max OD	p-value Rate	p-value Time	p-value OD	Variable sum
71	*SNT1*	*YCR033W*	1.25	5.00	0.98	0.627	**0.003**	0.136	7.23
72	*YNL198C*	*YNL198C*	1.16	5.00	1.02	0.663	**0.037**	**0.029**	7.18
73	*COX11*	*YPL132W*	1.58	4.00	1.56	**0.020**	**0.027**	0.251	7.14
74	*ATP11*	*YNL315C*	1.78	4.00	1.32	0.085	**0.011**	0.068	7.11
75	*SIC1*	*YLR079W*	1.64	4.00	1.33	0.169	**0.000**	0.525	6.96
76	*TRP2*	*YER090W*	1.52	4.00	1.38	0.252	**0.012**	0.652	6.91
77	*PET54*	*YGR222W*	1.54	4.00	1.36	0.220	**0.022**	0.692	6.89
78	*MRPL51*	*YPR100W*	1.49	4.00	1.36	0.172	**0.001**	0.648	6.85
79	*LGE1*	*YPL055C*	1.41	4.00	1.38	0.078	**0.012**	0.738	6.79
80	*YLR202C*	*YLR202C*	1.24	4.00	1.26	0.312	**0.001**	0.727	6.49

Rank	*Gene*	*ORF*	Max Rate	Time	Max OD	p-value Rate	p-value Time	p-value OD	Variable sum
81	*NPR3*	*YHL023C*	1.18	4.00	1.27	0.492	**0.017**	0.939	6.45
82	*WSS1*	*YHR134W*	1.21	4.00	1.22	0.503	**0.036**	0.378	6.44
83	*YDR417C*	*YDR417C*	1.69	3.00	1.70	**0.030**	**0.018**	**0.008**	6.38
84	*MRC1*	*YCL060C*	1.16	4.00	1.19	0.564	**0.005**	0.685	6.35
85	*NGG1*	*YDR176W*	1.16	4.00	1.14	0.854	**0.005**	0.225	6.30
86	*YGR219W*	*YGR219W*	1.17	4.00	1.07	0.572	**0.013**	0.256	6.24
87	*RSC1*	*YGR056W*	1.70	3.00	1.49	0.159	**0.015**	0.265	6.19
88	*RTF1*	*YGL244W*	1.66	3.00	1.48	0.292	**0.000**	0.296	6.14
89	*COX23*	*YHR116W*	1.05	4.00	1.05	0.646	**0.032**	**0.036**	6.10
90	*HOC1*	*YJR075W*	1.07	4.00	1.03	0.554	**0.001**	0.149	6.10

Rank	*Gene*	*ORF*	Max Rate	Time	Max OD	p-value Rate	p-value Time	p-value OD	Variable sum
91	*SKY1*	*YMR216C*	1.07	4.00	1.03	0.705	**0.014**	**0.007**	6.10
92	*DEP1*	*YAL013W*	1.69	3.00	1.32	**0.039**	**0.033**	0.772	6.01
93	*RSM27*	*YGR215W*	1.03	4.00	0.98	0.699	**0.000**	**0.006**	6.01
94	*MRPL9*	*YGR220C*	1.55	3.00	1.42	**0.002**	**0.003**	0.560	5.97
95	*YDR230W*	*YDR230W*	1.54	3.00	1.43	0.113	**0.006**	0.377	5.97
96	*VRP1*	*YLR337C*	1.62	3.00	1.33	0.118	**0.017**	0.934	5.96
97	*COQ6*	*YGR255C*	0.96	4.00	0.96	0.475	**0.003**	0.197	5.93
98	*LSM7*	*YNL147W*	1.57	3.00	1.35	0.106	**0.002**	0.580	5.92
99	*SPF1*	*YEL031W*	1.37	3.00	1.45	0.320	**0.026**	0.151	5.82
100	*PET117*	*YER058W*	1.49	3.00	1.24	0.267	**0.003**	0.784	5.73

Rank	*Gene*	*ORF*	Max Rate	Time	Max OD	p-value Rate	p-value Time	p-value OD	Variable sum
101	*CBP1*	*YJL209W*	1.34	3.00	1.31	0.116	**0.026**	0.300	5.65
102	*BCS1*	*YDR375C*	1.38	3.00	1.24	**0.050**	0.061	0.295	5.62
103	*MNN4*	*YKL201C*	1.35	3.00	1.22	0.615	**0.007**	0.656	5.57
104	*YMR031W-A*	*YMR031W-A*	1.41	3.00	1.09	0.093	**0.007**	0.241	5.50
105	*PCP1*	*YGR101W*	1.21	3.00	1.28	0.381	**0.008**	0.245	5.49
106	*YMR135W-A*	*YMR135W-A*	2.32	1.00	2.14	**0.006**	0.104	**0.004**	5.46
107	*RSM22*	*YKL155C*	1.82	2.00	1.60	**0.018**	**0.003**	0.275	5.43
108	*PET309*	*YLR067C*	1.30	3.00	1.08	0.446	**0.007**	0.072	5.38
109	*PHO23*	*YNL097C*	1.13	3.00	1.21	0.087	**0.001**	**0.026**	5.34
110	*KEX2*	*YNL238W*	1.26	3.00	1.05	0.228	**0.001**	0.155	5.31

Rank	*Gene*	*ORF*	Max Rate	Time	Max OD	p-value Rate	p-value Time	p-value OD	Variable sum
111	*SPT21*	*YMR179W*	1.16	3.00	1.08	**0.040**	0.057	**0.029**	5.24
112	*PEP3*	*YLR148W*	1.17	3.00	1.01	0.396	**0.001**	0.330	5.18
113	*YLR374C*	*YLR374C*	1.64	2.00	1.44	0.091	**0.015**	0.418	5.08
114	*MTM1*	*YGR257C*	1.59	2.00	1.42	**0.006**	**0.017**	0.269	5.01
115	*VPS64*	*YDR200C*	1.68	2.00	1.29	**0.045**	0.329	0.732	4.97
116	*LHP1*	*YDL051W*	1.54	2.00	1.43	0.306	**0.016**	0.742	4.97
117	*YHR009C*	*YHR009C*	0.85	3.00	0.92	**0.044**	**0.009**	0.122	4.77
118	*RAD6*	*YGL058W*	0.91	3.00	0.78	0.687	**0.006**	**0.025**	4.70
119	*MGR2*	*YPL098C*	1.40	2.00	1.25	0.292	**0.017**	0.626	4.64
120	*SOV1*	*YMR066W*	1.30	2.00	1.31	0.110	**0.003**	0.865	4.61

Rank	*Gene*	*ORF*	Max Rate	Time	Max OD	p-value Rate	p-value Time	p-value OD	Variable sum
121	*SHE3*	*YBR130C*	0.80	3.00	0.76	0.248	**0.000**	**0.015**	4.56
122	*MSW1*	*YDR268W*	1.23	2.00	1.29	0.157	**0.013**	0.669	4.52
123	*MEC3*	*YLR288C*	1.27	2.00	1.18	0.255	**0.008**	0.596	4.45
124	*MRPL7*	*YDR237W*	1.26	2.00	1.18	0.094	0.999	**0.035**	4.44
125	*VMA21*	*YGR105W*	1.11	2.00	1.28	0.618	**0.006**	0.141	4.40
126	*SAG1*	*YJR004C*	1.18	2.00	1.18	0.861	**0.038**	0.777	4.36
127	*HTB2*	*YBL002W*	0.66	3.00	0.67	**0.037**	**0.013**	**0.031**	4.33
128	*GRR1*	*YJR090C*	1.16	2.00	1.16	0.550	**0.013**	0.235	4.32
129	*ATP25*	*YMR098C*	1.12	2.00	1.19	0.383	**0.036**	0.207	4.31
130	*YBL094C*	*YBL094C*	1.74	1.00	1.54	**0.008**	0.099	0.477	4.28

Rank	*Gene*	*ORF*	Max Rate	Time	Max OD	p-value Rate	p-value Time	p-value OD	Variable sum
131	*RIC1*	*YLR039C*	1.24	2.00	1.02	0.171	0.079	**0.018**	4.27
132	*AIM22*	*YJL046W*	1.62	1.00	1.63	**0.002**	0.116	**0.011**	4.25
133	*CRD1*	*YDL142C*	1.74	1.00	1.51	**0.001**	0.051	0.259	4.25
134	*GLO3*	*YER122C*	1.06	2.00	1.15	0.144	**0.001**	0.130	4.22
135	*GCR2*	*YNL199C*	1.18	2.00	1.00	0.317	**0.020**	0.379	4.19
136	*YPR153W*	*YPR153W*	1.06	2.00	1.12	0.526	**0.013**	**0.013**	4.18
137	*CCE1*	*YKL011C*	1.74	1.00	1.37	0.196	**0.016**	0.449	4.11
138	*ELP3*	*YPL086C*	1.03	2.00	0.99	0.532	**0.020**	0.102	4.02
139	*QCR7*	*YDR529C*	1.51	1.00	1.50	**0.046**	0.060	0.082	4.01
140	*FRA2*	*YGL220W*	1.01	2.00	0.99	0.960	**0.023**	0.388	4.00

Rank	*Gene*	*ORF*	Max Rate	Time	Max OD	p-value Rate	p-value Time	p-value OD	Variable sum
141	*CAT5*	*YOR125C*	0.87	2.00	1.04	0.436	0.564	**0.034**	3.91
142	*RPS14A*	*YCR031C*	0.94	2.00	0.95	0.380	**0.000**	**0.032**	3.89
143	*SLI15*	*YBR156C*	0.91	2.00	0.91	0.456	**0.016**	0.075	3.83
144	*CSH1*	*YBR161W*	0.91	2.00	0.90	0.304	**0.016**	**0.026**	3.81
145	*MCT1*	*YOR221C*	1.11	1.00	1.11	0.556	0.393	**0.023**	3.21
146	*QCR8*	*YJL166W*	1.04	1.00	1.07	0.648	0.206	**0.011**	3.10
147	*MTC1*	*YJL123C*	1.47	0.00	1.36	**0.025**	0.074	0.858	2.83
148	*IMP2*	*YMR035W*	1.47	0.00	1.26	**0.016**	0.289	0.267	2.73
149	*SRB8*	*YCR081W*	0.84	1.00	0.87	0.600	**0.013**	0.728	2.71
150	*AEP1*	*YMR064W*	1.23	0.00	1.18	**0.048**	0.116	0.443	2.41

Rank	*Gene*	*ORF*	Max Rate	Time	Max OD	p-value Rate	p-value Time	p-value OD	Variable sum
151	*PET123*	*YOR158W*	1.13	0.00	1.15	0.064	0.051	**0.036**	2.28
152	*CTR1*	*YPR124W*	1.06	0.00	1.09	0.791	0.774	**0.004**	2.15
153	*RPS16A*	*YMR143W*	0.98	0.00	1.01	0.538	**0.001**	**0.014**	1.98
154	*YSY6*	*YBR162W-A*	0.75	0.00	0.76	0.177	**0.000**	**0.008**	1.52
155	*RPS28B*	*YLR264W*	1.27	-1.00	1.12	**0.037**	0.116	0.889	1.40
156	*RRP8*	*YDR083W*	1.02	-2.00	1.03	0.954	**0.001**	**0.009**	0.05

Table S2-2: Palmitoleate sensitive gene functions and human orthologs. Functional information on yeast genes obtained from *Saccharomyces* genome database (SGD). Human percentage values indicated refer to percent sequence identity. Ortholog conservation and function obtained from National Center for Biotechnology (NCBI) and Biobase PROTEOME databases. Genes ranked by phenotype seve rity, described in Table S-1.

Rank	*Yeast Gene*	*ORF*	Yeast Gene Function	*Human Ortholog*	Human Gene Function
1	*ARV1*	*YLR242C*	Protein functioning in transport of glycosylphosphatidylinositol intermediates into ER lumen; required for normal intracellular sterol distribution; human ARV1 required for normal cholesterol and bile acid homeostasis; similar to Nup120p	*ARV1 (conserved domain)*	ARV1 homolog, restores defective sterol uptake and intracellular distribution, and defective sphingolipid metabolism in yeast mutants, plays a role in cholesterol movement from the endoplasmic reticulum
2	*RPB9*	*YGL070C*	RNA polymerase II subunit B12.6; contacts DNA; mutations affect transcription start site selection and fidelity of transcription	*POLR2I (45%)*	Polymerase (RNA) II (DNA directed) polypeptide I 14.5kDa, a putative DNA-directed RNA polymerase that binds to zinc ion, may play a role in transcription start site selection
3	*ARO1*	*YDR127W*	Pentafunctional arom protein, catalyzes steps 2 through 6 in the biosynthesis of chorismate, which is a precursor to aromatic amino acids		
4	*GET1*	*YGL020C*	Subunit of the GET complex; involved in insertion of proteins into the ER membrane; required for the retrieval of HDEL proteins from the Golgi to the ER in an ERD2 dependent fashion and for normal mitochondrial morphology and inheritance	*CHD5 (23%)*	Basic nuelcear protein of unknown function. Receptor for the TRC40/Asna1-mediated insertion of tail anchored proteins into the ER membrane.
5	*VMA1*	*YDL185W*	Subunit A of the eight-subunit V1 peripheral membrane domain of the vacuolar H+-ATPase; protein precursor undergoes self-catalyzed splicing to yield the extein Tfp1p and the intein Vde (PI-SceI), which is a site-specific endonuclease	*ATP6V1A (37.8%)*	ATPase H+ transporting lysosomal subunit A1, a putative integral membrane protein that may play a role in ATP hydrolysis coupled proton transport
6	*FEN1*	*YCR034W*	Fatty acid elongase, involved in sphingolipid biosynthesis; acts on fatty acids of up to 24 carbons in length; mutations have regulatory effects on 1,3-beta-glucan synthase, vacuolar ATPase, and the secretory pathway	*ELOVL6 (30.6%)*	ELOVL family member 6 elongation of long chain fatty acids, a fatty acid elongase that plays a role in long-chain fatty acid biosynthesis; abundant mRNA expression correlates with geminoma, rat Elovl6 expression is downregulated in diabetic model
7	*YML095C-A*	*YML095C-A*	Dubious open reading frame unlikely to encode a protein, based on available experimental and comparative sequence data; partially overlaps the verified gene GIM5/YML094W; deletion confers sensitivity to GSAO		

Rank	*Yeast Gene*	*ORF*	Yeast Gene Function	*Human Ortholog*	Human Gene Function
8	*VMA7*	*YGR020C*	Subunit F of the eight-subunit V1 peripheral membrane domain of vacuolar H+-ATPase (V-ATPase), an electrogenic proton pump found throughout the endomembrane system; required for the V1 domain to assemble onto the vacuolar membrane	*ATP6V1F (52.6%)*	ATPase H+ transporting lysosomal 14kDa V1 subunit F, a putative ATPase and hydrogen ion transmembrane transporter that plays a role in proton transport
9	*VPS69*	*YPR087W*	Dubious open reading frame, unlikely to encode a protein; not conserved in closely related Saccharomyces species; 85% of ORF overlaps the verified gene SRP54		
10	*IES6*	*YEL044W*	Protein that associates with the INO80 chromatin remodeling complex under low-salt conditions; human ortholog INO80C is a member of the human INO80 complex; implicated in DNA repair based on genetic interactions with RAD52 epistasis genes		
11	*TRP5*	*YGL026C*	Tryptophan synthase, catalyzes the last step of tryptophan biosynthesis; regulated by the general control system of amino acid biosynthesis		
12	*FPS1*	*YLL043W*	Plasma membrane channel, member of major intrinsic protein (MIP) family; involved in efflux of glycerol and in uptake of acetic acid and the trivalent metalloids arsenite and antimonite; phosphorylated by Hog1p MAPK under acetate stress	*AQP9 (28%)*	Aquaporin 9, a transmembrane transporter that is involved in the transportation of water, polyol, antimonite, arsenite, glycerol, purine, pyrimidine, and urea, acts in filopodium formation, may play a role in osmosensory signaling pathway
13	*VPS71*	*YML041C*	Nucleosome-binding component of the SWR1 complex, which exchanges histone variant H2AZ (Htz1p) for chromatin-bound histone H2A; required for vacuolar protein sorting		
14	*SCS7*	*YMR272C*	Sphingolipid alpha-hydroxylase, functions in the alpha-hydroxylation of sphingolipid-associated very long chain fatty acids, has both cytochrome b5-like and hydroxylase/desaturase domains, not essential for growth	*CYB5M (42%)*	Cytochrome b5 type B an electron carrier and an enzyme activator that acts in L-ascorbic acid aldosterone and androgen biosynthesis and regulates lyase activity; mRNA expression is upregulated in Hodgkin Lymphoma and aggressive Non-Hodgkin Lymphoma
15	*ERV14*	*YGL054C*	Protein localized to COPII-coated vesicles, involved in vesicle formation and incorporation of specific secretory cargo; required for the delivery of bud-site selection protein Axl2p to cell surface; related to Drosophila cornichon	*CNIH4-isoform 1 (40%)*	Cornichon homolog 4; mRNA overexpression is observed in both primary and metastatic fibrolamellar carcinomas

Rank	*Yeast Gene*	*ORF*	Yeast Gene Function	*Human Ortholog*	Human Gene Function
16	*LOA1*	*YPR139C*	lysophosphatidic acid acyltransferase; involved in triacelglyceride homeostasis and lipid droplet formation; localized to lipid droplets and the ER; specificity for oleoyl-CoA		
17	*HSL7*	*YBR133C*	Protein arginine N-methyltransferase that exhibits septin and Hsl1p-dependent bud neck localization and periodic Hsl1p-dependent phosphorylation; required along with Hsl1p for bud neck recruitment, phosphorylation, and degradation of Swe1p	*PRMT5 (27.5%)*	Protein arginine methyltransferase 5, a transcriptional repressor that acts in protein complex assembly, skeletal muscle tissue development, and spliceosomal snRNP biogenesis, protein expression is upregulated in stomach neoplasm and gastric cancer
18	*YOR331C*	*YOR331C*	Dubious open reading frame unlikely to encode a protein, based on available experimental and comparative sequence data; open reading frame overlaps the verified gene VMA4/YOR332W		
19	*ITR1*	*YDR497C*	Myo-inositol transporter with strong similarity to the minor myo-inositol transporter Itr2p, member of the sugar transporter superfamily; expression is repressed by inositol and choline via Opi1p and derepressed via Ino2p and Ino4p	*GLUT2 (27%)*	Protein with strong similarity to solute carrier family 2 member 13 (rat Slc2a13) which is a myo-inositol:hydrogen symporter member of the major facilitator superfamily and the sugar (and other) transporter family
20	*MRP10*	*YDL045W-A*	Mitochondrial ribosomal protein of the small subunit; contains twin cysteine-x9-cysteine motifs		
21	*YBL100C*	*YBL100C*	Dubious open reading frame unlikely to encode a protein, based on available experimental and comparative sequence data; almost completely overlaps the 5' end of ATP1		
22	*CYT1*	*YOR065W*	Cytochrome c1, component of the mitochondrial respiratory chain; expression is regulated by the heme-activated, glucose-repressed Hap2p/3p/4p/5p CCAAT-binding complex	*CYC1 (56%)*	Protein with high similarity to A. thaliana AT5G40810, which is a component of mitochondrial respiratory chain complex that is involved in response to brassinosteroid stimulus
23	*VPS61*	*YDR136C*	Dubious open reading frame, unlikely to encode a protein; not conserved in closely related Saccharomyces species; 4% of ORF overlaps the verified gene RGP1; deletion causes a vacuolar protein sorting defec		

Rank	*Yeast Gene*	*ORF*	Yeast Gene Function	*Human Ortholog*	Human Gene Function
24	*GOS1*	*YHL031C*	v-SNARE protein involved in Golgi transport, homolog of the mammalian protein GOS-28/GS28	*GOSR1 (27.2%)*	Golgi SNAP receptor complex member 1, plays a role in retrograde and intra-Golgi vesicle-mediated transport
25	*GFD2*	*YCL036W*	Protein of unknown function, identified as a high-copy suppressor of a dbp5 mutation		
26	*YDL009C*	*YDL009C*	Dubious open reading frame unlikely to encode a protein, based on available experimental and comparative sequence data; partially overlaps the uncharacterized ORF YDL010W; YDL009C is not an essential gene		
27	*CTF8*	*YHR191C*	Subunit of a complex with Ctf18p that shares some subunits with Replication Factor C and is required for sister chromatid cohesion		
28	*YDL041W*	*YDL041W*	Dubious open reading frame unlikely to encode a protein, based on available experimental and comparative sequence data; overlaps the verified gene SIR2/YDL042C		
29	*PGI1*	*YBR196C-A*	Glycolytic enzyme phosphoglucose isomerase, catalyzes the interconversion of glucose-6-phosphate and fructose-6-phosphate; required for cell cycle progression and completion of the gluconeogenic events of sporulation (		
30	*IFM1*	*YOL023W*	Mitochondrial translation initiation factor 2	*MTIF2 (36%)*	Mitochondrial translational initiation factor 2, a putative translation initiation factor that may play a role in regulation of translational initiation
31	*VPS72*	*YDR485C*	Htz1p-binding component of the SWR1 complex, which exchanges histone variant H2AZ (Htz1p) for chromatin-bound histone H2A; required for vacuolar protein sorting		

Rank	*Yeast Gene*	*ORF*	Yeast Gene Function	*Human Ortholog*	Human Gene Function
32	*SAC1*	*YKL212W*	Phosphatidylinositol phosphate (PtdInsP) phosphatase involved in hydrolysis of PtdIns[4]P; transmembrane protein localizes to ER and Golgi; involved in protein trafficking and processing, secretion, and cell wall maintenance	*SACM1L (35%)*	SAC1 suppressor of actin mutations 1-like, a phosphatidylinositol-3-phosphatase that plays a role in Golgi and spindle organization and embryonic survival; haploinsufficiency of the mouse Sacm1l causes preimplantation lethality
33	*FES1*	*YBR101C*	Hsp70 (Ssa1p) nucleotide exchange factor, cytosolic homolog of Sil1p, which is the nucleotide exchange factor for BiP (Kar2p) in the endoplasmic reticulum		
34	*STP2*	*YHR006W*	Transcription factor, activated by proteolytic processing in response to signals from the SPS sensor system for external amino acids; activates transcription of amino acid permease genes		
35	*TCO89*	*YPL180W*	Subunit of TORC1 (Tor1p or Tor2p-Kog1p-Lst8p-Tco89p), a complex that regulates growth in response to nutrient availability; cooperates with Ssd1p in the maintenance of cellular integrity; deletion strains are hypersensitive to rapamycin	*DSPP (18%)*	Dentin sialophosphoprotein, a putative structural constituent of extracellular matrix that acts in odontogenesis and bone mineralization, upregulated in prostatic neoplasms; gene mutation is associated with dentinogenesis imperfecta and dentin dysplasia
36	*BUB1*	*YGR188C*	Protein kinase that forms a complex with Mad1p and Bub3p that is crucial in the checkpoint mechanism required to prevent cell cycle progression into anaphase in the presence of spindle damage, associates with centromere DNA via Skp1p	*BUB1 (22.7%)*	Budding uninhibited by benzimidazoles 1 homolog, a kinase that acts in spindle checkpoint and chromosome segregation; gene mutations are associated with T cell leukemia and Hodgkin lymphoma; mouse Bub1 is associated with aneuploidy and postnatal defects
37	*ARO2*	*YGL148W*	Bifunctional chorismate synthase and flavin reductase, catalyzes the conversion of 5-enolpyruvylshikimate 3-phosphate (EPSP) to form chorismate, which is a precursor to aromatic amino acids		
38	*GET3*	*YDL100C*	Guanine nucleotide exchange factor for Gpa1p; amplifies G protein signaling; subunit of the GET complex, which is involved in Golgi to ER trafficking and insertion of proteins into the ER membrane; has low-level ATPase activity		

Rank	*Yeast Gene*	*ORF*	Yeast Gene Function	*Human Ortholog*	Human Gene Function
39	*TPS1*	*YBR126C*	Synthase subunit of trehalose-6-phosphate synthase/phosphatase complex, which synthesizes the storage carbohydrate trehalose; also found in a monomeric form; expression is induced by the stress response and repressed by the Ras-cAMP pathway		
40	*SLX8*	*YER116C*	Subunit of the Slx5-Slx8 SUMO-targeted ubiquitin ligase (STUbL) complex; stimulated by prior attachment of SUMO to the substrate; contains a C-terminal RING domain		
41	*YER084W*	*YER084W*	Dubious open reading frame unlikely to encode a protein, based on available experimental and comparative sequence data		
42	*COX18*	*YGR062C*	Mitochondrial integral inner membrane protein required for membrane insertion of C-terminus of Cox2p; interacts genetically and physically with Mss2p and Pnt1p; similar to S. cerevisiae Oxa1, N. crassa Oxa2p, and E. coli YidC	*COX18 (24.7%)*	Protein with high similarity to COX18 cytochrome c oxidase assembly homolog (mouse Cox18), which acts in assembly of Cox2 into the cytochrome oxidase complex and is required for proper post-translation, member of the 60kDa inner membrane protein family
43	*NPL6*	*YMR091C*	Component of the RSC chromatin remodeling complex; interacts with Rsc3p, Rsc30p, Ldb7p, and Htl1p to form a module important for a broad range of RSC functions; involved in nuclear protein import and maintenance of proper telomere length		
44	*YLR184W*	*YLR184W*	Dubious ORF unlikely to encode a functional protein, based on available experimental and comparative sequence data		
45	*EMP24*	*YGL200C*	integral membrane component of endoplasmic reticulum-derived COPII-coated vesicles, which function in ER to Golgi transport	*TMED2 (32.4%)*	Transmembrane emp24 domain trafficking protein 2, plays a role in calcium sensing receptor maturation, plasma membrane targeting, and stabilization and embryonic placenta morphogenesis and heart looping
46	*YAF9*	*YNL107W*	Subunit of both the NuA4 histone H4 acetyltransferase complex and the SWR1 complex, may function to antagonize silencing near telomeres; interacts directly with Swc4p, has homology to human leukemogenic protein AF9, contains a YEATS domain	*YEATS2 (38%)*	YEATS domain containing 2, a scaffolding subunit of the ATAC (Ada Two-A containing) complex, forms a histone fold heterodimer with NC2-beta (DR1)

Rank	*Yeast Gene*	*ORF*	Yeast Gene Function	*Human Ortholog*	Human Gene Function
47	*RTG2*	*YGL252C*	Sensor of mitochondrial dysfunction; regulates the subcellular location of Rtg1p and Rtg3p, transcriptional activators of the retrograde (RTG) and TOR pathways; Rtg2p is inhibited by the phosphorylated form of Mks1p		
48	*CEM1*	*YER061C*	Mitochondrial beta-keto-acyl synthase with possible role in fatty acid synthesis; required for mitochondrial respiration	*OXSM (39%)*	This gene encodes a beta-ketoacyl synthetase. The enzyme is required for elogation of fatty acid chains in the mitochondria.
49	*AIM10*	*YER087W*	Protein with similarity to tRNA synthetases; non-tagged protein is detected in purified mitochondria; null mutant is viable and displays elevated frequency of mitochondrial genome loss	*PARS2 (29.3%)*	Protein containing a tRNA synthetase class II core domain (G, H, P, S and T), and an anticodon binding domain, has moderate similarity to C. elegans T27F6.5, which is involved in osmoregulation and positive regulation of body size and growth rate
50	*YBR144C*	*YBR144C*	Dubious open reading frame unlikely to encode a protein, based on available experimental and comparative sequence data; YBR144C is not an essential gene		
51	*YDR149C*	*YDR149C*	Dubious open reading frame unlikely to encode a functional protein, based on available experimental and comparative sequence data; overlaps the verified gene NUM1; null mutation blocks anaerobic growth		
52	*GET2*	*YER083C*	Subunit of the GET complex; involved in insertion of proteins into the ER membrane; required for the retrieval of HDEL proteins from the Golgi to the ER in an ERD2 dependent fashion and for meiotic nuclear division		
53	*LDB7*	*YBL006C*	Component of the RSC chromatin remodeling complex; interacts with Rsc3p, Rsc30p, Npl6p, and Htl1p to form a module important for a broad range of RSC functions		
54	*MDM32*	*YOR147W*	Mitochondrial inner membrane protein with similarity to Mdm31p, required for normal mitochondrial morphology and inheritance; interacts genetically with MMM1, MDM10, MDM12, and MDM34		

Rank	*Yeast Gene*	*ORF*	Yeast Gene Function	*Human Ortholog*	Human Gene Function
55	*VPS63*	*YLR261C*	Dubious open reading frame, unlikely to encode a protein; not conserved in closely related Saccharomyces species; 98% of ORF overlaps the verified gene YPT6; deletion causes a vacuolar protein sorting defec		
56	*CBP2*	*YHL038C*	Mitochondrial protein required for splicing of the group I intron aI5 of the COB pre-mRNA, binds to the RNA to promote splicing; also involved in but not essential for splicing of the COB bI2 intron and the intron in the 21S rRNA gene		
57	*RPL8A*	*YHL033C*	Ribosomal protein L4 of the large (60S) ribosomal subunit, nearly identical to Rpl8Bp and has similarity to rat L7a ribosomal protein; mutation results in decreased amounts of free 60S subunits	*rpl7a (57%)*	Ribosomal protein L7a, a putative component of the 60S ribosomal subunit that binds thyroid hormone receptor, inhibits transcription by antagonizing nuclear receptors; upregulated in colorectal cancer and acts as trk-2h fusion oncogene in breast cancer
58	*SSN3*	*YPL042C*	Cyclin-dependent protein kinase, component of RNA polymerase II holoenzyme; involved in phosphorylation of the RNA polymerase II C-terminal domain; involved in glucose repression	*CDK8 (44%)*	Cyclin dependent kinase 8, a transcription regulator that acts in notch signaling pathway, embryonic development, and protein stabilization; gene mutation correlates with colorectal cancer
59	*YNL296W*	*YNL296W*	ubious open reading frame unlikely to encode a functional protein; deletion adversely affects sporulation; deletion mutant exhibits synthetic phenotype under expression of mutant huntingtin fragment, but gene does not have human ortholog		
60	*VPS51*	*YKR020W*	Component of the GARP (Golgi-associated retrograde protein) complex, Vps51p-Vps52p-Vps53p-Vps54p, which is required for the recycling of proteins from endosomes to the late Golgi; links the (VFT/GARP) complex to the SNARE Tlg1p		
61	*MDJ1*	*YFL016C*	Co-chaperone that stimulates the ATPase activity of the HSP70 protein Ssc1p; involved in protein folding/refolding in the mitochodrial matrix; required for proteolysis of misfolded proteins; member of the HSP40 (DnaJ) family of chaperones	*DNAJB9 (46%)*	DnaJ homolog subfamily B member 9, a putative ATPase activator that may act in angiogenesis, cell cycle arrest, cell differentiation, protein folding, and ER overload response
62	*HAP3*	*YBL021C*	Subunit of the heme-activated, glucose-repressed Hap2p/3p/4p/5p CCAAT-binding complex, a transcriptional activator and global regulator of respiratory gene expression; contains sequences contributing to both complex assembly and DNA binding		

Rank	*Yeast Gene*	*ORF*	Yeast Gene Function	*Human Ortholog*	Human Gene Function
63	*GGC1*	*YDL198C*	Mitochondrial GTP/GDP transporter, essential for mitochondrial genome maintenance; has a role in mitochondrial iron transport; member of the mitochondrial carrier family		
64	*LSM1*	*YJL124C*	Lsm (Like Sm) protein; forms heteroheptameric complex (with Lsm2p, Lsm3p, Lsm4p, Lsm5p, Lsm6p, and Lsm7p) involved in degradation of cytoplasmic mRNAs	*Lsm1 (45%)*	LSM1 homolog, U6 small nuclear RNA associated (S. cerevisiae),LSM1,CASM,YJL124C,Cancer-associated Sm-like,Small nuclear ribonuclear CaSm,U6 snRNA-associated Sm-like protein LSm1,
65	*VPS52*	*YDR484W*	Component of the GARP (Golgi-associated retrograde protein) complex, Vps51p-Vps52p-Vps53p-Vps54p, which is required for the recycling of proteins from endosomes to the late Golgi; involved in localization of actin and chitin	*VPS52 (21.2%)*	Vacuolar protein sorting 52 homolog, a component of Golgi associated retrograde protein (GARP) complex that binds to Rab GTPase, involved in protein transport to lysosome and retrograde transport, regulates receptor recycling and protein localization
66	*PHO80*	*YOL001W*	Cyclin, interacts with cyclin-dependent kinase Pho85p; regulates the response to nutrient levels and environmental conditions, including the response to phosphate limitation and stress-dependent calcium signaling		
67	*GCN5*	*YGR252W*	Histone acetyltransferase, acetylates N-terminal lysines on histones H2B and H3; catalytic subunit of the ADA and SAGA histone acetyltransferase complexes; founding member of the Gcn5p-related N-acetyltransferase superfamily	*GCN5-L (46%)*	K(lysine) acetyltransferase 2A, a transcriptional coactivator that is involved in histone acetylation, DNA repair, and antiapoptosis, acts in retinoic acid receptor signaling, regulates embryonic stem cells shape and size through G2-M phase
68	*CTF4*	*YPR135W*	Chromatin-associated protein, required for sister chromatid cohesion; interacts with DNA polymerase alpha (Pol1p) and may link DNA synthesis to sister chromatid cohesion	*And-1 (20%)*	
69	*COQ3*	*YOL096C*	O-methyltransferase, catalyzes two different O-methylation steps in ubiquinone (Coenzyme Q) biosynthesis; component of a mitochondrial ubiquinone-synthesizing complex; phosphoprotein	*COQ (29%)*	Coenzyme Q3 homolog methyltransferase, an O-methyltransferase that catalyzes the methylation of 3,4-dihydroxy-5-polyprenylbenzoic acid and the conversion of demethyl-Q to ubiquinone in ubiquinone biosynthesis

Rank	*Yeast Gene*	*ORF*	Yeast Gene Function	*Human Ortholog*	Human Gene Function
70	*PFD1*	*YJL179W*	Subunit of heterohexameric prefoldin, which binds cytosolic chaperonin and transfers target proteins to it; involved in the biogenesis of actin and of alpha- and gamma-tubulin		
71	*SNT1*	*YCR033W*	Subunit of the Set3C deacetylase complex that interacts directly with the Set3C subunit, Sif2p; putative DNA-binding protein; mutant has increased aneuploidy tolerance	*NCOR1 (19.9%)*	Nuclear receptor corepressor 1, a transcriptional regulator that acts in histone acetylation, stem cell differentiation, and skeletal muscle tissue development; increased mRNA expression correlates with breast cancer and endometrial hyperplasia
72	*YNL198C*	*YNL198C*	Dubious open reading frame unlikely to encode a protein, based on available experimental and comparative sequence data		
73	*COX11*	*YPL132W*	Mitochondrial inner membrane protein required for delivery of copper to the Cox1p subunit of cytochrome c oxidase; association with mitochondrial ribosomes suggests that copper delivery may occur during translation of Cox1p	*COX11 (54%)*	Cytochrome c oxidase assembly protein COX11 homolog, a mitochondrial protein that may play a role in heme-A biosynthesis, regulation of oxidoreductase activity, and respiratory chain complex-IV assembly
74	*ATP11*	*YNL315C*	Molecular chaperone, required for the assembly of alpha and beta subunits into the F1 sector of mitochondrial F1F0 ATP synthase	*ATPAF1 (29%)*	ATP synthase mitochondrial F1 complex assembly factor 1, interacts with the F1 beta ATP synthase subunit (human ATP5B) and may mediate its assembly into the F1 complex; map position correlates with hereditary congenital ptosis and muscle-eye-brain disease
75	*SIC1*	*YLR079W*	Inhibitor of Cdc28-Clb kinase complexes that controls G1/S phase transition, preventing premature S phase and ensuring genomic integrity; phosphorylation targets Sic1p for SCF(CDC4)-dependent turnover; functional homolog of mammalian Kip1		
76	*TRP2*	*YER090W*	Anthranilate synthase, catalyzes the initial step of tryptophan biosynthesis, forms multifunctional hetero-oligomeric anthranilate synthase:indole-3-glycerol phosphate synthase enzyme complex with Trp3p		

Rank	*Yeast Gene*	*ORF*	Yeast Gene Function	*Human Ortholog*	Human Gene Function
77	*PET54*	*YGR222W*	Mitochondrial inner membrane protein that binds to the 5' UTR of the COX3 mRNA to activate its translation together with Pet122p and Pet494p; also binds to the COX1 Group I intron AI5 beta to facilitate exon ligation during splicing		
78	*MRPL51*	*YPR100W*	Mitochondrial Ribosomal Protein, Large subunit		
79	*LGE1*	*YPL055C*	Protein of unknown function; null mutant forms abnormally large cells, and homozygous diploid null mutant displays delayed premeiotic DNA synthesis and reduced efficiency of meiotic nuclear division		
80	*YLR202C*	*YLR202C*	Dubious open reading frame unlikely to encode a protein, based on available experimental and comparative sequence data; partially overlaps the verified ORF YLR201		
81	*NPR3*	*YHL023C*	Component, with Npr2p, of an evolutionarily conserved complex that mediates downregulation of TOR Complex 1 activity in response to amino acid limitation; null mutant displays delayed meiotic DNA replication and double-strand break repair		
82	*WSS1*	*YHR134W*	Sumoylated protein that localizes to a single spot on the nuclear periphery of mother cells but not daughters; interacts genetically with SMT3; UV-sensitive mutant phenotype and genetic interactions suggest a role in the DNA damage response		
83	*YDR417C*	*YDR417C*	Dubious open reading frame unlikely to encode a protein, based on available experimental and comparative sequence data; partially overlaps the verified ORF RPL12B/YDR418W		
84	*MRC1*	*YCL060C*	S-phase checkpoint protein required for DNA replication; interacts with and stabilizes Pol2p at stalled replication forks during stress, where it forms a pausing complex with Tof1p and is phosphorylated by Mec1p; protects uncapped telomeres		
85	*NGG1*	*YDR176W*	Transcriptional regulator involved in glucose repression of Gal4p-regulated genes; component of transcriptional adaptor and histone acetyltransferase complexes, the ADA complex, the SAGA complex, and the SLIK complex		

Rank	*Yeast Gene*	*ORF*	Yeast Gene Function	*Human Ortholog*	Human Gene Function
86	*YGR219W*	*YGR219W*	Dubious open reading frame unlikely to encode a protein, based on available experimental and comparative sequence data; partially overlaps the verified ORF MRPL9/YGR220C		
87	*RSC1*	*YGR056W*	Component of the RSC chromatin remodeling complex; required for expression of mid-late sporulation-specific genes; contains two essential bromodomains, a bromo-adjacent homology (BAH) domain, and an AT hook (	*PBRM1 (25.5%)*	Polybromo 1, a transcriptional co-regulator that binds to histone, acts in cell proliferation and organ development, may be involved in retinoic acid receptor signaling; genetic locus is associated with susceptibility to schizophrenia
88	*RTF1*	*YGL244W*	Subunit of the RNA polymerase II-associated Paf1 complex; directly or indirectly regulates DNA-binding properties of Spt15p and relative activities of different TATA elements; involved in telomere maintenance	*RTF1 (25.7%)*	Protein with low similarity to C. elegans F25B3.6, which is involved in larval development, gametogenesis, embryogenesis, body morphogenesis, and positive growth regulation
89	*COX23*	*YHR116W*	Mitochondrial intermembrane space protein that functions in mitochondrial copper homeostasis, essential for functional cytochrome oxidase expression; homologous to Cox17p; contains twin cysteine-x9-cysteine motifs		
90	*HOC1*	*YJR075W*	Alpha-1,6-mannosyltransferase involved in cell wall mannan biosynthesis; subunit of a Golgi-localized complex that also contains Anp1p, Mnn9p, Mnn11p, and Mnn10p; identified as a suppressor of a cell lysis sensitive pkc1-371 allele		
91	*SKY1*	*YMR216C*	SR protein kinase (SRPK) involved in regulating proteins involved in mRNA metabolism and cation homeostasis; similar to human SRPK1	*SRPK1 (49%)*	SFRS protein kinase 1, a protein kinase that plays a role in the regulation of RNA splicing, and AKT1 , MAPK3 and MAPK1 phosphorylation, may regulate cell cycle; protein expression is upregulated in adult T-cell leukemia, breast and colon tumors
92	*DEP1*	*YAL013W*	Transcriptional modulator involved in regulation of structural phospholipid biosynthesis genes and metabolically unrelated genes, as well as maintenance of telomeres, mating efficiency, and sporulation		
93	*RSM27*	*YGR215W*	Mitochondrial ribosomal protein of the small subunit		

Rank	*Yeast Gene*	*ORF*	Yeast Gene Function	*Human Ortholog*	Human Gene Function
94	*MRPL9*	*YGR220C*	Dubious open reading frame unlikely to encode a protein, based on available experimental and comparative sequence data; partially overlaps the verified ORF MRPL9/YGR220C	*MRPL3 (40%)*	Mitochondrial ribosomal protein L3, an RNA binding protein that may play a role in translation
95	*YDR230W*	*YDR230W*	Dubious open reading frame unlikely to encode a protein, based on available experimental and comparative sequence data; partially overlaps the verified gene COX20		
96	*VRP1*	*YLR337C*	Proline-rich actin-associated protein involved in cytoskeletal organization and cytokinesis; related to mammalian Wiskott-Aldrich syndrome protein (WASP)-interacting protein (WIP)	*WIP (35%)*	WAS-WASL interacting protein family member 1, binds to kinases and actin, stimulates mast cell degranulation and cytokine secretion, mediates focal adhesion assembly, Ca2+ transport, and PDGFR signaling, acts in actin polymerization and T cell activation
97	*COQ6*	*YGR255C*	Putative flavin-dependent monooxygenase, involved in ubiquinone (Coenzyme Q) biosynthesis; localizes to the matrix face of the mitochondrial inner membrane in a large complex with other ubiquinone biosynthetic enzymes	*COQ6 (32.9%)*	Protein with moderate similarity to C. elegans COQ-6, which participates in coenzyme Q9 biosynthesis and in determination of adult life span
98	*LSM7*	*YNL147W*	Lsm (Like Sm) protein; part of heteroheptameric complexes (Lsm2p-7p and either Lsm1p or 8p): cytoplasmic Lsm1p complex involved in mRNA decay; nuclear Lsm8p complex part of U6 snRNP and possibly involved in processing tRNA, snoRNA, and rRNA	*LSM7 (47%)*	U6 snRNA associated Sm like protein LSm7, a putative U6 snRNA binding protein that interacts with TACC1, may play a role in RNA processing
99	*SPF1*	*YEL031W*	P-type ATPase, ion transporter of the ER membrane involved in ER function and Ca2+ homeostasis; required for regulating Hmg2p degradation; confers sensitivity to a killer toxin (SMKT) produced by Pichia farinosa KK1	*ATP13A1 (39%)*	Protein with moderate similarity to A. thaliana AT5G23630, which is involved in cellular metal ion homeostasis and pollen maturation
100	*PET117*	*YER058W*	Protein required for assembly of cytochrome c oxidase		

Rank	*Yeast Gene*	*ORF*	Yeast Gene Function	*Human Ortholog*	Human Gene Function
101	*CBP1*	*YJL209W*	Mitochondrial protein that interacts with the 5'-untranslated region of the COB mRNA and has a role in its stability and translation; found in a complex at the inner membrane along with Pet309p		
102	*BCS1*	*YDR375C*	Mitochondrial protein of the AAA ATPase family; has ATP-dependent chaperone activity; required for assembly of Rip1p and Qcr10p into cytochrome bc(1) complex; mutations in human homolog BCS1L are linked to neonatal mitochondrial diseases	*BCS1L (50%)*	BCS1 like, plays a role in regulation of assembly of mitochondrial respiratory chain complex I, III, and IV; gene mutations are associated with GRACILE and Bjornstad syndrome, complex III deficiency, encephalopathy, tubulopathy, and metabolic diseases
103	*MNN4*	*YKL201C*	Putative positive regulator of mannosylphosphate transferase (Mnn6p), involved in mannosylphosphorylation of N-linked oligosaccharides; expression increases in late-logarithmic and stationary growth phases	*LEO1 (24.1%)*	Leo1 Paf1-RNA polymerase II complex component homolog, binds to parafibromin , plays a role in replicative cell aging, may regulate transcription
104	*YMR031W-A*	*YMR031W-A*	Dubious open reading frame unlikely to encode a protein, based on available experimental and comparative sequence data; null mutant displays shortened telomeres; partially overlaps the uncharacterized ORF YMR031C		
105	*PCP1*	*YGR101W*	Mitochondrial serine protease required for the processing of various mitochondrial proteins and maintenance of mitochondrial DNA and morphology; belongs to the rhomboid-GlpG superfamily of intramembrane peptidases	*PARL (32.3%)*	Presenilin associated rhomboid-like, a protease that acts in mitochondrial fragmentation initiation, regulates cytochrome c release during apoptosis via Opa1-dependent cristae remodeling; polymorphism is associated with Leber hereditary optic neuropathy
106	*YMR135W-A*	*YMR135W-A*	Dubious open reading frame unlikely to encode a functional protein, based on available experimental and comparative sequence data		
107	*RSM22*	*YKL155C*	Mitochondrial ribosomal protein of the small subunit; also predicted to be an S-adenosylmethionine-dependent methyltransferase		

Rank	*Yeast Gene*	*ORF*	Yeast Gene Function	*Human Ortholog*	Human Gene Function
108	*PET309*	*YLR067C*	Specific translational activator for the COX1 mRNA, also influences stability of intron-containing COX1 primary transcripts; localizes to the mitochondrial inner membrane; contains seven pentatricopeptide repeats (PPRs)		
109	*PHO23*	*YNL097C*	Probable component of the Rpd3 histone deacetylase complex, involved in transcriptional regulation of PHO5; C-terminus has similarity to human candidate tumor suppressor p33(ING1) and its isoform ING3	*EAF4-isoform1 (66%)*	Inhibitor of growth family member 3, an NuA4 histone acetyltransferase complex subunit that regulates p53-mediated transcription, cell cycle, and apoptosis, expression is downregulated in head and neck squamous cell carcinomas and melanoma
110	*KEX2*	*YNL238W*	Subtilisin-like protease (proprotein convertase), a calcium-dependent serine protease involved in the activation of proproteins of the secretory pathway	*PC7 (41%)*	Proprotein convertase subtilisin-kexin type 7, a putative serine-type endopeptidase that is involved in proteolysis, may play a role in cell differentiation, cell proliferation, vasculogenesis, and in utero embryonic development
111	*SPT21*	*YMR179W*	Protein with a role in transcriptional silencing; required for normal transcription at several loci including HTA2-HTB2 and HHF2-HHT2, but not required at the other histone loci; functionally related to Spt10p		
112	*PEP3*	*YLR148W*	Component of CORVET tethering complex; vacuolar peripheral membrane protein that promotes vesicular docking/fusion reactions in conjunction with SNARE proteins, required for vacuolar biogenesis	*vps18-isoform 1 (23%)*	Vacuolar protein sorting 18 homolog, a syntaxin binding ubiquitin ligase that plays a role in monoubiquitylation of GGA3 , vesicle-mediated transport, and negative regulation of S phase cell cycle
113	*YLR374C*	*YLR374C*	Dubious open reading frame unlikely to encode a protein, based on available experimental and comparative sequence data; partially overlaps the uncharacterized ORF STP3/YLR375W		
114	*MTM1*	*YGR257C*	Mitochondrial protein of the mitochondrial carrier family, involved in activating mitochondrial Sod2p probably by facilitating insertion of an essential manganese cofacto	*SLC25A39 (34%)*	Protein with strong similarity to solute carrier family 25 member 39 (mouse Slc25a39), which exhibits induced expression in brown adipose tissue exposed to cold, member of the mitochondrial carrier protein family of membrane transporters

Rank	*Yeast Gene*	*ORF*	Yeast Gene Function	*Human Ortholog*	Human Gene Function
115	*VPS64*	*YDR200C*	Protein required for cytoplasm to vacuole targeting of proteins; forms a complex with Far3p and Far7p to Far11p involved in recovery from pheromone-induced cell cycle arrest; mutant has increased aneuploidy tolerance		
116	*LHP1*	*YDL051W*	RNA binding protein required for maturation of tRNA and U6 snRNA precursors; acts as a molecular chaperone for RNAs transcribed by polymerase III; homologous to human La (SS-B) autoantigen	*LARP7 (27.1%)*	La ribonucleoprotein domain family member 7 (P-TEFb-interaction protein for 7SK stability), contains an La domain, stably associated with and required for 7SK snRNP integrity, suppresses P-TEFb-dependent transcriptional elongation and tumorigenesis
117	*YHR009C*	*YHR009C*	Putative protein of unknown function; not an essential gene		
118	*RAD6*	*YGL058W*	Ubiquitin-conjugating enzyme (E2), involved in postreplication repair (as a heterodimer with Rad18p), DSBR and checkpoint control (as a heterodimer with Bre1p), ubiquitin-mediated N-end rule protein degradation (as a heterodimer with Ubr1p	*Ube2A (69%)*	Ubiquitin-conjugating enzyme E2A , a ubiquitin-protein ligase that acts in mitotic cell cycle G2 to M transition, DNA repair, and histone ubiquitination, involved in embryonic development; gene mutation correlates with X linked mental retardation syndrome
119	*MGR2*	*YPL098C*	Protein required for growth of cells lacking the mitochondrial genome	*ROMO1 (43%)*	Reactive oxygen species modulator 1, induces reactive oxygen species production in mitochondria, regulates cellular properties such as replicative senescence, drug resistance to 5-FU, and cell proliferation
120	*SOV1*	*YMR066W*	Mitochondrial protein of unknown function		
121	*SHE3*	*YBR130C*	Protein that acts as an adaptor between Myo4p and the She2p-mRNA complex; part of the mRNA localization machinery that restricts accumulation of certain proteins to the bud; also required for cortical ER inheritance		

Rank	*Yeast Gene*	*ORF*	Yeast Gene Function	*Human Ortholog*	Human Gene Function
122	*MSW1*	*YDR268W*	Mitochondrial tryptophanyl-tRNA synthetase	*WARS2 (41.2%)*	Tryptophanyl tRNA synthetase 2 mitochondrial, a mitochondrial class I aminoacyl-tRNA synthetase catalyzing covalent attachment of tryptophan to cognate tRNA; gene locus is associated with waist hip ratio, a measure of body fat distribution
123	*MEC3*	*YLR288C*	DNA damage and meiotic pachytene checkpoint protein; subunit of a heterotrimeric complex (Rad17p-Mec3p-Ddc1p) that forms a sliding clamp, loaded onto partial duplex DNA by a clamp loader complex; homolog of human and S. pombe Hus1		
124	*MRPL7*	*YDR237W*	Mitochondrial ribosomal protein of the large subunit		
125	*VMA21*	*YGR105W*	ntegral membrane protein that is required for vacuolar H+-ATPase (V-ATPase) function, although not an actual component of the V-ATPase complex; functions in the assembly of the V-ATPase; localized to the yeast endoplasmic reticulum (ER)		
126	*SAG1*	*YJR004C*	Alpha-agglutinin of alpha-cells, binds to Aga1p during agglutination, N-terminal half is homologous to the immunoglobulin superfamily and contains binding site for a-agglutinin, C-terminal half is highly glycosylated and contains GPI anchor		
127	*HTB2*	*YBL002W*	Histone H2B, core histone protein required for chromatin assembly and chromosome function; nearly identical to HTB1; Rad6p-Bre1p-Lge1p mediated ubiquitination regulates transcriptional activation, meiotic DSB formation and H3 methylation	*HIST1H2BL (73%)*	Protein with very strong similarity to histone 1 H2bd (human HIST1H2BD), which is a putative nucleosome core histone that acts in chromatin remodeling and binds to human HIRA, contains a core histone H2A, H2B, H3 or H4 domain
128	*GRR1*	*YJR090C*	F-box protein component of the SCF ubiquitin-ligase complex; involved in carbon catabolite repression, glucose-dependent divalent cation transport, high-affinity glucose transport, morphogenesis, and sulfite detoxification	*FBLX20 (24%)*	Protein with high similarity to f-box and leucine-rich repeat protein 2 (F box leucine rich repeat 3, human FBXL2), which is a putative subunit of SCF ubiquitin ligase involved in protein degradation, contains an F-box domain

Rank	*Yeast Gene*	*ORF*	Yeast Gene Function	*Human Ortholog*	Human Gene Function
129	*ATP25*	*YMR098C*	Mitochondrial protein required for the stability of Oli1p (Atp9p) mRNA and for the Oli1p ring formation; YMR098C is not an essential gene		
130	*YBL094C*	*YBL094C*	Dubious open reading frame unlikely to encode a protein, based on available experimental and comparative sequence data; partially overlaps uncharacterized ORF YBL095W		
131	*RIC1*	*YLR039C*	Protein involved in retrograde transport to the cis-Golgi network; forms heterodimer with Rgp1p that acts as a GTP exchange factor for Ypt6p; involved in transcription of rRNA and ribosomal protein genes		
132	*AIM22*	*YJL046W*	Putative lipoate-protein ligase, required along with Lip2 and Lip5 for lipoylation of Lat1p and Kgd2p; similar to E. coli LplA; null mutant displays reduced frequency of mitochondrial genome loss	*LIPT (33%)*	Lipoyltransferase 1, putative enzyme that transfers the lipoyl group from lipoyl AMP to the lysine residue of lipoate-dependent enzymes, may be involved in lipoic acid metabolic process
133	*CRD1*	*YDL142C*	Cardiolipin synthase; produces cardiolipin, which is a phospholipid of the mitochondrial inner membrane that is required for normal mitochondrial membrane potential and function; also required for normal vacuolar ion homeostasis	*CRLS1 (34.7%)*	Cardiolipin synthase 1, catalyzes synthesis of cardiolipin from cytidinediphosphate diacylglycerol and phosphatidylglycerol, activity is optimal at alkaline pH and requires divalent cations, highly expresses in skeletal and cardiac muscles
134	*GLO3*	*YER122C*	ADP-ribosylation factor GTPase activating protein (ARF GAP), involved in ER-Golgi transport; shares functional similarity with Gcs1p	*ARFGAP1 (46.9%)*	GTPase-activating protein (GAP) which associates with the Golgi apparatus and which interacts with ADP-ribosylation factor 1 (ARF1). The encoded protein promotes hydrolysis of ARF1-bound GTP and is required for the dissociation of coat proteins from Golgi-derived membranes and vesicles.
135	*GCR2*	*YNL199C*	Transcriptional activator of genes involved in glycolysis; interacts and functions with the DNA-binding protein Gcr1p		
136	*YPR153W*	*YPR153W*	Putative protein of unknown function		

Rank	*Yeast Gene*	*ORF*	Yeast Gene Function	*Human Ortholog*	Human Gene Function
137	*CCE1*	*YKL011C*	Mitochondrial cruciform cutting endonuclease, cleaves Holliday junctions formed during recombination of mitochondrial DNA		
138	*ELP3*	*YPL086C*	Subunit of Elongator complex, which is required for modification of wobble nucleosides in tRNA; exhibits histone acetyltransferase activity that is directed to histones H3 and H4; disruption confers resistance to K. lactis zymotoxin	*ELP3 (72%)*	Elongation protein 3 homolog, subunit of the core elongator complex that interacts with RNA polymerase II, may play a role in mitochondrial function, actin organization, and cell motility
139	*QCR7*	*YDR529C*	Subunit 7 of the ubiquinol cytochrome-c reductase complex, which is a component of the mitochondrial inner membrane electron transport chain; oriented facing the mitochondrial matrix; N-terminus appears to play a role in complex assembly	*UZCRB (42%)*	Ubiquinol-cytochrome c reductase binding protein, a putative ubiquinol-cytochrome-c reductase, may mediate aerobic respiration and oxidative phosphorylation; gene mutation is associated with hypoglycaemia and lactic acidosis
140	*FRA2*	*YGL220W*	Protein involved in negative regulation of transcription of iron regulon; forms an iron independent complex with Fra2p, Grx3p, and Grx4p; null mutant fails to repress iron regulon and is sensitive to nickel		
141	*CAT5*	*YOR125C*	Protein required for ubiquinone (Coenzyme Q) biosynthesis; localizes to the matrix face of the mitochondrial inner membrane in a large complex with ubiquinone biosynthetic enzymes; required for gluconeogenic gene activation	*COQ7 (45%)*	Coenzyme Q7 homolog ubiquinone, a putative oxidoreductase that plays a role in ubiquinone and quinone cofactor biosynthesis, mitochondrial organization and function, neuron generation, and embryonic development, regulates gluconeogenesis
142	*RPS14A*	*YCR031C*	Ribosomal protein 59 of the small subunit, required for ribosome assembly and 20S pre-rRNA processing; mutations confer cryptopleurine resistance; nearly identical to Rps14Bp and similar to E. coli S11 and rat S14 ribosomal proteins	*RSP14 (82.6%)*	Ribosomal protein S14, a putative structural constituent of ribosome that may play a role in the chemical reactions and pathways resulting in the formation of a protein; gene haploinsufficiency correlates with myelodysplastic syndrome
143	*SLI15*	*YBR156C*	Subunit of the conserved chromosomal passenger complex (CPC; Ipl1p-Sli15p-Bir1p-Nbl1p), which regulates kinetochore-microtubule attachments, activation of the spindle tension checkpoint, and mitotic spindle disassembly		

Rank	*Yeast Gene*	*ORF*	Yeast Gene Function	*Human Ortholog*	Human Gene Function
144	*CSH1*	*YBR161W*	Probable catalytic subunit of a mannosylinositol phosphorylceramide (MIPC) synthase, forms a complex with probable regulatory subunit Csg2p; function in sphingolipid biosynthesis is overlapping with that of Sur1p		
145	*MCT1*	*YOR221C*	Predicted malonyl-CoA:ACP transferase, putative component of a type-II mitochondrial fatty acid synthase that produces intermediates for phospholipid remodeling		
146	*QCR8*	*YJL166W*	Subunit 8 of ubiquinol cytochrome-c reductase complex, which is a component of the mitochondrial inner membrane electron transport chain; oriented facing the intermembrane space; expression is regulated by Abf1p and Cpf1p		
147	*MTC1*	*YJL123C*	Protein of unknown function that may interact with ribosomes; green fluorescent protein (GFP)-fusion protein localizes to the cytoplasm and to COPI-coated vesicles (early Golgi); mtc1 is synthetically lethal with cdc13-1		
148	*IMP2*	*YMR035W*	Catalytic subunit of the mitochondrial inner membrane peptidase complex, required for maturation of mitochondrial proteins of the intermembrane space; complex contains Imp1p and Imp2p (both catalytic subunits), and Som1p	*IMMP2L (43%)*	Inner mitochondrial membrane peptidase 2 like, may act in nervous system development; gene mutation is associated with Tourette syndrome, gene SNP may correlate with susceptibility to autism, gene structural variant may be associated with ADHD
149	*SRB8*	*YCR081W*	Subunit of the RNA polymerase II mediator complex; associates with core polymerase subunits to form the RNA polymerase II holoenzyme; essential for transcriptional regulation; involved in glucose repression		
150	*AEP1*	*YMR064W*	Protein required for expression of the mitochondrial OLI1 gene encoding subunit 9 of F1-F0 ATP synthase		
151	*PET123*	*YOR158W*	Mitochondrial ribosomal protein of the small subunit; PET123 exhibits genetic interactions with PET122, which encodes a COX3 mRNA-specific translational activator		

Rank	*Yeast Gene*	*ORF*	Yeast Gene Function	*Human Ortholog*	Human Gene Function
153	*RPS16A*	*YMR143W*	Protein component of the small (40S) ribosomal subunit; identical to Rps16Bp and has similarity to E. coli S9 and rat S16 ribosomal proteins	*RPS16 (65%)*	Ribosomal protein S16 , a putative structural constituent of ribosome, binds to 18S rRNA and plays a role in translation
154	*YSY6*	*YBR162W-A*	Protein whose expression suppresses a secretory pathway mutation in E. coli; has similarity to the mammalian RAMP4 protein involved in secretion		
155	*RPS28B*	*YLR264W*	Protein component of the small (40S) ribosomal subunit; nearly identical to Rps28Ap and has similarity to rat S28 ribosomal protein	*RPS28 (75%)*	Protein with strong similarity to C. elegans Y41D4B.5, which is involved in reproduction, physiological processes, and positive regulation of growth, member of the ribosomal protein S28e family
156	*RRP8*	*YDR083W*	Nucleolar protein involved in rRNA processing, pre-rRNA cleavage at site A2; also involved in telomere maintenance; mutation is synthetically lethal with a gar1 mutation	*RRP8 (32.1%)*	Member of the hypothetical methyltransferase family, has moderate similarity to C. elegans T07A9.8

Table S2-3: Additional phenotypes of palmitoleate sensitive strains. Breakdown of additional lipid related phenotypes in single deletion mutants based on lipid droplet screen (Table 2-3) nystatin and myriocin sensitivity vulnerability to low (16°) or high (37°) temperatures and identification in genome-wide screen for altered basal unfolded protein response (UPR) (Jonikas et al). Sensitivity levels on a scale of 0-4 0 being no sensitivity and 4 being complete inviability. Blank values for Nystatin Myriocin Cold and Heat columns indicate that strain was not tested. Blank values for UPR column indicate that no significant change was evident. Yeast genes ranked by palmitoleate phenotype severity

Rank	*Gene*	*ORF*	LD phenotype	UPR	Nystatin	Myriocin	Cold (16°C)	Heat (37°C)
1	*ARV1*	*YLR242C*	NORMAL	4.0	4	0	0	4
2	*RPB9*	*YGL070C*	NORMAL					
3	*ARO1*	*YDR127W*	NORMAL	1.1	1	0	0	0
4	*GET1*	*YGL020C*	LESS	2.0	4	0	2	3
5	*VMA1*	*YDL185W*	LESS		4	3	4	0
6	*FEN1*	*YCR034W*	MORE	0.3	4	0	2	0
7	*YML095C-A*	*YML095C-A*	NORMAL		2	0	3	0
8	*VMA7*	*YGR020C*	NORMAL		3	0	3	0
9	*VPS69*	*YPR087W*	MORE		4	0	3	0
10	*IES6*	*YEL044W*	NORMAL		4	0	4	3

Rank	*Gene*	*ORF*	LD phenotype	UPR	Nystatin	Myriocin	Cold (16°C)	Heat (37°C)
11	*TRP5*	*YGL026C*	NORMAL					
12	*FPS1*	*YLL043W*	NORMAL		0	0	3	0
13	*VPS71*	*YML041C*	MORE	0.4	0	0	3	0
14	*SCS7*	*YMR272C*	NORMAL		0	0	0	0
15	*ERV14*	*YGL054C*	NORMAL	2.0				
16	*LOA1*	*YPR139C*	NORMAL					
17	*HSL7*	*YBR133C*	MORE		0	0	0	0
18	*YOR331C*	*YOR331C*	LESS		4	0	4	3
19	*ITR1*	*YDR497C*	NORMAL		0	0	0	0
20	*MRP10*	*YDL045W-A*	NORMAL		0	0	0	0

Rank	*Gene*	*ORF*	LD phenotype	UPR	Nystatin	Myriocin	Cold (16°C)	Heat (37°C)
21	*YBL100C*	*YBL100C*	LESS		3	0	4	0
22	*CYT1*	*YOR065W*	LESS		2	0	2	0
23	*VPS61*	*YDR136C*	MORE	1.3	0	0	0	0
24	*GOS1*	*YHL031C*	SMALLER	0.6	4	0	0	0
25	*GFD2*	*YCL036W*	NORMAL		3	0	0	0
26	*YDL009C*	*YDL009C*	NORMAL		0	0	0	0
27	*CTF8*	*YHR191C*	MORE		2	0	2	0
28	*YDL041W*	*YDL041W*	NORMAL		0	0	0	0
29	*PGI1*	*YBR196C-A*	MORE					
30	*IFM1*	*YOL023W*	LESS		3	0	3	0

Rank	*Gene*	*ORF*	LD phenotype	UPR	Nystatin	Myriocin	Cold (16°C)	Heat (37°C)
31	*VPS72*	*YDR485C*	MORE	0.5	2	0	3	0
32	*SAC1*	*YKL212W*	NORMAL	1.6	0	0	2	0
33	*FES1*	*YBR101C*	MORE		1	0	1	0
34	*STP2*	*YHR006W*	NORMAL	3.8				
35	*TCO89*	*YPL180W*	NORMAL	0.2	4	0	1	0
36	*BUB1*	*YGR188C*	NORMAL	0.3	3	0	3	0
37	*ARO2*	*YGL148W*	NORMAL		0	0	4	0
38	*GET3*	*YDL100C*	LESS	1.0	3		0	0
39	*TPS1*	*YBR126C*	NORMAL	-0.3	4	0	1	0
40	*SLX8*	*YER116C*	MORE		0	0	2	0

Rank	*Gene*	*ORF*	LD phenotype	UPR	Nystatin	Myriocin	Cold (16°C)	Heat (37°C)
41	*YER084W*	*YER084W*	NORMAL					
42	*COX18*	*YGR062C*	LESS		2	0	2	0
43	*NPL6*	*YMR091C*	NORMAL		4	0	3	3
44	*YLR184W*	*YLR184W*	NORMAL					
45	*EMP24*	*YGL200C*	NORMAL		1	0	0	0
46	*YAF9*	*YNL107W*	NORMAL		4	0	4	0
47	*RTG2*	*YGL252C*	NORMAL		0	0	0	0
48	*CEM1*	*YER061C*	LESS					
49	*AIM10*	*YER087W*	LESS					
50	*YBR144C*	*YBR144C*	NORMAL	0.3	0	0	0	0

Rank	*Gene*	*ORF*	LD phenotype	UPR	Nystatin	Myriocin	Cold (16°C)	Heat (37°C)
51	*YDR149C*	*YDR149C*	NORMAL					
52	*GET2*	*YER083C*	NORMAL	1.4	4	0	3	3
53	*LDB7*	*YBL006C*	LESS					
54	*MDM32*	*YOR147W*	NORMAL		0	0	0	0
55	*VPS63*	*YLR261C*	NORMAL					
56	*CBP2*	*YHL038C*	NORMAL					
57	*RPL8A*	*YHL033C*	MORE	-1.2	2	0	2	0
58	*SSN3*	*YPL042C*	LESS					
59	*YNL296W*	*YNL296W*	MORE	0.4	4	0	3	0
60	*VPS51*	*YKR020W*	MORE	1.9	2	0	1	0

Rank	*Gene*	*ORF*	LD phenotype	UPR	Nystatin	Myriocin	Cold (16°C)	Heat (37°C)
61	*MDJ1*	*YFL016C*	LESS					
62	*HAP3*	*YBL021C*	MORE					
63	*GGC1*	*YDL198C*	LESS		2	0	3	0
64	*LSM1*	*YJL124C*	LESS		2	0	2	3
65	*VPS52*	*YDR484W*	NORMAL	1.5	0	0	3	0
66	*PHO80*	*YOL001W*	NORMAL					
67	*GCN5*	*YGR252W*	LESS	-1.3	1	0	1	0
68	*CTF4*	*YPR135W*	LESS					
69	*COQ3*	*YOL096C*	LESS		1	0	2	0
70	*PFD1*	*YJL179W*	MORE		3	0	0	0

Rank	*Gene*	*ORF*	LD phenotype	UPR	Nystatin	Myriocin	Cold (16°C)	Heat (37°C)
71	*SNT1*	*YCR033W*	NORMAL					
72	*YNL198C*	*YNL198C*	LESS					
73	*COX11*	*YPL132W*	LESS		0	0	2	0
74	*ATP11*	*YNL315C*	NORMAL					
75	*SIC1*	*YLR079W*	NORMAL					
76	*TRP2*	*YER090W*	NORMAL		0	0	3	0
77	*PET54*	*YGR222W*	NORMAL					
78	*MRPL51*	*YPR100W*	LESS					
79	*LGE1*	*YPL055C*	NORMAL					
80	*YLR202C*	*YLR202C*	LESS					

Rank	*Gene*	*ORF*	LD phenotype	UPR	Nystatin	Myriocin	Cold (16°C)	Heat (37°C)
81	*NPR3*	*YHL023C*	LESS					
82	*WSS1*	*YHR134W*	LESS					
83	*YDR417C*	*YDR417C*	NORMAL					
84	*MRC1*	*YCL060C*	NORMAL					
85	*NGG1*	*YDR176W*	NORMAL	-2.0				
86	*YGR219W*	*YGR219W*	NORMAL					
87	*RSC1*	*YGR056W*	MORE					
88	*RTF1*	*YGL244W*	NORMAL					
89	*COX23*	*YHR116W*	LESS					
90	*HOC1*	*YJR075W*	MORE					

Rank	*Gene*	*ORF*	LD phenotype	UPR	Nystatin	Myriocin	Cold (16°C)	Heat (37°C)
91	*SKY1*	*YMR216C*	NORMAL					
92	*DEP1*	*YAL013W*	NORMAL		2	0	1	0
93	*RSM27*	*YGR215W*	NORMAL					
94	*MRPL9*	*YGR220C*	LESS		2	0	2	0
95	*YDR230W*	*YDR230W*	LESS					
96	*VRP1*	*YLR337C*	NORMAL	1.0				
97	*COQ6*	*YGR255C*	NORMAL					
98	*LSM7*	*YNL147W*	NORMAL	-0.4				
99	*SPF1*	*YEL031W*	NORMAL	3.8				
100	*PET117*	*YER058W*	LESS					

Rank	*Gene*	*ORF*	LD phenotype	UPR	Nystatin	Myriocin	Cold (16°C)	Heat (37°C)
101	*CBP1*	*YJL209W*	NORMAL					
102	*BCS1*	*YDR375C*	LESS		0	0	2	0
103	*MNN4*	*YKL201C*	NORMAL					
104	*YMR031W-A*	*YMR031W-A*	NORMAL					
105	*PCP1*	*YGR101W*	NORMAL					
106	*YMR135W-A*	*YMR135W-A*	LESS		0	0	0	0
107	*RSM22*	*YKL155C*	LESS		1	0	1	0
108	*PET309*	*YLR067C*	LESS					
109	*PHO23*	*YNL097C*	NORMAL	-0.6	1	0	2	0
110	*KEX2*	*YNL238W*	NORMAL	1.2				

Rank	*Gene*	*ORF*	LD phenotype	UPR	Nystatin	Myriocin	Cold (16°C)	Heat (37°C)
111	*SPT21*	*YMR179W*	NORMAL	0.9	0	0	3	0
112	*PEP3*	*YLR148W*	NORMAL					
113	*YLR374C*	*YLR374C*	MORE					
114	*MTM1*	*YGR257C*	LESS		0	0	3	0
115	*VPS64*	*YDR200C*	MORE		4	0	3	0
116	*LHP1*	*YDL051W*	MORE					
117	*YHR009C*	*YHR009C*	NORMAL					
118	*RAD6*	*YGL058W*	NORMAL					
119	*MGR2*	*YPL098C*	NORMAL					
120	*SOV1*	*YMR066W*	LESS					

Rank	*Gene*	*ORF*	LD phenotype	UPR	Nystatin	Myriocin	Cold (16°C)	Heat (37°C)
121	*SHE3*	*YBR130C*	NORMAL					
122	*MSW1*	*YDR268W*	LESS					
123	*MEC3*	*YLR288C*	NORMAL					
124	*MRPL7*	*YDR237W*	NORMAL					
125	*VMA21*	*YGR105W*	NORMAL	0.9				
126	*SAG1*	*YJR004C*	LESS					
127	*HTB2*	*YBL002W*	LESS	0.5				
128	*GRR1*	*YJR090C*	LESS					
129	*ATP25*	*YMR098C*	LESS	-0.4				
130	*YBL094C*	*YBL094C*	NORMAL					

Rank	*Gene*	*ORF*	LD phenotype	UPR	Nystatin	Myriocin	Cold (16°C)	Heat (37°C)
131	*RIC1*	*YLR039C*	NORMAL					
132	*AIM22*	*YJL046W*	LESS		0	0	3	0
133	*CRD1*	*YDL142C*	NORMAL		1	0	2	0
134	*GLO3*	*YER122C*	NORMAL	2.2				
135	*GCR2*	*YNL199C*	NORMAL	0.7				
136	*YPR153W*	*YPR153W*	LESS					
137	*CCE1*	*YKL011C*	NORMAL	-0.4				
138	*ELP3*	*YPL086C*	NORMAL					
139	*QCR7*	*YDR529C*	LESS		1	0	2	0
140	*FRA2*	*YGL220W*	NORMAL					

Rank	*Gene*	*ORF*	LD phenotype	UPR	Nystatin	Myriocin	Cold (16°C)	Heat (37°C)
141	*CAT5*	*YOR125C*	NORMAL					
142	*RPS14A*	*YCR031C*	NORMAL	-0.5				
143	*SLI15*	*YBR156C*	NORMAL					
144	*CSH1*	*YBR161W*	NORMAL					
145	*MCT1*	*YOR221C*	NORMAL	-0.5				
146	*QCR8*	*YJL166W*	LESS					
147	*MTC1*	*YJL123C*	NORMAL	0.4	0	0	3	0
148	*IMP2*	*YMR035W*	LESS		0	0	2	0
149	*SRB8*	*YCR081W*	LESS	1.2				
150	*AEP1*	*YMR064W*	LESS		0	3	2	0

Rank	*Gene*	*ORF*	LD phenotype	UPR	Nystatin	Myriocin	Cold (16°C)	Heat (37°C)
151	*PET123*	*YOR158W*	LESS					
152	*CTR1*	*YPR124W*	LESS	-0.5				
153	*RPS16A*	*YMR143W*	NORMAL	-1.0				
154	*YSY6*	*YBR162W-A*	NORMAL					
155	*RPS28B*	*YLR264W*	LESS	-0.8				
156	*RRP8*	*YDR083W*	NORMAL	-0.6				

Table S3-1: Yeast Tail-Anchored (TA) proteins and sensitivity to palmitoleate. List of yeast tail anchored proteins, their cellular localization and function and their sensitivity to palmitoleate based on the palmitoleate screen, or a retesting on solid media (solid + palmitoleate) and liquid media (liquid + palmitoleate). Blank wells indicate that the mutant was not tested. '0' indicates no sensitivity, '+' slight sensitivity and '++' completely inviable.

TA Protein	Location	Function	Palmitoleate screen	Lipid droplets	Solid + palmitoleate	Liquid + palmitoleate
YFL046W	mitochondria	?	0			
Fis1	mitochondria	organelle fission	0			
Tom5	mitochondria	protein import	0			
Tom6	mitochondria	protein import	0			
Tom7	mitochondria	protein import	0			
Tom22	mitochondria	protein import	0			
Prm3	NE	karyogamy	0		0	0
Kar1	NE	karyogamy	0		0	0
Ubc6	ER	ubiquitination	0			
Scs2	ER	lipid metabolism	sensitive (time)	more		
Csm4	ER	?	0		0	0
Hlj1	ER	protein turnover	0		0	0
Ysy6	ER	secretion	sensitive (time/ OD)	normal	0	0
YBL100C	ER	?	sensitive (time/ OD)	less	++	++
Sbh2	ER	secretion	0		0	0
Pgc1	ER (Lipid body)	lipid metabolism	0		0	0
Pex15	ER/peroxisome	peroxisomoge	0		0	0
Cyb5	ER	cytochrome	0		0	0
Frt1	ER	?	0		0	0
Frt2	ER	?	0		0	
Far10	ER	?	0		0	0
Vps64	ER/actin	?	sensitive (rate)	more	0	0
Sec20	ER	SNARE	0		0	0
Sec22	ER	SNARE	0		0	0

TA Protein	Location	Function	Palmitoleate screen	Lipid droplets	Solid + palmitoleate	Liquid + palmitoleate
Ufe1	ER	SNARE	0		0	0
Slt1	ER	SNARE	0		0	0
Sed5	ER-Golgi	SNARE	0		0	0
Gos1	ER-Golgi	SNARE	sensitive (time)	smaller	++	++
Bet1	ER-Golgi	SNARE	0		0	
Bos1	ER-Golgi	SNARE	0		0	0
Tlg1	Golgi	SNARE	0		0	0
Sft1	Golgi	SNARE	0			
Tlg2	Golgi	SNARE	0		+	0
Syn8	Golgi-vacuole	SNARE	0		0	0
Pep12	Golgi-vacuole	SNARE	0		0	0
Vti1	Golgi-vacuole	SNARE	0		0	0
Nyv1	Golgi-vacuole	SNARE	0		0	0
Vam3	vacuole	SNARE	0		0	0
Snc1	PM-vesicles	SNARE	0		0	0
Snc2	PM-vesicles	SNARE	0		0	0
Sso1	PM	SNARE	0		0	0
Sso2	PM	SNARE	0		0	0
YDL012C	PM	?	0		0	
Sps2	PM	sporulation	0		0	
YBR016W	PM	?	0		0	
Cwh36	?	?	0			
Phm6	?	?	0		0	
YDL241W	?	?	0		0	
YEL010W	?	?	0		0	
YEL073C	?	?	0			
YBL091C-A	?	?	0		0	
YML036W	?	?	0		0	
YJL119c	?	?	0		0	